Development, Optimization and Pharmacokinetic Evaluation of Rotigotine-Loaded Nanocarriers for Nose-to-Brain Delivery

THESIS

Submitted in partial fulfilment

of the requirements for the degree of

DOCTOR OF PHILOSOPHY

by

PARAMITA SAHA

ID. No. 2017PHXF0425P

Under the Supervision of

Dr. Murali Monohar Pandey

BITS Pilani

Pilani | Dubai | Goa | Hyderabad

BIRLA INSTITUTE OF TECHNOLOGY AND SCIENCE, PILANI

MAY 2023

Dedication

This thesis work is wholeheartedly dedicated to my parents ***Mr. Prabhas Chandra Saha*** and ***Mrs. Mitali Saha***, who never gave up on me, and to my M.Pharm Supervisor ***Prof. Punna Rao Ravi***, who has been my source of inspiration.

Declaration

I hereby declare that the work carried out in this thesis titled **"Development, Optimization and Pharmacokinetic Evaluation of Rotigotine-Loaded Nanocarriers for Nose-to-Brain Delivery"** is an original piece of research work carried out under the guidance of Dr. Murali Monohar Pandey at BITS-Pilani, Pilani Campus, Pilani, India. This thesis has not been submitted by me for the award of any other degree of any other University/Institute.

Name: PARAMITA SAHA

Signature:

Date:

BIRLA INSTITUTE OF TECHNOLOGY AND SCIENCE, PILANI

CERTIFICATE

This is to certify that the thesis titled **Development, Optimization and Pharmacokinetic Evaluation of Rotigotine-Loaded Nanocarriers for Nose-to-Brain Delivery** submitted by **PARAMITA SAHA** ID No **2017PHXF0425P** for award of Ph.D. of the Institute embodies original work done by him/her under my supervision.

Signature of the Supervisor:
Name in capital letters: Dr. MURALI MONOHAR PANDEY
Designation: **Assistant Professor**

Date:

Acknowledgment

"Of all the 'attitudes' we can acquire, surely the attitude of gratitude is the most important and by far the most life-changing."

-Zig Ziglar

The completion of any project depends upon the co-operation, co-ordination, and combined efforts of several resources of knowledge, inspiration, and energy. Therefore, I approach the important matters of project through these lines trying my best to give full credit where it deserves.

With all my gratitude and love I would like to thank the almighty GOD for taking me so far in life and showering blessing on me. You were there so I am here.

Let the word of thanks I would like to start with my supervisor ***Dr. Murali Monohar Pandey****, Assistant Professor; Department of Pharmacy****, BITS Pilani, Pilani Campus****. He is a wonderful adviser and true researcher. It was due to his support, valuable suggestion and timely advice during my doctoral thesis the project have been completed authentically. Apart from that I would also like to thank him for all his inspirational and motivational words in past few years. I consider myself fortunate enough to work with him professionally and know him personally.*

I also expressed my profound gratitude to ***Prof. Anil B. Gaikwad****, Professor and Head, Department of Pharmacy, for his support and extending the facilities to work at the institute. I would like to thank all the former Head, Department of Pharmacy* ***Prof. Atish T. Paul*** *and* ***Prof. Hemant R. Jadav*** *for providing all the facilities timely.*

I am deeply grateful to ***Prof. Aniruddha Roy*** *and* ***Prof. Gautam Singhvi*** *who have acted as Doctoral Advisory Committee (DAC) members and provided their detailed constructive comments and support throughout this work.*

I sincerely acknowledge the help provided by other faculty members, ***Prof R. Mahesh, Prof. Hemant R. Jadhav, Prof. Anil B. Gaikwad, Prof. Atish T Paul, Prof. S. Murugesan, Prof. Rajeev Taliyan, Prof. Deepak Chitkara, Prof. Anupama Mittal, Prof. Anil Jindal, Dr. Richa Shrivastava*** *and* ***Dr. Sandeep Sundriyal*** *for sharing their vast experience and technical knowledge with me when required.*

Acknowledgement

*I want to thank **Dr. Sushil K. Yadav**, Senior Veterinary In-charge, Animal house, Department of Pharmacy, for timely providing all the required animal facilities.*

*In life, we met very few people who make our life worth it and even fewer who actually change our attitude toward life. I express my warmest and most humble gratitude to one of them, my master's supervisor **Prof. Punna Rao Ravi**, Professor, BITS Pilani, Hyderabad Campus for always being there for me, for helping me, and for inspiring me throughout the progress of my academics.*

*I would like to take the privilege of thanking my lab mate **Ms. Nikita S. Hinge** for her constant support throughout my Ph.D. tenure. She is an inspiring colleague, a helpful individual with a great scientific mind.*
*I would also like to thank my colleagues and friends - **Dr. Himanshu, Dr. Swetha, Dr. Sarathlal, Geetika, Prabhjeet, Karan, Rajesh, Arihant, Moumita, Kedar, Srividya, Kavya, Shreya, Sharyu, Manisha, Atharva, Mahipal, Nisha, Vishwadeep,** and **Sriravali** for supporting me professionally.*
*I would like to take an opportunity to especially thank two of my colleagues **Dr. Violina** and **Dr. Swati** whom I met here and who will be a part for the rest of my life. They were my adviser, inspiration, and biggest supporter during my entire Ph.D. journey.*
*I owe my heartiest thanks to all my seniors **Dr. Vajir Malik, Dr. K. V. Krishna, Dr. Kishan Italiya, Dr. Ginson George, Dr. Pracheta Sengupta, Dr. Nisha Sharma, Dr. Dhanashree Surve,** and **Dr. Vamshi Krishna** for the professional and personal guidance during their stay in the campus.*
*I would like to also thank all my M.Pharm students **Mr. Souradeep, Ms. Chandni, Ms. Shreya,** and **Ms. Deepthi** for helping me out during my project duration.*

*I want to express my sincere gratitude to **Dr. Avantika Dalvi** and **Dr. Chandra Teja Uppuluri**, two of my fellow colleagues, for their unwavering support during the extent of my Ph.D. journey.*

I thank all the non-teaching staff for all the support they provided me with resources and helping hands.

*Finally, I take this opportunity to say my very special thanks to my parents **Mr. Prabhas Chandra Saha** and **Mrs. Mitali Saha** for being my constant source of inspiration, strength, and confidence and in one word everything.*

*I owe thanks to a very special person, my spouse, **Dr. Vishal Singh** for his continued and unfailing love, support, and understanding during my pursuit of Ph.D. degree that made the accomplishment of the thesis possible. You were always around at times I thought that it is impossible to continue, you helped me to keep things in perception. I owe him for selflessly letting his intellect, desires, and aspirations collide with mine.*

*I express my deep sense of gratitude to my in-laws **Mr. Dipen Singh** and **Mrs. Chanchal Singh** for their understanding and support.*

*It will be incomplete without thanking a person who enlightens my life with her existence. My younger sister **Ms. Debarpita** who always stood by me and provided strength in pursuing my thesis work.*

Besides this, there are numerous other people who have knowingly or unknowingly facilitated me in the successful accomplishment of my thesis. I thank all the people for every grain of effort they contributed.

Lastly, I owe a countless debt of gratitude to the animals who were sacrificed during my P.hD. due to the essential basis of my research work.

Date: ***Paramita Saha***

Table of Content

List of Tables

List of Figures

List of Abbreviations and Symbols

%RSD	Percentage relative standard deviation
^{o}C	Degree Celsius
µg	Microgram
µL	Microlitre
µm	Micrometre
Å	Angstrom
ACN	Acetonitrile
ADME	Absorption, distribution, metabolism and elimination
AD	Alzheimer's Disease
ANOVA	Analysis of variance
AUC	Area under the curve
ASR	Application site reaction
BBB	Blood-brain barrier
BBD	Box-Behnken design
CS	Chitosan
cm	Centimetre
C_{max}	Maximum plasma concentration of the drug
CMVs	Critical method variables
CNS	Central Nervous system
CSF	Cerebrospinal fluid
Da	Dalton
DE	Dissolution efficiency
DoE	Design of experiments
DSC	Differential scanning calorimetry
DTE (%)	Drug targeting efficiency percentage
DTP (%)	Direct transport percentage
EDAC	N-(3- Dimethylaminopropyl)-N′-ethylcarbodiimide hydrochloride
%EE	Entrapment efficiency
EMA	European medicines agency
FI	Fluorescence intensity

g	Gram
GAA	Glacial acetic acid
GIT	Gastrointestinal tract
GSE	Grape seed extract
h	Hour
HCl	Hydrochloric acid
HQC	High quality control
H_2O_2	Hydrogen peroxide
FTIR	Fourier transform infrared
f_1	Dissimilarity
f_2	Similarity
IAEC	Institutional animal ethics committee
ICH	International council of harmonization
IS	Internal standard
IV	Intravenous
IN	Intranasal
KH_2PO_4	Potassium dihydrogen phosphate
L	Litre
LB	Lewy bodies
Lf	Lactoferrin
LLOQ	Lower limit of quantification
LN	Lewy neurites
Log P	Logarithm of partition coefficient
LOD	Limit of detection
LOQ	Limit of quantitation
LOC	Lower quality control
MDT	Mean dissolution time
MeOH	Methanol
mg	Milligram
mL	Millilitre
mM	Millimolar
mm	Millimetre

MDR	Mean dissolution time
MQC	Middle quality control
mV	Millivolt
MW	Molecular weight
n	Number of replicates
NaOH	Sodium hydroxide
nm	Nanometre
NC	Nanocrystals
NE	Nanoemulsion
N2B	Nose-to-brain
NLC	Nanostructured lipid carriers
NP	Nanoparticles
OFAT	One factor at a time approach
PBD	Placket-Burman design
PBS	Phosphate buffer saline
PD	Parkinson's disease
PDI	Polydispersity index
PG	Propylene glycol
pH	Potential of hydrogen
PLGA	Poly lactic-co-glycolic acid
PM	Polymeric micelles
pXRD	Powder X-ray diffraction
QoL	Quality Of Life
R^2	Regression coefficient
rpm	Rotations per minute
RP-HPLC	Reverse phase High-performance liquid chromatography
RTG	Rotigotine
RTG-LCNP	Rotigotine Lecithin-chitosan hybrid nanoparticle
SD	Standard deviation
SEM	Scanning electron microscopy
SLN	Solid lipid nanoparticle
SPC	Soya phosphatidylcholine

Sol-gel	Solution to gel
$t_{1/2}$	Elimination half life
T_{max}	Time taken to reach maximum plasma concentration
TEM	Transmission electron microscopy
USP	United States Pharmacopoeia
UV	Ultraviole
v/v	Volume by volume
w/v	Weight by volume
σ	Standard deviation of the intercepts

Abstract

Rotigotine (RTG) is a non-ergoline dopamine receptor agonist approved by United States Food and Drug Administration for the treatment of Parkinson's disease (PD) and restless leg syndrome. RTG is currently available as a transdermal patch, Neupro®. RTG is effective as monotherapy to treat early symptoms of PD and as a combination therapy with levodopa through course of the disease. RTG shows efficiency in managing the motor symptoms of PD. It also improves major non-motor PD symptoms such as sleep disturbances, apathy, and anhedonia. Although RTG is one of the important and frontline drugs in PD management but, it is associated with various problems in clinical treatment. RTG shows poor aqueous solubility. It undergoes high first-pass metabolism, limiting its oral bioavailability to less than 1%. Also, systemic bioavailability of RTG from the transdermal patch is limited to only 37%, which is further reported to vary with respect to its site of application. Another challenge with RTG transdermal patches is the development of snowflake-like crystals during storage due to RTG crystallization. This leads to poor drug absorption through the skin and results in variable therapeutic responses. After systemic absorption from the transdermal patch, the brain availability of RTG remains a problem due to poor permeation of the drug across the blood-brain barrier (BBB).

Despite all the problems, in the market, RTG is available as a transdermal patch. The literature report revealed that very few attempts were taken to solve the delivery-related issues of RTG. Due to the shortcomings of orally and transdermally administered RTG, it is important to first look for an alternative route for the administration of RTG and then to find out some different formulations for the same delivery route.

Intranasal (i.n.) or precisely nose-to-brain (N2B) drug delivery route overcomes several problems of oral administration *viz.*, avoidance of hepatic first-pass metabolism,

gastrointestinal enzymatic degradation, systemic toxicity, etc. This route delivers the drugs via the olfactory or trigeminal nerve pathway directly to the brain by avoiding the BBB and improves the brain bioavailability of the drugs. The route also possesses advantages such as rapid onset of action, rapid absorption, and ease of self-administration which might be further beneficial for PD patients. Though, poor permeation of hydrophilic drugs, enzymatic degradation in nasal cavity, mucociliary clearance, shorter residence time, and improper installation of the formulation are the major limitations of i.n. route. However, these prime problems can effectively be addressed by using suitable nanocarrier-based i.n. formulations.

In this present research work, we have investigated different i.n. nanocarrier-based formulation strategies to increase the brain availability of RTG via direct N2B uptake, by minimizing systemic exposure of the drug.

Therefore, two analytical methods (a simple fluorescence-based and another advanced liquid chromatographic based) were developed and validated as per ICH guidelines. A fluorescence-based method was developed and validated to rapidly and accurately estimate the solubility of RTG in different surfactants and solvents during the preliminary screening of excipients for the preparation of nanocarriers. Further, design of expert (DoE) based RP-HPLC analytical method was developed and validated to quantify RTG with accuracy and precision in several *in vitro* and *ex vivo* samples. A rapid, sensitive, and specific RP-HPLC bioanalytical method was developed and validated as per ICH guidelines to estimate RTG in biological matrices i.e., brain and plasma. The applicability of the validated bioanalytical method for quantification of RTG in plasma and brain tissue samples was demonstrated by carrying out intravenous and i.n. pharmacokinetics (PK) studies of pure drug in male Wistar rats.

One of the significant disadvantages of RTG is its poor solubility, which results in lower saturation solubility of the drug in nasal fluid. A nanosuspension for RTG was developed to

solve the solubility issue of RTG. Several factors affecting nanosuspension were studied employing the concept of DoE. The formulation was characterized for particle size (nm), *in vitro* drug dissolution, *ex vivo* nasal permeation, nasal ciliotoxicity, and *in vivo* mucociliary transport time. The optimized nanosuspension showed a particle size of 73.55 ± 4.04 nm and PDI of 0.286 ± 0.028. The nanosuspension significantly improved the aqueous solubility of RTG as demonstrated by the *in vitro* dissolution study. Finally, *in vivo* PK study was performed for brain and plasma after i.n. administration of RTG-Nanosuspension and compared with pure drug suspension. RTG-Nanosuspension showed a 1.86-fold increased brain C_{max} when compared to pure drug suspension. The drug targeting efficiency percentage (DTE (%)) value for RTG-Nanosuspension was 885.1. This work confirmed that the RTG-Nanosuspension solved the issue of drug solubility and the i.n. administration enhanced the overall brain exposure of RTG as compared to pure drug.

To further enhance the direct N2B uptake and sustain the drug in the brain for a longer time, RTG-Proposomes was developed. Proposomes is a propylene glycol containing liposomal system that helps to overcome the stability issues associated with conventional ethosomes. Soya phosphatidylcholine, a mixture of phospholipids reported as nonimmunogenic and biocompatible, was used in the preparation of RTG-Proposomes to ensure safe delivery of the drug to brain via i.n. route. Optimized RTG-Proposomes were evaluated for stability, *in vitro* drug release, *ex vivo* nasal permeation, and *in vivo* PK studies in brain and plasma. RTG-Proposomes exhibited particle size of 115.63 ± 5.22 nm, PDI of 0.267 ± 0.028, and zeta potential of −14.8 ± 1.2 mV. The optimized proposomes showed mucociliary transport time of 32.5 ± 3.53 min. It enhanced the brain C_{max} and $AUC_{0\rightarrow tlast}$ by 2.68-fold and 5.21-fold, respectively than pure drug suspension. The DTE (%) value for RTG-Proposomes was found to be 1556.4. This signifies that the formulation further enhanced the delivery of RTG to the brain better than both pure RTG suspension and previously prepared RTG-Nanosuspension.

Finally, we have developed lecithin-chitosan hybrid nanoparticles (LCNP) using solvent injection method to further improve residence time of formulation in the nasal cavity which improves the brain uptake of nanocarrier. Chitosan is well-reported for its mucoadhesive and permeation enhancement properties and lecithin is considered a safe and biocompatible phospholipid. Both were used for the preparation of LCNP by ionic gelation method. The RTG-LCNP were characterized for particle size (nm), zeta potential, entrapment efficiency, surface morphology, and physical stability. Optimized RTG-LCNP showed a particle size of 108.2 ± 1.09 nm and zeta potential of 14.9 ± 0.5 mV. The morphology of RTG-LCNP was studied using FESEM and TEM. The electron microscopic images showed that the LCNP was smooth and predominantly of spherical shape. The brain PK study showed that RTG-LCNP improved brain C_{max} and $AUC_{0\rightarrow tlast}$ by 3.84-fold and 8.76-fold, respectively as compared to pure RTG suspension. From *in vivo* PK study, DTE (%) and direct transport percentage (DTP (%)) for RTG-LCNP were found to be 3673.7 and 97.3, respectively. This work indicates that RTG-LCNP improved the direct N2B uptake of RTG to the highest level as compared to the other two nanocarriers.

Finally, it was concluded that the prepared nanocarriers considerably enhanced RTG availability to the brain through direct N2B pathways and addressed the problems associated with RTG.

Chapter 1: Introduction

1.1 Parkinson's disease

In the year 1817, a neurologist, James Parkinson for the first time described a disease by the terms Shaking Palsy/paralysis agitans. Soon after, Jean-Martin Charcot, along with Alfred Vulpian in around 1861 and 1862, marked a place in medical history for incorporating more symptoms *viz.*, irresistible propulsion, muscle rigidity, slowness of speech, etc. to James Parkinson's clinical description of Shaking Palsy and created the umbrella term Parkinson's disease (PD) for all those symptoms. PD is an idiopathic nervous system disease characterized by both motor and non-motor symptoms.

PD is the 2nd leading neurodegenerative disease after Alzheimer's, mainly caused due to dopaminergic neuronal death in pars compacta of substantia nigra and ventral tegmental area, which eventually results in dopamine depletion in the brain [1–3]. PD affects approximately 7 – 10 million population across the globe [4] and the population affected by the disease is directly proportionate with age. Since last century, the PD prevalence rate has increased by 117.8% and death rates by 149.8% [5]. The combined direct and indirect expenses of PD are estimated to be 52 billion dollars per year just in the USA. It comprises treatment costs, caregiver expenditures, loss of income, etc. This economic burden is projected to cross 79 billion dollars by the end of 2037 [6]. According to the Global Burden of Disease, Injuries, and Risk Factors Study 2015, PD is the fastest spreading in prevalence, disability, and deaths [7]. As of 2016, 0.58 million people in India suffered from PD [8]. It is reported that PD has a severe adverse impact on patients' quality of life (QoL) [9]. QoL of PD patients includes mental, physical, and social domains [10]. Studies demonstrated that PD patients face the second worst impact on QoL's mental and physical realm [11]. Between 30 – 40% of people

with PD affected population are also affected by anxiety and depression like stress associated psychiatric disorders.

1.1.1 Pathophysiology of PD

PD affects multiple segments of the brain simultaneously and regarded as one of the primary causes of neurological disabilities. Dopaminergic nerve cells of the substantia nigra, the pigmented nuclei of midbrain and brainstem, olfactory nucleus, and cerebral cortex are parts of brain majorly affected in the disease. PD causes neuronal degeneration in different parts of CNS and peripheral nervous system as well [12,13]. Pathophysiology of PD includes combination of complex series of incidents *viz.*, accumulation of α-synuclein, loss of dopamine, mitochondrial dysfunction, neuroinflammation, etc. The characteristic pathological features in conclusive identification of PD are lowering of dopamine neurons in the substantia nigra and presence of Lewy bodies (LB). These two features start developing in stage 1 of the disease and get aggravated in further stages.

1.1.1.1 Loss of dopamine in striatum

Degeneration of dopaminergic neurons in pars compacta of substantia nigra and their projections in the striatum is one of the main pathophysiological features of PD. The loss of dopamine results in functional changes in striatum which plays a key role in motor dysfunctions [14]. After a significant amount (at least up to 70%) of dopamine neuron degeneration in striatum, the motor symptoms of PD can be observed [15]. Dopamine loss promotes changes in the sensitivity of dopamine receptors and reduces the density of dendritic spines in the putamen [16,17]. Dopamine loss in the striatum leads to the appearance of three motor symptoms called bradykinesia, rigidity, and tremor, which conventionally characterize PD [18].

1.1.1.2 Appearance of Lewy bodies (LB)

Existence of spherical aggregates called LB is another histopathological character of PD. The aggregates are usually comprised of insoluble fibrillary clusters containing misfolded proteins. The fibrillary cluster consists of varieties of proteins but, α-synuclein protein is considered as its critical element. The formation of LB is another result of neuronal degeneration [19]. Dysfunction of α- synuclein protein seems to be one common hallmark of all stages of PD [20].

PD is a complex disorder involving several factors like mitochondrial dysfunction, gene variation, oxidative stress, and neuroinflammation. Functional loss of genes causes damaged mitophagy which results in the growth of dysfunctional mitochondria and leads to the pathogenesis of PD. Neuroinflammation substantially up-regulates aggregation of α-synuclein, which finally causes formation of LB [21,22]. Even head injury [23], active and passive exposure to environmental toxins [24] may increase the probability of PD. Both head injury and environmental toxins increase the risk of accretion of LB [25] and finally results in PD.

1.1.2 Symptoms of PD

PD is an idiopathic nervous system disease characterized by both motor and non-motor symptoms. The onset of motor symptoms occurs in later stages of the disease when dopamine levels drop below normal. Slowness and erratic movements i.e., bradykinesia, rigidity, and tremor categories motor symptoms of the disease. As the disease advances, it affects the facial muscles involved in speech, resulting in slurred speech.

Though PD, is a motor disease, but patients show non-motor symptoms *viz.*, anxiety, sleep disorders, apathy, depression, etc. PD patients also show autonomic systematic dysfunction causing in symptoms i.e., sexual dysfunction, constipation, orthostatic hypotension, incontinence, and changes in thermoregulation, etc.

1.1.3 Stages of PD

PD develops in six pathological stages, wherein every stage leads to the continuous growth of inclusion bodies in a spindle-like structure called Lewy neurites (LN) in axons or as granular aggregates or spherical pale bodies called LB in the somata [26]. These inclusion bodies predominantly consist of misfolded aggregations of α- synuclein protein [27,28].

Mostly in stage 1, very few isolated LN are observed to be present in dorsal part of the motor nucleus of vagal nerve, and some LN are found in the axon of same nerve [29,30]. At this stage, tremors and other movement issues typically only affect one side of the body. A slight change in posture, in walk, and facial expressions are noticeable.

In stage 2, the number of LN increases significantly in the dorsal motor nucleus and also arises in brainstem nuclei of the lower medulla. Inclusion bodies existence does not initiate in the substantia nigra during the first two stages of PD [31,32]. For the first time, LN starts appearing in the pars compacta of the substantia nigra in the 3rd stage of PD [27]. In stage 2 symptoms *viz.*, tremors, stiffness, and trembling are visibly noticeable. This stage is not associated with balance impairment. Stage 3 signifies a critical turning point in the progression of the disease. Balance impairment and loss of reflex are common symptoms in this stage along with stiffness, tremors, etc.

In stage 4, LB also starts appearing along with LN, and hereafter the disease becomes severe and clinically diagnosable [33]. At this stage 4 of PD, the movement and reaction times of patients significantly decreased. In stages 5 and 6, neuronal degeneration attains its greatest extent. LN and LB progressively invade the entire neocortex [34] leading to severe impairment of somatic, limbic, and autonomic nervous systems which results in extreme manifestation of PD [35].

Later stages of the disease have also been associated with sensory abnormalities such as smell impairment, hallucinations, and illusions etc. These non-motor symptoms considerably lower the productivity and QoL of PD patients in addition to the motor symptoms. Till now no cure is available for PD, and the present treatment focuses on extending symptomatic relief. Due to the tremendous burden that PD poses in social, economic, and emotional life of patients, it is necessary to understand the condition in depth and develop novel management strategies for treating PD.

1.1.4 USFDA approved anti-Parkinson drugs

Drug therapy used for PD treatment can broadly be categorized as dopaminergic drugs and non-dopaminergic drugs. Dopaminergic drugs essentially act by modifying dopaminergic transmission. Non-dopaminergic drugs work by controlling the abnormal striatal neurotransmitters [36]. Dopaminergic drugs are mainly classified as dopamine precursors, dopamine agonists, monoamine oxidase B (MAO-B) inhibitors, and catechol-O-methyl transferase (COMT) inhibitors. Recently a non-dopaminergic drug is approved by USFDA for treating PD.

Levodopa (dopamine precursor) is used as first-line therapy for the symptomatic treatment of PD [37]. COMT inhibitors (tolcapone, entacapone, and opicapone), MAO-B inhibitors (rasagiline, selegiline, and safinamide), and dopamine agonist (bromocriptine, ropinirole, apomorphine, and rotigotine) are other drugs used for the treatment of PD [38]. Istradefylline (non-dopaminergic drug) is a selective adenosine A_{2A} receptor inhibitor recently approved to treat PD [39]. USFDA approved anti-Parkinson drugs are compiled and presented in **Table 1.1**. Non-pharmacological treatment approaches in PD include physiotherapy, occupational and speech therapy, deep brain stimulation, and cognitive training [40–42].

Table 1.1 USFDA approved anti-Parkinson drugs, their mechanism of action, available dosage form, and available dose strength

Drugs	Mechanism of action	Commercial dosage forms	Dose (mg)
Levodopa	Act by converting to neurotransmitter (dopamine)	Tablets	100 to 250
Entacapone	Block COMT enzyme & inhibit break down of dopamine in Brain	Tablets	200
Tolcapone		Tablets	100, 200
Opicapone		Capsules	25 & 50
Bromocriptine	Act on dopamine receptors (D_1 & D_2) by mimic action of neurotransmitter (dopamine)	Tablets	2.5, 5
Pergolide		Capsules	0.25 to 5
Ropinirole		Tablets	1 to 8
Rotigotine		Transdermal patches	0.05 to 1
Selegiline hydrochloride	Block MAO-B enzyme & inhibit break down of dopamine in Brain	Tablets	1.25 to 12
Rasagiline mesylate		Tablets	0.5 & 1
Safinamide		Flim coated tablets	50 & 100
Istradefylline	Inhibit adenosine A_{2A} receptor that restore the basal ganglia balance	Tablets	20 & 40

1.1.5 Blood-brain barrier (BBB)

Blood-brain barrier (BBB) is the most selective and dynamic barrier present in all organisms with well-developed central nervous system (CNS). The BBB applies the tightest control over direct microenvironment of brain cells, as it immediately interacts with the circulating blood. The BBB comprises blood capillaries of specialized endothelial cells, astrocytes, pericytes, and neuronal terminals. It allows only a few essential molecules to permeate into the brain from systemic circulation and protect the brain from circulating neurotoxin that may enter into systemic circulation accidentally [43].

Being the most restrictive endothelium in body, BBB is the principal barrier for transport of drugs into brain [44]. Most of the approved CNS drugs have limited or to no permeability

across the BBB which resulted in poor brain availability of them [44,45]. Because of this several strategies are explored for drug delivery of CNS drugs.

1.1.6 Strategies to improve the brain availability of drugs

Strategies for enhancing the brain delivery of drugs can be broadly categorized into two classes. Firstly, strategies enhanced the delivery of drugs to the brain through BBB. In recent years, liposomes, dendrimers [46], micelles [47,48], viral vectors [49], exosomes [50], nanoparticles, and surface modified-nanoparticles [51], etc. have been used to improve the brain availability of drugs by crossing the BBB.

For over a decade, several strategies have been explored for delivering drugs directly to the brain by avoiding the BBB. The strategies can be classified into two types *viz.*, invasive and non-invasive techniques. Invasive techniques include chemical disruption of BBB, craniotomy based drug delivery [52], convection-enhanced delivery [53,54], polymeric wafers, and microchip technologies [55]. But all these delivery techniques are associated with high risk. The non-invasive approaches include efflux pump inhibition [56,57], prodrug approaches [58], targeted nanocarrier based drug delivery [59–61], cell-based therapy [62], and intranasal (i.n.) drug delivery [63–65]. On the other hand, several non-invasive direct drug delivery methods are also being explored that bypass the BBB and reach the brain and cerebrospinal fluid (CSF). The i.n. drug delivery is one technique that has demonstrated promising results in recent times. The i.n. delivery of drugs overcomes the problems of oral administration by avoiding the hepatic first-pass metabolism and enzymatic degradation of drugs in the gastrointestinal tract. Additionally, i.n. delivery also possesses advantages such as rapid onset of action, rapid absorption [66], enhanced therapeutic effects without systemic exposure, reduced peripheral organ toxicity, etc. Absolute absence of any kind of pain and ease of self-administration make this delivery approach patient-friendly for the chronic neurodegenerative disease including PD.

1.2 Intranasal (i.n.) delivery of small molecules

The i.n. administration of any drug molecule refers to absorption of drug through nasal mucosa and then exhibit the action in body. The i.n. administration for brain delivery of drugs presents several advantages over any other route such as presence of highly permeable endothelial membrane, non-invasive painless easy mode of administration, avoidance of gastrointestinal enzymatic degradation, and hepatic first past metabolism. Transmucosal delivery of drugs via the olfactory or trigeminal nerve pathway directly to the brain by avoiding the BBB is often referred as nose-to-brain (N2B).

1.2.1 Anatomy of the nose

Nose is a complex organ that serves an essential role in respiration and olfaction of human and other vertebrates. The nasal cavity is divided by a septum into two symmetrical segments. Each segment are further divided into four areas - nasal vestibule, nasal atrium, respiratory region, and olfactory region. Nasal vestibule is the anterior portion that opens to the face via nostrils. Nasal atrium is the transitional region between vestibule and respiratory region. Respiratory region is further subdivided into inferior, middle, and superior nasal turbinate. This region is lined with a respiratory epithelium layer consisting of ciliated pseudostratified columnar and goblet cells. The trigeminal nerve's second branch (maxillary) goes directly from the nasal cavity to the brain stem.

The olfactory region is positioned on top of nasal cavity and continues to the septum and lateral wall of nose. The olfactory region comprises pseudostratified columnar epithelium (olfactory neuroepithelium), basal cells, supporting cells, microvillar cells, and a characteristic receptor (olfactory cells). Olfactory neuroepithelium is the only CNS component that is directly exposed to the external environment via olfactory region of nasal cavity [67].

1.2.2 Nose-to-brain (N2B) pathways

1.2.2.1 Uptake pathway of N2B delivery

Nose is the only part of human body which is directly connected to the brain and meets the external environment [68]. The i.n. route gives a direct entry from the external environment to the brain without any peripheral sensory receptor relay. The first and fifth cranial nerves *viz.*, olfactory and trigeminal nerves, respectively play an important role in the transport of drugs to CNS from deep area of nose. This pathway is usually called N2B transport [4,69]. The direct N2B delivery of drugs or nanocarriers majorly follows trigeminal and olfactory pathways.

1.2.2.1.1 Olfactory pathway

The olfactory region of nasal cavity has a surface area of 10 cm^2, contributing 5% of the total nasal surface area [70]. Olfactory epithelium is the only CNS part exposed directly to environment, so this pathway contributes a substantial role in the transport of drugs directly to brain upon i.n. administration [71]. This region comprises of olfactory epithelium, lamina propria, and olfactory bulb. Olfactory epithelium consists of olfactory receptor neurons. This neuronal pathway is considered to act as a determining transport mechanism pathway for direct delivery of drugs to brain. The olfactory neuronal pathway helps drugs enter to CSF directly via N2B route [72]. In this pathway, drugs via axon cross the cribriform plate and reach the olfactory bulb, which is opened to various parts of brain region like the amygdale, piriform cortex, and hypothalamus and thus help in transport [71,73]. The olfactory pathway takes only a few minutes to deliver the drugs directly into the brain by transporting them from CSF to brain's interstitial fluid [71].

1.2.2.1.2 Trigeminal pathway

Trigeminal nerve is the largest and fifth cranial nerve. It comprises of three branches such as ophthalmic, maxillary, and mandibular. The trigeminal nerve pathway joins to the end part of the brain, such as the spinal cord, the medulla, and the pons [71]. N2B delivery uses the

trigeminal pathway as a channel to carry drugs from nose to the brainstem opening. Then the drug enters through pons and then transfers through the rest of hindbrain [74]. Maxillary and ophthalmic branches of the trigeminal nerve play a very essential role in direct N2B delivery of drugs. These two branches of trigeminal nerves directly pass through the nasal mucosa to the forebrain and supply innervention to different parts of nasal mucosa and also anterior part of nose [75–77]. Trigeminal pathway is advantageous than olfactory pathway because it delivers drugs to both caudal and rostral parts of the brain [73]. This pathway is essential for the transport of drugs directly to brain to treat PD because, at the early stage of the disease, accumulation of α-synuclein occurs in caudo-rostral part of brain [70,78].

1.2.2.2 Cellular transport for N2B delivery

Drugs or nanocarriers following i.n. administration, first need to pass through the mucus layer by overcoming mucociliary clearance, and then only they would get absorbed from the nasal cavity. Two mechanisms are involved in transporting drugs and nanocarriers after passing through the mucus: paracellular (extracellular) and transcellular (intracellular).

1.2.2.2.1 Paracellular transport

Paracellular route for drug transport involves a quick mobilization of drugs between the nasal epithelial layers [73,75,79]. Nasal epithelium cells are inter-connected through various junctions like tight junctions, zonula adherens, and macular adherens [80]. Transport of drugs to the brain through olfactory pathway via perineural channels might involve a paracellular transport mechanism [81]. As most of the reported N2B drug delivery systems exhibit an immediate delivery of drugs, with high concentrations in the brain. This indicates that brain delivery of drug via i.n. route largely follows paracellular transport [82,83].

1.2.2.2.2 Transcellular transport

Upon i.n. administration, transcellular transport mechanism for brain drug delivery involves transfer of drug molecules through the cells either by endocytosis or carrier-mediated transport. Clathrin-dependent, caveolae dependant, caveolae/clathrin independent or receptor mediated endocytosis are involved in transcellular transport. Various receptors like nicotinic acetylcholine receptors and olfactory receptors are present in the olfactory region and trigeminal ganglions involving receptor-mediated endocytosis through transcellular mechanism [73]. Transport of drugs which follows transcellular mechanism sometimes takes few hours to an entire day for delivery of drug to the brain via olfactory pathway. Transcellular transport mechanism involves passive diffusion of drugs for uptake. Further, the drugs are taken up by carrier-mediated endocytosis for transportation to olfactory bulbs and eventually into brain [84,85]. The transport pathway and mechanism of direct N2B delivery of drugs are demonstrated in **Figure 1.1**.

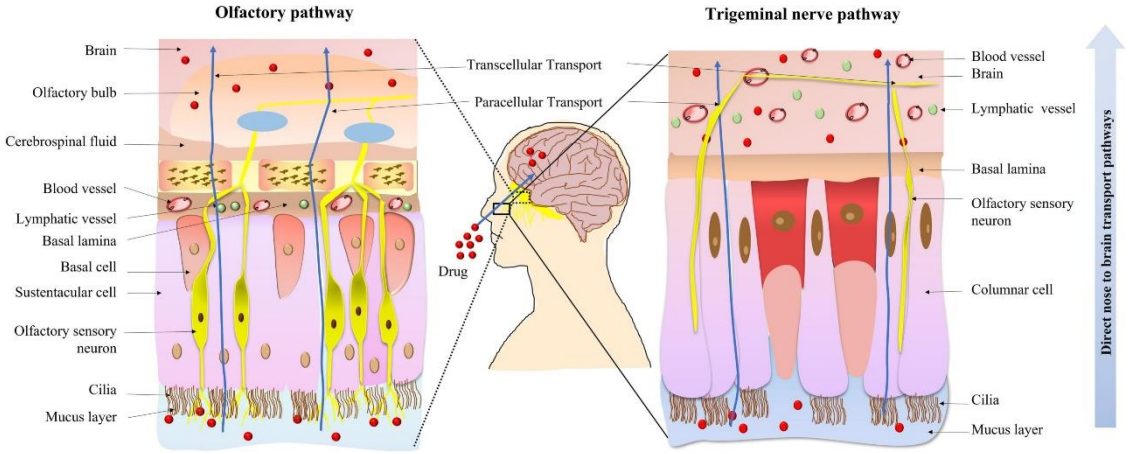

Figure 1.1 Transport pathway and mechanism of direct N2B delivery of drug

1.3 Formulation approaches to improve N2B delivery of drugs

Several formulation approaches are reported in the literature to enhance N2B delivery of drugs with low brain availability. Drug loaded *in situ* gel, different nanocarriers, and nanocarrier embedded *in situ* gel have been widely explored in last few years for enhancing the brain uptake

of drugs via N2B route. These formulation approaches are concisely stated in the following sections:

1.3.1 *In situ* gelling systems

In situ gel are a special type of hydrogels prepared with polymers that transform in the site of application from solution to gel (sol-gel) in response to physiological stimuli like temperature, pH, and ionic concentration. *In situ* gel ensure precise dosing inside the nasal cavity and reduce loss of drug [86]. *In situ* gel prolongs nasal retention duration, lowers mucociliary clearance, enhances drug absorption via nasal epithelium, and finally increases the availability of the drug to brain [87].

1.3.1.1 Thermoresponsive in situ gel

Thermoresponsive *in situ* gel are hydrogels that respond to a specific range of temperatures and convert from sol to gel. Polymers like poloxamer, xyloglucan, and cellulose-derivatives are mostly used as excipients for thermosensitive *in situ* gel. Uppuluri *et al.* prepared and evaluated piribedil loaded methyl cellulose based thermosensitive nasal *in situ* gel to improve its brain delivery for treatment of PD. The absolute brain bioavailability of piribedil increased from 4.71% to 35.92% from oral to i.n. administration of *in situ* gel [88]. Rao *et al.* developed and evaluated ropinirole loaded i.n. thermoresponsive *in situ* gel to treat PD. A combination of Pluronic F 127 and hydroxy methyl propyl cellulose was used as a thermoresponsive polymer for the *in situ* gel that increased brain bioavailability of i.n. ropinirole as compared to intravenous (i.v.) dose of the drug [89]. Ravi *et al.* developed thermoresponsive rasagiline loaded *in situ* gel to enhance brain delivery of drug and for the effective treatment of PD. *In situ* i.n. rasagiline gel substantially increased brain bioavailability of drug as compared to oral solution [90].

1.3.1.2 Ion-responsive in situ gel

Ion-responsive *in situ* gel are composed of polymers that show sol-gel transformation in the presence of ions in the site of administration. Gellan gum is an anionic polymer widely used for ion-responsive *in situ* gel preparation. This anionic polymer interacts with cations Ca^{++} sufficiently present in the nasal fluid and results in formation of *in situ* gel. As per best of our knowledge, no literature reports are available for i.n. ion-responsive *in situ* gel to treat PD till now. Literature reports very few ion-responsive *in situ* gel used to deliver CNS drugs via i.n. route for better brain targeting [91–93].

1.3.1.3 pH-responsive in situ gel

pH-responsive *in situ* gel system comprised of polymers that undergoes phase transition upon change in pH of the microenvironment of site of administration. Carbopol is one of the widely used pH-responsive polymers used for the sol-gel transformation. Due to the variation in nasal fluid pH, pH-responsive *in situ* gel systems are not widely explored. To best of our knowledge, no i.n. pH-responsive *in situ* gel system is investigated for PD till now. Very few CNS drugs are explored for better brain delivery using i.n. pH-responsive *in situ* gel and are reported in the literature [94].

1.3.2 Nanocarrier based N2B delivery

Several clinical and preclinical studies demonstrated that i.n. administration of different nanocarrier based drug delivery systems are advantageous for direct brain targeting of anti-Parkinson drugs as compared to conventional formulation using other routes. Nanocarriers, due to their physicochemical properties like size and shape, can also be directly taken up by the olfactory region of nasal cavity. Surface modified nanocarriers can help in achieving better targeting to brain and at the same time reduce drug distribution to the other organs. Surface modified nanocarriers finally result in lower systemic toxicity when administered intranasally.

1.3.2.1 Polymeric nanoparticles (NP)

Polymeric nanoparticles (NP) are one of the important nanocarrier systems investigated for direct N2B delivery of anti-Parkinson drugs. Polymeric NP are mostly composed of synthetic, semisynthetic, and natural biodegradable polymers wherein, drugs are encapsulated into a polymeric matrix [95,96]. These NP extend various advantages such as small particle size, high drug loading efficiency, prolonged circulation time, suffice distribution of drugs to the target site, better cellular uptakes, etc. [97].

1.3.2.1.1 Chitosan (CS) NP

The most suited natural polymer for design of polymeric drug nanocarrier system intended for i.n. administration is CS because of its biodegradable characteristic, higher stability, low toxicity, and mucoadhesive nature [98,99]. The mucoadhesive nature of this polymer leads to lower mucociliary clearance and extends a longer residence time of NP on the nasal mucosa [100,101]. Rukmangathen *et al.* prepared i.n. selegiline hydrochloride loaded CS NP intended for N2B delivery. PK studies demonstrated improvement in the drug's plasma $t_{1/2}$, C_{max}, and Ke compared to the marketed tablets of selegiline hydrochloride. Pharmacodynamics studies depicted that NP significantly reversed the catalepsy and akinesia activities in rats [102]. Sridhar *et al.* formulated NP using CS for N2B delivery of selegiline hydrochloride [103]. PK studies demonstrated increment in C_{max} of the drug in brain as compared to oral solution. The enhanced brain bioavailability was attributed to i.n. administration of NP which reduced first-pass metabolism of the drug. and Pharmacodynamics depicted that the intranasal CS NP caused increase in dopamine level as compared to oral solution. The i.n. CS NP also facilitated better therapeutic effect in locomotor activity, catalepsy and stride length tests [103]. Gulati *et al.* prepared sustained release selegiline hydrochloride-loaded CS NP intended for intranasal delivery. Study concluded that CS NP could be promising for treating PD as a targeted delivery system [104]. In another study, i.n. pramipexole dihydrochloride-loaded CS NP was prepared

for the effective brain delivery. This NP showed significantly high activity scores in the photoactometer and catalepsy test, and substantially increased dopamine level in brain compared to intranasal and oral pramipexole dihydrochloride solutions [105]. Jafarieh *et al.* prepared ropinirole hydrochloride-loaded CS NP for brain delivery of the drug. The *ex vivo* nasal permeation study depicted improvement of in flux ratio with ropinirole hydrochloride-CS NP compared to the drug solution. Biodistribution study showed significant improvement in the brain availability of drug from i.n. NP as compared to i.n. solution. Furthermore, gamma scintigraphic studies also supported the result and depicted high brain uptake of NP. Study demonstrated that mucoadhesive nature of CS resulted in longer retention of NP at site of action [106]. The i.n. rasagiline-loaded CS glutamate NP was prepared to achieve better brain uptake. The *ex vivo* nasal permeation study showed that NP improved rasagiline permeation. This was attributed to the interaction of CS with nasal cell membrane resulting in the opening of tight junctions. In the biodistribution study, they found that i.n. NP caused enhanced rasagiline brain concentration as compared to the same dose of i.n. solution. The enhanced brain concentration of drug from NP was because of its reduced mucociliary clearance compared to the pure solution [107]. Another i.n. bromocriptine-CS NP showed an increase C_{max} and $AUC_{0\rightarrow 48h}$ in Brain respectively, as compared to i.n. solution. The increased brain distribution of drug was assigned to the ability of NP to protect the drug from degrading in nasal environment [108]. The scintigraphy study of i.n. bromocriptine-CS NP demonstrated significantly high localization of the drug in brain as compared to the intravenously administered NP. The result indicated that bromocriptine NP reached to brain via direct N2B pathway by avoiding the BBB [109].

1.3.2.1.2 Poly lactic-co-glycolic acid (PLGA) NP

PLGA is another commonly used polymer for formulating NP because of its biocompatible, biodegradable, and long-circulating properties [110]. In a study, i.n. rasagiline encapsulated

PLGA NP surface coated with CS was found to improve the brain uptake of rasagiline. Study demonstrated that positive surface charge of NP due to surface coating resulted in increased *ex vivo* permeation of rasagiline from NP over drug solution. The i.n. NP compared to i.n. solution demonstrated increased C_{max} and $AUC_{0\rightarrow 24h}$. The improved result was attributed to initial burst release of the drug from NP than solution. Significantly improved drug targeting efficiency percentage (DTE (%)) and direct transport percentage (DTP (%)) of NP was attributed to the mucoadhesive property of the prepared NP [111]. Gambaryan *et al.* evaluated i.n. levodopa-loaded PLGA NP Which resulted prolonged circulation effect and better restoration of motor function as compared to i.n. pure levodopa solution [112]. Arisoy *et al.* reported an i.n. PLGA based N-(3- Dimethylaminopropyl)-N′-ethylcarbodiimide hydrochloride (EDAC) modified levodopa NP for direct brain targeting. The surface modified NP increased dopamine level as compared to oral and i.n. levodopa solution respectively. Study demonstrated that EDAC improved nasal absorption of NP and resulted better dopamine availability [113]. Chatzitaki *et al.* prepared a nasal ropinirole hydrochloride-PLGA NP surface coated with CS which improved nasal permeability of the drug. Increased permeability was attributed to the tight junction opening property of CS [114].

1.3.2.2 Nanoemulsions (NE)

NE are another interesting formulation approach for the N2B delivery of drugs, especially lipophilic ones [115]. Lipophilic NE with smaller globule size (<200 nm) are extensively used to enhance nasal permeability and to improve brain uptake of drugs via nasal mucosa [115,116]. Mustafa *et al.* reported an i.n. CS modified ropinirole-loaded NE for PD. The *ex vivo* study showed a significantly higher drug distribution in various parts of the rat brain. The study demonstrated that the presence of CS-modified NE caused destabilization of nasal mucosa which finally resulted easy contact of NE with the trigeminal and olfactory nerves and facilitated rapid extracellular uptake [117]. Kumar *et al.* prepared an i.n. selegiline-loaded NE

for direct brain delivery. *In vitro* nasal permeation study concluded that nasal permeation fluxes and permeation coefficient values of selegiline from NE were higher than drug suspensions. The higher permeation of NE was ascribed to the high solubilization of selegiline due to the low droplet size of NE. Furthermore, presence of tween 80 in NE blocked the P-gp efflux resulting in increased diffusion of drug from NE across the nasal mucosa as compared to suspensions. The i.n. NE significantly restored the level of dopamine towards its normal value compared to i.v. and i.n. drug solutions [118]. In another study, Kumar *et al.* developed an i.n. NE using grape seed oil and Sefsol 218® for selegiline hydrochloride with a particle size of 61.43 ± 4.10 nm. In PK and brain distribution studies, i.n. NE showed increased brain C_{max} compared to i.v. solution. The study revealed that due to the lower droplet size of NE as compared to the diameter of axons (<100 nm) present in filia olfactoria, helped in higher uptake of NE. Result demonstrated that due to the very low droplet size NE were taken up through intra-axonal pathway via endocytic process [119]. Nehal *et al.* developed CS surface coated ropinirole hydrochloride-loaded NE. The CS coated NE exhibited improved flux as compared to drug suspensions. The increased permeation was attributed to the fact that CS which interacts with negative charges of the sialic acid present in mucosa and open the tight junctions. The smaller globule size of NE was regarded as another important factor for increased permeation of drug from NE than that of the drug suspension. PK studies showed that i.n. NE resulted an increased brain C_{max} as compared to i.v. pure drug suspensions. Study demonstrated that direct transport of drug to brain via i.n. route by avoiding BBB, resulted in increased brain C_{max} [120].

1.3.2.3 Lipid-based NP

Lipid-based NP are preferred for direct N2B delivery of drugs because of their smaller particle size, biocompatible nature and ability to easily get transported via transcellular nasal pathway [121]. This NP are broadly classified in two generations *viz.*, solid lipid nanoparticles (SLN) and lipid nanocarriers (NLC).

1.3.2.3.1 Solid lipid nanoparticles (SLN)

SLN is the first generation of lipid-based NP, which is considered to be an attractive colloidal carrier system for delivery of drugs to brain [122]. SLN are lipid matrix which is solid at room temperature, mostly dispersed in aqueous or aqueous surfactant phase. They have the potential to carry both lipophilic and hydrophilic drugs with a wide variety of size range between 80 – 1000 nm [123]. SLN are used as carrier for N2B delivery because they allow control release of drug for a longer time and the excipients used are non-toxic to nasal mucosa. Pardeshi *et al.* developed i.n. ropinirole hydrochloride-loaded SLN intended for improved brain delivery. The optimized SLN showed around 69.88% permeation through sheep nasal mucosa and no evidence of injury like presence of epithelial necrosis or sloughing in nasal mucosa was observed in histopathological study. *In vivo* pharmacodynamics studies showed that even at a lower dose, i.n. SLN showed enhanced anti-tremor activity as compared to marketed oral formulation of the drug [124].

1.3.2.3.2 Nanostructured lipid carriers (NLC)

Second generation lipid-based NP are named as nanostructured lipid carriers (NLC) which are composed with binary mixture of both liquid and solid lipids [125]. Due to presence of both types of lipids in the structure, organization of NLC are usually imperfect and this phenomenon helps to overcome the problems of low drug loading, low entrapment efficiency, and burst release associated with the first generation lipid based NP, the SLN system [126,127]. NLC demonstrate better brain uptake because of their high biocompatibility and bioacceptability nature. NLC could also be easily delivered via i.n. route due to their low toxicity attributes [125]. Mishra *et al.* formulated i.n. selegiline hydrochloride loaded NLC for direct brain delivery of the drug. The i.n. NLC demonstrated increase in brain selegiline hydrochloride concentration as compared to the pure drug solution. In pharmacodynamics study, the i.n. NLC formulation resulted improved grip strength and restored locomotor activities compared to

plain drug [128]. Pardeshi and Belgamwar explored the impact of i.n. N,N,N-trimethyl CS surface modified ropinirole encapsulated NLC when delivered via N2B route. Surface modified NLC showed high nasal permeation flux compared to ropinirole-NLC. The study revealed that the absorption enhancing property of N,N,N-trimethyl CS helped in opening the tight junction of nasal mucosa resulting better permeation. The i.n. surface modified NLC caused increase in brain C_{max} as compared to i.n. ropinirole solution. The study concluded that the small size and hydrophobic nature of the surface modified NLC resulted in enhancement of brain availability of drug [129].

1.3.2.4 Nanocarrier embedded in situ gel systems

In recent years, i.n. nanocarriers embedded into *in situ* gel systems are investigated to overcome the disadvantage of mucociliary clearance and to increase the nasal residence time. Sharma *et al.* prepared levodopa loaded CS NP embedded in thermosensitive *in situ* gel for efficient delivery of levodopa. *In vivo* study depicted that brain recovery of levodopa was highest from NP and low from the gel incorporated NP. The study concluded that the NP embedded gel might not have allowed enough release of drug at the site of action which eventually resulted in lower brain recovery of levodopa as compared to NP. NP showed higher recovery than that of drug solution which was attributed to the fact that NP uptake improved through paracellular route by inhibiting P-gp efflux [130]. Gabal *et al.* prepared ropinirole-loaded both anionic and cationic NLC embedded in thermoresponsive *in situ* gel. Cationic NLC-embedded gel exhibited higher mucoadhesive strength than anionic gel might be because cationic gel had higher binding affinity towards the negative charge of mucin cells present in nasal mucosa. PK study for i.n. solution, NLC, and gel formulation showed increased DTE (%) in case of anionic NLC as compared to cationic one which might be result of direct transport of drug to brain via olfactory pathway [131]. Uppuluri *et al.* developed i.n. piribedil-loaded SLN and lecithin-CS hybrid NP embedded into thermoresponsive *in situ* gel for better brain bioavailability of the

drug for treatment of PD. The i.n. SLN and NP embedded *in situ* gel enhanced improved brain bioavailability as compared to i.n. drug suspensions [132,133].

1.4 Problem definition and objectives of the research

PD is one of the world's fastest spreading neurodegenerative disorders that poses a substantial financial burden on patients and the overall global economy. Studies have demonstrated that PD patients also suffer mentally and socially to a high extent [10,11]. Thus, it is crucial to efficiently manage PD to reduce the social and economic burden. Most of the clinically approved anti-Parkinson drugs are associated with limitations *viz.*, high therapeutic doses, frequent administration, high first-pass metabolism or enzymatic degradation, organ toxicity, poor brain availability due to presence of BBB, etc. There is an unmet need for an alternative route for delivering the currently available anti-Parkinson drugs directly to the brain to avoid drawbacks associated with the conventional routes. The i.n. route overcomes several problems *viz.*, bypass BBB, avoid hepatic first-pass metabolism, negate gastrointestinal enzymatic degradation, reduce systemic toxicity, etc. [52,134,135]. Additionally, i.n. delivery also possesses advantages such as rapid onset of action, rapid absorption [66], enhanced therapeutic effects without systemic exposure, reduced peripheral organ toxicity, etc. Absolute absence of any pain and ease in self-administration make i.n. delivery approach is patient-friendly.

However, poor permeation of hydrophilic drugs, enzymatic degradation in the nasal cavity, mucociliary clearance, shorter residence time, and improper formulation installation are the major limitations of i.n. delivery [66]. These prime problems could effectively be addressed by using suitable nanocarrier based i.n. formulations. Nanocarrier based systems intended for brain delivery via i.n. route allows easy crossing of the therapeutic molecules through the nasal mucosal membrane [136].

Rotigotine (RTG) is one of the newest and promising anti-Parkinson drugs approved by regulatory authorities, the USFDA and Europe Medical Agency, and has a better affinity toward dopamine receptors than other dopamine agonists [137]. It shows efficiency in managing the motor symptoms of PD. It also improves major non-motor PD symptoms such as sleep disturbances, apathy, and anhedonia [138,139]. It is a BCS class 2 molecule used for treating PD in early and advanced stage patients as monotherapy or in combination. Currently approved formulation of RTG is a transdermal patch since the drug shows poor oral bioavailability (<1%) because of its extensive first-pass metabolism [140]. Although successfully marketed, RTG potential has not been fully utilized owing to the challenges and drawbacks associated with its delivery. For instance, the absolute bioavailability from the transdermal patch is reported to be only 37% [140]. The absolute bioavailability of transdermal patches varies depending on its site of application [140]. Moreover, RTG forms crystals in the transdermal patch upon storage and shows variations in drug release and bioavailability as well [141]. Furthermore, systemic absorption of the drug is compromised due to its slower transport from patch to the dermal surface after application. After absorption into the systemic circulation, lower amount of drug reaches to brain due to the hindrance of BBB. To avoid these problems, high dose of RTG are prescribed even in early stage of PD. Higher and frequent dosing of transdermal patch leads to both peripheral and systemic adverse effects.

Considering the drawbacks of the currently available RTG transdermal patch, it is necessary to develop suitable formulations of RTG that can be administered via an alternative route, avoiding BBB and first-pass metabolism as well, leading to effective increase in the drug's brain availability.

Recent studies showed that i.n. nanocarriers have been explored to deliver RTG directly to the brain. Bi *et al.* prepared lactoferrin (Lf) modified RTG-loaded PEG-PLGA NP intended for direct N2B delivery [142]. Bhattamisra *et al.* prepared an i.n. CS NP for RTG for brain delivery

[143]. Wang *et al.* evaluated i.n. RTG-loaded polymeric micelles embedded in thermoresponsive *in situ* gel [144]. *Prajapati and Patel* reported preparation of RTG loaded SLN and Choudhury *et al.* prepared a mucoadhesive CS coated RTG-loaded NE [145,146]. However, the brain availability of RTG from SLN and NE was not evaluated. The i.n. nanocarriers of RTG appear to be an appropriate alternative to overcome limitations of the drug and to fill the existing gap. Delivery of RTG via i.n. route can reduce the dose, decrease systemic exposure, and dose-dependent side effects by enhancing the drug's brain availability. Nanosuspensions, liposomes, and CS-lecithin NP have been reported to enhance the brain availability of hydrophobic drugs via N2B pathway [132,147–150]. This research work aimed to enhance the brain bioavailability of RTG by administering it through i.n. route.

Therefore, objectives of the current research work were envisioned as follows:

Objective I: Development and optimization of suitable nanocarriers of RTG for i.n. administration

i. Development and optimization of RTG-Nanosuspension for N2B delivery
ii. Development and optimization of RTG-Proposomes for N2B delivery
iii. Development and optimization of RTG-loaded LCNP for N2B delivery

Objective II: *In vitro* characterization of the RTG-loaded i.n. nanocarriers

Objective III: *Ex vivo* assessment of the RTG-loaded i.n. nanocarriers

Objective IV: *In vivo* brain and plasma PK studies of the RTG-loaded i.n. nanocarriers in Wistar rats

In this current research, we have developed and evaluated RTG-Nanosuspension using Poloxamer 407 as a stabilizer to increase the solubility of RTG. Solubility enhancement of RTG helped in drug availability in nasal fluid and finally increased its brain availability. We

have also prepared RTG-Proposomes using soya phosphatidylcholine and propylene glycol for improved brain availability of RTG. Finally, RTG Lecithin-CS nanoparticles (RTG-LCNP) is prepared to increase retention time of drug in nasal cavity and enhance its brain availability in a controlled manner. All nanocarriers are characterized using differential scanning calorimetry, fourier-transform infrared spectroscopy, powder x-ray diffraction, field emission scanning electron microscopy, and transmission electron microscopy. *Ex vivo* nasal permeation study is performed to evaluate the nasal permeability of RTG from optimized nanocarriers. Finally, *in vivo* brain and plasma PK studies are performed to assess the direct N2B delivery of RTG from optimized nanocarriers. To evaluate the brain targeting efficiency of optimized nanocarriers DTE (%) and DTP (%) are calculated for all the developed nanocarriers.

References

1. Przedborski, W.D.S. Parkinson's Disease: Mechanisms and Models. *Neuron* **2003**, *39*, 889–909, doi:10.1017/CCOL9780521851282.008.

2. Raza, C.; Anjum, R.; Shakeel, N. ul A. Parkinson's Disease: Mechanisms, Translational Models and Management Strategies. *Life Sciences* **2019**, *226*, 77–90, doi:10.1016/j.lfs.2019.03.057.

3. Rodríguez-Nogales, C.; Garbayo, E.; Carmona-Abellán, M.M.; Luquin, M.R.; Blanco-Prieto, M.J. Brain Aging and Parkinson's Disease: New Therapeutic Approaches Using Drug Delivery Systems. *Maturitas* **2016**, *84*, 25–31, doi:10.1016/j.maturitas.2015.11.009.

4. Paul, A.; Yadav, K.S. Parkinson's Disease: Current Drug Therapy and Unraveling the Prospects of Nanoparticles. *Journal of Drug Delivery Science and Technology* **2020**, *58*, 101790, doi:10.1016/j.jddst.2020.101790.

5. Cohen, A.J.; Brauer, M.; Burnett, R.; Anderson, H.R.; Frostad, J.; Estep, K.; Balakrishnan, K.; Brunekreef, B.; Dandona, L.; Dandona, R.; et al. Estimates and 25-Year Trends of the Global Burden of Disease Attributable to Ambient Air Pollution: An Analysis of Data from the Global Burden of Diseases Study 2015. *The Lancet* **2017**, *389*, 1907–1918, doi:10.1016/S0140-6736(17)30505-6.

6. Yang, W.; Hamilton, J.L.; Kopil, C.; Beck, J.C.; Tanner, C.M.; Albin, R.L.; Ray Dorsey, E.; Dahodwala, N.; Cintina, I.; Hogan, P.; et al. Current and Projected Future Economic Burden of Parkinson's Disease in the U.S. *NPJ Parkinson's Disease* **2020**, *6*, eCollection 2020, doi:10.1038/s41531-020-0117-1.

7. Feigin, V.L.; Krishnamurthi, R. V.; Theadom, A.M.; Abajobir, A.A.; Mishra, S.R.; Ahmed, M.B.; Abate, K.H.; Mengistie, M.A.; Wakayo, T.; Abd-Allah, F.; et al. Global,

Regional, and National Burden of Neurological Disorders during 1990–2015: A Systematic Analysis for the Global Burden of Disease Study 2015. *The Lancet Neurology* **2017**, *16*, 877–897, doi:10.1016/S1474-4422(17)30299-5.

8. Ray Dorsey, E.; Elbaz, A.; Nichols, E.; Abd-Allah, F.; Abdelalim, A.; Adsuar, J.C.; Ansha, M.G.; Brayne, C.; Choi, J.Y.J.; Collado-Mateo, D.; et al. Global, Regional, and National Burden of Parkinson's Disease, 1990–2016: A Systematic Analysis for the Global Burden of Disease Study 2016. *The Lancet Neurology* **2018**, *17*, 939–953, doi:10.1016/S1474-4422(18)30295-3.

9. Opara, J.A.; Brola, W.; Leonardi, M.; Błaszczyk, B. Quality of Life in Parkinson's Disease. *Journal of medicine and life* **2012**, *5*, 375–381, doi:10.5005/jp/books/10538_43.

10. Stocchi, F.; Martínez-Martin, P.; Reichmann, H. Quality of Life in Parkinson's Disease - Patient, Clinical and Research Perspectives. *European Neurological Review* **2014**, *9*, 12–18, doi:10.17925/enr.2014.09.01.12.

11. Gage, H.; Hendricks, A.; Zhang, S.; Kazis, L. The Relative Health Related Quality of Life of Veterans with Parkinson's Disease. *Journal of Neurology Neurosurgery and Psychiatry* **2003**, *74*, 163–169, doi:10.1136/jnnp.74.2.163.

12. Schaffernicht, G.; Shang, Q.; Stievenard, A.; Bötzel, K.; Dening, Y.; Kempe, R.; Toussaint, M.; Gündel, D.; Kranz, M.; Reichmann, H.; et al. Physiological and Pathological Changes in the Enteric Nervous System of Rotenone-Exposed Mice as Early Biomarkers for Parkinson's Disease. *bioRxiv* **2020**, doi:10.1101/2020.12.11.421164.

13. Comi, C.; Magistrelli, L.; Oggioni, G.D.; Carecchio, M.; Fleetwood, T.; Cantello, R.;

Mancini, F.; Antonini, A. Peripheral Nervous System Involvement in Parkinson's Disease: Evidence and Controversies. *Parkinsonism and Related Disorders* **2014**, *20*, 1329–1334, doi:10.1016/J.PARKRELDIS.2014.10.010.

14. Calabresi, P.; Picconi, B.; Tozzi, A.; … V.G.-N.; 2014, undefined Direct and Indirect Pathways of Basal Ganglia: A Critical Reappraisal. *nature.com* **2014**, doi:10.1038/nn.3743.

15. Bernheimer, H.; Birkmayer, W.; Hornykiewicz, O.; Jellinger, K.; Seitelberger, F. Brain Dopamine and the Syndromes of Parkinson and Huntington Clinical, Morphological and Neurochemical Correlations. *Journal of the Neurological Sciences* **1973**, *20*, 415–455, doi:10.1016/0022-510X(73)90175-5.

16. Aubert, I.; Guigoni, C.; Håkansson, K.; Li, Q.; Dovero, S.; Barthe, N.; Bioulac, B.H.; Gross, C.E.; Fisone, G.; Bloch, B.; et al. Increased D1 Dopamine Receptor Signaling in Levodopa-Induced Dyskinesia. *Annals of Neurology* **2005**, *57*, 17–26, doi:10.1002/ana.20296.

17. Zaja-Milatovic, S.; Milatovic, D.; Schantz, A.M.; Zhang, J.; Montine, K.S.; Samii, A.; Deutch, A.Y.; Montine, T.J. Dendritic Degeneration in Neostriatal Medium Spiny Neurons in Parkinson Disease. *Neurology* **2005**, *64*, 545–547, doi:10.1212/01.WNL.0000150591.33787.A4.

18. Magrinelli, F.; Picelli, A.; Tocco, P.; Federico, A.; Roncari, L.; Smania, N.; Zanette, G.; Tamburin, S. Pathophysiology of Motor Dysfunction in Parkinson's Disease as the Rationale for Drug Treatment and Rehabilitation. *Parkinson's Disease* **2016**, *2016*, doi:10.1155/2016/9832839.

19. Wakabayashi, K.; Tanji, K.; Mori, F.; Akahashi, H. The Lewy Body in Parkinson's Disease: Molecules Implicated in the Formation and Degradation of α-Synuclein

Aggregates. *Neuropathology* **2007**, *27*, 494–506, doi:10.1111/j.1440-1789.2007.00803.x.

20. Soper, J.H.; Trojanowski, J.Q.; Lee, V.M.Y. α-Synuclein and Parkinson's Disease. *Parkinson's Disease: Genetics and Pathogenesis* **2007**, 167–186, doi:10.1096/fj.03-0338rev.

21. Kannarkat, G.T.; Boss, J.M.; Tansey, M.G. The Role of Innate and Adaptive Immunity in Parkinson's Disease. *Journal of Parkinson's Disease* 2013, *3*, 493–514.

22. Croisier, E.; Moran, L.B.; Dexter, D.T.; Pearce, R.K.B.; Graeber, M.B. Microglial Inflammation in the Parkinsonian Substantia Nigra: Relationship to Alpha-Synuclein Deposition. *Journal of Neuroinflammation* **2005**, *2*, doi:10.1186/1742-2094-2-14.

23. Kenborg, L.; Rugbjerg, K.; Lee, P.C.; Ravnskjær, L.; Christensen, J.; Ritz, B.; Lassen, C.F. Head Injury and Risk for Parkinson Disease: Results from a Danish Case-Control Study. *Neurology* **2015**, *84*, 1098–1103, doi:10.1212/WNL.0000000000001362.

24. Goldman, S.M. Environmental Toxins and Parkinson's Disease. *Annual Review of Pharmacology and Toxicology* **2014**, *54*, 141–164, doi:10.1146/annurev-pharmtox-011613-135937.

25. Crane, P.K.; Gibbons, L.E.; Dams-O'Connor, K.; Trittschuh, E.; Leverenz, J.B.; Dirk Keene, C.; Sonnen, J.; Montine, T.J.; Bennett, D.A.; Leurgans, S.; et al. Association of Traumatic Brain Injury With Late-Life Neurodegenerative Conditions and Neuropathologic Findings. *JAMA Neurology* **2016**, *73*, 1062–1069, doi:10.1001/JAMANEUROL.2016.1948.

26. Wakabayashi, K.; Takahashi, H.; Ohama, E.; Ikuta, F. Parkinson's Disease: An Immunohistochemical Study of Lewy Body-Containing Neurons in the Enteric Nervous

System. *Acta Neuropathologica* **1990**, *79*, 581–583, doi:10.1007/BF00294234.

27. Gibb, W.R.G.; Lees, A.J. Anatomy, Pigmentation, Ventral and Dorsal Subpopulations of the Substantia Nigra, and Differential Cell Death in Parkinson's Disease. *Journal of Neurology Neurosurgery and Psychiatry* **1991**, *54*, 388–396, doi:10.1136/jnnp.54.5.388.

28. Goedert, M. The Significance of Tau and α-Synuclein Inclusions in Neurodegenerative Diseases. *Current Opinion in Genetics and Development* **2001**, *11*, 343–351, doi:10.1016/S0959-437X(00)00200-8.

29. Saha, A.R.; Hill, J.; Utton, M.A.; Asuni, A.A.; Ackerley, S.; Grierson, A.J.; Miller, C.C.; Davies, A.M.; Buchman, V.L.; Anderton, B.H.; et al. Parkinson's Disease α-Synuclein Mutations Exhibit Defective Axonal Transport in Cultured Neurons. *Journal of Cell Science* **2004**, *117*, 1017–1024, doi:10.1242/jcs.00967.

30. Hopkins, D.A.; Bieger, D.; De Vente, J.; Steinbusch, H.W.M. *Vagal Efferent Projections: Viscerotopy, Neurochemistry and Effects of Vagotomy*; 1996; Vol. 107;.

31. Del Tredici, K. Where Does P.D Pathology Begin in the Brain. *Journal of neuropathy and experimental neurology*, **2002**, *61*, 413–426, doi:10.1093/jnen/61.5.413.

32. Braak, H.; Bohl, J.R.; Müller, C.M.; Rüb, U.; de Vos, R.A.I.; Del Tredici, K. Stanley Fahn Lecture 2005: The Staging Procedure for the Inclusion Body Pathology Associated with Sporadic Parkinson's Disease Reconsidered. *Movement Disorders* **2006**, *21*, 2042–2051, doi:10.1002/mds.21065.

33. Braak, H.; Braak, E.; Yilmazer, D.; de Vos, R.A.I.; Jansen, E.N.H.; Bohl, J.; Jellinger, K. Amygdala Pathology in Parkinson's Disease. *Acta Neuropathologica* **1994**, *88*, 493–500, doi:10.1007/BF00296485.

34. Braak, H.; Del Tredici, K.; Rüb, U.; De Vos, R.A.I.; Jansen Steur, E.N.H.; Braak, E. Staging of Brain Pathology Related to Sporadic Parkinson's Disease. *Neurobiology of Aging* **2003**, *24*, 197–211, doi:10.1016/S0197-4580(02)00065-9.

35. Braak, H.; Ghebremedhin, E.; Rüb, U.; Bratzke, H.; Del Tredici, K. Stages in the Development of Parkinson's Disease-Related Pathology. *Cell and Tissue Research* **2004**, *318*, 121–134, doi:10.1007/s00441-004-0956-9.

36. Mizuno, Y. Definition and Classification of Parkinsonian Drugs. *NeuroPsychopharmacotherapy* **2020**, 1–30, doi:10.1007/978-3-319-56015-1_213-1.

37. Reich, S.G.; Savitt, J.M. Parkinson's Disease. *The Medical clinics of North America* **2019**, *103*, 337–350, doi:10.1016/J.MCNA.2018.10.014.

38. Muzerengi, S.; Clarke, C.E. Initial Drug Treatment in Parkinson's Disease. *BMJ* **2015**, *351*, h4669, doi:10.1136/bmj.h4669.

39. Chen, J.F.; Cunha, R.A. The Belated US FDA Approval of the Adenosine A2A Receptor Antagonist Istradefylline for Treatment of Parkinson's Disease. *Purinergic Signalling* **2020**, *16*, 167–174, doi:10.1007/S11302-020-09694-2/FIGURES/1.

40. Herd, C.P.; Tomlinson, C.L.; Deane, K.H.; Brady, M.C.; Smith, C.H.; Sackley, C.M.; Clarke, C.E. Speech and Language Therapy versus Placebo or No Intervention for Speech Problems in Parkinson's Disease. *The Cochrane database of systematic reviews* **2012**, *8*, CD002812, doi:10.1002/14651858.CD002812.PUB2.

41. Tomlinson, C.L.; Patel, S.; Meek, C.; Herd, C.P.; Clarke, C.E.; Stowe, R.; Shah, L.; Sackley, C.M.; Deane, K.H.O.; Wheatley, K.; et al. Physiotherapy versus Placebo or No Intervention in Parkinson's Disease. *The Cochrane database of systematic reviews* **2013**, *9*, CD002817, doi:10.1002/14651858.CD002817.PUB4.

42. Klamroth, S.; Steib, S.; Devan, S.; Pfeifer, K. Effects of Exercise Therapy on Postural Instability in Parkinson Disease: A Meta-Analysis. *Journal of neurologic physical therapy : JNPT* **2016**, *40*, 3–14, doi:10.1097/NPT.0000000000000117.

43. Dong, X. Current Strategies for Brain Drug Delivery. *Theranostics* **2018**, *8*, 1481–1493, doi:10.7150/thno.21254.

44. Bellettato, C.M.; Scarpa, M. Possible Strategies to Cross the Blood–Brain Barrier. *Italian Journal of Pediatrics* **2018**, *44*, 131, doi:Dong, X. (2018). Current Strategies for Brain Drug Delivery. Theranostics, 8(6), 1481-1493. https://doi.org/10.7150/thno.21254.

45. Abbott, N.J. Blood-Brain Barrier Structure and Function and the Challenges for CNS Drug Delivery. *Journal of inherited metabolic disease* **2013**, *36*, 437–449, doi:10.1007/s10545-013-9608-0.

46. Gao, X.; Qian, J.; Zheng, S.; Changyi, Y.; Zhang, J.; Ju, S.; Zhu, J.; Li, C. Overcoming the Blood–Brain Barrier for Delivering Drugs into the Brain by Using Adenosine Receptor Nanoagonist. *ACS Nano* **2014**, *8*, 3678–3689, doi:10.1021/nn5003375.

47. Huo, H.; Gao, Y.; Wang, Y.; Zhang, J.; Wang, Z. you; Jiang, T.; Wang, S. Polyion Complex Micelles Composed of Pegylated Polyasparthydrazide Derivatives for SiRNA Delivery to the Brain. *Journal of Colloid and Interface Science* **2015**, *447*, 8–15, doi:10.1016/j.jcis.2015.01.043.

48. Zhan, C.; Li, B.; Hu, L.; Wei, X.; Feng, L.; Fu, W.; Lu, W. Micelle-Based Brain-Targeted Drug Delivery Enabled by a Nicotine Acetylcholine Receptor.Pdf. *Angew Chem Int Ed Engl* **2011**, *50*, 5482–5485, doi:10.1002/anie.201100875.

49. Xie, B.S.; Wang, X.; Pan, Y.H.; Jiang, G.; Feng, J.F.; Lin, Y. Apolipoprotein E, Low-

Density Lipoprotein Receptor, and Immune Cells Control Blood-Brain Barrier Penetration by AAV-PHP.EB in Mice. *Theranostics* **2021**, *11*, 1177–1191, doi:10.7150/thno.46992.

50. Khan, H.; Pan, J.J.; Li, Y.; Zhang, Z.; Yang, G.Y. Native and Bioengineered Exosomes for Ischemic Stroke Therapy. *Frontiers in Cell and Developmental Biology* **2021**, *9*, 450, doi:10.3389/FCELL.2021.619565/BIBTEX.

51. Xu, J.; Wang, X.; Yin, H.; Cao, X.; Hu, Q.; Lv, W.; Xu, Q.; Gu, Z.; Xin, H. Sequentially Site-Specific Delivery of Thrombolytics and Neuroprotectant for Enhanced Treatment of Ischemic Stroke. *ACS Nano* **2019**, *13*, 8577–8588, doi:10.1021/acsnano.9b01798.

52. Groothuis, D.R.; Benalcazar, H.; Allen, C. V.; Wise, R.M.; Dills, C.; Dobrescu, C.; Rothholtz, V.; Levy, R.M. Comparison of Cytosine Arabinoside Delivery to Rat Brain by Intravenous, Intrathecal, Intraventricular and Intraparenchymal Routes of Administration. *Brain Research* **2000**, *856*, 281–290, doi:10.1016/S0006-8993(99)02089-2.

53. Nordling-David, M.M.; Yaffe, R.; Guez, D.; Meirow, H.; Last, D.; Grad, E.; Salomon, S.; Sharabi, S.; Levi-Kalisman, Y.; Golomb, G.; et al. Liposomal Temozolomide Drug Delivery Using Convection Enhanced Delivery. *Journal of Controlled Release* **2017**, *261*, 138–146, doi:10.1016/j.jconrel.2017.06.028.

54. Saucier-Sawyer, J.K.; Seo, Y.E.; Gaudin, A.; Quijano, E.; Song, E.; Sawyer, A.J.; Deng, Y.; Huttner, A.; Saltzman, W.M. Distribution of Polymer Nanoparticles by Convection-Enhanced Delivery to Brain Tumors. *Journal of Controlled Release* **2016**, *232*, 103–112, doi:10.1016/j.jconrel.2016.04.006.

55. Staples, M. Microchips and Controlled-Release Drug Reservoirs. *Wiley*

Interdisciplinary Reviews: Nanomedicine and Nanobiotechnology **2010**, *2*, 400–417, doi:10.1002/wnan.93.

56. Callaghan, R.; Luk, F.; Bebawy, M. Inhibition of the Multidrug Resistance P-Glycoprotein: Time for a Change of Strategy? *Drug Metabolism and Disposition* **2014**, *42*, 623–631, doi:10.1124/dmd.113.056176.

57. Patel, N.R.; Rathi, A.; Mongayt, D.; Torchilin, V.P. Reversal of Multidrug Resistance by Co-Delivery of Tariquidar (XR9576) and Paclitaxel Using Long-Circulating Liposomes. *International Journal of Pharmaceutics* **2011**, *416*, 296–299, doi:10.1016/j.ijpharm.2011.05.082.

58. Singh, R.K.; Prasad, D.N.; Bhardwaj, T.R. Design, Synthesis, Chemical and Biological Evaluation of Brain Targeted Alkylating Agent Using Reversible Redox Prodrug Approach. *Arabian Journal of Chemistry* **2017**, *10*, 420–429, doi:10.1016/j.arabjc.2013.12.008.

59. Martins, S.; Tho, I.; Reimold, I.; Fricker, G.; Souto, E.; Ferreira, D.; Brandl, M. Brain Delivery of Camptothecin by Means of Solid Lipid Nanoparticles: Formulation Design, in Vitro and in Vivo Studies. *International Journal of Pharmaceutics* **2012**, *439*, 49–62, doi:10.1016/j.ijpharm.2012.09.054.

60. Gaillard, P.J.; Appeldoorn, C.C.M.; Dorland, R.; Van Kregten, J.; Manca, F.; Vugts, D.J.; Windhorst, B.; Van Dongen, G.A.M.S.; De Vries, H.E.; Maussang, D.; et al. Pharmacokinetics, Brain Delivery, and Efficacy in Brain Tumor-Bearing Mice of Glutathione Pegylated Liposomal Doxorubicin (2B3-101). *PLoS ONE* **2014**, *9*, e82331, doi:10.1371/journal.pone.0082331.

61. Bruun, J.; Larsen, T.B.; Jølck, R.I.; Eliasen, R.; Holm, R.; Gjetting, T.; Andresen, T.L. Investigation of Enzyme-Sensitive Lipid Nanoparticles for Delivery of SiRNA to

Blood–Brain Barrier and Glioma Cells. *International Journal of Nanomedicine* **2015**, *10*, 5995–6008, doi:10.2147/IJN.S87334.

62. Baek, S.K.; Makkouk, A.R.; Krasieva, T.; Sun, C.H.; Madsen, S.J.; Hirschberg, H. Photothermal Treatment of Glioma; An in Vitro Study of Macrophage-Mediated Delivery of Gold Nanoshells. *Journal of Neuro-Oncology* **2011**, *104*, 439–448, doi:10.1007/s11060-010-0511-3.

63. Fatouh, A.M.; Elshafeey, A.H.; Abdelbary, A. Agomelatine-Based in Situ Gels for Brain Targeting via the Nasal Route: Statistical Optimization, in Vitro, and in Vivo Evaluation. *Drug Delivery* **2017**, *24*, 1077–1085, doi:10.1080/10717544.2017.1357148.

64. Abbas, H.; Refai, H.; El Sayed, N. Superparamagnetic Iron Oxide–Loaded Lipid Nanocarriers Incorporated in Thermosensitive in Situ Gel for Magnetic Brain Targeting of Clonazepam. *Journal of Pharmaceutical Sciences* **2018**, *107*, 2119–2127, doi:10.1016/j.xphs.2018.04.007.

65. Ravi, P.R.; Aditya, N.; Patil, S.; Cherian, L. Nasal In-Situ Gels for Delivery of Rasagiline Mesylate: Improvement in Bioavailability and Brain Localization. *Drug Delivery* **2015**, *22*, 903–910, doi:10.3109/10717544.2013.860501.

66. Erdő, F.; Bors, L.A.; Farkas, D.; Bajza, Á.; Gizurarson, S. Evaluation of Intranasal Delivery Route of Drug Administration for Brain Targeting. *Brain Research Bulletin* **2018**, *143*, 155–170, doi:10.1016/j.brainresbull.2018.10.009.

67. Ramvikas, M.; Arumugam, M.; Chakrabarti, S.R.; Jaganathan, K.S. Chapter Fifteen - Nasal Vaccine Delivery. In *Micro- and Nanotechnology in Vaccine Development*; William Andrew Publishing, 2017; pp. 279–301 ISBN 9780323400299.

68. Djupesland, P.G.; Mahmoud, R.A.; Messina, J.C. Accessing the Brain: The Nose May

Know the Way. *Journal of Cerebral Blood Flow & Metabolism* **2013**, *33*, 793–794, doi:10.1038/JCBFM.2013.41.

69. Djupesland, P.G.; Messina, J.C.; Mahmoud, R.A. The Nasal Approach to Delivering Treatment for Brain Diseases: An Anatomic, Physiologic, and Delivery Technology Overview. *Ther. Deliv* **2014**, *5*, 709–733, doi:10.4155/tde.14.41.

70. Charlton, S.; Jones, N.S.; Davis, S.S.; Illum, L. Distribution and Clearance of Bioadhesive Formulations from the Olfactory Region in Man: Effect of Polymer Type and Nasal Delivery Device. *European Journal of Pharmaceutical Sciences* **2007**, *30*, 295–302, doi:10.1016/j.ejps.2006.11.018.

71. Selvaraj, K.; Gowthamarajan, K.; Karri, V.V.S.R. Nose to Brain Transport Pathways an Overview: Potential of Nanostructured Lipid Carriers in Nose to Brain Targeting. *Artificial Cells, Nanomedicine and Biotechnology* **2018**, *46*, 2088–2095, doi:10.1080/21691401.2017.1420073.

72. Dhuria, S. V.; Hanson, L.R.; Frey, W.H. Novel Vasoconstrictor Formulation to Enhance Intranasal Targeting of Neuropeptide Therapeutics to the Central Nervous System. *Journal of Pharmacology and Experimental Therapeutics* **2009**, *328*, 312–320, doi:10.1124/jpet.108.145565.

73. Khan, A.R.; Liu, M.; Khan, M.W.; Zhai, G. Progress in Brain Targeting Drug Delivery System by Nasal Route. *Journal of Controlled Release* **2017**, *268*, 364–389, doi:10.1016/j.jconrel.2017.09.001.

74. Kyrkanides, S.; Yang, M.; Tallents, R.H.; Miller, J. nie H.; Brouxhon, S.M.; Olschowka, J.A. The Trigeminal Retrograde Transfer Pathway in the Treatment of Neurodegeneration. *Journal of Neuroimmunology* **2009**, *209*, 139–142, doi:10.1016/j.jneuroim.2009.02.006.

75. V.Dhuria, S.; R.Hanson, L.; H.Frey, W.I. Intranasal Delivery to the Central Nervous System: Mechanisms and Experimental Considerations. *Journal of pharmaceutical sciences* **2010**, *99*, 1654–1673, doi:10.1002/jps.21924.

76. Thorne, R.G.; Pronk, G.J.; Padmanabhan, V.; Frey, W.H. Delivery of Insulin-like Growth Factor-I to the Rat Brain and Spinal Cord along Olfactory and Trigeminal Pathways Following Intranasal Administration. *Neuroscience* **2004**, *127*, 481–496, doi:10.1016/j.neuroscience.2004.05.029.

77. Liu, X.F.; Fawcett, J.R.; Hanson, L.R.; Frey, W.H. The Window of Opportunity for Treatment of Focal Cerebral Ischemic Damage with Noninvasive Intranasal Insulin-like Growth Factor-I in Rats. *Journal of Stroke and Cerebrovascular Diseases* **2004**, *13*, 16–23, doi:10.1016/j.jstrokecerebrovasdis.2004.01.005.

78. Ulusoy, A.; Rusconi, R.; Pe´rez-Revuelta, B.I.; Musgrove, R.E.; Helwig, M.; Winzen-Reichert, B.; Monte, D.A. Di Caudo-rostral Brain Spreading of A-synuclein through Vagal Connections. *EMBO Molecular Medicine* **2013**, *5*, 1051–1059, doi:10.1002/emmm.201302475.

79. Altner, H.; Altner-Kolnberger, I. Freeze-Fracture and Tracer Experiments on the Permeability of the Zonulae Occludentes in the Olfactory Mucosa of Vertebrates. *Cell and Tissue Research* **1974**, *154*, 51–59, doi:10.1007/BF00221071.

80. Van Itallie, C.M.; Anderson, J.M. Claudins and Epithelial Paracellular Transport. *Annual Review of Physiology* **2006**, *68*, 403–429, doi:10.1146/annurev.physiol.68.040104.131404.

81. Chen, X.Q.; Fawcett, J.R.; Rahman, Y.E.; Ala, T.A.; Frey, W.H. Delivery of Nerve Growth Factor to the Brain via the Olfactory Pathway. *Journal of Alzheimer's Disease*

1998, *1*, 35–44, doi:10.3233/JAD-1998-1102.

82. Trotta, V.; Pavan, B.; Ferraro, L.; Beggiato, S.; Traini, D.; Gomes, L.; Reis, D.; Scalia, S.; Dalpiaz, A. Brain Targeting of Resveratrol by Nasal Administration of Chitosan-Coated Lipid Microparticles. *European Journal of Pharmaceutics and Biopharmaceutics* **2018**, *127*, 250–259, doi:10.1016/j.ejpb.2018.02.010.

83. Banks, W.A.; During, M.J.; Niehoff, M.L. Brain Uptake of the Glucagon-like Peptide-1 Antagonist Exendin(9-39) after Intranasal Administration. *Journal of Pharmacology and Experimental Therapeutics* **2004**, *309*, 469–475, doi:10.1124/jpet.103.063222.

84. Baker, H.; Spencer, R.F. Transneuronal Transport of Peroxidase-Conjugated Wheat Germ Agglutinin (WGA-HRP) from the Olfactory Epithelium to the Brain of the Adult Rat. *Experimental Brain Research* **1986**, *63*, 461–473, doi:10.1007/BF00237470.

85. Lorenzo, A.J.D. De *The Olfactory Neuron and the Blood-Brain Barrier*; Wolstenholme, G.E.W., Knight, J., Eds.; Wiley online library, 1970; doi: 10.1002/9780470715369.ch9

86. Aderibigbe, B.A. In Situ-Based Gels for Nose to Brain Delivery for the Treatment of Neurological Diseases. *Pharmaceutics* **2018**, *10*, doi:10.3390/pharmaceutics10020040.

87. Karavasili, C.; Fatouros, D.G. Smart Materials: In Situ Gel-Forming Systems for Nasal Delivery. *Drug Discovery Today* **2016**, *21*, 157–166, doi:https://doi.org/10.1016/j.drudis.2015.10.016.

88. Uppuluri, C.T.; Ravi, P.R.; Dalvi, A. V.; Shaikh, S.S.; Kale, S.R. Piribedil Loaded Thermo-Responsive Nasal in Situ Gelling System for Enhanced Delivery to the Brain: Formulation Optimization, Physical Characterization, and in Vitro and in Vivo Evaluation. *Drug Delivery and Translational Research* **2021**, *11*, 909–926, doi:10.1007/S13346-020-00800-W/FIGURES/11.

89. Rao, M.; Agrawal, D.K.; Shirsath, C. Thermoreversible Mucoadhesive in Situ Nasal Gel for Treatment of Parkinson's Disease. *Drug Development and Industrial Pharmacy* **2017**, *43*, 142–150, doi:10.1080/03639045.2016.1225754.

90. Ravi, P.R.; Aditya, N.; Patil, S.; Cherian, L. Nasal In-Situ Gels for Delivery of Rasagiline Mesylate: Improvement in Bioavailability and Brain Localization. *Drug delivery* **2015**, *22*, 903–910, doi:10.3109/10717544.2013.860501.

91. Galgatte, U.C.; Kumbhar, A.B.; Chaudhari, P.D. Drug Delivery Development of in Situ Gel for Nasal Delivery: Design, Optimization, in Vitro and in Vivo Evaluation. *Drug Deliv* **2014**, *21*, 62–73, doi:10.3109/10717544.2013.849778.

92. Zhao, Y.; Yue, P.; Tao, T.; Chen, Q.-H. Drug Brain Distribution Following Intranasal Administration of Huperzine A in Situ Gel in Rats. *Acta Pharmacol Sin* **2007**, *28*, 273–278, doi:10.1111/j.1745-7254.2007.00486.x.

93. Cai, Z.; Song, X.; Sun, F.; Yang, Z.; Hou, S.; Liu, Z. Formulation and Evaluation of in Situ Gelling Systems for Intranasal Administration of Gastrodin. *AAPS PharmSciTech* **2011**, *12*, 1102–1109, doi:10.1208/S12249-011-9678-Y/TABLES/5.

94. Sherje, A.P.; Londhe, V. Development and Evaluation of PH-Responsive Cyclodextrin-Based in Situ Gel of Paliperidone for Intranasal Delivery. *AAPS PharmSciTech* **2018**, *19*, 384–394, doi:10.1208/S12249-017-0844-8/FIGURES/7.

95. Gao, H. Progress and Perspectives on Targeting Nanoparticles for Brain Drug Delivery. *Acta Pharmaceutica Sinica B* **2016**, *6*, 268–286, doi:10.1016/j.apsb.2016.05.013.

96. Pires, P.C.; Santos, A.O. Nanosystems in Nose-to-Brain Drug Delivery: A Review of Non-Clinical Brain Targeting Studies. *Journal of Controlled Release* **2018**, *270*, 89–100, doi:10.1016/j.jconrel.2017.11.047.

97. Badwaik, H.R.; Kumari, L.; Nakhate, K.; Verma, V.S.; Sakure, K. *Phytoconstituent Plumbagin: Chemical, Biotechnological and Pharmaceutical Aspects*; 1st ed.; Elsevier Inc., 2019, 63, 415–460, doi: 10.1016/B978-0-12-817901-7.00013-7 .

98. Di Gioia, S.; Trapani, A.; Mandracchia, D.; De Giglio, E.; Cometa, S.; Mangini, V.; Arnesano, F.; Belgiovine, G.; Castellani, S.; Pace, L.; et al. Intranasal Delivery of Dopamine to the Striatum Using Glycol Chitosan/Sulfobutylether-β-Cyclodextrin Based Nanoparticles. *European Journal of Pharmaceutics and Biopharmaceutics* **2015**, *94*, 180–193, doi:10.1016/j.ejpb.2015.05.019.

99. Ieva, E.; Trapani, A.; Cioffi, N.; Ditaranto, N.; Monopoli, A.; Sabbatini, L. Analytical Characterization of Chitosan Nanoparticles for Peptide Drug Delivery Applications. *Analytical and Bioanalytical Chemistry* **2009**, *393*, 207–215, doi:10.1007/s00216-008-2463-4.

100. Abdel-Bar, H.M.; Abdel-Reheem, A.Y.; Awad, G.A.S.; Mortada, N.D. Evaluation of Brain Targeting and Mucosal Integrity of Nasally Administrated Nanostructured Carriers of a CNS Active Drug, Clonazepam. *Journal of Pharmacy and Pharmaceutical Sciences* **2013**, *16*, 456–469, doi:10.18433/j30s31.

101. Nour, S.A.; Abdelmalak, N.S.; Naguib, M.J.; Rashed, H.M.; Ibrahim, A.B. Intranasal Brain-Targeted Clonazepam Polymeric Micelles for Immediate Control of Status Epilepticus: In Vitro Optimization, Ex Vivo Determination of Cytotoxicity, in Vivo Biodistribution and Pharmacodynamics Studies. *Drug Delivery* **2016**, *23*, 3681–3695, doi:10.1080/10717544.2016.1223216.

102. Rukmangathen, R.; Yallamalli, I.M.; Yalavarthi, P.R. Biopharmaceutical Potential of Selegiline Loaded Chitosan Nanoparticles in the Management of Parkinson's Disease. *Current Drug Discovery Technologies* **2018**, *16*, 417–425,

doi:10.2174/1570163815666180418144019.

103. Sridhar, V.; Gaud, R.; Bajaj, A.; Wairkar, S. Pharmacokinetics and Pharmacodynamics of Intranasally Administered Selegiline Nanoparticles with Improved Brain Delivery in Parkinson's Disease. *Nanomedicine: Nanotechnology, Biology, and Medicine* **2018**, *14*, 2609–2618, doi:10.1016/j.nano.2018.08.004.

104. Gulati, N.; Nagaich, U.; Saraf, S. Fabrication and in Vitro Characterization of Polymeric Nanoparticles for Parkinson's Therapy: A Novel Approach. *Brazilian Journal of Pharmaceutical Sciences* **2014**, *50*, 869–876, doi:10.1590/S1984-82502014000400022.

105. Raj, R.; Wairkar, S.; Sridhar, V.; Gaud, R. Pramipexole Dihydrochloride Loaded Chitosan Nanoparticles for Nose to Brain Delivery: Development, Characterization and in Vivo Anti-Parkinson Activity. *International Journal of Biological Macromolecules* **2018**, *109*, 27–35, doi:10.1016/j.ijbiomac.2017.12.056.

106. Jafarieh, O.; Md, S.; Ali, M.; Baboota, S.; Sahni, J.K.; Kumari, B.; Bhatnagar, A.; Ali, J. Design, Characterization, and Evaluation of Intranasal Delivery of Ropinirole-Loaded Mucoadhesive Nanoparticles for Brain Targeting. *Drug Development and Industrial Pharmacy* **2015**, *41*, 1674–1681, doi:10.3109/03639045.2014.991400.

107. Mittal, D.; Md, S.; Hasan, Q.; Fazil, M.; Ali, A.; Baboota, S.; Ali, J. Brain Targeted Nanoparticulate Drug Delivery System of Rasagiline via Intranasal Route. *Drug Delivery* **2016**, *23*, 130–139, doi:10.3109/10717544.2014.907372.

108. Md, S.; Haque, S.; Fazil, M.; Kumar, M.; Baboota, S.; Sahni, J.K.; Ali, J. Optimised Nanoformulation of Bromocriptine for Direct Nose-to-Brain Delivery: Biodistribution, Pharmacokinetic and Dopamine Estimation by Ultra-HPLC/Mass Spectrometry Method. *Expert Opinion on Drug Delivery* **2014**, *11*, 827–842,

doi:10.1517/17425247.2014.894504.

109. Shadab, M.D.; Khan, R.A.; Mustafa, G.; Chuttani, K.; Baboota, S.; Sahni, J.K.; Ali, J. Bromocriptine Loaded Chitosan Nanoparticles Intended for Direct Nose to Brain Delivery: Pharmacodynamic, Pharmacokinetic and Scintigraphy Study in Mice Model. *European Journal of Pharmaceutical Sciences* **2013**, *48*, 393–405, doi:10.1016/j.ejps.2012.12.007.

110. Danhier, F.; Ansorena, E.; Silva, J.M.; Coco, R.; Le Breton, A.; Préat, V. PLGA-Based Nanoparticles: An Overview of Biomedical Applications. *Journal of Controlled Release* **2012**, *161*, 505–522, doi:10.1016/j.jconrel.2012.01.043.

111. Ahmad, N. Rasagiline-Encapsulated Chitosan-Coated PLGA Nanoparticles Targeted to the Brain in the Treatment of Parkinson's Disease. *Journal of Liquid Chromatography and Related Technologies* **2017**, *40*, 677–690, doi:10.1080/10826076.2017.1343735.

112. Gambaryan, P.Y.; Kondrasheva, I.G.; Severin, E.S.; Guseva, A.A.; Kamensky, A.A. Increasing the Effciency of Parkinson's Disease Treatment Using a Poly(Lactic-Co-Glycolic Acid) (PLGA) Based L-DOPA Delivery System. *Experimental Neurobiology* **2014**, *23*, 246–252, doi:10.5607/en.2014.23.3.246.

113. Arisoy, S.; Sayiner, O.; Comoglu, T.; Onal, D.; Atalay, O.; Pehlivanoglu, B. In Vitro and in Vivo Evaluation of Levodopa-Loaded Nanoparticles for Nose to Brain Delivery. *Pharmaceutical Development and Technology* **2020**, *25*, 735–747, doi:10.1080/10837450.2020.1740257.

114. Chatzitaki, A.; Jesus, S.; Karavasili, C.; Andreadis, D. Chitosan-Coated PLGA Nanoparticles for the Nasal Delivery of Ropinirole Hydrochloride : In Vitro and Ex Vivo Evaluation of Efficacy and Safety. *International Journal of Pharmaceutics* **2020**, *589*, 119776, doi:10.1016/j.ijpharm.2020.119776.

115. Choudhury, H.; Gorain, B.; Chatterjee, B.; Mandal, U.K.; Sengupta, P.; Tekade, R.K. Pharmacokinetic and Pharmacodynamic Features of Nanoemulsion Following Oral, Intravenous, Topical and Nasal Route. *Current Pharmaceutical Design* **2017**, *23*, 2504–2531, doi:10.2174/1381612822666161201143600.

116. Colombo, M.; Figueiró, F.; de Fraga Dias, A.; Teixeira, H.F.; Battastini, A.M.O.; Koester, L.S. Kaempferol-Loaded Mucoadhesive Nanoemulsion for Intranasal Administration Reduces Glioma Growth in Vitro. *International Journal of Pharmaceutics* **2018**, *543*, 214–223, doi:10.1016/j.ijpharm.2018.03.055.

117. Mustafa, G.; Ahuja, A.; Al Rohaimi, A.H.; Muslim, S.; Hassan, A.A.; Baboota, S.; Ali, J. Nano-Ropinirole for the Management of Parkinsonism: Blood-Brain Pharmacokinetics and Carrier Localization. *Expert Review of Neurotherapeutics* **2015**, *15*, 695–710, doi:10.1586/14737175.2015.1036743.

118. Kumar, S.; Ali, J.; Baboota, S. Design Expert® Supported Optimization and Predictive Analysis of Selegiline Nanoemulsion via the Olfactory Region with Enhanced Behavioural Performance in Parkinson's Disease. *Nanotechnology* **2016**, *27*, doi:10.1088/0957-4484/27/43/435101.

119. Kumar, S.; Dang, S.; Nigam, K.; Ali, J.; Baboota, S. Selegiline Nanoformulation in Attenuation of Oxidative Stress and Upregulation of Dopamine in the Brain for the Treatment of Parkinson's Disease. *Rejuvenation Research* **2018**, *21*, 464–476, doi:10.1089/rej.2017.2035.

120. Nehal, N.; Nabi, B.; Rehman, S.; Pathak, A.; Iqubal, A.; Khan, S.A.; Yar, M.S.; Parvez, S.; Baboota, S.; Ali, J. Chitosan Coated Synergistically Engineered Nanoemulsion of Ropinirole and Nigella Oil in the Management of Parkinson's Disease: Formulation Perspective and In Vitro and In Vivo Assessment. *International Journal of Biological*

Macromolecules **2021**, *167*, 605–619, doi:10.1016/j.ijbiomac.2020.11.207.

121. Joseph, E.; Narayan Saha, R. Advances in Brain Targeted Drug Delivery: Nanoparticulate Systems. *Journal of PharmaSciTech* **2013**, *3*.

122. Cacciatore, I.; Ciulla, M.; Fornasari, E.; Marinelli, L.; Di Stefano, A. Solid Lipid Nanoparticles as a Drug Delivery System for the Treatment of Neurodegenerative Diseases. *Expert Opinion on Drug Delivery* **2016**, *13*, 1121–1131, doi:10.1080/17425247.2016.1178237.

123. Blasi, P.; Giovagnoli, S.; Schoubben, A.; Ricci, M.; Rossi, C. Solid Lipid Nanoparticles for Targeted Brain Drug Delivery. *Advanced Drug Delivery Reviews* **2007**, *59*, 454–477, doi:10.1016/j.addr.2007.04.011.

124. Pardeshi, C. V.; Rajput, P. V.; Belgamwar, V.S.; Tekade, A.R.; Surana, S.J. Novel Surface Modified Solid Lipid Nanoparticles as Intranasal Carriers for Ropinirole Hydrochloride: Application of Factorial Design Approach. *Drug Delivery* **2013**, *20*, 47–56, doi:10.3109/10717544.2012.752421.

125. Jazuli, I.; Annu; Nabi, B.; Moolakkadath, T.; Alam, T.; Baboota, S.; Ali, J. Optimization of Nanostructured Lipid Carriers of Lurasidone Hydrochloride Using Box-Behnken Design for Brain Targeting: In Vitro and in Vivo Studies. *Journal of Pharmaceutical Sciences* **2019**, *108*, 3082–3090, doi:10.1016/j.xphs.2019.05.001.

126. Müller, R.H.; Petersen, R.D.; Hommoss, A.; Pardeike, J. Nanostructured Lipid Carriers (NLC) in Cosmetic Dermal Products. *Advanced Drug Delivery Reviews* **2007**, *59*, 522–530, doi:10.1016/j.addr.2007.04.012.

127. Chakraborty, T.; Das, M.K.; Dutta, L.; Mukherjee, B. *Successful Delivery of Zidovudine-Loaded Docosanol Nanostructured Lipid Carriers (Docosanol NLCs) into*

Rat Brain; 2019; doi: 10.1007/978-3-030-06115-9_26.

128. Mishra, N.; Sharma, S.; Deshmukh, R.; Kumar, A.; Sharma, R. Development and Characterization of Nasal Delivery of Selegiline Hydrochloride Loaded Nanolipid Carriers for the Management of Parkinson's Disease. *Central Nervous System Agents in Medicinal Chemistry* **2018**, *19*, 46–56, doi:10.2174/1871524919666181126124846.

129. Pardeshi, C. V.; Belgamwar, V.S. Improved Brain Pharmacokinetics Following Intranasal Administration of N,N,N-Trimethyl Chitosan Tailored Mucoadhesive NLCs. *Materials Technology* **2020**, *35*, 249–266, doi:10.1080/10667857.2019.1674522.

130. Sharma, S.; Lohan, S.; Murthy, R.S.R. Formulation and Characterization of Intranasal Mucoadhesive Nanoparticulates and Thermo-Reversible Gel of Levodopa for Brain Delivery. *Drug Development and Industrial Pharmacy* **2014**, *40*, 869–878, doi:10.3109/03639045.2013.789051.

131. Gabal, Y.M.; Kamel, A.O.; Sammour, O.A.; Elshafeey, A.H. Effect of Surface Charge on the Brain Delivery of Nanostructured Lipid Carriers in Situ Gels via the Nasal Route. *International Journal of Pharmaceutics* **2014**, *473*, 442–457, doi:10.1016/j.ijpharm.2014.07.025.

132. Uppuluri, C.T.; Ravi, P.R.; Dalvi, A. V. Design and Evaluation of Thermo-Responsive Nasal in Situ Gelling System Dispersed with Piribedil Loaded Lecithin-Chitosan Hybrid Nanoparticles for Improved Brain Availability. *Neuropharmacology* **2021**, *201*, 108832, doi:10.1016/J.NEUROPHARM.2021.108832.

133. Uppuluri, C.T.; Ravi, P.R.; Dalvi, A. V. Design, Optimization and Pharmacokinetic Evaluation of Piribedil Loaded Solid Lipid Nanoparticles Dispersed in Nasal in Situ Gelling System for Effective Management of Parkinson's Disease. *International*

Journal of Pharmaceutics **2021**, *606*, 120881, doi:10.1016/J.IJPHARM.2021.120881.

134. Singh, R.M.; Kumar, A.; Pathak, K. Mucoadhesive in Situ Nasal Gelling Drug Delivery Systems for Modulated Drug Delivery. *Expert Opinion on Drug Delivery* **2013**, *10*, 115–130, doi:10.1517/17425247.2013.746659.

135. Xie, J.; Shen, Z.; Anraku, Y.; Kataoka, K.; Chen, X. Nanomaterial-Based Blood-Brain-Barrier (BBB) Crossing Strategies. *Biomaterials* **2019**, *224*, 119491, doi:10.1016/j.biomaterials.2019.119491.

136. Gorain, B.; Rajeswary, D.C.; Pandey, M.; Kesharwani, P.; Kumbhar, S.A.; Choudhury, H. Nose to Brain Delivery of Nanocarriers Towards Attenuation of Demented Condition. *Current Pharmaceutical Design* **2020**, *26*, 2233–2246, doi:10.2174/1381612826666200313125613.

137. Millan, M.J.; Maiofiss, L.; Cussac, D.; Audinot, V.; Boutin, J.A.; Newman-Tancredi, A. Differential Actions of Antiparkinson Agents at Multiple Classes of Monoaminergic Receptor. I. A Multivariate Analysis of the Binding Profiles of 14 Drugs at 21 Native and Cloned Human Receptor Subtypes. *Journal of Pharmacology and Experimental Therapeutics* **2002**, *303*, 791–804, doi:10.1124/JPET.102.039867.

138. Rosa-Grilo, M.; Qamar, M.A.; Taddei, R.N.; Pagonabarraga, J.; Kulisevsky, J.; Sauerbier, A.; Chaudhuri, K.R. Rotigotine Transdermal Patch and Sleep in Parkinson's Disease: Where Are We Now? *NPJ Parkinson's disease* **2017**, *3*, 28, doi:10.1038/s41531-017-0030-4.

139. Ray Chaudhuri, K.; Martinez-Martin, P.; Antonini, A.; Brown, R.G.; Friedman, J.H.; Onofrj, M.; Surmann, E.; Ghys, L.; Trenkwalder, C. Rotigotine and Specific Non-Motor Symptoms of Parkinson's Disease: Post Hoc Analysis of RECOVER. *Parkinsonism & related disorders* **2013**, *19*, 660–665, doi:10.1016/j.parkreldis.2013.02.018.

140. Elshoff, J.P.; Cawello, W.; Andreas, J.O.; Mathy, F.X.; Braun, M. An Update on Pharmacological, Pharmacokinetic Properties and Drug-Drug Interactions of Rotigotine Transdermal System in Parkinson's Disease and Restless Legs Syndrome. *Drugs* **2015**, *75*, 487–501, doi:10.1007/s40265-015-0377-y.

141. Sharma, P.K.; Panda, A.; Pradhan, A.; Zhang, J.; Thakkar, R.; Whang, C.H.; Repka, M.A.; Murthy, S.N. Solid-State Stability Issues of Drugs in Transdermal Patch Formulations. *AAPS PharmSciTech* **2018**, *19*, 27–35, doi:10.1208/S12249-017-0865-3.

142. Bi, C.C.; Wang, A.P.; Chu, Y.C.; Liu, S.; Mu, H.J.; Liu, W.H.; Wu, Z.M.; Sun, K.X.; Li, Y.X. Intranasal Delivery of Rotigotine to the Brain with Lactoferrin-Modified PEG-PLGA Nanoparticles for Parkinson's Disease Treatment. *International Journal of Nanomedicine* **2016**, *11*, 6547–6559, doi:10.2147/IJN.S120939.

143. Bhattamisra, S.K.; Shak, A.T.; Xi, L.W.; Safian, N.H.; Choudhury, H.; Lim, W.M.; Shahzad, N.; Alhakamy, N.A.; Anwer, M.K.; Radhakrishnan, A.K.; et al. Nose to Brain Delivery of Rotigotine Loaded Chitosan Nanoparticles in Human SH-SY5Y Neuroblastoma Cells and Animal Model of Parkinson's Disease. *International Journal of Pharmaceutics* **2020**, *579*, 119148, doi:10.1016/j.ijpharm.2020.119148.

144. Wang, F.; Yang, Z.; Liu, M.; Tao, Y.; Li, Z.; Wu, Z.; Gui, S. Facile Nose-to-Brain Delivery of Rotigotine-Loaded Polymer Micelles Thermosensitive Hydrogels: In Vitro Characterization and in Vivo Behavior Study. *International Journal of Pharmaceutics* **2020**, *577*, 119046, doi:10.1016/j.ijpharm.2020.119046.

145. Prajapati, J.B.; Patel, G.C. Nose to Brain Delivery of Rotigotine Loaded Solid Lipid Nanoparticles: Quality by Design Based Optimization and Characterization. *Journal of Drug Delivery Science and Technology* **2021**, *63*, 102377, doi:10.1016/j.jddst.2021.102377.

146. Choudhury, H.; Zakaria, N.F.B.; Tilang, P.A.B.; Tzeyung, A.S.; Pandey, M.; Chatterjee, B.; Alhakamy, N.; Bhattamishra, S.K.; Kesharwani, P.; Gorain, B.; et al. Formulation Development and Evaluation of Rotigotine Mucoadhesive Nanoemulsion for Intranasal Delivery. *Journal of Drug Delivery Science and Technology* **2019**, *54*, 101301, doi:https://doi.org/10.1016/j.jddst.2019.101301.

147. Wavikar, P.; Pai, R.; Vavia, P. Nose to Brain Delivery of Rivastigmine by In Situ Gelling Cationic Nanostructured Lipid Carriers: Enhanced Brain Distribution and Pharmacodynamics. *Journal of Pharmaceutical Sciences* **2017**, *106*, 3613–3622, doi:10.1016/J.XPHS.2017.08.024.

148. Pailla, S.R.; Talluri, S.; Rangaraj, N.; Ramavath, R.; Challa, V.S.; Doijad, N.; Sampathi, S. Intranasal Zotepine Nanosuspension: Intended for Improved Brain Distribution in Rats. *DARU, Journal of Pharmaceutical Sciences* **2019**, *27*, 541–556, doi:10.1007/s40199-019-00281-4.

149. Narayan, R.; Singh, M.; Ranjan, O.P.; Nayak, Y.; Garg, S.; Shavi, G. V.; Nayak, U.Y. Development of Risperidone Liposomes for Brain Targeting through Intranasal Route. *Life Sciences* **2016**, *163*, 38–45, doi:10.1016/J.LFS.2016.08.033.

150. Katona, G.; Sabir, F.; Sipos, B.; Naveed, M.; Schelz, Z.; Zupkó, I.; Csóka, I. Development of Lomustine and N-Propyl Gallate Co-Encapsulated Liposomes for Targeting Glioblastoma Multiforme via Intranasal Administration. *Pharmaceutics* **2022**, *14*, doi:10.3390/pharmaceutics14030631.

Chapter 2: Drug Profile

2.1 Introduction

Rotigotine (RTG) is the newest member of dopamine agonist and is effective as monotherapy to treat early PD and as a combination therapy with levodopa through course of the disease. Overall, RTG along with motor symptoms diversely improves non-motor symptoms of PD, particularly sleep disturbances and health-related quality of life [1,2].

2.2 Rotigotine for the management of PD

RTG is a non-ergoline dopamine receptor agonist having higher affinity towards all dopamine receptors (D2, D3, D4, and D5) than D1 receptors [3]. Chemical name of RTG is 6-{propyl[2-(thiophen-2-yl)ethyl]amino}-5,6,7,8-tetrahydronaphthalen-1-ol. The chemical structure of RTG is given in **Figure 2.1**.

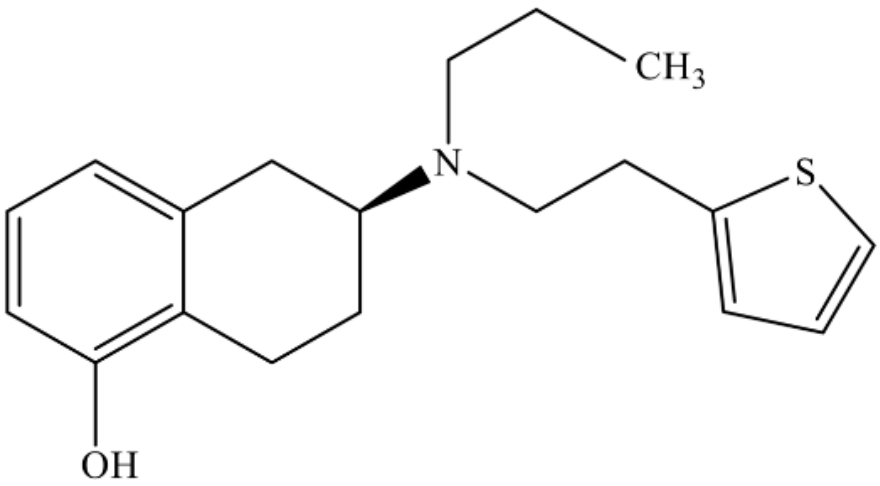

Figure 2.1 Chemical structure of RTG

RTG was approved by both USFDA and EMA for treatment of PD and restless leg syndrome in 2007 as a controlled release transdermal patch under the trade name Neupro®. RTG has been indicated for the symptoms of early-stage idiopathic PD as monotherapy. It is also prescribed in combination with levodopa at later stages of the disease.

2.3 Physicochemical properties of RTG

2.3.1 Solubility

RTG is freely soluble in dimethyl formamide (30 mg/mL), dimethyl sulfoxide (20 mg/mL), and ethanol (1 mg/mL) at 25 ^{o}C. It is insoluble in water [4]. The partition coefficient (Log P) value of RTG is 4.96.

2.3.2 Polymorphic form

RTG exhibits two polymorphic forms namely Form (I) and Form (II). Among two polymorphic forms, polymorph II is more stable. Polymorph I and polymorph II exhibit endothermic peak at 77 ± 2 ^{o}C and 97 ± 2 ^{o}C, respectively [5]. Polymorph I of RTG exhibits a characteristic powder x-ray diffraction peak at about 20.23 ± 0.2 ($^{o}2\theta$) which is found to be absent in Form II [6]. Whereas, polymorph II is characterized by 13.68 ± 0.2 and 17.72 ± 0.2 ($^{o}2\theta$) [6]. The crystal lattice of polymorph I is tetragonal in shape whereas, polymorph II is orthorhombic in shape [5]. RTG (Polymorph II) is used for this research work. Physicochemical properties of RTG (Polymorph II) are given in **Table 2.1**.

Table 2.1 Physicochemical properties of RTG

Parameters*	**Description**
Drug name and BCS Class	Rotigotine, Class 2
Therapeutic class	Anti-Parkinson drugs
Chemical name	6-{propyl[2-(thiophen-2-yl)ethyl]amino}-5,6,7,8-tetrahydronaphthalen-1-ol
Chemical formula	$C_{19}H_{25}NOS$
Molecular weight	315.474 g/mol
Physical state	Crystalline powder
Melting point	97 ± 2 ^{o}C
Water solubility (at pH of ~ 7.0)	0.00904 mg/mL
Hydrophobicity (Log P)	4.96
Ionization constant (pKa)	10.03 (Strongest acidic), 10.97 (Strongest basic)

* Data taken from available literatures

2.4 Clinical pharmacology of RTG

2.4.1 Mechanism of Action

The exact mechanism of action of RTG is not yet fully understood. RTG acts by its ability to stimulate D2 dopamine receptors within the dorsal striatum of brain. RTG is more similar to dopamine and apomorphine than other dopamine agonists since it exhibits binding affinity for D1 receptors as well as D2 and D3 receptors [7]. Studies have also reported that it possesses *in vitro* binding affinity to $5HT_{1A}$ and the α_{2B} receptor subtypes [8].

2.5 Pharmacokinetics (PK) of RTG

2.5.1 Absorption after transdermal administration

RTG exhibits extremely poor oral bioavailability due to extensive first-pass metabolism [9]. Absolute bioavailability of the currently marketed transdermal patch is 37% after 24 h of delivery [10]. Literature reported that RTG showed maximum plasma concentration (C_{max}) of 0.56 ng/mL with T_{max} of 19 h following transdermal application [11]. Systemic bioavailability of the drug varied depending on site of application (thigh, belly, hip, shoulder, flank, and upper arm) of the patch [12]. From the transdermal patch, RTG showed a dose-proportional PK up to therapeutic dose rates of 24 mg upto 24 h.

2.5.2 Distribution

RTG demonstrates high distribution towards adrenals, kidneys, harderian gland, and prostate gland. A high apparent volume of distribution for RTG indicates a quick and extensive distribution across tissues.

2.5.3 Metabolism and Elimination

RTG gets rapidly metabolized and 71% of metabolites are excreted in urine and 23% into feces. Literature revealed that CYP2C19 is involved in the metabolism of RTG. *In vitro* studies have demonstrated that RTG does not act as a substrate of P-glycoprotein [13]. Upon intravenous

(i.v.) administration, elimination half-life of RTG is reported to be about 1.8 h and 0.7 h in rat and monkey, respectively [13]. The plasma terminal half-life of RTG after transdermal administration was found to be 5 – 7 h in human [14].

2.5.4 Adverse effect of RTG

The adverse effects of RTG are well tolerated and of mild to moderate severity. The most common adverse effects of RTG are application site reaction (ASR), nausea, somnolence, headache, dizziness, vomiting, back pain, insomnia, fatigue, and constipation [13]. Several studies report dose-dependent ASR such as localized erythema, edema, and pruritus [15].

2.5.5 Dosage and administration

As per USFDA and EMA, RTG dose for PD patients is initiated from 1 mg/24 h. Depending on patient response, the dose can be increased to a maximum of 3 mg/24 h on weekly basis. In early stage of PD, the maximum dose is 8 mg/24 h, and in case of advanced stage of disease the maximum recommended dose is 16 mg/24 h [16].

RTG is marketed as Neupro® and Leganto® in USA and Europe, respectively. Both Neupro® and Leganto® are available as 1, 2, 3, 4, 6, and 8 mg/24 h extended release transdermal patches.

2.6 Drawbacks of the currently available RTG formulation

RTG shows high first-pass metabolism and low oral bioavailability (<1%) [11]. Therefore, the drug is currently available as extended release transdermal patch. The systemic bioavailability of RTG from transdermal patch is only 37%, which varies with its application site [10]. Furthermore, in transdermal patch RTG develops snowflake-like crystals during storage due to RTG crystallization [17]. This leads to poor drug absorption through the skin and results in variable therapeutic responses. Additionally, systemic absorption of drug is compromised due to its slower transport from the patch. Once systemically absorbed, RTG has to cross the tight

and rigid blood-brain barrier (BBB) to reach into brain. This additionally lowers the brain availability of RTG.

2.7 Conclusion

RTG is a newly approved drug for the management of PD that efficiently treat motor and non-motor symptoms. However, potential of the drug is not fully utilized due to its lower and varied systemic bioavailability from marketed transdermal formulation. Its brain availability from transdermal patch is further compromised due to the restrictions posed by BBB. The drug is well tolerated and safe as required for the treatment of PD. Thus, there is a need to formulate novel delivery systems for RTG to improve its brain availability.

References

1. Frampton, J.E. Rotigotine Transdermal Patch: A Review in Parkinson's Disease. *CNS Drugs* **2019**, *33*, 707–718, doi:10.1007/S40263-019-00646-Y.

2. Valldeoriola, F.; Salvador, A.; Gómez-Arguelles, J.M.; Marey, J.; Moya, M.; Ayuga, Á.; Ramírez, F. The Effects of Transdermal Rotigotine on Non-Motor Symptoms of Parkinson's Disease: A Multicentre, Observational, Retrospective, Post-Marketing Study. *The International journal of neuroscience* **2018**, *128*, 369–375, doi:10.1080/00207454.2017.1387111.

3. Wood, M.; Dubois, V.; Scheller, D.; Gillard, M. Rotigotine Is a Potent Agonist at Dopamine D1 Receptors as Well as at Dopamine D2 and D3 Receptors. *British journal of pharmacology* **2015**, *172*, 1124–1135, doi:10.1111/BPH.12988.

4. Williams, M. The Merck Index: An Encyclopedia of Chemicals, Drugs, and Biologicals, 15th Edition. *Drug Development Research* **2013**, *74*, 339, doi:10.1002/DDR.21085.

5. Wolff, H.-M.; Quere, L.; Riedner, J. Polymorphic Form of Rotigotine 2008.

6. Hans-Michael Wolff; Quere, L.; Riedner, J. Polymorphic Form of Rotigotine and Process for Production.

7. De Rijk, M.C.; Tzourio, C.; Breteler, M.M.B.; Dartigues, J.F.; Amaducci, L.; Lopez-Pousa, S.; Manubens-Bertran, J.M.; Alperovitch, A.; Rocca, W.A. Prevalence of Parkinsonism and Parkinson's Disease in Europe: The EUROPARKINSON Collaborative Study. European Community Concerted Action on the Epidemiology of Parkinson's Disease. *Journal of Neurology, Neurosurgery & Psychiatry* **1997**, *62*, 10–15, doi:10.1136/JNNP.62.1.10.

8. Scheller, D.; Ullmer, C.; Berkels, R.; Gwarek, M.; Lübbert, H. The in Vitro Receptor

Profile of Rotigotine: A New Agent for the Treatment of Parkinson's Disease. *Naunyn-Schmiedeberg's Archives of Pharmacology* **2009**, *379*, 73–86, doi:10.1007/S00210-008-0341-4.

9. Lafuente, J.V.; Requejo, C.; Ugedo, L. Chapter 8 - Nanodelivery of Therapeutic Agents in Parkinson's Disease. In *Nanoneuroprotection and Nanoneurotoxicology Research*; Aruna Sharma, H.S.S., Ed.; Elsevier, 2019, *245*, 263–279 doi: 10.1016/bs.pbr.2019.03.004

10. Saha, P.; Pandey, M.M. Spectrochimica Acta Part A : Molecular and Biomolecular Spectroscopy A New Fluorescence-Based Method for Rapid and Specific Quantification of Rotigotine in Chitosan Nanoparticles. *Spectrochimica Acta Part A: Molecular and Biomolecular Spectroscopy* **2022**, *267*, 120555, doi:10.1016/j.saa.2021.120555.

11. Elshoff, J.P.; Cawello, W.; Andreas, J.O.; Mathy, F.X.; Braun, M. An Update on Pharmacological, Pharmacokinetic Properties and Drug-Drug Interactions of Rotigotine Transdermal System in Parkinson's Disease and Restless Legs Syndrome. *Drugs* **2015**, *75*, 487–501, doi:10.1007/s40265-015-0377-y.

12. Kujirai, H.; Itaya, S.; Ono, Y.; Takahashi, M.; Inaba, A.; Shimo, Y.; Hattori, N.; Orimo, S. A Study for Expanding Application Sites for Rotigotine Transdermal Patch. *Parkinson's Disease* **2020**, *2020*, 5892163, doi:10.1155/2020/5892163.

13. EMEA Rotigotine Scientific Discussion. *European Medicines Agency - Pre-Authorisation Evaluation of Medicines for Human Use* 2006, 1–27.

14. Neupro 3mg/24h Transdermal Patch - Summary of Product Characteristics (SmPC) - (Emc) Available online: https://www.medicines.org.uk/emc/product/6576/smpc#gref (accessed on 10 December 2022).

15. Nakaki, T. Chapter 13 - Drugs That Affect Autonomic Functions or the Extrapyramidal System. In *A Worldwide Yearly Survey of New Data in Adverse Drug Reactions*; Ray, S.D.B.T.-S.E. of D.A., Ed.; Elsevier, 2014,*35*, 255–272, doi: 10.1016/B978-0-444-62635-6.00013-9.

16. Hauser, R.A.; Slawek, J.; Barone, P.; Dohin, E.; Surmann, E.; Asgharnejad, M.; Bauer, L. Evaluation of Rotigotine Transdermal Patch for the Treatment of Apathy and Motor Symptoms in Parkinson's Disease. *BMC Neurology* **2016**, *16*, 90, doi:10.1186/s12883-016-0610-7.

17. Sharma, P.K.; Panda, A.; Pradhan, A.; Zhang, J.; Thakkar, R.; Whang, C.H.; Repka, M.A.; Murthy, S.N. Solid-State Stability Issues of Drugs in Transdermal Patch Formulations. *AAPS PharmSciTech* **2018**, *19*, 27–35, doi:10.1208/s12249-017-0865-3.

Chapter 3: Development and Validation of Analytical and Bioanalytical Methods for Quantification of Rotigotine

3.1 Introduction

Accurate quantification of drugs is an important requirement to pursue research and development of any drug delivery system. Analysis is an essential and basic component in the formulation development process. It is necessary to develop a suitable analytical method to analyze and quantify drugs. After development, there is a need to validate the method in order to show its competency. It is not only important to quantify the drug in any formulation but, also it is necessary to prove that the quantified results are accurate and precise [1]. Thus, validation is required after method development which is also a prerequisite of regulatory bodies. A rapid, accurate, precise, and simple analytical method can make formulation development quick and successful. Hence, development and validation of an analytical method is vital before starting dosage form design of any drug [2]. Furthermore, assessment of drug in plasma and other biological matrices is another crucial aspect of product development [3]. The quantitative estimation of drugs in plasma and other bio-matrices plays a major role in the evaluation of pharmacokinetics (PK) studies.

Rotigotine (RTG) is a non-ergoline dopamine agonist which acts by stimulating dopaminergic receptors in the brain and reduces symptoms of Parkinson's disease (PD) [4]. Commercially available RTG transdermal patch exhibits only 37% systemic bioavailability. Additionally, brain delivery of RTG from the transdermal patch is compromised due to slow release of drug from dermal surface, hindrance caused by the blood-brain barrier (BBB), etc. In the present research work, it is proposed to develop and optimize nose-to-brain nanocarriers for enhancing transport of RTG directly into the brain.

Screening of excipients for preparation of nanocarriers on the basis of drug's solubility in surfactants, lipids, and solvents is an important aspect of formulation development. The particle size, PDI, drug loading, and entrapment efficiency of drug is dependent on solubility of drug in several excipients *viz.*, surfactants, lipids, solvents, etc. To rapidly estimate the solubility of RTG in different surfactants and solvents during preliminary screening of excipients for the preparation of nanocarriers, a fluorescence-based analytical method was developed and validated. An accurate, specific, precise, and stability-indicating reverse phase high performance liquid chromatography (RP-HPLC) analytical method was developed and validated to assess different aspects of developed nanocarriers *viz.*, drug content, drug loading, entrapment efficiency, *in vitro* drug dissolution and release, *ex vivo* drug permeation, stability during storage etc. Finally, to evaluate efficiency of the optimized nanocarriers, PK studies are required to perform. A RP-HPLC bioanalytical method was developed and validated in plasma and brain matrices to quantify drug in plasma and other biological matrices obtained during the PK studies.

3.2 Analytical methods for estimation of RTG

There have been a few RP-HPLC analytical methods reported for the analysis of RTG in bulk and pharmaceutical dosage forms. Swarupa *et al.* reported a stability-indicating RP-HPLC method for quantification of RTG in bulk and pharmaceutical formulations with a linearity range between 10 – 60 µg/mL and the lowest quantity that could be detected using this method is 0.05 µg/mL [5]. Krishna *et al.* reported another RP-HPLC method for assay of RTG using 70% v/v methanol as a non-aqueous solvent in the mobile phase [6]. Patil *et al.* reported an ultra-performance LC method for the simultaneous analysis of RTG and its impurities where a longer retention time and usage of high proportion of organic phase was observed [7]. All these methods are time-consuming, expensive, and non-ecofriendly due to longer run time and usage

of high organic solvents. There have been a few bioanalytical methods reported for analysis of RTG in bio matrices *viz.*, rat serum, rat plasma, monkey plasma, and rat brain [8–11]. Kehr *et al.* reported a microdialysis technique to analyse RTG in rat brain combined with microbore column liquid chromatography using electrochemical detection [8]. Den *et al.* have reported a RP-HPLC method for quantification of RTG in rat serum with a limit of detection (LOD) of 0.05 nmol/mL [9]. Walters *et al.* have worked on HPLC method using electrochemical detector to estimate RTG in monkey plasma with LOD of 1.5 ng/mL and a linearity range of 1.5 – 1000 ng/mL [10]. Sha *et al.* reported a LC-MS/MS method for estimation of RTG in rat plasma with a linearity range of 0.100 – 10.0 ng/mL [11]. Despite the several detectors used for LC separation, detection using UV is still the most frequently used for bioanalysis. Furthermore, though LC-MS/MS techniques offer good sensitivity and selectivity but, less costly methods are mostly preferred for routine analysis [12].

Fluorescence-based methods are regarded as rapid, sensitive, accurate, cost-effective, easy to execute, and require relatively simple instrumentation [13]. Literature revealed that to date, there is no fluorescence-based analytical method reported to estimate RTG in bulk and pharmaceutical formulations. As required, we have developed a fluorescence-based analytical method for quantification of RTG in preliminary screening of formulation development.

All reported RP-HPLC methods are costly and time-consuming due to usage of high organic solvents and longer run time, respectively. Therefore, it was necessary to develop an in-house RP-HPLC analytical method that would be sensitive, rapid, specific, and economic compared to the already available methods.

Few bioanalytical RP-HPLC methods are available for estimation of RTG in biological matrices. But, these methods are costly and required high-end instruments. So, there was a need to develop RP-HPLC bioanalytical method for analyzing RTG in both plasma and brain using

a simple UV detector. Hence, we also developed a specific, sensitive, and rapid bioanalytical RP-HPLC method for quantification of RTG in plasma and brain matrices. All the developed methods were validated as per the International Conference on Harmonization (ICH) as well as USP guidelines [14].

3.3 Method I: Fluorescence-based method for estimation of RTG in aqueous samples

3.3.1 Materials

RTG was kindly gifted by Mylan Laboratories (Hyderabad, India). Poloxamer 188 and Phospholipon 80 H (Soya lecithin) were received as gift samples from BASF (Navi- Mumbai, India) and Lipoid (GmBH, Germany), respectively. Medium molecular weight (MMW) chitosan (CS) (99% deacetylated), potassium dihydrogen phosphate (KH_2PO_4), hydrochloric acid (HCl), sodium hydroxide (NaOH) were purchased from SISCO Research Laboratories (SRL) Pvt. Ltd (Delhi, India).

3.3.2 Instrumentation

The fluorescence-based estimations were performed in Fluorolog^{TM} (HORIBA Ltd. Kyoto, Japan) equipped with Xenon arc lamp. For both excitation and emission, 4 nm slit width was used with the cuvette size being 0.6 cm. The fluorescence-based method parameters are provided in **Table 3.1**. All the hardware regulation and data processing were done using FluorEssence™ software version 3.8. Regression and statistical analysis were performed using Microsoft Excel 2013.

Table 3.1 Fluorescence-based method parameters

Spectrum type	Excitation and Emission
Scan range	200 - 400 nm
Scanning speed	Medium
Slit width (nm)	Excitation : 4; Emission : 4

3.3.3 Methods

3.3.3.1 Preparation of standard and calibration curve standards

The stock solution of RTG was prepared by dissolving accurately weighed 5 mg of the drug into 5 mL of ethanol to get a final concentration of 1 mg/mL. A working standard solution of 10 µg/mL was prepared by stepwise diluting the stock solution using phosphate buffer pH 6.4. The working standard solution was diluted with phosphate buffer (pH 6.4) to get calibration curve standards of 250, 500, 1000, 1500, 2000, and 2500 ng/mL. Fluorescence intensity (FI) of the calibration curve standards was measured at 298 nm (λ_{em}) after excitation at 277 nm (λ_{ex}). FI of the blank solution was measured using the same emission and excitation parameters.

3.3.3.2 Effect of pH

The effect of pH on FI of RTG (1300 ng/mL) was investigated using phosphate buffers within a range of pH 3 – 8. Phosphate buffers (10 mM) were prepared by taking an accurately weighed amount of KH_2PO_4 in Milli-Q water and pH of the buffers was adjusted by using either 0.1 (M) HCl or 0.1 (N) NaOH.

3.3.3.3 Method validation

The developed method was validated as per the ICH Q2(R1) guidelines [14]. For validation of the developed method, analytical parameters including linearity, range, accuracy, precision, limit of detection, limit of quantification, specificity, and robustness were evaluated.

3.3.3.3.1 Calibration curve, linearity, and range

The corrected FI values were plotted against respective concentrations of RTG to get the calibration curves (n = 6). Each calibration curve was constructed using six different calibration curve standards in a range of 250 – 2500 ng/mL. Linearity of the method was estimated with help of the linear regression equation and correlation coefficient equation. Statistical analysis and model predictability were evaluated by regression coefficient (R^2).

3.3.3.3.2 Sensitivity

Limit of detection (LOD) is defined as the lowest concentration of an analyte that can be detected and distinguished from the level of noise [14]. The lowest concentration of an analyte that can be quantified with appropriate accuracy and precision is termed as limit of quantification (LOQ). LOD and LOQ of the developed method were estimated using the standard deviation of y-intercept and mean of the slope of all six calibration curves. The following equations were used for the determination of LOD and LOQ, Equation 3.1 and 3.2, respectively [14].

$$LOD = \frac{3.3\sigma}{S} \quad (3.1)$$

$$LOD = \frac{3.3\sigma}{S} \quad (3.2)$$

where, σ = standard deviation of FI of analyte and S = mean slope of the calibration curves (n = 6).

3.3.3.3.3 Accuracy and precision

Accuracy and precision of the developed method were determined using three quality control (QC) concentrations. QC samples at three concentration levels- lower QC (LQC; 375 ng/mL), medium QC (MQC; 1300 ng/mL) and higher QC (HQC; 2350 ng/mL) were prepared by appropriately diluting the working standard solution with the phosphate buffer (pH 6.4). Six

replicates of each QC sample were used for checking the accuracy of the developed method and the result was represented as % recovery. Inter-day and intra-day precision studies were performed using all three QC samples and the intermediate precision data was represented as % RSD. For the inter-day precision study, QC samples were analyzed on three subsequent days whereas, the intra-day precision study was performed three times in a single day for all three QC samples. All the samples were analyzed in triplicate.

3.3.3.3.4 Robustness

Robustness of the method was assessed by analyzing all three QC samples by introducing intentional minor variations in experimental conditions such as a change in pH of buffer (± 0.5) and sample temperature (± 0.5 min of heating). Percent recovery was calculated for each standard QC sample.

3.3.3.3.5 Specificity

Specificity of the developed method was evaluated using blank Lecithin-chitosan nanoparticles (LCNP). A dispersion of blank LCNP were prepared using all the excipients (Soya lecithin, MMW Ch, P-188, acetic acid glacial) except the drug. A known concentration of RTG solution (10 μg/mL) was spiked to the dispersion and vigorously vortexed. From the mixture, 1 mL aliquot was withdrawn and RTG was extracted using ACN (up to 10 mL). After complete extraction of the drug, samples were filtered through 0.22 μm membrane filter and appropriately diluted. All the samples were analyzed in triplicate to determine the specificity of the developed method [15].

3.3.4 Results and discussion

3.3.4.1 Effect of pH

FI of pure RTG was found to be highly dependent on pH of the buffer as shown in **Figure 3.1**. The study shows that increase in pH from pH 3 – 8 results in a decrease in FI of the pure drug. A sharp decrease in the FI from pH 3 – 5 and a slight change in FI can be observed between pH 5 – 6. Again, FI of RTG started to decrease with an increase in pH of buffer in the range of pH 6 – 8. This result could be attributed to the change in ionization of drug with the change in pH of buffer solution (pKa values; 10.77, 8.93) [16,17]. Although RTG exhibited maximum FI at pH 3 but, the method is developed at phosphate buffer pH 6.4 as pH of nasal cavity is reported to be 5.5 - 6.5 [18]. The primary objective of developing this method is to employ it in the future for *in vitro* release and *ex vivo* nasal permeation studies of the prepared intranasal (i.n.) RTG-loaded LCNP.

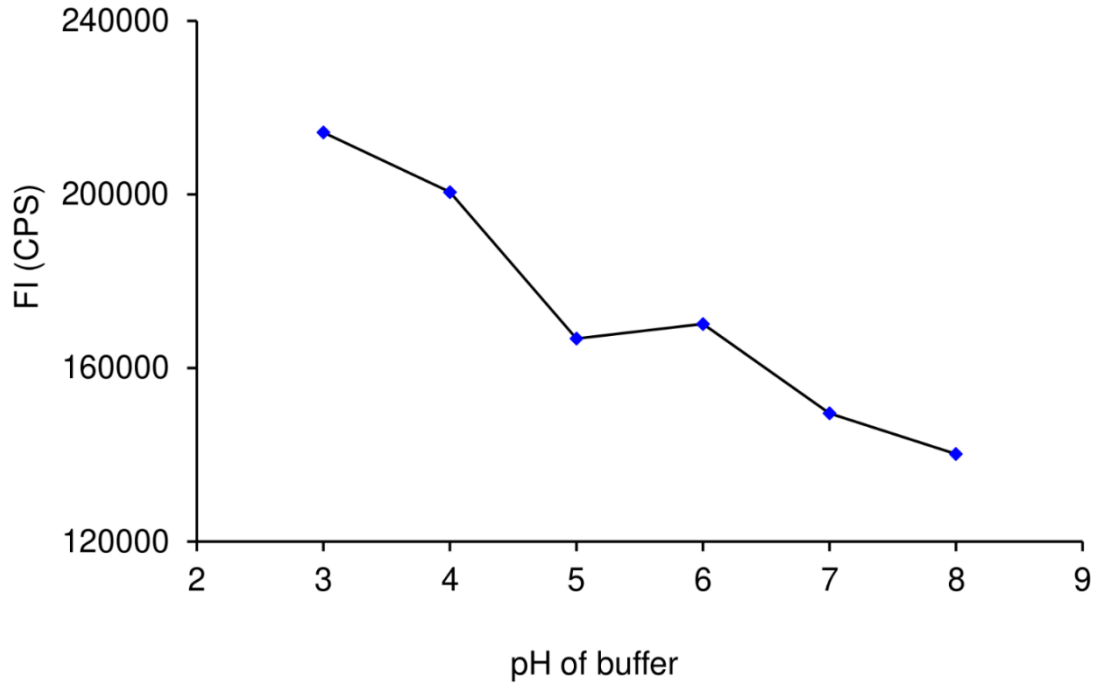

Figure 3.1 Effect of pH on FI of pure RTG (750 ng/mL)

3.3.4.2 Method development and validation

RTG is reported to be insoluble in water but freely soluble in ethanol and ACN [4,19]. To effectively apply the proposed method in the characterization of i.n. formulation, the method was developed in phosphate buffer pH 6.4 (nasal pH 5.5 – 5.6) [18]. RTG was found to exhibit emission maxima (λ_{em}) at 298 nm after excitation at 277 nm (λ_{ex}). A fluorescence contour plot and an excitation-emission spectrum of the drug (750 ng/mL) in phosphate buffer pH 6.4 are shown in **Figure 3.2** (A) and (B) respectively.

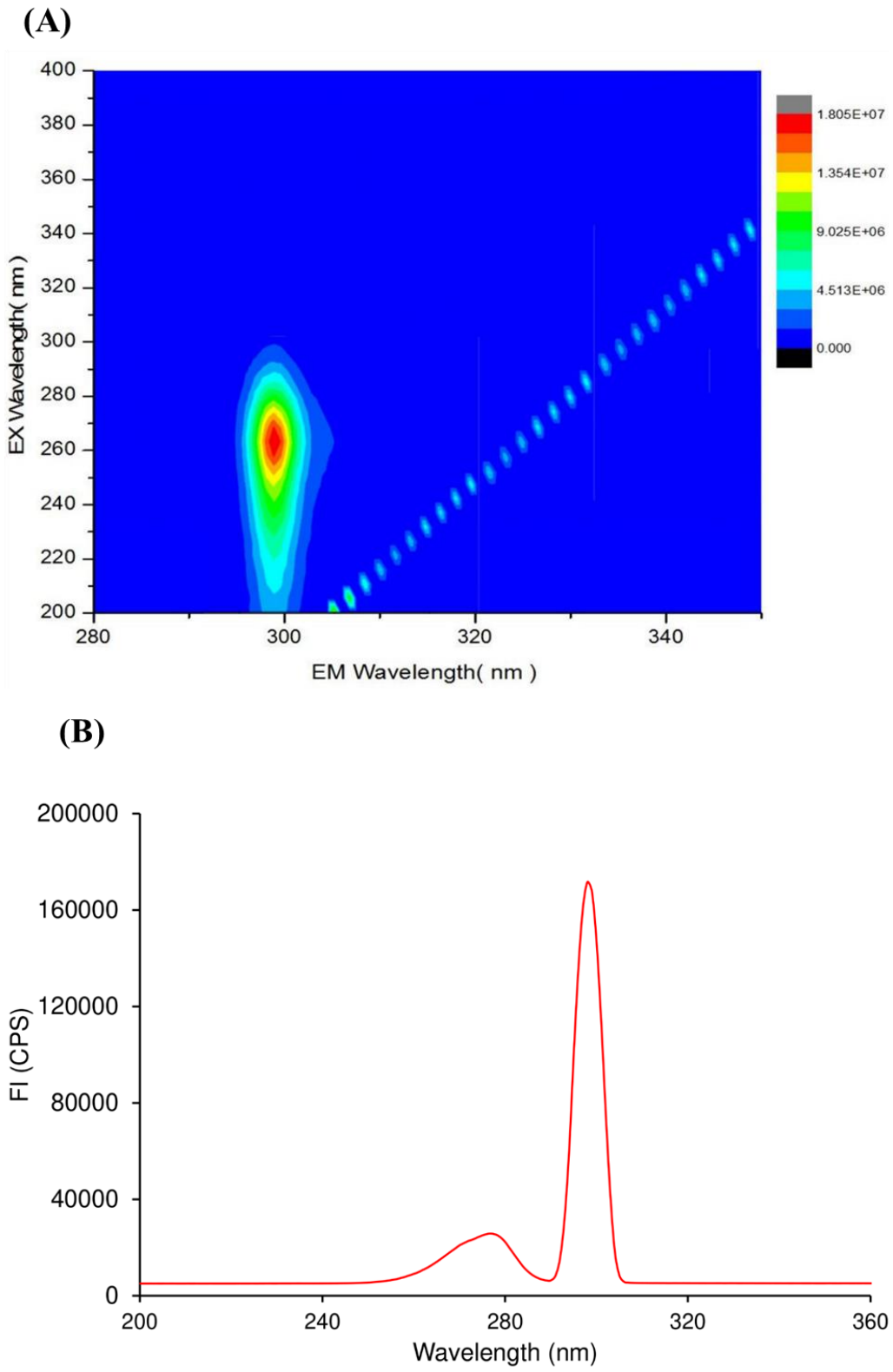

Figure 3.2 (A) Contour plot for excitation and emission wavelengths of RTG (750 ng/mL), (B) Excitation and emission spectra of RTG (750 ng/ml)

3.3.4.2.1 Calibration curve, linearity, and range

Calibration curve **Figure 3.3A** plotted using six standard concentrations was found to be linear over the range of 250 – 2500 ng/mL with a correlation coefficient (R^2) value of 0.9995. Upon statistical evaluation of the calibration curve, the Adjusted R^2 value was found to be 0.9994 which indicates that fit of the model is good. F-calculated (7863.91) value was observed to be significantly higher than that of F-critical (5.19), at a p-value of 0.000000969 which implies that regression is significant between FI and concentrations of the analyte. An overlay of fluorescence emission spectra of different calibration curve points along with the blank is presented in **Figure 3.3B**. The statistical data of regression equations are expressed as mean ± SD (**Table 3.2**). All the validation parameters of the developed method are illustrated in **Table 3.2**.

Table 3.2 Analytical parameters and statistical data of the regression equations (n = 6) attained from the developed fluorescence-based method

Parameters	**Developed method**
Excitation wavelength (nm)	277
Emission wavelength (nm)	298
Linear range (ng/mL)	250 - 2500
Correlation coefficient (R)	0.9997
Determination coefficient (R^2)	0.9995
Adjusted R^2 (R^2 adj)	0.9994
Slope ± SD	146.75 ± 1.47
Intercept ± SD	55719.6 ± 1612.03
LOD (ng/mL)	36.25
LOQ (ng/mL)	109.85

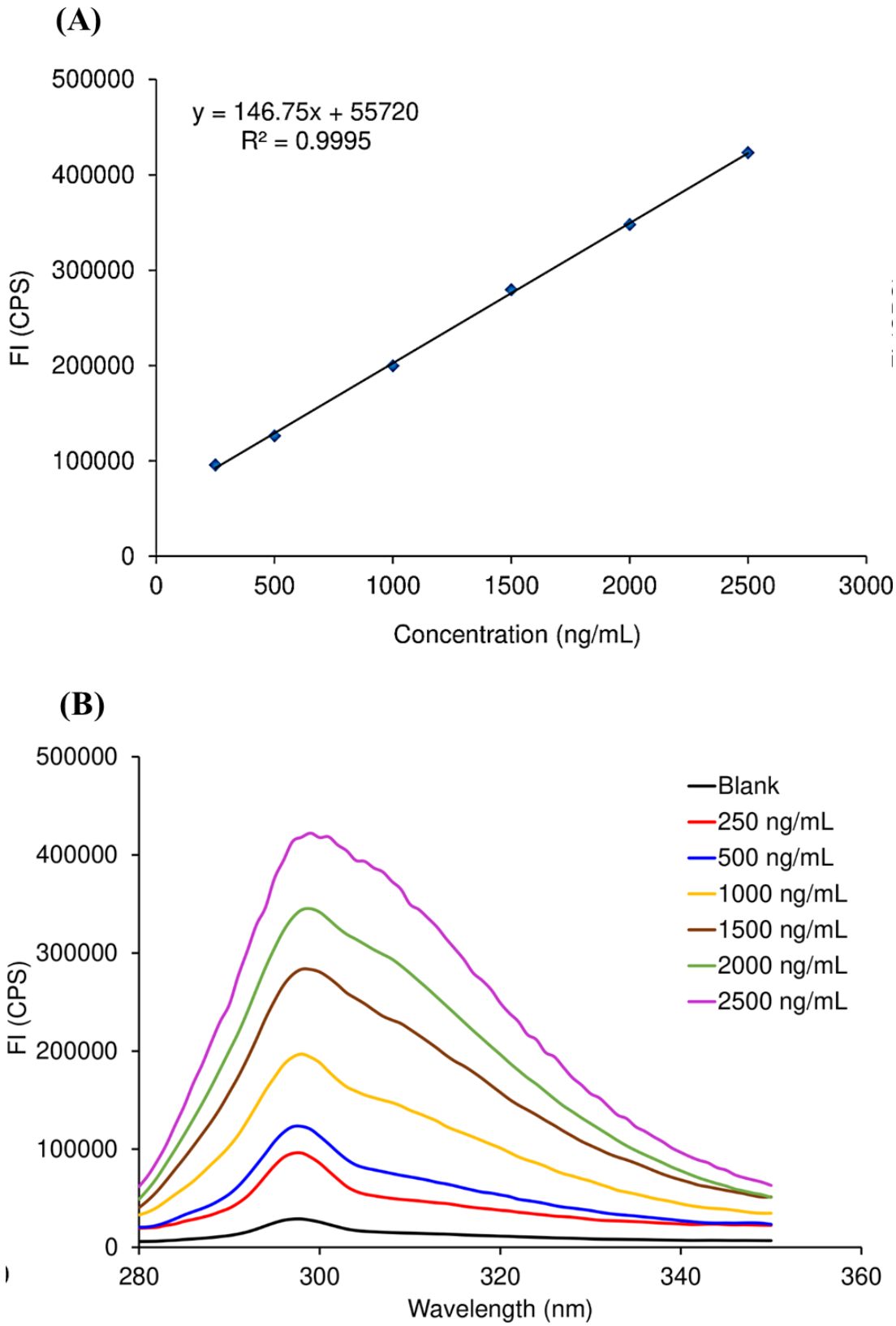

Figure 3.3 (A) Linearity plot of RTG in pH 6.4 phosphate buffer by Fluorescence-based method, (B) Overlaid spectra of blank and calibration curve points

3.3.4.2.2 Sensitivity

LOD and LOQ were determined by applying the equations given in ICH guidelines Q2(R1) [14]. The LOD and LOQ values calculated using Equations 3.1 and 3.2 were found to be 36.25 ng/mL and 109.85 ng/mL respectively. These results indicate that the developed analytical method is very sensitive.

3.3.4.2.3 Accuracy and precision

Accuracy of the developed method was determined using three QC concentrations (LQC, MQC and HQC), and the results are represented as % recovery in **Table 3.3**. Percentage recovery for all the three QC concentrations was observed to be within a range of 99.72% to 102.04%. The high values of percentage recoveries along with % RSD lower than 0.5% indicate that the developed method is highly accurate. Inter and intra-day precision data are shown in **Table 3.4**. In inter-day precision study, % RSD values for all three QC samples were found in a range of 0.28 to 1.33 and in intra-day precision study, % RSD values were observed in a range of 0.73 to 1.98. The intermediate (inter and intra-day) precision data was found to be in accordance with the ICH guidelines (% RSD < 2%) and the results confirmed that developed analytical method possesses good repeatability and reliability as well.

Table 3.3 Accuracy of the developed fluorescence-based method at three concentration levels within the linear range

QC levels [a]	**Predicted concentration** [b]			**% recovery Mean ± SD**	**% Bias**
	Range	**Mean ± SD**	**% RSD**		
LQC	373.98 - 378.41	376.68 ± 1.46	0.39	100.45 ± 0.39	0.45
MQC	1301.95 - 1317.28	1307.95 ± 6.14	0.47	100.61 ± 0.47	0.61
HQC	2380.11 - 2391.96	2383.89 ± 7.02	0.29	101.44 ± 0.29	1.44

Standard deviation (SD), % relative standard deviation (% RSD), n = 6 samples in all cases.
[a] LQC, MQC, HQC are 375, 1300, 2375 ng/mL of RTG
[b] Predicted concentrations of RTG were calculated using linear average regression equation, given in ng/mL

Table 3.4 Inter-day and intra-day precisions for the fluorescence-based method

QC levels [a]	Inter-day precision (n = 3)			Intra-day precision (n = 3)		
	Measured concentrations [b]	SD	% RSD	Measured concentrations [b]	SD	% RSD
LQC	384.18	5.12	1.33	377.35	6.08	1.61
MQC	1325.43	11.12	0.84	1271.83	25.15	1.98
HQC	2330.33	6.58	0.28	2361.33	17.17	0.73

Standard deviation (SD), % relative standard deviation (% RSD)
[a] LQC, MQC, HQC are 375, 1300, 2375 ng/mL of RTG, [b] Measured concentrations of RTG were calculated using linear average regression equation, given in ng/mL

3.3.4.2.4 Robustness

Results of the robustness study are presented as % recovery in **Table 3.5**. It was found that the effect of slight changes in experimental conditions on FI of the drug was not significant and % recovery for all three QC concentrations was obtained within a range of 99.22% to 101.94%. The results were found to be in good agreement with the ICH guidelines Q2(R1) [14]. As deliberate changes could not affect the method parameters hence, it can be concluded that the developed method is desirably robust.

3.3.4.2.5 Specificity

Specificity of the developed method was evaluated using blank LCNP. The amount recovered from blank NP formulation was 99.25 ± 0.28% (n = 3). The result demonstrates that the method is specific for quantification of the drug and there is no interference of excipients used in the preparation of LCNP on the FI of pure RTG.

3.4 Method II: RP-HPLC analytical method for quantification of RTG in aqueous samples

3.4.1 Materials

Emplura® grade o-phosphoric acid 85% (OPA) and ethanol were purchased from Merck (Mumbai, India). Hydrogen peroxide (H_2O_2) was purchased from SISCO Research Laboratories (SRL) Pvt. Ltd (Delhi, India). Three different molar concentration of buffers were prepared by dissolving weighed amount of KH_2PO_4 in Mili-Q water and pH of buffers were adjusted using 0.1 (N) OPA. HPLC grade acetonitrile (ACN) and methanol (MeOH) were purchased from Merck (Mumbai, India). Glipizide, internal standard for bioanalytical method was purchased from TCI Chemicals Pvt Ltd. (Chennai, India).

3.4.2 Instrument

The HPLC system (LC-2010CHT, Shimadzu Corporation, Japan) comprised of pulse-free solvent system delivering two pumps, 5-line degasser, block heating type column oven, sample cooler, intelligent auto-sampler with UV-visible detector of dual-wavelength was used for the study. The software used was LC solution, version 1.6.

3.4.3 Chromatographic conditions

Hypersil BDS-C18 column, (250 mm × 4.6 mm, 5 µ) purchased from Agilent (Mumbai, India) was used for the chromatographic separation. In the optimized method, a ratio of 54:46% v/v of ACN and 10 mM KH_2PO_4 buffer (pH 5.0) was used as the mobile phase in isocratic mode at a flow rate of 0.65 mL/min. UV detection wavelength used was 226 nm and injection volume of the samples was 20 µL. The column and auto-sampler temperature were set at 25 ^oC during the entire analysis.

3.4.4 Methods

3.4.4.1 Preparation of stock solution, calibration curve standards, and quality control (QC) samples

RTG stock solution of 1 mg/mL was prepared in ACN and stepwise diluted using the mobile phase to get a working standard solution of 500 ng/mL for both screening and optimization studies. For preparing calibration curve standards of RTG, 1 µg/mL working standard solution was stepwise diluted to get 25, 50, 100, 200, 400, and 600 ng/mL solutions using the mobile phase. The QC samples of three concentration levels- lower QC (LQC; 30 ng/mL), medium QC (MQC; 150 ng/mL), and higher QC (HQC; 510 ng/mL) were prepared from 1 µg/mL working standard solution. Before analysis, all the samples were filtered through a 0.45 µm Millipore™ membrane filter.

3.4.4.2 Experimental design

3.4.4.2.1 Preliminary study

Preliminary study was performed using one factor at a time approach (OFAT) to select the type of organic solvent used in the mobile phase. MeOH and ACN were studied to select the suitable solvent. Peak parameters like peak area, tailing factor (10%), number of theoretical plates (N), and height equivalent to theoretical plate (HETP) were evaluated to select the appropriate organic solvent for further studies.

3.4.4.2.2 Factor screening study

Screening study was performed employing Plackett-Burman design (PBD) for the selection of critical method variables (CMVs) for the RP-HPLC method of RTG. PBD is a screening design which helps to analyse a large number of variables more economically using lesser number of runs as compared to other screening design like 2^k fractional design, Taguchi design etc. The

design involved 12 experimental runs, help to find the CMVs from 7 independent method variables like ACN proportion (% v/v), flow rate (mL/min), pH of buffer, the molarity of buffer (mM), column temperature (^oC), injection volume (µL) and detection wavelength (nm) and study their effect on two responses namely the number of theoretical plates (N), response 1 (R_1) and retention time (min), response 2 (R_2). The respective values of two levels of all 7 independent variables are shown in **Table 3.5**. All 12 experiments, as shown in **Table 3.6** were suggested by the Design-Expert® Software (Version 8.1, Stat-Ease, USA).

Table 3.5 List of the analytical method variables and their levels employed for Plackett-Burman design

Name of method variables studied		**Levels**	
		High	**Low**
		(+1)	**(–1)**
ACN proportion	(%)	55	45
pH of buffer		5.0	3.0
Flow rate	(mL/min)	0.80	0.50
Molarity of buffer	(mM)	10	5
Column temperature	(^oC)	30	25
Injection volume	(µL)	20	40
Detection wavelength	(nm)	230	226

Table 3.6 Plackett-Burman design matrix for screening of various independent variables for RP-HPLC analytical method

Run[a]	ACN proportion (% v/v)	pH of buffer	Flow Rate (mL/min)	Molarity of buffer (mM)	Column Temperature (ºC)	Injection Volume (µL)	Detection Wavelength (nm)
1	55	3.0	0.50	5	30	20	230
2	45	3.0	0.50	5	25	20	226
3	45	3.0	0.50	10	25	40	230
4	45	5.0	0.50	10	30	20	230
5	55	5.0	0.80	5	25	20	230
6	55	5.0	0.50	10	30	40	226
7	55	5.0	0.80	10	25	20	226
8	45	5.0	0.80	5	30	40	230
9	55	5.0	0.50	5	25	40	226
10	45	3.0	0.80	5	30	40	226
11	55	3.0	0.80	10	25	40	230
12	55	3.0	0.80	10	30	20	226

[a] The run order is allocated randomly by DoE software

3.4.4.2.3 Optimization study

Three CMVs were identified on the basis of results obtained from the factor screening study, which were affecting both the responses (R_1 and R_2) and taken up for further optimization using Box-Behnken design (BBD). BBD is a three-level optimization design that provides significant optimization information in comparison to other three-level optimization designs like full factorial design, central composite design, etc. using fewer resources and less number of experimental runs. In this study, BBD was employed using Design-Expert® Software for optimization of CMVs, i.e. Factor A: ACN proportion, Factor B: pH of the buffer, and Factor C: flow rate. CMVs were investigated at three levels represented high as (+1), middle as (0), and low as (−1). Respective values of three CMVs are presented in **Table 3.7**. The experiments were executed in randomized order and in a single block with a total number of 17 runs that comprised of 5 center point runs (**Table 3.8**). After performing all the experiments, obtained data was found to be best fitted in the second-order polynomial equation for both the responses. The quadratic model polynomial equation is as follows:

$$R_i = b_0 + b_1A + b_2B + b_3C + b_4AB + b_5BC + b_6CA + b_7A^2 + b_8B^2 + b_9C^2 \qquad (3.3)$$

where, R_i = responses; b_0 = intercept; b_i (i = 1, 2, 3…n) = coefficients of individual linear, quadratic, and cubic effects along with their interactions; A, B, C = CMVs of the design.

3.4.4.2.4 Statistical analysis of data

Data obtained from all the experimental results were represented as mean ± SD (n = 3). Statistical analysis of data was performed at a 5% level of significance (α = 0.05). In PBD, t-calculated value for the magnitude of each of the variables was compared with Bonferroni limits and t-critical value for identification of the significant term. In BBD, P-value for each of the terms involved in the model was determined and finally used to select the significant terms.

Table 3.7 Box-Behnken design matrix for optimization of various CMVs for RP-HPLC analytical method

Run [a]	A	B	C
	ACN proportion (% v/v)	pH of buffer	Flow rate (mL/min)
1	50	4.0	0.65
2	50	4.0	0.65
3	50	4.0	0.65
4	45	3.0	0.65
5	50	5.0	0.80
6	50	4.0	0.65
7	45	4.0	0.80
8	50	5.0	0.80
9	50	3.0	0.50
10	50	3.0	0.80
11	45	5.0	0.65
12	45	4.0	0.50
13	55	3.0	0.65
14	55	4.0	0.80
15	55	5.0	0.65
16	50	4.0	0.65
17	55	4.0	0.50

[a] Run order is allocated randomly by DoE software

3.4.4.2.5 Desirability function and validation run

Desirability function was used to achieve the best favorable conditions for both the responses. Desirability function for R_1, number of theoretical plates (N), was set between a range of 10,000 – 12,000 , whereas, in the case of R_2, retention time (min), was set within a range of 6 – 8 min (**Table 3.8**). Experimental conditions extending the highest desirability function using above mentioned constraints were selected for the validation run. Validation run was performed in triplicate and experimental results were compared with the predicted values given by the model.

Table 3.8 List of CMVs and their levels employed for Box-Behnken design for RP-HPLC analytical method

Name of critical method variables studied	**Levels**		
	High	**Medium**	**Low**
	(+1)	**(0)**	**(–1)**
ACN proportion (% v/v)	55	50	45
pH of buffer	5.0	4.0	3.0
Flow rate (min)	0.80	0.65	0.50
Responses	**Constrain**		
Number of theoretical plates (N)	10,000 - 12,000		
Retention time (min)	6 - 8		

3.4.4.3 *Method validation*

Method development and validation were executed as per the recommended guidelines of the ICH referred in Q2 (R1) [20].

3.4.4.3.1 System suitability study

System suitability test was implemented to confirm the suitability of chromatographic system for the anticipated analysis. Six replicate of a standard solution of RTG (500 ng/mL) were injected into the HPLC and variations in retention time (min), tailing factor (10%), N, and HETP were presented in terms of % RSD of respective parameters.

3.4.4.3.2 Specificity

Specificity of the method was determined by spiking a standard solution of RTG (500 ng/mL) into the solution of excipients used for preparation of nanocrystals and the components of dissolution media as well. Chromatograms of both samples were studied for the presence of interfering peaks corresponding to RTG. Furthermore, forced degradation studies were performed to evaluate the stability-indicating property of the developed RP-HPLC method. For this, RTG was exposed to acid, alkali, oxidation, and thermal degradation. Briefly, RTG stock solution was first prepared by simply dissolving 5 mg of RTG in 10 mL solvent [i.e., ACN and Mili-Q® water 50:50% v/v]. For acid degradation, 1 mL of 2 (N) HCl was added into 1 mL of RTG stock solution and refluxed for 8 h. Similarly, for alkali and oxidative degradation, 1mL of 2 (N) NaOH and 1 mL of 30% v/v H_2O_2 were added separately into 1 mL of RTG stock solution and the resultant solutions were refluxed for 2 h and 8 h respectively. All the above-mentioned degradation studies were performed at 60 ^oC. For solid-state degradation study, 5 mg of the pure drug was kept under ultraviolet (UV) radiation for 48 h, and analyzed by RP-HPLC after dissolving 1 mg of it in 1 mL ACN and further appropriately diluting the stock solution with mobile phase [7]. All the exposed samples were analyzed for degradation peaks using the developed RP-HPLC method.

3.4.4.3.3 Calibration curve, linearity, and range

Calibration curve (n = 6) plot of peak area versus concentration of RTG was constructed by using six different drug concentrations in a range of 25 – 600 ng/mL and the linearity of the method was estimated. Linearity can be defined as the ability of a specific method to produce test results that are directly proportional to the drug concentration within a particular range.

3.4.4.3.4 Accuracy and precision

Method accuracy was determined using the QC concentrations (LQC, MQC, and HQC) and results are articulated as % recovery. Precision of the method was also estimated, and results are expressed as % RSD. Intra-day and inter-day precision studies were conducted by evaluating three QC concentrations (in triplicate) at three different times of a day and, in three successive days respectively.

3.4.4.3.5 Robustness

Robustness of the method was assessed by analyzing the QC samples by introducing intentional variation in chromatographic conditions such as pH of buffer (± 0.5), flow rate (± 0.2 mL/min), column temperature (± 5 ^{o}C) and performing the study at a different HPLC instrument (HPLC 2: Shimadzu Corporation, Japan; comprised of LC 20AD pump, DGU-20ASR degasser, SIL-20AC HT column oven, SPD-20A UV detector of dual-wavelength). Percent recovery was evaluated as a chromatographic response for each variation with respect to the standard QC samples.

3.4.4.3.6 Sensitivity

LOD and LOQ can be used to describe the sensitivity of the analytical method. LOD and LOQ were determined using the standard deviation of y-intercept and the mean of slope of all six calibration curves. Equations used for the determination of LOD and LOQ are as described in **Section 3.3.3.3.2**.

3.4.4.3.7 Stability studies

The solution state stability of RTG was carried out in different storage conditions such as atmospheric temperature (benchtop stability; 24 h), at auto-sampler stability (25 ^{o}C; 24 h), short-term (4 ^{o}C; 7 days), and long-term stability (–20 ^{o}C; 1 month). QC samples kept for

stability were compared with freshly prepared QC solutions on the aforementioned time points to test the stability of RTG solutions.

3.4.5 Results and discussion

3.4.5.1 Experimental design

3.4.5.1.1 Preliminary study

Peak parameters evaluated for the selection of organic solvents are shown in **Table 3.9**. Among the two organic solvents, ACN yielded better peak parameters like peak area, N, tailing factor (10%), and HETP. Therefore, ACN was selected as the organic solvent in the further study.

Table 3.9 Comparison of peak parameters for selection of organic solvent

Parameters	MeOH	ACN
Peak Area (mV*min)	29560	36664
Tailing factor (10%)	1.121	1.001
Number of theoretical plates (N)	6645	9161
Height equivalent to theoretical plate (HETP)	22.57	14.37

3.4.5.1.2 Factor screening study

The influence of each independent method variable on the responses (R_1 and R_2) as obtained from PBD is shown in respective Pareto charts, **Figure 3.4A** for the number of theoretical plates (N) and **Figure 3.4B** for retention time (min) depict that t-value for ACN proportion, pH of buffer and flow rate is significantly higher than Bonferroni limits and t-critical value which indicates that these three independent method variables are critical amongst all method variables screened using PBD. Henceforth, these three were selected as CMVs for the analytical method and further used for optimization study.

3.4.5.1.3 Optimization study

As discussed in **Section 3.4.4.2.3**, the suggested 17 runs were performed, and the respective values of R_1 and R_2 are presented in **Table 3.10**. Statistically assessed data and fit of the model for the number of theoretical plates (N) and retention time (min) are given in **Table 3.11**. F-value obtained for the quadratic model related to the number of theoretical plates (N), with model F-calculated value (258.35) was found to be significant ($p < 0.0001$). Similarly, the F-value for quadratic model related to retention time (min), with model F-calculated value (12420.29) was also found to be significant ($p < 0.0001$) demonstrating that both the models were highly significant for the respective responses. A High predicted R^2 (R^2 pred) value is regarded as an indicator of a high degree of predictability of any model. The R^2 pred values for response R_1 and response R_2 were found to be 0.97520 and 0.99901, respectively. In addition, the 'lack of fit' value relating to the number of theoretical plates (F-value = 11.81, P-value = 0.0159) and retention time (F-value = 173.26, P-value = 0.0001), for both regression models were found to be statistically insignificant (P-value < 0.05) which further indicated that the acquired models are suitable in predicting the responses. P-value is used to determine the significance of each coefficient. The terms showing P-value < 0.05 were significant and incorporated in the model equation. The model equation for R_1 (number of theoretical plates) and R_2 (retention time) in terms of coded factors are given below in Equation 3.4 and 3.5, respectively:

$$R_1 = 9895.434 - 1603.207A + 626.381B - 1061.304C + 408.730A^2 + 470.679B^2 + \quad (3.4)$$

$$R_2 = 6.879 - 1.468A + 0.728B - 1.730C - 0.175AB + 0.312AC - 0.148BC + 0.292A^2 + 0.343B^2 + 0.414C^2 \quad (3.5)$$

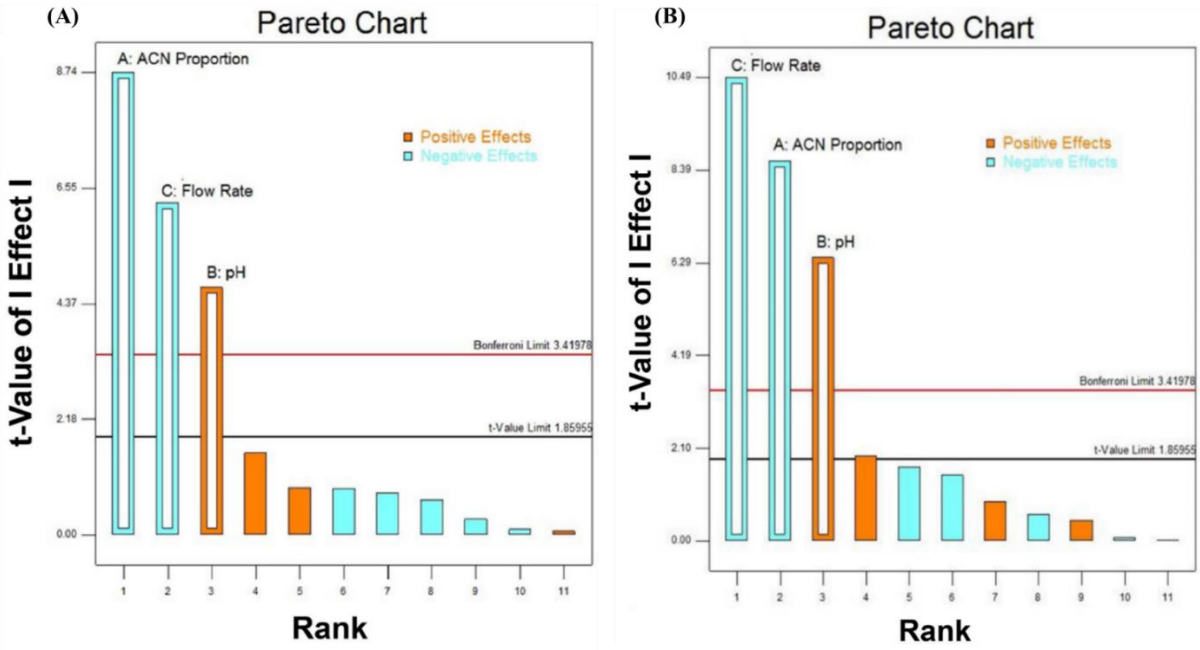

Figure 3.4 Pareto charts representing the influence of various independent variables critically on the selected responses, (A) number of theoretical plates (N) and (B) retention time (min)

Table 3.10 Experimental responses obtained for runs given by Box-Behnken design

Run [a]	Number of theoretical plates (N)	Retention time (min)
1	9,842	6.88
2	9,919	6.87
3	9,931	6.87
4	11,511	8.08
5	12,299	10.21
6	9,831	6.88
7	11,382	7.01
8	10,503	6.46
9	11.404	8.51
10	9,144	5.35
11	13,027	9.90
12	13,593	11.09
13	8,660	5.48
14	7,951	4.71
15	9,901	6.60
16	9,954	6.88
17	10,176	7.55

[a] Run order is allocated randomly by DoE software

Table 3.11 Regression coefficients and statistical analysis for Box-Behnken design matrix for analytical method

Response model	Factor	Factor coefficient	P value	Adj R^2	Pred R^2	Lack of fit	Model F-value
R_1: Number of theoretical plates (Quadratic model)	Intercept	9895.434	0.0001	0.98974	0.97520	F-value =11.81	258.35
	A- ACN proportion	-1603.207	0.0001				
	B- pH of buffer	626.381	0.0001				
	C- Flow rate	-1061.304	0.0001			P-value = 0.0159	(P < 0.0001)
	A^2	408.730	0.0002				
	B^2	470.679	0.0001				
	C^2	471.290	0.0001				
R_2: Retention time (Quadratic model)	Intercept	6.879	0.0001	0.99986	0.99901	F-value =173.26	12420.29
	A- ACN proportion	-1.468	0.0001				
	B- pH of buffer	0.728	0.0001				
	C- Flow rate	-1.730	0.0001				
	AB	-0.175	0.0001				
	AC	0.3121	0.0001			P-value = 0.0001	(P < 0.0001)
	BC	-0.148	0.0001				
	A^2	0.292	0.0001				
	B^2	0.343	0.0001				
	C^2	0.414	0.0001				

3.4.5.1.4 Response surface plots

3D-response surface plots **Figure 3.5** (**A** – **F**) were utilized for understanding the relationship between the variables and responses. Response surface plot **Figure 3.5A** showed that increase in pH of buffer led to an increase in number of theoretical plates. This could be a result of higher ionization of RTG in high pH, which might improve the diffusion coefficient of RTG in buffer proportion of the mobile phase [21,22]. As per **Figure 3.5A** and **B**, an increase in ACN proportion in the mobile phase has caused decrease in the number of theoretical plates. This result might be attributed to a fact that, an increase in the proportion of ACN causes reduction in ionization and diffusion coefficient of the hydrophobic drug in buffer portion of

the mobile phase which eventually leads into decrease in the number of theoretical plates [21]. **Figure 3.5** (**B** and **C**) illustrated that increase in flow rate has caused in decrease in the number of theoretical plates. This could be attributed to the lower interaction of RTG with the stationary phase, which has finally resulted in compromised separation quality.

3D-response surface plots **Figure 3.5** (**D** – **F**) showed the effect of CMVs on retention time. **Figure 3.5** (**D** and **E**) indicated that an increase in ACN proportion had caused a sharp decrease in retention time which could be linked to higher solubility of the drug in ACN than to the buffer. **Figure 3.5** (**E** and **F**) depicted that increase in flow rate has significantly reduced the retention time. This result might be attributed to lipophilic nature of RTG which causes higher affinity of RTG towards the mobile phase as compared to the stationary phase and finally resulted in faster elution [23]. **Figure 3.5D** and **Figure 3.5F** depicted that the pH of buffer has a negligible effect on retention time.

3.4.5.1.5 Determination of optimized method and its validation

Depending on the constraints defined in **Section 3.4.4.2.5** for the number of theoretical plates (R_1) and retention time (R_2), a high desirability function (1.000) was obtained for optimized RP-HPLC analytical method. Optimum conditions found for CMVs using DoE model were- factor A (ACN proportion): 54% v/v; factor B (pH of buffer): 5.0; factor C (flow rate): 0.65 mL/min and the responses were- number of theoretical plates (R_1): 10,023 and retention time (R_2): 7.01 min. Applying above-mentioned chromatographic conditions, three experiments were performed and the respective responses for R_1 and R_2 were obtained. The experimental results were compared with the predicted results given by model using unpaired t-test for the model validity. Statistical analysis indicated that experimental mean values and standard error values were not statistically different (P-value < 0.05) from predicted values of both the responses.

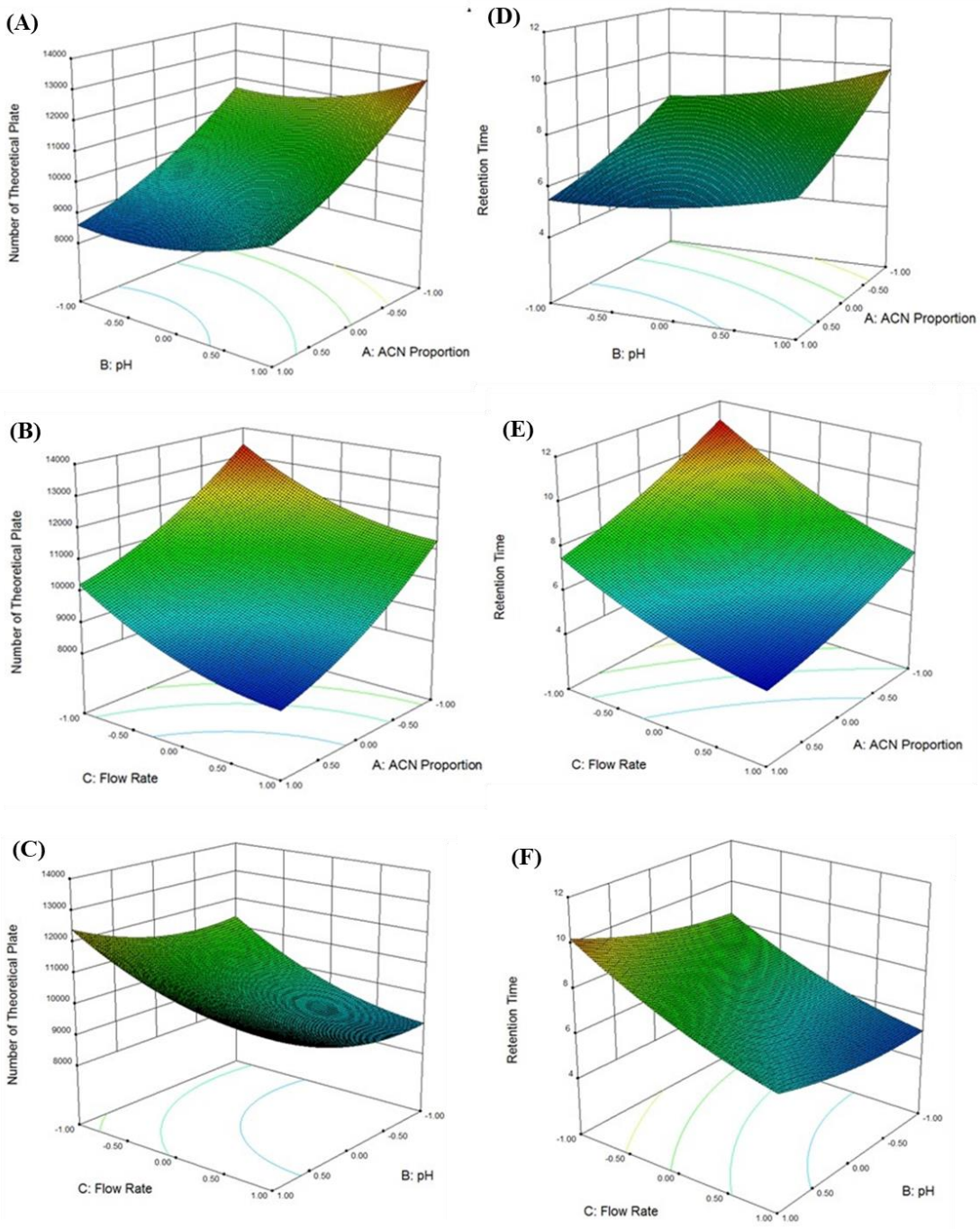

Figure 3.5 3D-response surface plots showing the impact of CMVs *viz.*, Acetonitrile proportion (factor A), pH of buffer (factor B), and flow rate (factor C) on (R_1) number of theoretical plates (A, B, and C) and on (R_2) retention time (D, E, and F).

3.4.5.2 Method Validation

3.4.5.2.1 System suitability study

Peak area and retention time for 500 ng/mL of RTG were found to be 42101 ± 312.23 mV*min and 7.65 ± 0.09 min, respectively. Results of all the chromatographic parameters i.e. tailing factor (10%), HETP, N, and retention factor (k) are expressed as % RSD and given in Supporting Information **Table 3.12**. % RSD for all the parameters was found to be less than 2%. Furthermore, the values for tailing factor (10%), k, and N also lie under the acceptance criteria of United States Pharmacopeia (< 1.2 and > 2000 respectively) for system suitability parameters.

Table 3.12 Results of system suitability parameters using RTG solution (500 ng/mL)

Parameters	Acceptance criteria	Mean	SD	% RSD
Peak Area (mV*min)	-	42101	312.23	0.74
Retention time (min)	-	7.65	0.09	0.81
Tailing factor (10%)	0.8 - 1.5	1.19	0.01	0.81
Retention factor	2 < k <10	2.14	0.01	0.52
Number of theoretical plates (N)	> 2000	11,206	0.03	1.36
HETP	-	13.26	0.19	1.43

Standard deviation (SD), % Relative standard deviation (% RSD); data represented for n = 6

3.4.5.2.2 Specificity

Absence of any other interfering peak of nanocrystals formulation excipients, dissolution media components, and degradants at the retention time of RTG (7.65 ± 0.09 min) in the chromatogram indicated the specificity of the developed RP-HPLC method **Figure 3.6** (**C – H**). Figure 2B represents the blank matrix chromatogram containing all the excipients (without drug) used in the preparation of NC. Absence of any peak in the particular chromatogram at retention time of drug illustrates specificity of the developed method. **Figure 3.6** (**C** and **D**) depicted that there is no additional peak present at the retention time of RTG when the drug is present with nanocrystals excipients and dissolution media components, respectively.

Furthermore, **Figure 3.6** (**E** – **H**) represented the chromatograms of RTG in different force degradation conditions. In **Figure 3.6E**, a well-separated acid degradant peak (7.16 ± 0.23 min) was observed along with RTG peak (7.79 ± 0.01 min) which corresponds to 28.09 ± 1.31% degradation of the pure drug. Alkali treatment led to a 15.53 ± 1.37% degradation of RTG, and the degradant of drug was eluted at 8.23 ± 0.02 min in **Figure 3.6F**. Oxidative stress treatment resulted in 60.04 ± 1.28% degradation of the pure drug, and a degradant peak was observed at 6.79 ± 0.25 min (**Figure 3.6G**). The acid, alkali, and oxidative degradant products might be regarded as rotigotine thienyl ether or thiophene rotigotine as per previously reported literature [7]. UV exposure of the drug for 48 h resulted in no additional peak suggesting high stability of RTG in the condition as shown in **Figure 3.6H**. Forced degradation studies demonstrated that the developed RP-HPLC method is significantly specific for estimation of RTG. Retention time and % recovery for RTG in different stress conditions are presented in **Table 3.13**.

Table 3.13 Assay of RTG solution (500 ng/mL) under different stress conditions

Stress Condition	**Sample treatment**	**Retention time of RTG (min)**	**Additional peaks (min)**	**% recovery [a]**
Reference	-	7.65 ± 0.09	No	99.97 ± 2.16
Acid treated	2 (N) HCl, 60 ^{o}C, 8 h	7.79 ± 0.01	Yes, 7.16 ± 0.23	71.06 ± 1.31
Alkali treated	2 (N) NaOH, 60 ^{o}C, 2 h	7.44 ± 0.14	Yes, 8.23 ± 0.02	84.44 ± 1.37
Oxidation	30 % H_2O_2, 60 ^{o}C, 8 h	7.88 ± 0.03	Yes, 6.79 ± 0.25	39.93 ± 1.28
UV light	48 h	7.44 ± 0.06	No	99.51 ± 1.59

[a] % recovery = [(Measured concentration / Actual concentration) × 100].

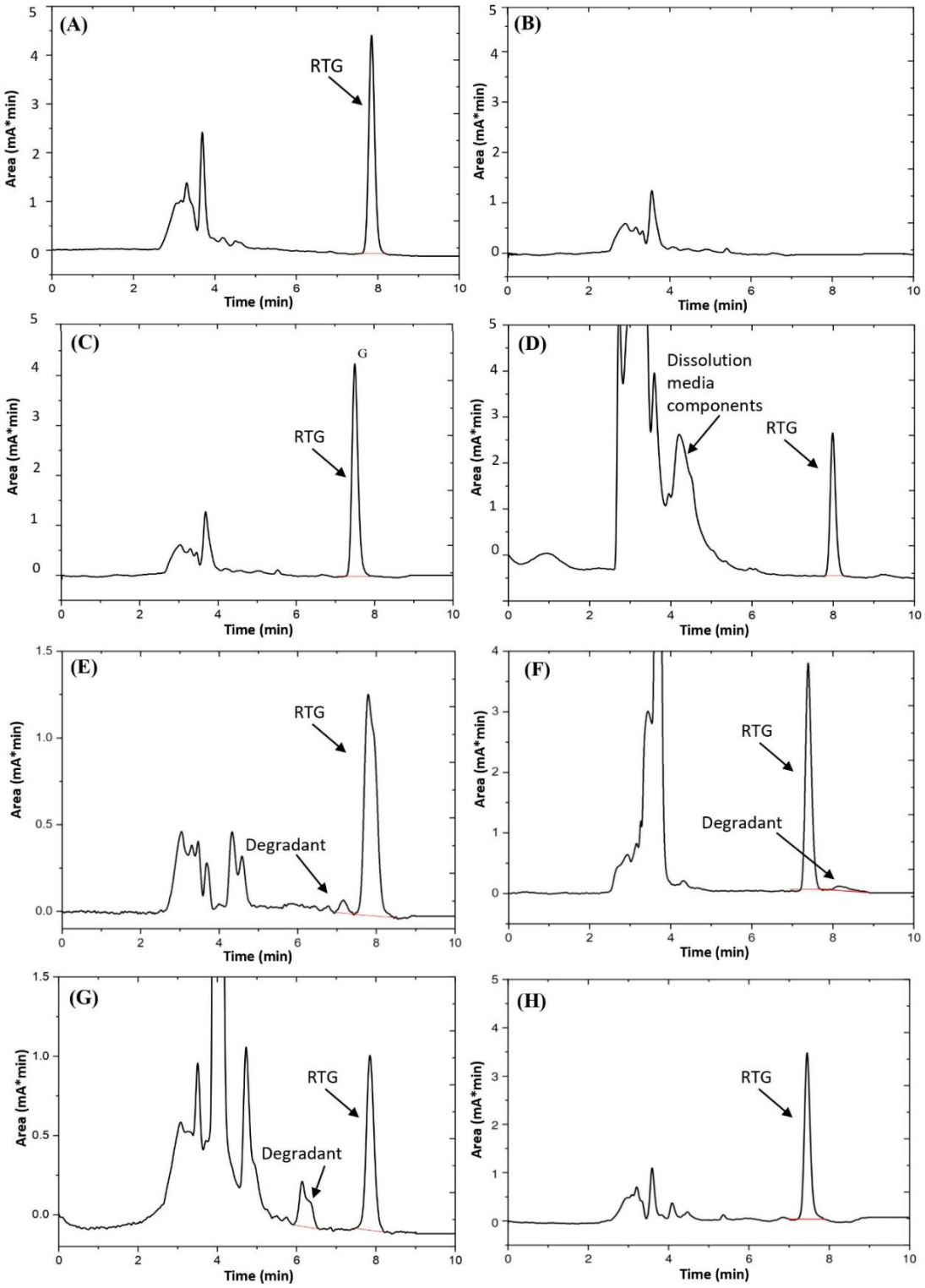

Figure 3.6 Chromatogram of (A) standard RTG (500 ng/mL), (B) Blank matrix of nanocrystals excipients, (C) RTG in presence of Nanocrystals excipients, (D) RTG in presence of dissolution media components, Chromatogram of RTG after degradation at (E) acidic pH for 8 h, (F) alkaline pH for 2 h, (G) H_2O_2 exposure for 8 h, (H) UV exposure for 48 h

3.4.5.2.3 Calibration curve, linearity, and range

All six calibration curves exhibited good linearity within the ranges of 25 – 600 ng/mL for RTG. The calibration curve points were 25, 50, 100, 200, 400, 600 ng/mL. Regression coefficient (R^2) for RTG over aforementioned range was found to be 0.9995 as shown in **Figure 3.7**. Following is the regression equation for RTG (n = 6):

$$y = 95.115x - 606.898 \quad (3.6)$$

where, y corresponds to the peak area for corresponding concentration (ng/mL). Statistical evaluation of the calibration curves yielded adjusted R^2 (R^2 adj) of 0.9994 which demonstrates that fit of model is good. F-calculated (8076.69) was found to be significantly higher than F-critical (4.95), at a P-value of 0.000000092. Result shows that the regression is significant between peak area and concentration.

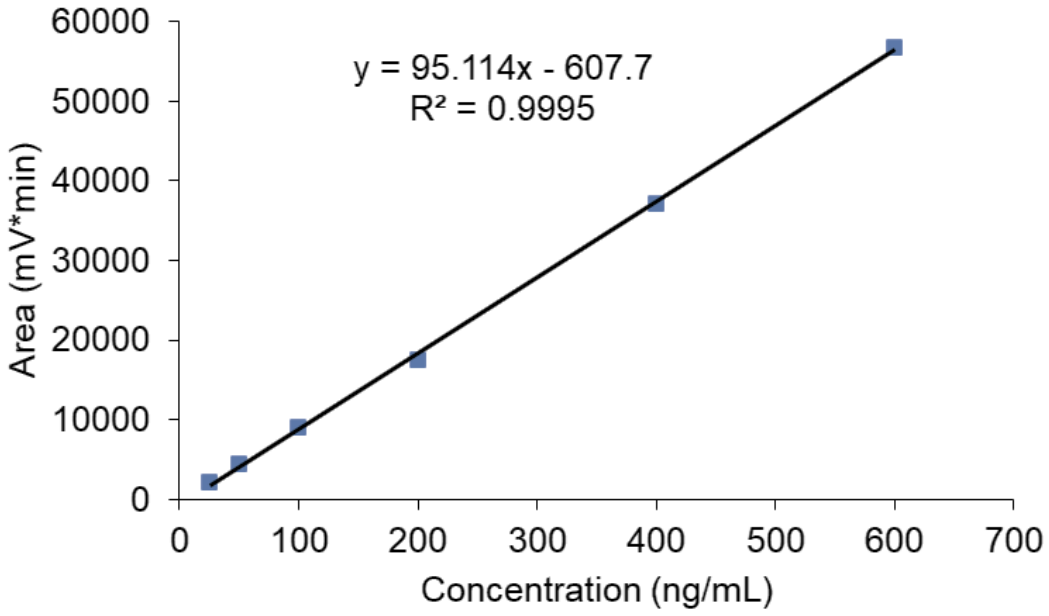

Figure 3.7 Calibration curve of RTG by RP-HPLC method

3.4.5.2.4 Accuracy and precision

Accuracy of the method was represented as overall % recovery for all three different concentrations at LQC, MQC, and HQC levels. For all these three concentrations, % recovery

was found to be ranged between 99.33 ± 0.57 to 100.93 ± 1.47% (**Table 3.14**). Precision data for all three QC samples are expressed as % RSD for both intra-day and inter-day and were observed to be less than 2% (**Table 3.15**). Both accuracy and precision data were found to be in agreement with ICH guidelines [14].

Table 3.14 Accuracy data of developed RP-HPLC analytical method for RTG

QC levels [a]	Measured concentration [b]			Mean accuracy [c]	%recovery [d]	
	Range	Mean ± SD	% RSD	% bias	Mean ± SD	% RSD
LQC	29.57-30.68	30.17 ± 0.38	1.25	0.58	100.58 ± 1.26	1.25
MQC	148.37-153.00	151.39 ± 2.20	1.45	0.93	100.93 ± 1.47	1.45
HQC	503.86-512.24	506.58 ± 2.88	0.57	-0.67	99.33 ± 0.57	0.57

Standard deviation (SD), % relative standard deviation (% RSD), n = 6 samples in all cases.
[a] LQC, MQC, and HQC are 30, 150, 510 ng/mL of RTG, [b] Measured concentrations of RTG were calculated by linear average regression equation, given in ng/mL, [c] Accuracy (% bias) = [(Measured concentration − Actual concentration)/Actual concentration × 100], [d] % recovery = [(Measured concentration / Actual concentration) × 100]

Table 3.15 Precision data of developed RP-HPLC analytical method for RTG

QC levels [a]	Inter-day precision (n = 3)			Intra-day precision (n = 3)		
	Mean measured concentration [b]	SD	% RSD	Mean measured concentration [b]	SD	% RSD
LQC	29.55	0.32	1.07	30.34	0.36	1.18
MQC	150.35	3.21	1.81	151.71	1.54	1.02
HQC	496.23	4.84	0.98	501.10	1.98	0.40

Standard deviation (SD), % Relative standard deviation (% RSD); Intra-day repeatability was assessed by replicate analysis (n=3) thrice a day at each QC level
[a] LQC, MQC, and HQC are 30, 150, 510 ng/mL

3.4.5.2.5 Robustness

Robustness of developed method was evaluated by changing instrument, pH of buffer, column oven temperature and flow rate. After a deliberate changing of different chromatographic conditions and HPLC instrument, % recovery for all three QC samples of RTG was found to be within 98.27 ± 5.81% and 109.65 ± 1.65% (**Table 3.16**).

Table 3.16 Different conditions and results of robustness study for RP-HPLC analytical method for RTG

Conditions / QC levels [a]	**% recovery** [b] **(± SD)**		
	LQC	**MQC**	**HQC**
HPLC 2	106.39 ± 0.94	99.85 ± 4.87	100.28 ± 1.82
pH (± 0.5)	102.78 ± 1.79	100.03 ± 7.85	99.24 ± 4.10
Flow rate (± 0.2)	109.65 ± 1.65	99.54 ± 2.97	98.27 ± 5.81
Temperature (± 5 ^{0}C)	108.90 ± 3.07	103.62 ± 0.62	99.19 ± 2.11

Standard deviation (SD)
[a] LQC, MQC, and HQC are 30, 150, 510 ng/mL, [b] % recovery = [(Nominal concentration/Mean measured concentration)×100]

3.4.5.2.6 Sensitivity

LOD and LOQ were calculated by applying Equations 3.1 and 3.2, respectively [24], and used to indicate sensitivity of the developed RP-HPLC method. LOD and LOQ of the method for RTG were found to be 2.58 ng/mL and 7.81 ng/mL, respectively. To further validate theoretically obtained LOD and LOQ, another independent analysis of samples was performed for following concentrations: 3, 6, 9, 12, 15, and 18 ng/mL and provided in **Table 3.17**. For 3 and 6 ng/mL concentrations, no peaks were observed at retention time of RTG. Drug peak was started to be observed from 9 ng/mL but, the % RSD value was greater than acceptable limit. From 12 ng/mL onwards, the % RSD values were found to be within the acceptable limit (less than 2%). This result portrays that although theoretically calculated LOD and LOQ values of the method were 2.58 and 7.81 ng/mL respectively but, practically LOD and LOQ were found to be 9 ng/mL and 12 ng/mL, respectively [25].

Table 3.17 Concentration levels and their %RSD data below LOD and LOQ for RP-HPLC analytical method

Concentration levels (ng/mL)	Actual average concentration	SD	% RSD
9	9.301	0.124	3.349
12	12.221	0.198	1.839
15	15.218	0.252	1.453
18	18.238	0.489	1.322

Standard deviation (SD), % relative standard deviation (% RSD), n = 3 samples in all cases.

3.4.5.2.7 Stability studies

Stability of RTG in the solution state was estimated in terms of benchtop stability, autosampler stability, short and long-term stability and the results are presented in **Table 3.18**. For all the three QC samples, between zero-day and after exposure to respective conditions (benchtop stability; 24 h), auto-sampler (25 ^{o}C; 24 h)**,** short-term (4 ^{o}C; 7 days) and long-term (–20 ^{o}C; 1 month) storage, no significant changes (% RSD < 2) in the peak area were observed. These results advocate the stability of RTG in solution state under different storage conditions.

Table 3.18 Results for stability study for RP-HPLC analytical method

QC levels [a]	Mean measured concentration [b]	Nominal concentration [c]	% RSD	% recovery [d]
Bench top stability (Room Temperature, 24 h)				
LQC	30.15	29.59	1.69	97.88
MQC	147.64	151.39	1.73	101.79
HQC	504.73	505.80	0.39	100.10
Auto sampler stability (25 ºC, 24 h)				
LQC	30.15	29.97	2.04	99.15
MQC	147.64	147.63	1.50	99.26
HQC	504.73	501.82	0.74	99.32
Short-term stability (4 ºC, 7 days)				
LQC	30.15	30.61	1.82	101.28
MQC	147.64	151.29	1.68	101.72
HQC	504.73	507.38	0.99	100.42
Long-term stability (–20 ºC, 1 month)				
LQC	30.15	30.98	0.90	102.49
MQC	147.64	151.03	1.45	101.54
HQC	504.73	500.16	1.65	98.99

[a] LQC, MQC, and HQC are 30, 150, 510 ng/mL of RTG, [b] Mean measured concentration of RTG on day zero for LQC = 30 ng/mL, MQC = 150 ng/mL, and HQC = 510 ng/mL, [c] Nominal concentration of RTG during stability studies; % relative standard deviation (% RSD)
[d] % recovery = [(Nominal concentration/Mean measured concentration)×100]

3.5 Method III: Bioanalytical method for quantification of RTG from plasma and brain samples

3.5.1 Materials and Instrument

Materials and instrument mentioned in **Sections 3.4.1** and **3.4.2** were used for bioanalytical method for quantification of RTG.

3.5.2 Method Development

3.5.2.1 Collection of brain tissue and plasma from rats

All *in vivo* experiments were approved by the Institute's Animal Ethics Committee (IAEC), Protocol number- IAEC/RES/26/07/REV-1/30/19. Male Wistar rats of 9 – 10 weeks old and weighed between 250 – 260 g were used for experiments. Blood was collected in centrifuge tubes (Tarson, Kolkata, India) containing 4.5% (w/v) solution of disodium EDTA as anticoagulant and was centrifuged (Eppendorf®, Hamburg, Germany) at 7,500 rpm for 10 min at 4 °C to separate plasma and stored at –20 °C till further analysis.

Similarly, for brain homogenate, the brain samples were weighed and PBS (pH 7.4) was added in 1:3 ratios and homogenised (Kinematica, GmBH, Germany) for 5 min at 12,000 rpm. The brain homogenate was centrifuged (Eppendorf®, Hamburg, Germany) at 7,500 rpm for 10 min at 4 °C to separate brain matrices. The supernatant i.e., brain matrices was collected carefully using micropipettes and stored at –20 ^{o}C till further use.

3.5.2.2 Processing of brain matrices and plasma from rats

A simple protein-precipitation technique was used to extract RTG and internal standard (IS) from brain matrices and plasma. A 90 µL of brain matrices and plasma was mixed separately with 10 µL of IS (Glipizide) solution and vortexed for 30 s. Standard stock of RTG was prepared as mentioned in **Section 3.4.4.1**. ACN was used as protein-precipitating agent. 300

μL of ACN was added and vortexed for 7 min. The samples were centrifuged (Eppendorf®, Hamburg, Germany) at 15,000 rpm for 10 min at 4 ^{o}C to obtained protein-free brain matrices and plasma. The supernatants were transferred into microcentrifuge tube (Tarsons, Kolkata, India) and evaporated to dryness under vacuum. The dried samples were reconstituted using 100 μL of mobile phase and vortexed (Tarsons, Kolkata, India) for 5 min. Finally, samples were transferred into a HPLC vials and injected on to the column for quantification.

3.5.2.3 Calibration curve and quality control standards

Stock solutions of 1 mg/mL for RTG and IS were prepared in ACN. In order to study absolute recovery from brain matrices and plasma, working standard solutions were prepared by step-wise diluting the stock solutions using mobile phase. For both brain matrices and plasma, seven non-zero calibration standards of RTG in range of 100 – 1200 ng/g and 100 – 1200 ng/mL respectively, were prepared. Sample preparation process was same as mentioned in **Section 3.5.2.2**. For brain matrices, IS at 2 μg/g; and for plasma, IS at 2 μg/mL were spiked as mentioned in **Section 3.5.2.2**. For brain matrices, QC samples at three concentration levels, *viz.*, LQC; 150 ng/g, MQC; 750 ng/g, and HQC; 1150 ng/g were considered. For plasma sample, LQC; 150 ng/mL, MQC; 750 ng/mL, and HQC; 1150 ng/mL were considered.

3.5.3 Method Validation

Validation of developed method for both brain matrices and plasma was achieved as per guidelines of USFDA and EMA [26,27]. Evaluation of samples was perfomed to determine selectivity, linearity, sensitivity, accuracy, precision, recovery, and stability.

3.5.3.1 Selectivity

Selectivity of method was determined by comparing chromatograms of blank (without RTG and IS) in brain matrices and plasma against chromatograms of RTG and IS spiked brain matrices and plasma.

3.5.3.2 Linearity

Linearity of the method was measured by plotting ratio of peak areas of RTG/IS against the nominal concentration of RTG. Unweighted linear regression analysis was used to fit the calibration curves.

3.5.3.3 Sensitivity

Sensitivity of the method was assessed as described in **Section 3.4.4.3.6**.

3.5.3.4 Accuracy and precision

Accuracy of the method was estimated as %bias for all three QC standards (n = 6) for both plasma and brain matrices. For accuracy study, percentage bias was calculated from the observed concentration from peak area ratio of RTG/IS using average regression equation with respective nominal concentrations. To assess precision of the method, all QC standards were analyzed in replicates and percentage relative standard deviation (%RSD) was reported. Intraday precision was determined by analyzing QC samples (n = 3), twice a day; and for intra-day precision assessment, QC standards were analyzed on three different days (n = 18). Recovery of drug was estimated for all QC standards in triplicate by comparing peak area ratio of RTG/IS attained from extracted brain matrices and plasma with the peak area of analytical standards at same nominal concentration.

3.5.3.5 Stability studies

The stability studies of RTG in plasma and brain matrices were determined at three different conditions. All three QC standards were analyzed in triplicates in the autosampler, freeze-thaw and long-term stability. For autosampler, samples were stored at 15 ^{o}C for 24 h and analyzed at intervals of 0, 8, 16, and 24 h. In freeze-thaw, three cycles (−20 ^{o}C) were performed for all three QC standards for both the matrices. Finally, for long-term stability, QC standards were stored upto 27th day. To test the stability of RTG stock solutions, QC samples kept under above mentioned conditions were compared with freshly prepared QC standards.

3.5.4 Single dose intranasal (i.n.) and intravenous (i.v.) PK study in Wistar rats

Wistar rats (male), weighing 250 – 260 g, were used in the study. All animal experiments were performed in compliance with the IAEC of BITS-Pilani University with the approved protocol (IAEC/RES/26/07/REV-1/30/19). All the rats were kept in polyacrylic cages and housed under ambient temperature of 22 ± 3 ^{o}C with 65% relative humidity in central animal facility of institute. All the animals were housed for at least for 7 days preceding the experiment to acclimate with the environment. The animals were fasted for 12 h prior dosing to avoid coprophagia. After 4 h of dosing, water, and feed were provided *ad libitum* till the end of study.

RTG was administered via i.n. and i.v. route at a dose of 2 mg/Kg. For i.n. administration, a 1.3 cm long soft and flexible cannula (Instech Laboratories, PA, USA) was fixed in front of a 100 μL microtips (Tarsons, Kolkata, India). For i.v. dosing, RTG was administered via tail vein at a dose of 2 mg/Kg body weight. Before both i.n. and i.v. administration, rats were anaesthetised using isoflurane.

The required dose of pure RTG was solubilized in 0.2% v/v propylene glycol just before the beginning of i.n. PK study. For blood collection, retro-orbital puncture technique was employed. Blood was collected in 1.5 mL microcentrifuge tubes, containing an anticoagulant

(disodium EDTA), at 0 (before administration of the drug), and 0.08, 0.25, 0.5, 1, 2, 4, 6, and 8 h following i.n. and i.v. administration of RTG. At each time point, 200 µL of blood was collected from every animal.

Brains were collected at 0.5, 1, 2, 4, 6, and 8 h following both i.n. and i.v. dosing, after blood sampling. At every time point animals (n = 4) were sacrificed for brain sample collection. All blood and brain samples were processed as described in **Sections 3.5.2.1** and **3.5.2.2.** Finally, processed bio samples were analyzed using validated RP-HPLC bioanalytical method.

3.5.5 Results and discussions

3.5.5.1 Selectivity

Protein-precipitation method for analysis of samples was observed to be efficient and consistent for the estimation of RTG in both plasma and brain matrices. No interfering peaks were found at retention times of RTG or IS in both the bio matrices. **Figure 3.8** presents overlays of chromatograms for both brain and plasma of their respective blanks and *in vivo* PK samples.

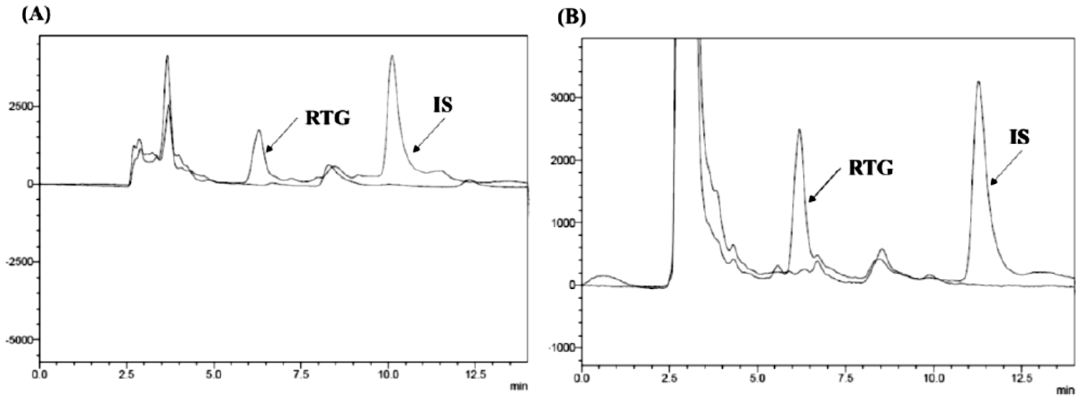

Figure 3.8 Overlaid chromatograms of (A) blank plasma and *in vivo* PK sample; (B) blank brain matrix and *in vivo* PK sample.

3.5.5.2 Linearity

Calibration curves were linear in the concentration range of 100 – 1200 ng/mL and 100 – 1200 ng/g for plasma and brain matrices, respectively. The mean regression coefficient, R^2 was found 0.9978 and 0.9966 for brain matrices and plasma, respectively. Calibration curves were constructed with peak area ratio of RTG/IS on y-axis and concentration (ng/mL for plasma; and ng/g for brain) of RTG on x-axis. From linear regression analysis, slope, intercept, and R^2 values were calculated, and results are presented in **Table 3.19**.

3.5.5.3 Sensitivity

LOD and LOQ obtained using Equation 3.1 and 3.2 are the indicative of sensitivity of the method. For plasma, LOD and LOQ values were found to be 9.75 ng/mL and 32.51 ng/mL, respectively (**Table 3.19**). For the brain matrices, LOD and LOQ values were found to be 9.95 ng/mL and 33.18 ng/mL, respectively (**Table 3.19**). Hence, lower limit of quantification (LLOQ) values *viz.*, 100 ng/g and 100 ng/mL for brain matrices and plasma are accurate, reproducible, and reliable. Furthermore, the LLOQ values were sufficient for quantification of RTG in both plasma and brain PK studies.

Table 3.19 Results attained from linear regression analysis of calibration curves, LOD, and LOQ for RTG for bioanalytical method

Parameter	Brain matrices	Plasma
Slope (mean ± SD)	5562.33 ± 193.70	5775.67 ± 199.30
Intercept (mean ± SD)	58.37 ± 2.55	61.31 ± 1.77
R^2	0.9978	0.9966
LOD	9.95 ng/g	9.75 ng/mL
LOQ	33.18 ng/g	32.51 ng/mL

Mean, Standard deviation(SD), regression coefficient (R^2) all are calculated for n = 6

3.5.5.4 Accuracy and precision

In plasma, %bias of the QC samples were found to be ranging from –5.67 to 9.09. For brain matrices, %bias of the QC samples were found to be ranging from –0.74 to –12.18. The results

indicated that method was accurate to quantify RTG in both the bio matrices (**Table 3.20**). Repeatability study for intra-day precision showed that %RSD was not more than 4.69 and 5.78 for plasma and brain matrices, respectively. The inter-day precision study showed that %RSD value was not more than 2.53 and 2.82 for brain matrices and plasma, respectively (**Table 3.21**). The accuracy and intermediate precision study results were well accepted within the limits which revealed the developed bioanalytical method is accurate and precise for quantification of RTG in both the matrices.

3.5.5.5 Recovery

The absolute recovery study result is presented in **Table 3.20** for all the QC samples. The peak areas of aqueous QC samples were compared against the drug peak areas spiked in plasma and brain matrices. In plasma, %recovery was ranged between 90.91 to 94.33% with %RSD not more than 4.50 in all cases whereas, in brain matrices, the %recovery was found between a range of 87.82 – 92.26 (**Table 3.20**). High recovery values obtained from both the bio matrices indicated that the protein precipitation process was a reliable extraction method and also revealed that ACN was a good protein-precipitating agent in this case.

Table 3.20 Accuracy and absolute recovery data of bioanalytical methods for RTG

QC level*	Predicted concentration [a]			%Recovery [b]	% Mean bias [c]
	Range	Mean ± SD	%RSD		
Plasma (ng/mL)					
LQC	135.08 - 147.69	140.99 ± 6.34	4.50	92.17 ± 2.26	-7.83
MQC	752.60 - 764.38	758.49 ± 5.89	0.78	90.91 ± 0.93	-9.09
HQC	1142.22 - 1193.59	1163.43 ± 26.82	2.31	94.33 ± 1.09	-5.67
Brain matrices (ng/g)					
LQC	144.14 - 150.25	147.19 ± 4.31	2.93	87.82 ± 5.45	-12.18
MQC	756.46 - 763.67	760.07 ± 5.09	0.67	90.71 ± 4.25	-9.29
HQC	1139.62 - 1155.36	1147.49 ± 11.13	0.97	92.26 ± 1.63	-7.74

Mean, Standard deviation (SD), % relative standard deviation (% RSD), for n = 6 samples.[*] LQC, MQC, and HQC are 150, 750, 1150 ng/mL for plasma. LQC, MQC, and HQC are 150, 750, 1150 ng/g for brain matrices.[a] Predicted concentrations of RTG were calculated using linear average regression equation, given in ng/mL for plasma and ng/g for brain matrices, [b] %

recovery = [(Measured concentration / Actual concentration) × 100], [c] Accuracy i(% bias) = [(Measured concentration − Actual concentration)/Actual concentration × 100]

Table 3.21 Intermediate precision study results of bioanalytical method for RTG

Matrix	QC level*	Intra-day repeatability (% RSD) (n = 3)			Inter-day repeatability (%RSD) (n = 18)
		Day 1	Day 2	Day 3	
Plasma	LQC	1.91	4.69	1.15	2.82
		3.03	2.31	2.67	
	MQC	3.67	2.77	0.68	2.55
		2.81	1.37	1.03	
	HQC	1.89	2.10	1.45	2.47
		3.84	2.94	2.97	
Brain	LQC	4.90	5.49	3.48	2.24
		2.96	1.69	2.07	
	MQC	1.18	4.11	2.25	1.23
		5.78	2.33	1.89	
	HQC	5.32	4.85	1.53	2.53
		3.33	4.92	1.86	

Percent relative standard deviation (%RSD);
Intra-day repeatability was calculated using (n = 3) replicate analysis twice a day at every QC level. Inter-day repeatability was calculated using (n = 18) replicate analysis of each QC samples over three days.
* For plasma, LQC, MQC and HQC are 150, 750 and 1150 ng/mL. LQC, MQC and HQC are 150, 750 and 1150 ng/g for brain matrices

3.5.5.6 Stability studies

Stability of RTG in both matrices was assessed using QC samples under several stress conditions. Results are presented in **Figure 3.9**. No significant degradation of RTG in plasma samples was observed under all stress conditions i.e., auto-injector stability (at 15 °C) study of processed plasma samples over 24 h post-preparation, freeze-thaw (–20 °C) stability studied for 3 cycles on 3 consecutive days and long term stability (–20 °C) for period of 27 days. The deviation from zero-time samples in all the stress conditions was observed to be in the range of –2.11 – 3.98%.

RTG spiked brain samples showed no degradation with auto-injector over 24 h, with %deviation from zero-time samples in the range of −1.78 – 2.77%. In case of freeze-thaw stability and long-term stability studies, the %deviation with respect to zero-time samples was between −1.35 – 3.89% up to 1st freeze-thaw cycle and 18th day samples. However, the samples showed interfering peaks and noise around the retention times of both RTG and IS with rest of the 3 freeze-thaw cycles and the 27th day long-term stability samples. Hence, it can be concluded that when stored at −20 °C from zero-time samples in all the stress conditions was observed to be in the range of −3.01 – 3.51%.

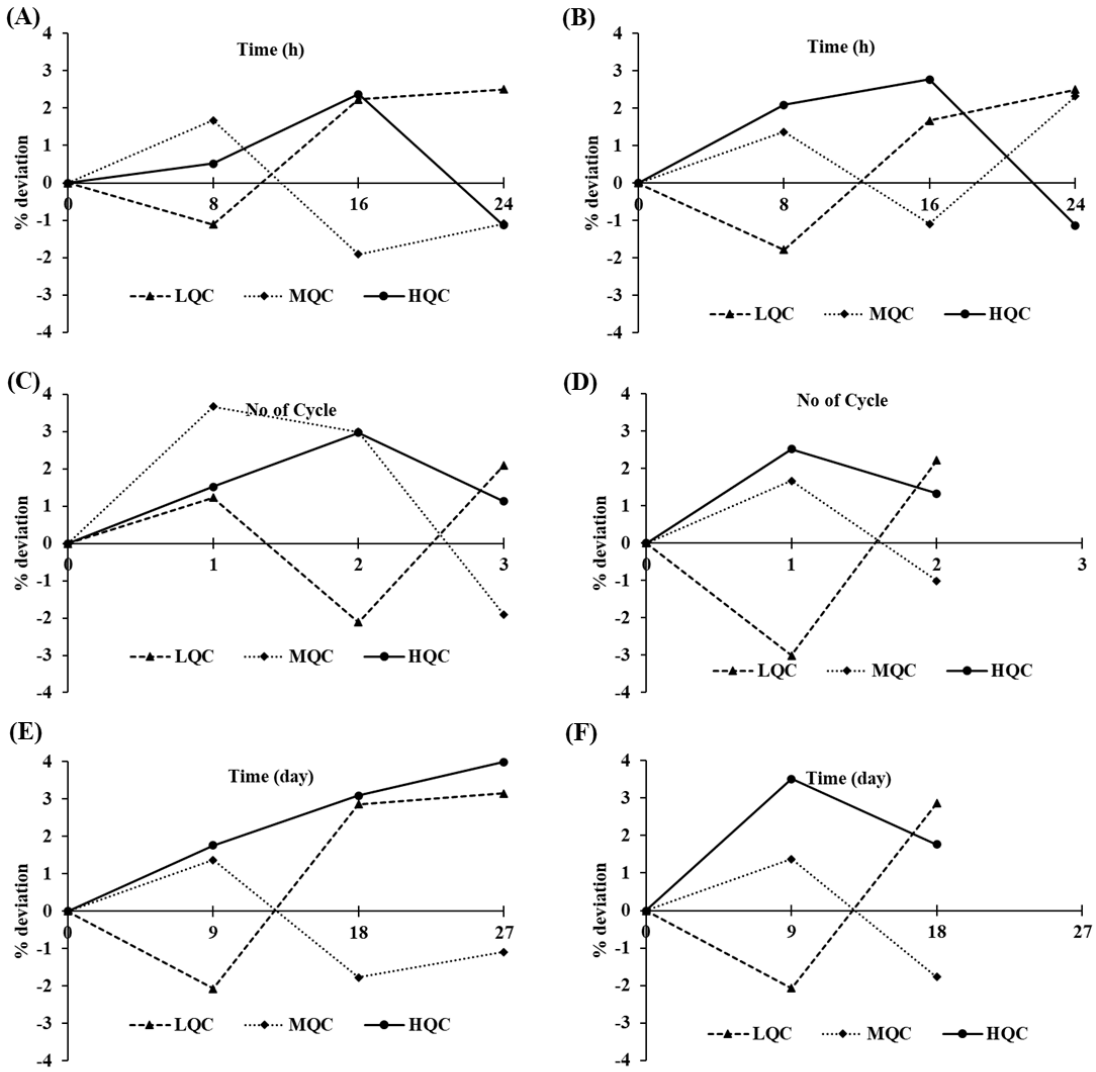

Figure 3.9 Autosampler stability in (A) plasma and (B) brain; Freeze-thaw stability in (C) plasma and (D) brain; Long-term stability in (E) plasma and (F) brain

3.5.6 Single dose i.n. and i.v. PK study

Plasma and brain PK profiles for single i.v. bolus and i.n. dose administration are presented in **Figure 3.10**. The C_{max} in brain after i.v. and i.n. administration was found to be 155.08 ± 15.04 ng/g and 264.71 ± 13.31 ng/g, respectively. The $AUC_{0\rightarrow tlast}$ in brain was found to be 462.36 ± 23.11 ng*h/g and 628.11 ± 17.92 ng*h/g after i.v. and i.n. administration, respectively. The result shows that the developed bioanalytical method is sensitive and can detect nearly the complete time profile of RTG in rat brain at the given dose. The study further shows that i.n. administration of pure RTG increased brain C_{max} and $AUC_{0\rightarrow tlast}$ by 1.70-fold and 2.10-fold, respectively as compared to i.v. bolus dose of pure RTG solution.

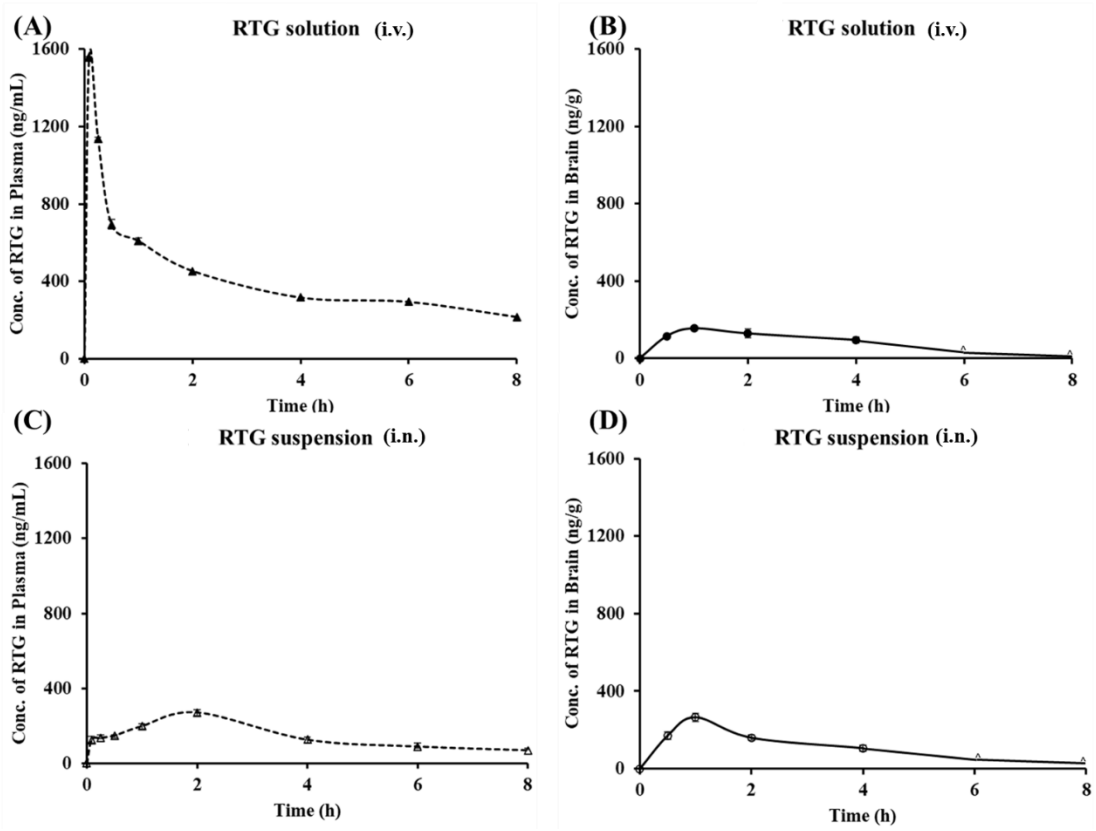

Figure 3.10 Plasma and brain PK profiles of pure RTG after i.v. and i.n. administration; (A) and (B): PK profiles of RTG for plasma and brain respectively after i.v. administration (2 mg/Kg); (C) and (D): PK profiles of RTG for plasma and brain respectively after i.n. administration (2 mg/Kg); All data points are represented as mean ± SD (n = 4). For plasma PK study, n = 4 animals were used and for PK study in brain, n = 4 rats' were used at each time point to collect the brains. '^' denote that the concentration of RTG was not detected at those time points in brain matrices

3.6 Conclusion

A simple, effective, rapid, sensitive, robust and accurate fluorescence-based analytical method was developed and validated for the first time to estimate RTG in presence of excipients. Further a DoE based rapid, specific, sensitive and stability indicating RP-HPLC method was developed and validated for effectively quantify RTG from several *in vitro, ex vivo* study samples. Critically effecting variables that can affect the analytical methods were selected and further critical factors were optimized to obtain desired conditions for the final analytical method. Application of DoE helped to finalize the optimum number of theoretical plates and retention time for the analytical method. The RP-HPLC method was rapid with a run time of 10 min and cost-effective due to usage of only 46% ACN. The developed method was linear between the range of 25 – 600 ng/mL. The present chapter also discusses the development and validation of rapid, selective sensitive RP-HPLC bioanalytical method for quantification of RTG in bio matrices (rat plasma and brain matrix). Finally, i.v. and i.n. PK studies were performed for effective application of the developed bioanalytical method. The method was efficient to estimate RTG in both plasma and brain matrices after i.v. and i.n. administration. The bioanalytical method was additionally applied in quantification of RTG in bio samples obtained from *in vivo* PK studies using several nanocarriers presented in the consequent chapters.

References

1. Kumar, A.; Kishore, L.; Kaur, N.; Nair, A. Method Development and Validation: Skills and Tricks. *Chronicles of Young Scientists* **2012**, *3*, 3–11,doi: 10.4103/2229-5186.94303.

2. Bende, G.; Kollipara, S.; Kolachina, V.; Saha, R. Development and Validation of an Stability Indicating RP-LC Method for Determination of Imatinib Mesylate. *Chromatographia* **2007**, *11–12*, 859–866, doi:10.1365/S10337-007-0415-3.

3. Tiwari, G.; Tiwari, R. Bioanalytical Method Validation: An Updated Review. *Pharmaceutical Methods* **2010**, *1*, 25–38, doi:10.1016/S2229-4708(10)11004-8.

4. McAfee, D.A.; Hadgraft, J.; Lane, M.E. Rotigotine: The First New Chemical Entity for Transdermal Drug Delivery. *European Journal of Pharmaceutics and Biopharmaceutics* **2014**, *88*, 586–593, doi:10.1016/j.ejpb.2014.08.007.

5. Swarupa P; Krishna, D.; Prasad, K.; Babu, K. Stability Indicating Method Development and Validation for the Estimation of Rotigotine by Rp-Hplc in Bulk and Pharmaceutical Dosage Form. *Oriental Journal of Chemistry* **2015**, *31*, 2499–2505, doi: 10.13005/ojc/310486.

6. Krishna, P.M.; Rao, B.T.; Kumar, R.K.; Venkateswarlu, P. A Stability Indicating of Rotigotine in Bulk Drugs by HPLC Assay Method. *Research Journal of Pharmaceutical, Biological and Chemical Sciences* **2010**, *1*, 848–857.

7. Patil, A.S.; Sait, S.S.; Deshpande, G.; Acharya, P.; Kaki, V.S. An Improved Validated Ultra High Pressure Liquid Chromatography Method for Separation of Rotigotine Impurities in Rotigotine Transdermal Patch. *Der Pharma Chemica* **2015**, *7*, 26–34.

8. Kehr, J.; Hu, X.J.; Yoshitake, T.; Scheller, D. Determination of the Dopamine Agonist

Rotigotine in Microdialysates from the Rat Brain by Microbore Column Liquid Chromatography with Electrochemical Detection. *Journal of Chromatography B: Analytical Technologies in the Biomedical and Life Sciences* **2007**, *845*, 109–113, doi:10.1016/j.jchromb.2006.07.066.

9. Den Daas, I.; Rollema, H.; De Vries, J.B.; Tepper, P.G.; Horn, A.S. Analysis of the Dopamine Agonist N-0437 in Rat Serum Using Reversed-Phase High-Performance Liquid Chromatography with Electrochemical Detection. *Journal of Chromatography B: Biomedical Sciences and Applications* **1989**, *487*, 210–214, doi:10.1016/S0378-4347(00)83027-3.

10. Ruckmick, S.C.; Hench, B.D. Direct Analysis of the Dopamine Agonist (-)-2-(N-Propyl-N-2-Thienylethylamino)-5-Hydroxytetralin Hydrochloride in Plasma by High-Performance Liquid Chromatography Using Two-Dimensional Column Switching. *Journal of Chromatography B: Biomedical Sciences and Applications* **1991**, *565*, 277–295, doi:10.1016/0378-4347(91)80390-X.

11. Sha, C.; Han, J.; Zhao, F.; Shao, X.; Yang, H.; Wang, L.; Yu, F.; Liu, W.; Li, Y. Validated LC–MS/MS Method for the Simultaneous Determination of Rotigotine and Its Prodrug in Rat Plasma and an Application to Pharmacokinetics and Biological Conversion in Vitro. *Journal of Pharmaceutical and Biomedical Analysis* **2017**, *146*, 24–28, doi:10.1016/j.jpba.2017.07.018.

12. Swartz, M. HPLC Detectors: A Brief Review. *Journal of Liquid Chromatography & Related Technologies* **2010**, *33*, 1130–1150, doi:10.1080/10826076.2010.484356.

13. Omar, M.A.; Nagy, D.M.; Halim, M.E. Simple Ultrasensitive Spectrofluorimetric Method for Determination of Midodrine in Its Tablet Form: Application to Content Uniformity Testing. *Luminescence* **2019**, *34*, 854–858, doi:10.1002/bio.3682.

14. ICH *ICH; Validation of Analytical Procedures: Text and Methodology Q2 (R1). In International Conference on Harmonization,Geneva, Switzerland (2005)*; ICH, 2005;

15. Rapalli, V.K.; Kaul, V.; Gorantla, S.; Waghule, T.; Dubey, S.K.; Pandey, M.M.; Singhvi, G. UV Spectrophotometric Method for Characterization of Curcumin Loaded Nanostructured Lipid Nanocarriers in Simulated Conditions: Method Development, in-Vitro and Ex-Vivo Applications in Topical Delivery. *Spectrochimica Acta - Part A: Molecular and Biomolecular Spectroscopy* **2020**, *224*, 117392, doi:10.1016/j.saa.2019.117392.

16. Zidan, D.W.; Hassan, W.S.; Elmasry, M.S.; Shalaby, A.A. A Novel Spectrofluorimetric Method for Determination of Imatinib in Pure, Pharmaceutical Preparation, Human Plasma, and Human Urine. *Luminescence* **2018**, *33*, 232–242, doi:10.1002/bio.3406.

17. Andleeb, S.; Ahmed, S.; Sheraz, M.A.; Anwar, Z.; Ahmad, I. Development and Validation of a Spectrofluorimetric Method for the Analysis of Tolfenamic Acid in Pure and Tablet Dosage Form. *Luminescence* **2020**, *35*, 1017–1027, doi:10.1002/bio.3810.

18. England, R.J.A.; Homer, J.J.; Knight, L.C.; Ell, S.R. Nasal PH Measurement: A Reliable and Repeatable Parameter. *Clinical Otolaryngology and Allied Sciences* **1999**, *24*, 67–68, doi:10.1046/j.1365-2273.1999.00223.x.

19. Mortazavi, M.; Hoja, J.; Aerts, L.; Quéré, L.; van de Streek, J.; Neumann, M.A.; Tkatchenko, A. Computational Polymorph Screening Reveals Late-Appearing and Poorly-Soluble Form of Rotigotine. *Communications Chemistry* **2019**, *2*, 1–7, doi:10.1038/s42004-019-0171-y.

20. (R1), I.G.-Q.; 2005, U. Validation of Analytical Procedures: Text and Methodology Q2(R1). In Proceedings of the somatek.com; 2014.

21. Garg, N.K.; Sharma, G.; Singh, B.; Nirbhavane, P.; Katare, O.P. Quality by Design (QbD)-Based Development and Optimization of a Simple, Robust RP-HPLC Method for the Estimation of Methotrexate. *Journal of Liquid Chromatography and Related Technologies* **2015**, *38*, 1629–1637, doi:10.1080/10826076.2015.1087409.

22. Gritti, F.; Guiochon, G. The van Deemter Equation: Assumptions, Limits, and Adjustment to Modern High Performance Liquid Chromatography. *Journal of Chromatography A* **2013**, *1302*, 1–13, doi:10.1016/j.chroma.2013.06.032.

23. Patil, T.S.; Deshpande, A.S. Development of an Innovative Quality by Design (QbD) Based Stability-Indicating HPLC Method and Its Validation for Clofazimine from Its Bulk and Pharmaceutical Dosage Forms. *Chromatographia* **2019**, *82*, 579–590, doi:10.1007/s10337-018-3660-8.

24. ICH, Q. ICH Q10 Pharmaceutical Quality Systems. In *Federal Register, Geneva, Switzerland*; 2009; Vol. 74, pp. 15990–15991 ISBN 1574911090.

25. Saha, P.; Pandey, M. Design of Experiment (DoE)-Approach Based RP-HPLC Analytical Method Development and Validation for Estimation of Efavirenz in Bulk and Formulations. *Journal of Chromatographic Science* **2021**, *60*, 35–44, doi:10.1093/CHROMSCI/BMAB029.

26. FDA; Cder Bioanalytical Method Validation Guidance for Industry Biopharmaceutics Bioanalytical Method Validation Guidance for Industry Biopharmaceutics Contains Nonbinding Recommendations. **2018**.

27. Medicines Agency, E. ICH Guideline M10 on Bioanalytical Method Validation 4 Step 2b 5. **2019**.

Chapter 4: Development, Optimization, *In vitro, Ex vivo* and *In vivo* Evaluation of Rotigotine Nanosuspension for Improved N2B Delivery

4.1 Introduction

Presence of blood-brain barrier (BBB) poses a serious challenge in achieving desired brain bioavailability of drugs used for the PD treatment. To improve brain bioavailability of drugs by evading the BBB, several techniques such as intracerebroventricular injections, cerebral implants, convection-enhanced delivery, nose-to-brain (N2B) delivery etc. have been reported in literature [1,2]. N2B delivery approach has widely been explored in last few decades which significantly increases the brain availability of drugs by delivering through olfactory neuronal pathway and trigeminal nerves [3,4]. Nanocarriers have been currently explored as an effective delivery approach to deliver drugs directly to brain via N2B route [5]. Different nanocarriers *viz.*, PLGA nanoparticles (NP), chitosan NP, solid lipid NP, nanoemulsions, polymeric micelles etc. have been explored to deliver Rotigotine (RTG) directly to the brain. These formulations have been reported to show better nasal permeability, improved residence time, better brain targeting etc. [6–10]. However, research in these works was directed only towards solving the problems of permeability or brain bioavailability of the drug, but the issue of poor solubility of RTG was not addressed. Whereas, it is important to increase the solubility of RTG which would enhance the solubility of drug in nasal fluid. Thus improved solubility would enhance the passive diffusion of drug molecule due to its increased surface area across the nasal mucosa [11].

Amongst different nanocarriers, nanosuspension stabilized by surfactants, can effectively enhance the aqueous solubility of hydrophobic drugs by virtue of its calibre to have high loading of drugs (almost 100%) and extends improved permeation profiles as well [12,13].

Furthermore, nanocrystals of less than 100 nm in size are reported to be internalized by neuronal cells of the nose-to-brain pathway directly upon intranasal (i.n.) administration [14]. Additionally, in case of i.n. delivery, the dose volume and amount of formulation that can be administered in the nasal cavity is restricted by physiological constraints [15,16]. Due to significantly high drug loading capacity, nanosuspension also effectively combat the problem of small dose volume of nasal formulations.

Nanosuspension can be prepared by mainly two methods *viz.*, bottom-up approach and top-down approach. Top-down method is an energy driven process where bigger particle size is broken down into small particles by high pressure homogenizer or wet ball mill. Among bottom-up approaches, anti-solvent precipitation method is widely used for the preparation. Though the bottom-up approach have advantages i.e., simple and rapid processing, cost effective etc. But, this method is dependent on optimization of various factors to produce desired particle size. Factors *viz.*, solubility of drug in solvent and surfactant, solvent-antisolvent ratio, concentration of drug and surfactant etc. affect the particle size and other attributes of nanosuspension [17]

Therefore, in the current work, we have fabricated nanosuspension for RTG using anti-solvent precipitation ultrasonication method. We have exhaustively evaluated DoE based optimization for the development of nanosuspension-based RTG formulation intended for N2B delivery. Further, *in vitro* dissolution, nasal *ex vivo* permeability behaviour, nasal ciliotoxicity study and *in vivo* brain and plasma pharmacokinetic (PK) study of the optimized RTG-Nanosuspension were performed and compared with that of pure drug suspension.

4.2 Materials and methods

4.2.1 Materials

RTG was generously gifted by Mylan Laboratories (Hyderabad, India). Glipizide, internal standard was purchased from TCI Chemicals Pvt Ltd. (Chennai, India). Poloxamer 407, Poloxamer 188 and Soluplus® were obtained as kind gift samples from BASF (Mumbai, India). Span 20, sodium lauryl sulphate, and tween 20 were purchased from SRL Pvt. Ltd. (Mumbai, India) and PVP K-30 was purchased from Sigma Aldrich (Bengaluru, India). HPLC grade acetonitrile, orthophosphoric acid were procured from Merck (Mumbai, India). Milli-Q water obtained from an in-house Milli-Q® Reference water purification system (GmbH, Germany) was used in all experimental processes and analysis.

4.2.2 Solubility of RTG in various solvents

The solubility of RTG was determined in three different water miscible organic solvents for the selection of the suitable one for preparation of RTG-Nanosuspension. An excess amount of RTG (n = 3) was added to 1 mL of different solvents and kept in the orbital shaker incubator (Macro scientific works, Delhi, India) for 24 h maintained at 37 ± 1 ^{o}C. After 24 h, samples were centrifuged (Eppendorf®, Hamburg, Germany) at 15,000 rpm for 15 min and supernatant was collected and filtered through 0.45 μm membrane filter. Filtered samples were suitably diluted with mobile phase and the solubility of RTG was determined with help of previously discussed Fluorescence-based analytical method discussed in **Chapter 3**, **Method II** [18].

4.2.3 Screening of surfactant

Surfactants play an important role in the preparation of nanosuspension. Surfactants not only offer physical stability to the nanosuspension by decreasing free surface energy or inhibiting particle aggregation but, also act as cryoprotectant during lyophilization [19]. Various

surfactants were investigated in order to select the appropriate one for preparation of nanosuspension. For this, the equilibrium solubility of RTG was assessed in different surfactants such as span 20, PVP K-30, Soluplus®, tween 20, sodium lauryl sulphate, Poloxamer 188 and Poloxamer 407 using analytical method described in **Chapter 3**, **Method I** [18]. Briefly, an excess amount of RTG was added into the vials (n = 3) containing 5 mL of different surfactant solutions (0.1% w/v) and kept on shaking in water bath shaker (Remi, Mumbai, India) for 24 h at 37 ± 1 ^{o}C temperature. Afterwards, nanosuspension using all the surfactants were separately prepared and analysed for their particle size (nm).

4.2.4 Preparation of RTG-Nanosuspension

Based on the solubility studies of RTG in various solvents and surfactants, ethanol and Poloxamer 407 were selected as the solvent and surfactant respectively, for the preparation of RTG nanosuspension. The nanosuspension was prepared by antisolvent precipitation-ultrasonication method (**Figure 4.1**). Briefly, RTG was dissolved in ethanol and Poloxamer 407 was solubilized in Milli-Q water to prepare the solvent and antisolvent phase, respectively. Afterwards, the freshly prepared solvent phase was rapidly injected to the ice-cold antisolvent phase containing surfactant under ultrasonication (Vibra cell model, Sonics & Materials, Inc., Connecticut, USA) for 3 min to obtain the nanosuspension. Concentration of drug (mg/mL), surfactant (% w/v) and solvent:antisolvent ratio used in the preparation were optimized employing the concept of design of experiments (DoE). The organic solvent was evaporated from nanosuspension using rotaevaporator (Buchi, Mumbai, India) for 10 min and was freeze-dried (Labconco™, South Kansas City, USA) to obtained final RTG-Nanosuspension. The prepared nanosuspension was stored under refrigeration (2 – 8 ^{o}C) until further use.

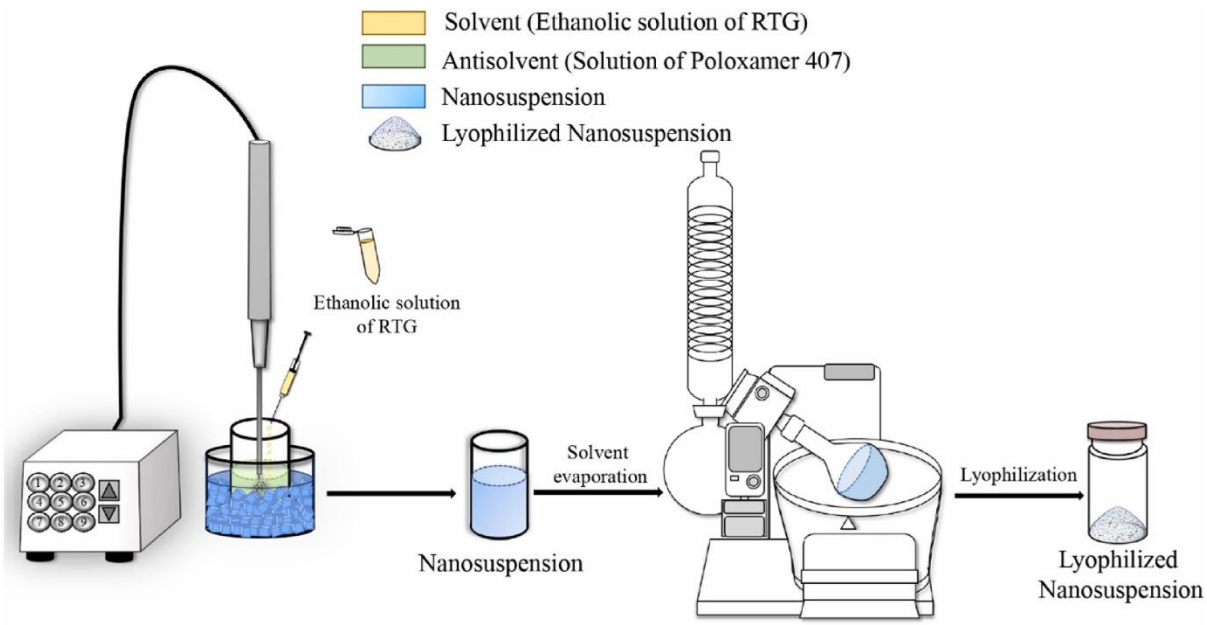

Figure 4.1 Schematic representation of preparation of RTG-Nanosuspension

4.2.5 Experimental design for the preparation of RTG-Nanosuspension

4.2.5.1 Experimental design

A design approach involving optimization design using response surface methodology (RSM), was considered to optimize the components used in the preparation of RTG-Nanosuspension. Design Expert® software (Version 8.1, Stat-Ease Inc., Minneapolis, USA) was used in building the design matrices for the optimization of variables and analysis of the data obtained. Particle size (nm) and nanosuspension PDI are important parameters affecting its uptake via neuronal pathways into the brain upon i.n. administration [14]. Hence, particle size (nm); R_1 and PDI; R_2 were identified as responses for the optimization of nanosuspension. Based on preliminary trials, 3 method variables, i.e., drug concentration (A), solvent:antisolvent ratio (B), and surfactant concentration (C) were chosen, and their respective high, medium, and low levels were determined. Further, a high-resolution RSM design, Box-Behnken Design (BBD), was employed to understand the impact of method variables and their interactions on both responses. In BBD, experiments were designed with 3 method variables at 3 different levels with 2 responses (**Table 4.1**). Seventeen experiments comprising 5 centre points (**Table 4.2**) were performed. The corresponding responses were

fitted to linear, 2-FI, quadratic, cubic, special cubic or quadratic polynomial models. The best fit model for each of the responses was determined depending on statistical parameters such as lack of fit, analysis of variance (ANOVA), square correlation coefficient (R^2), R^2-adjusted (Adj R^2), and R^2-predicted (Pred R^2). The obtained polynomial equation for each response was used for the design space. The same was visually illustrated using 3D response surface plots.

Table 4.1 List of the method variables for RTG-Nanosuspension and their levels

Name of method variables studied	**Levels**		
	High	**Medium**	**Low**
	(+1)	**(0)**	**(–1)**
A : Drug concentration (mg/mL)	30	20	10
B : Solvent:antisolvent	20	15	10
C : Surfactant concentration (% w/v)	0.3	0.2	0.1
Responses	**Goal**		
R_1 : Particle Size (nm)	Minimize		
R_2 : PDI	Minimize		

4.2.5.2 Desirability function and model validation

Design-Expert software provided the optimum values for all 3 factors based on the desirability function criteria. The desirability function was calculated based on the constrains set for the dependent variables: minimizing the particle size (nm) and PDI. A batch with the highest desirability function was selected, prepared (n = 3) and characterized for particle size and PDI to validate the model. The actual values obtained experimentally were compared with the predicted values given by the software. Further, t-test was applied to the predicted and actual values to check statistical difference between the values.

Table 4.2 Box-Behnken Design matrix of various method variables for RTG-Nanosuspension

Run[a]	Drug concentration (mg/mL)	Solvent:antisolvent	Surfactant concentration (% w/v)
1	10	20	0.2
2	20	15	0.2
3	10	15	0.1
4	30	10	0.2
5	20	20	0.1
6	30	15	0.1
7	20	15	0.2
8	20	15	0.2
9	20	20	0.3
10	20	15	0.2
11	20	10	0.3
12	10	15	0.3
13	30	15	0.3
14	20	15	0.2
15	20	10	0.1
16	10	10	0.2
17	30	20	0.2

[a] The run order is allocated randomly by DoE software.

4.2.6 Characterization of RTG- nanosuspension

4.2.6.1 Measurement of drug content (%)

The drug content of RTG-Nanosuspension was determined by resuspending 2 mg equivalent of lyophilized nanosuspension in Milli-Q water. Further, samples were centrifuged (Eppendorf®, Hamburg, Germany) at 15,000 rpm for 10 min at 4 ºC, and the supernatant was filtered through 0.45 μm membrane filter. Filtered samples (n = 3) were analysed using validated RP-HPLC method [20].

4.2.6.2 Measurement of particle size, PDI, and zeta potential

Average particle size (d.nm) and PDI of optimization batches were measured using dynamic light scattering at 25 ºC (Nano ZS, Malvern Instrument Ltd., UK). Zeta potential (ζ) of the optimized nanosuspension was measured using electrophoretic dynamic light scattering at 25

^{o}C. Before the measurements, an equilibration time of 20 s was set for all samples. All the samples were diluted 10 times with Milli-Q water to avoid cross-reflectivity from the adjacent particles.

4.2.6.3 Field emission scanning electron microscopy (FESEM)

The characteristic surface morphology of lyophilized RTG-Nanosuspension was studied using field emission scanning electron microscopy (FEI, Washington, USA). The solid samples of pure RTG, Poloxamer 407 and lyophilized RTG-Nanosuspension were deposited on double sided carbon tape and tape was then placed on aluminium stubs. Samples were gold coated for 50 s by Q150TES sputter coater (Quorum Technologies, East Sussex, England). Gold-coated samples were analysed using FESEM at high vacuum at 10 kV.

4.2.6.4 Transmission electron microscopy (TEM)

The particle size and shape of RTG-Nanosuspension and pure-RTG was further evaluated using transmission electron microscopy (JEOL, Tokyo, Japan) at an accelerating voltage of 120 kilovolts. A simple drop caste method on carbon coated copper grids were used to prepare the samples for TEM analysis. Liquid sample of formulations was dropped on the carbon grid, allowed to caste on the grid, then excess formulation was soaked using blotting paper before measurement.

4.2.6.5 Differential scanning calorimetry (DSC)

The thermograms of drug, surfactant, and lyophilized RTG-Nanosuspension were acquired by DSC-60 Plus (Shimadzu, Kyoto, Japan), and TA-60 WS, thermal analyser software, was used for data analysis. Approximately 3 – 5 mg samples were weighed and crimped inside standard aluminium pans. Samples were heated at a rate of 10 ^{o}C/min from 25 – 200 ^{o}C with a nitrogen flow rate of 50 mL/min.

4.2.6.6 Powder X-ray diffraction (PXRD)

PXRD analysis was performed to discern the crystalline or amorphous nature of pure RTG, Poloxamer 407, physical mixture and the lyophilized RTG-Nanosuspension. Miniflex II, powder-X-ray diffractometer (Rigaku, Tokyo, Japan) was used to analyse the samples. PXRD experiment was carried out using Cu Kα line as the source of radiation at a wavelength of 1.5405 Å. The instrument was operated at a scanning rate of 2 ^{o}/min and scanned between 2θ range of 5 – 60 ^{o} [21]. The physical mixture of RTG and Poloxamer 407 was prepared by geometric mixing using mortar pestle.

4.2.6.7 Fourier-transform infrared spectroscopy (FT-IR)

FT-IR was performed to identify interactions between ingredients. FT-IR (Bruker, Massachusetts, USA) equipped with attenuated total reflectance (ATR) probe was used to analyse the IR spectroscopy of the samples. Pure RTG, Poloxamer 407, and lyophilized RTG-Nanosuspension were analysed directly using ATR accessory. Each spectrum was scanned in a range from 600 – 4000 cm^{-1}.

4.2.6.8 Raman spectroscopy

Raman spectroscopy was used to characterize the interaction between RTG and surfactant. It can also interpret the crystalline and amorphous nature of the pure drug and lyophilized RTG-Nanosuspension. Analysis was performed using surface-enhanced Raman spectroscope (HORIBA Scientific, Kyoto, Japan) equipped with laser excitation energy of 633 nm (17 mW power). Spectra measurements were conducted in the frequency range 100 – 4500 cm^{-1}.

4.2.7 *In vitro* dissolution

In vitro drug dissolution study of lyophilized RTG-Nanosuspension and pure RTG was carried out in small volumes to imitate the volume of nasal fluid. Several drug dissolution studies are reported using lower volume and modified dissolution apparatus to mimic the *in*

vivo environment of the administration site [3,22,23]. The study was performed using an in-house modified USP Type I dissolution apparatus (Electrolab-Tablet Dissolution Tester, Mumbai, India). 250 mL beakers of uniform dimensions were placed inside the dissolution apparatus jar, and the samples were kept inside the basket. Further, the baskets containing samples were immersed into the beaker containing 100 mL of dissolution medium maintained at 33 ± 1 ^{o}C as the temperature of nasal cavity is 33.5 ^{o}C [24]. The rotational speed of the baskets was set at 50 rpm. The study used phosphate buffer saline (PBS) pH 6.4, containing 0.2% sodium lauryl sulphate as the dissolution media. Samples (1 mL) were withdrawn at predetermined time points (5, 10, 15, 30, 45, and 60 min) and replenished with an equal volume of fresh dissolution media. Processing and analysis of samples were performed using our previously reported RP-HPLC method discussed in **Chapter 3, Method II** [20]. Dissolution profiles for pure RTG and lyophilized RTG-Nanosuspension were compared employing model-independent approach. Dissolution efficiency (DE), mean dissolution time (MDT), mean dissolution rate (MDR), and similarity factor (f_2) were determined for both the pure drug and lyophilized nanosuspension to effectively compare the dissolution behaviour.

4.2.8 *Ex vivo* nasal permeation

Ex vivo nasal permeation study was performed using Franz diffusion cell (Orchid Scientific, Nashik, India). Goat nasal mucosa was used for the nasal permeation study [10]. The whole nose of goat was obtained immediately after the sacrifice of goat from a local slaughterhouse. The nose was cleaned in saline solution to remove any traces of blood. The adherent muscles were properly removed using scissors. Mucosa was stored in PBS (pH 7.4) immediately after processing. The receptor compartment of the diffusion cell was filled with 5 mL of PBS (pH 6.4) as diffusion media. The nasal mucosa, with a diffusion area of 0.785 cm^2 and thickness of 0.22 ± 0.03 mm was placed in contact with receptor compartment keeping the mucosal side facing toward the donor compartment. The mucosa was allowed to stabilize for a pre-

incubation time of 30 min with PBS (pH 6.4) in both donor and receptor compartments [25]. The whole diffusion assembly was set at 33 ± 1 ^{o}C and stirred at 50 rpm. One mL of RTG-dispersion (dispersed in PBS pH 6.4) and RTG-Nanosuspension (dispersed in PBS pH 6.4) equivalent to 2 mg RTG were placed on the donor compartment. Samples of 500 µL were withdrawn at predetermined time intervals (5, 10, 15, 30, 60, 120, 240, and 360 min) and replaced with the same amount of pre-heated fresh media. All the samples were centrifuged (Eppendorf®, Hamburg, Germany) at 15,000 rpm for 15 min, and supernatant was filtered through 0.45 µm syringe filter. Filtered samples were suitably diluted to determine the permeated amount of RTG per unit area and the % drug permeability at various time points from pure RTG-dispersion and RTG-Nanosuspension using validated RP-HPLC method discussed in **Chapter 3, Method II** [20].

4.2.9 Nasal ciliotoxicity study

The effect of pure drug and RTG-Nanosuspension on the structural integrity of nasal mucosa, was investigated and suitably compared with positive and negative control groups. Goat nasal mucosa was carefully separated, cleaned with saline solution, and cut into four pieces. Two pieces of mucosae were treated with PBS pH 6.4 (negative control) and isopropyl alcohol (positive control) for 6 h, respectively. Other two pieces of mucosae were treated with pure drug suspension and optimized RTG-Nanosuspension for 6 h. Afterwards, all the mucosae were washed with saline solution and fixed in 10% formalin solution. The mucosal sections were stained with hematoxylin and eosin after the preparation of histopathological slides [26]. The sections were examined for nasal mucosal damages and sign of toxicity, if any, using inverted microscope (Carl Zeiss, Jena, Germany).

4.2.10 Stability study

Lyophilized RTG-Nanosuspension samples were tightly sealed in glass vials (15 mL) and stored at refrigerated conditions (4 ^{o}C). Samples (n = 3) were collected at 1-month intervals for 3 months. After collection, stored samples were dissolved in Milli-Q water and assessed for mean particle size, PDI, and drug content. The data acquired at sampling points (1st, 2nd and 3rd month) were compared with that of the freshly prepared RTG-Nanosuspension. The stability of the RTG-Nanosuspension was evaluated for 3 months.

4.2.11 *In vivo* studies in Wistar rats

All *in vivo* experiments were approved by the Institute's Animal Ethics Committee (IAEC), Protocol number- IAEC/RES/26/07/REV-1/30/19. All *in vivo* studies for RTG nanosuspension and suspension were performed in male Wistar rats of 9 – 10 weeks old, which weighed between 250 – 260 g. RTG suspension was prepared by suspending the drug in 0.2% w/v of methylcellulose (400 cps). Formulations were administered at 2 mg/Kg of rat weight. Food and water were supplied *ad libitum* to the rats during their housing. Animals were fasted overnight with only access to water before dosing.

4.2.11.1 Intranasal (i.n.) administration

Formulations were administered intranasally using a soft cannula (Instech Laboratories, PA, USA). It was 1.3 cm long and attached to a 100 µL microtip to ensure delivery to an olfactory region in the nasal cavity. Rats were anesthetized before dosing and sample collection using isoflurane in the anaesthetic chamber. 50 µL of the formulation was administered in each nostril, and animals were kept supine until anaesthesia recovery.

4.2.11.2 Evaluation of mucociliary transport time

Mucociliary transport time was evaluated to assess the mucociliary clearance of the formulations [27]. Both formulations were administered (50 µL) to each nostril as mentioned

in **Section 4.2.11.1** and the oropharyngeal cavity was swabbed using cotton buds at every 5 min till 90 min. Rats were not allowed to take food for 1 h after starting the study. The samples collected at each time point were 10-times diluted using RP-HPLC mobile phase (ACN:KH_2PO_4,pH 5::54:46) and measured using the validated RP-HPLC method described in previous **Chapter 3**, **Method II** [20]. The first time point at which RTG was detected in the oropharyngeal swab was the mucociliary transport time of respective formulations.

4.2.11.3 Brain and plasma PK analysis

Lyophilized RTG-Nanosuspension was dissolved in Milli-Q® just before i.n. dosing. Blood samples were collected (n = 4 rats) via Retro-orbital puncture at predetermined intervals (0, 0.08, 0.25, 0.5, 1, 2, 4, 6, and 8 h). A separate group of rats (n = 4) was assigned for the brain PK study. The whole brain was collected at predetermined intervals (0.5, 1, 2, 4, 6, and 8 h) after sacrificing the rats using cervical dislocation. Brain and plasma samples were processed and analysed using validated RP-HPLC bioanalytical method described previously in **Chapter 3, Method III**. PK parameters (C_{max}, T_{max}, $AUC_{0\rightarrow tlast}$, MRT, clearance) for both brain and plasma were determined by non-compartmental analysis (NCA) using Phoenix WinNonlin (Version 8.0, Pharsight Corporation, NC, USA).

Direct transport percentage DTP (%) and drug targeting efficiency percentage DTE (%) of the formulations were measured to assess brain targeting efficiency. DTP (%) indicates the drug percentage reaching directly to the brain via nose. In contrast, DTE (%) indicates the total drug transported to the brain, which includes direct nose-to-brain and indirect nose-to-systemic circulation-to-brain [28]. Positive and high DTP (%) and DTE (%) are indicative of efficient brain drug delivery [29]. These were calculated using the following equations, Equation 4.1 and 4.2, respectively:

$$DTP(\%) = \frac{AUC_{brain_{i.n.}} - B_x}{AUC_{brain_{i.n.}}} \times 100 \qquad (4.1)$$

where,

$$B_x = \frac{AUC_{brain_{i.v.}}}{AUC_{plasma_{i.v.}}} \times AUC_{plasma_{i.n.}}$$

where, AUC_{brain} = $AUC_{0\rightarrow tlast}$ in brain, AUC_{plasma} = $AUC_{0\rightarrow tlast}$ in plasma. B_x is the fraction of $AUC_{0\rightarrow last(brain)}$ from systemic circulation (via indirect pathway) after i.n. administration of a given formulation.

$$DTE\ (\%) = \frac{(AUC_{brain}/AUC_{plasma})_{i.n.}}{(AUC_{brain}/AUC_{plasma})_{i.v.}} \times 100 \quad (4.2)$$

where, AUC_{brain} = $AUC_{0\rightarrow tlast}$ in brain, AUC_{plasma} = $AUC_{0\rightarrow tlast}$ in plasma.

4.2.12 Histopathology of brain

For histopathology of brain, brains were isolated from rats at 0 time (as control) and at 8th h (as treated) after i.n. administration of RTG-Nanosuspension. The isolated brains were washed in PBS (pH 7.4) to remove traces of blood and connective tissues. The cleaned brains were weighed and then fixed in 10% v/v formalin solution. A series of ethanol concentration (*v/v*) i.e., 70%, 80%, 95%, and finally using 100%, dehydration of brain tissue was performed. The brain tissue was embedded in paraffin wax and sectioned using microtome. The deparaffinization process was performed using xylene. Slides were first treated with xylene, then ethanol concentrations (*v/v)*of 100%, 80%, and 70%, and finally using phosphate buffer saline (pH 7.4) rehydration was achieved. Finally the slides were stained with hematoxylin and eosin. The histopathological slides were examined using inverted light microscope (Carl Zeiss, Jena, Germany) for toxicity. The histopathological slides of brain were analyzed qualitatively, and three rats per group was used in the study.

4.3 Results and discussion

4.3.1 Solubility of RTG in various solvents

Solubility of RTG was determined in methanol, ethanol, and acetone. All these solvents are miscible with water which is one of the prerequisites in solvent selection. The solubility of RTG was highest in methanol, followed by ethanol and acetone (**Figure 4.2A**). Ethanol and acetone are classified as class 3 solvents in the ICH guidelines and regarded as safer compared to methanol, a class 2 solvent [30]. Hence, the further solvent selection was carried out using ethanol and acetone. The effect of these two solvents on the particle size and PDI of nanosuspension was assessed. Nanosuspension prepared with ethanol yielded smaller particle size and narrow PDI than nanosuspension prepared with acetone (**Figure 4.2B**). This result can be ascribed to the effect of boiling point of the two solvents. The acetone (56 ^{o}C) has lower boiling point than ethanol (78 ^{o}C). Therefore, acetone rapidly evaporates during the sonication process resulting in quick supersaturation of RTG in the aqueous phase. Additionally, ethanol has been widely reported to be used as solvent phase in various nanosuspension intended for oral, parenteral and nasal delivery In contrast, ethanol has been widely used as the solvent phase in various nanosuspension intended for oral, parenteral, and nasal delivery [31,32]. Therefore, ethanol was selected as the solvent for the preparation of nanosuspension.

4.3.2 Screening of surfactant

RTG showed significantly low solubility in Poloxamer 188, Poloxamer 407, and Soluplus®. Nanosuspension prepared using these surfactants showed considerably lower particle size (**Figure 4.2C**). In Poloxamer 407, RTG showed the lowest solubility (5.83 ± 2.33 µg/mL) and resulted in size of 360.50 ± 9.26 nm. The decreased drug solubility in the antisolvent phase results in higher nucleation rates and inhibits Ostwald's ripening rendering smaller particle size [33,34]. Hence, Poloxamer 407 yielded the lowest particle size compared to

other surfactants. One of the most important challenges associated with nanosuspension is Ostwald ripening and particle aggregation [35]. Surfactants offer a steric barrier, inhibiting Ostwald ripening and agglomeration, resulting in a physically stable nanosuspension [36]. Furthermore, the lower viscosity with surfactant helps in achieving smaller particle size. An increase in antisolvent viscosity inhibits the diffusion across solvent phase, leading to a lower nucleation rate and increased particle agglomeration. Thus, the lower viscosity of Poloxamer 407, Soluplus® and Poloxamer 188 solution might have resulted in smaller particle size than other surfactants [33,37]. Therefore, Poloxamer 407 was selected as surfactant for further optimization of nanosuspension. In contrast, span 20, PVP K-30, sodium lauryl sulphate, and tween 20, RTG showed significantly high solubility and larger particle size (**Figure 4.2C**).

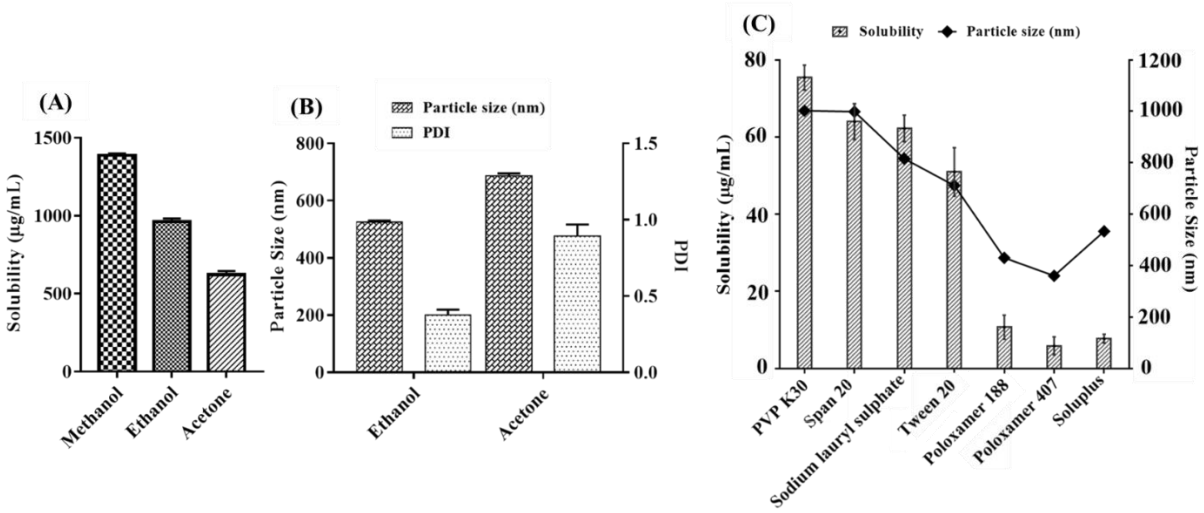

Figure 4.2 Selection of formulation excipients for nanosuspension: (A) Effect of organic solvents on solubility of RTG, (B) Effect of organic solvent on particle size and PDI, (C) Effect of surfactant on solubility of RTG and particle size

4.3.3 Experimental design for the preparation of RTG-Nanosuspension

4.3.3.1 BBD analysis

A three-factor, three-level BBD was employed for the optimization of RTG-Nanosuspension. According to the design matrix obtained from Design-Expert software, 17 batches of RTG-Nanosuspension were prepared. Their corresponding results for particle size (nm) and PDI are presented in **Table 4.3**. For all 17 batches of prepared nanosuspension, particle size was

found to be in the range of 61.2 to 434.1 nm, and PDI was observed to be within the range of 0.181 to 0.495. The obtained responses for all 17 batches were subjected to statistical evaluation using Design-Expert software. Particle size (nm) and PDI variability are best explained using a reduced cubic model. The ANOVA result from regression analysis for both dependent responses (R_1 and R_2) and their significant terms, is presented in **Table 4.4**. The regression models obtained for both of the responses were statistically significant ($P < 0.0001$). The R^2 and Adj R^2 for the best-fit models were found to be 0.999 and 0.999 for R_1 (particle size, nm) and 0.998 and 0.992 for R_2 (PDI), respectively. High R^2 values and its closeness to Adj R^2 values signify that the models are well fitted for both of the dependent responses. The model equations for R_1 (particle size, nm) and R_2 (PDI) in terms of coded factors are given below:

$$R_1 = 64.384 + 30.9A + 10.1875B + 44.35C + 49.025AB + 25.85AC - 36.60BC + 162.63A^2 + 111.08B^2 + 52.27C^2 - 39.11A^2B + 4.49A^2C - 48.22AB^2$$

$$R_2 = 0.186 + 0.025A + 0.037B + 0.016C + 0.015AB + 0.029AC - 0.068BC + 0.167A^2 + 0.076B^2 + 0.063C^2 - 0.087A^2B - 0.087A^2C - 0.087AB^2$$

Table 4.3 Box-Behnken design batches composition and experimental results for RTG-Nanosuspension

Run[a]	Drug concentration (mg/mL)	Solvent: antisolvent	Surfactant concentration (% w/v)	Particle size (nm)	PDI
1	10	20	0.2	278.2 ± 1.21	0.366 ± 0.009
2	20	15	0.2	61.2 ± 5.22	0.181 ± 0.028
3	10	15	0.1	225.4 ± 0.98	0.446 ± 0.034
4	30	10	0.2	301.4 ± 6.11	0.464 ± 0.076
5	20	20	0.1	226.9 ± 2.04	0.415 ± 0.024
6	30	15	0.1	235.5 ± 3.83	0.439 ± 0.003
7	20	15	0.2	63.6 ± 0.99	0.185 ± 0.009
8	20	15	0.2	65.3 ± 1.01	0.187 ± 0.023
9	20	20	0.3	250.4 ± 2.58	0.312 ± 0.024
10	20	15	0.2	66.2 ± 0.90	0.188 ± 0.019
11	20	10	0.3	295.2 ± 5.25	0.373 ± 0.028
12	10	15	0.3	271.4 ± 3.17	0.336 ± 0.034
13	30	15	0.3	384.9 ± 2.95	0.445 ± 0.001
14	20	15	0.2	65.6 ± 1.62	0.189 ± 0.008
15	20	10	0.1	141.3 ± 3.83	0.203 ± 0.098
16	10	10	0.2	434.1 ± 11.29	0.495 ± 0.002
17	30	20	0.2	341.6 ± 1.22	0.396 ± 0.021

[a] The run order is allocated randomly by DoE software.

Table 4.4 Regression coefficients and statistical analysis for Box-Behnken design matrix for RTG-Nanosuspension

Response model	Factor	Factor coefficient	P value	Adj R^2	Pred R^2	Model F-value
R_1: Particle size (Cubic model)	Intercept	64.384	0.0001	0.99993	0.9997	4786.37 (P < 0.0001)
	B- Solvent : antisolvent	10.1875	0.0005			
	C- Surfactant concentration	44.3525	0.0001			
	AB	49.025	0.0001			
	AC	25.85	0.0001			
	BC	-32.6025	0.0001			
	A^2	162.63925	0.0001			
	B^2	111.80175	0.0001			
	C^2	52.27675	0.0001			
	A^2B	-39.1125	0.0001			
	A^2C	4.4975	0.0001			
	AB^2	-48.225	0.0001			
R_2: PDI (Cubic model)	Intercept	0.186	0.0001	0.99982	0.99926	1821.93 (P < 0.0001)
	A- Drug concentration	0.0255	0.0001			
	B- Solvent : antisolvent	0.03775	0.0001			
	C- Surfactant concentration	0.01675	0.0004			
	AB	0.01525	0.0006			
	AC	0.029	0.0001			
	BC	-0.06825	0.0001			
	A^2	0.1675	0.0001			
	B^2	0.07675	0.0001			
	C^2	0.063	0.0001			
	A^2B	-0.087	0.0001			
	A^2C	-0.04275	0.0001			
	AB^2	-0.02575	0.0003			

4.3.3.2 Response surface plots

The 3D response surface plots were used for understanding the relationship between the 3 critical method variables with the two responses i.e., the particle size (R_1) and PDI (R_2). 3D-response surface plots **Figure 4.3** (**A** – **F**) demonstrates the effect of drug concentration (A), solvent:antisolvent ratio (B) and surfactant concentration (C) on R_1 and R_2 of RTG nanosuspension.

Figure 4.3A and **B** shows the effect of drug concentration (A) and surfactant concentration (C) on R_1; particle size, and R_2; PDI, respectively. An increase in drug concentration (A) results in a significant increase in R_1. This could be attributed to the fact that an increase in drug concentration promotes particle agglomeration resulting in larger particle size [38]. An increase in surfactant concentration (C) causes an increase in R_1 **Figure 4.3A** This result might be ascribed to the fact that high surfactant concentration leads to higher antisolvent phase viscosity, reducing fluid velocity, weakening the cavitation effect, and ultimately yielding increased particle size [39]. Decreased surfactant concentration also results in increased R_1. This could be attributed to the low surfactant concentration failing to provide sufficient electrostatic stabilization resulting in particle agglomeration [40,41]. **Figure 4.3B** demonstrated that high drug concentration increases PDI. Here, high supersaturation caused by very high drug concentrations led to particle agglomeration [42]. High surfactant concentration (C) significantly increased R_2; PDI (**Figure 4.3B**). This result might be attributed to the fact that high surfactant concentration causes a reduction in nucleation rate, which promotes particle agglomeration driving increased PDI [41].

Figure 4.3C and **D** depicted the effect of drug concentration (A) and solvent:antisolvent ratio (B) on R_1 and R_2. **Figure 4.3C** depicted that increased drug concentration (A) has significantly increased R_1. The increase in drug concentration causes particle agglomeration during precipitation [43–45]. An increase in solvent:antisolvent ratio (B) has caused an increase in R_1 **Figure 4.3C**. This might be due to reduced supersaturation and poor nucleation rate resulting in larger particle size [46,47]. An increase in solvent:antisolvent ratio (B) has reduced R_2 (**Figure 4.3D)**, which could be caused by reduced Ostwald ripening.

Figure 4.3E and **F** presents the effect of solvent:antisolvent ratio (B) and surfactant concentration (C) on R_1 and R_2. **Figure 4.3E** indicated that increased surfactant concentration

(C) causes a sharp increase in R_1. This can be attributed to the combined effect of higher viscosity of antisolvent phase, lower fluid velocity, and cavitation effect [46,47]. Increased solvent:antisolvent ratio resulted in higher R_2 (**Figure 4.3F**), which could be due to reduced supersaturation. It also causes a reduction of the mixing efficiency during the nanoprecipitation process. The combined effect of these two processes finally results in increased R_2.

4.3.3.3 Desirability function and model validation

The desirability function was used for the simultaneous optimization of both critical responses. The constrain for desirability function were set in the software as per the desired properties of nanosuspension intended for i.n. administration i.e., minimizing both the particle size and PDI. The i.n. nanocrystals of less than 100 nm are directly taken up by the cells or neurons in the nose-to-brain pathway [14]. Lower PDI provides monodisperse system that ensures the stability, safety and efficiency of nanosuspension [48]. Based on the model obtained for each response (R_1 and R_2), the software generated several solutions with the respective predicted values for particle size, PDI, and various desirability factors

The proposed conditions for the optimized RTG-Nanosuspension were: 22.63 mg/mL drug concentration (A), 1:15.25 solvent:antisolvent ratio (B), and 0.15% w/v surfactant concentration (C) with the highest desirability function of 0.89. At the proposed conditions, optimized RTG-Nanosuspension was predicted to have a particle size of 73.27 nm and PDI of 0.241. Based on the predicted conditions given by the desirability function, batches (n = 3) of RTG-Nanosuspension were prepared. The particle size (nm) and PDI were statistically compared with the predicted values using t-test. The difference between the obtained and predicted values for both responses was statistically insignificant ($P > 0.05$), confirming the regression models' validity. The experimentally obtained values (n = 3) for the optimized RTG-Nanosuspension were 73.55 ± 4.04 nm for particle size and 0.286 ± 0.028 for PDI

(**Figure 4.4A**). The zeta potential (ζ) of RTG nanosuspension **Figure 4.4B** was observed to be −24.7 ± 0.7 mV (n = 3), indicating that the nanosuspension is stable [49,50].

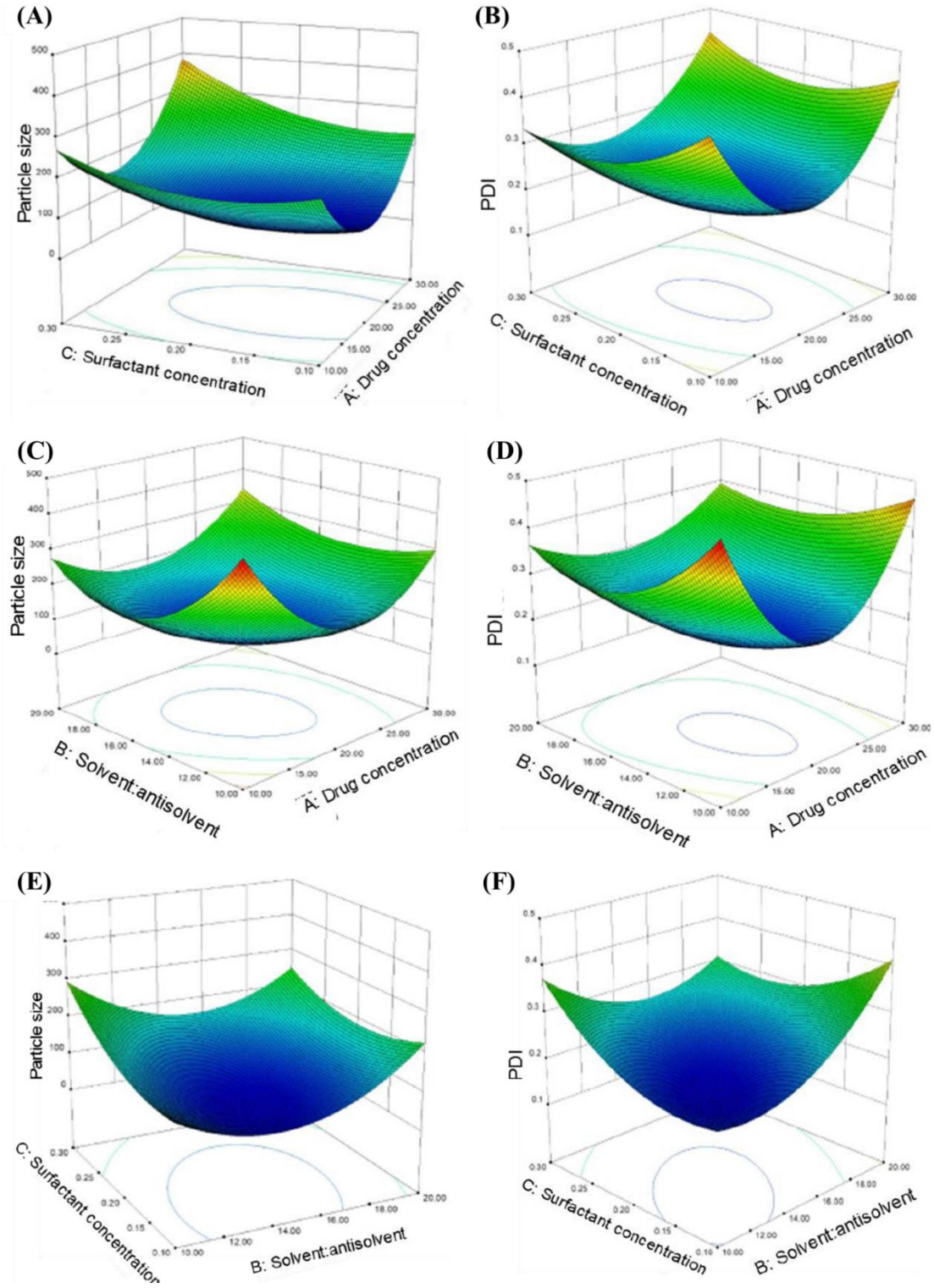

Figure 4.3 3D Contour plot for (A) Effect of drug and surfactant concentration on particle size, (B) Effect of drug and surfactant concentration on PDI, (C) Effect of drug concentration and solvent:antisolvent ratio on particle size, (D) Effect of drug concentration and

solvent:antisolvent ratio on PDI, (E) Effect of solvent:antisolvent ratio and surfactant concentration on particle size, (F) Effect of solvent:antisolvent ratio and surfactant concentration on PDI.

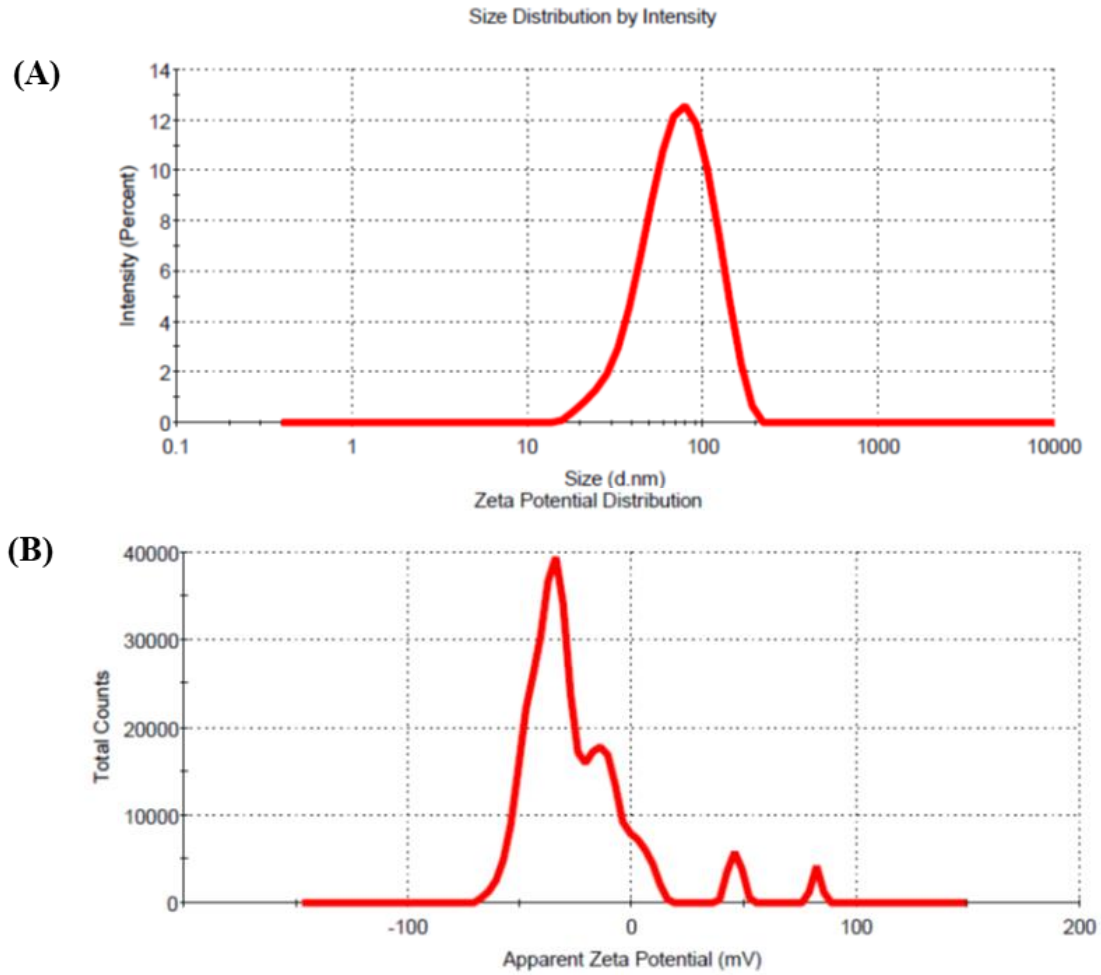

Figure 4.4 RTG-Nanosuspension characterization (A) Hydrodynamic diameter of optimized RTG nanosuspension based on the % intensity with an average diameter of 73.55 nm, (B) Zeta potential of optimized nanosuspension (−24.7 mV)

4.3.4 Characterization of RTG-Nanosuspension

4.3.4.1 Measurement of drug content (%)

Drug content (%) has a major effect on efficacy and safety of lyophilized nanosuspension. Drug content (%) was measured for the final lyophilized nanosuspension using previously discussed RP-HPLC method discussed in **Chapter 3, Method II** [20]. The drug content (%) of the optimized RTG-Nanosuspension was found 101.61 ± 3.69 % w/w.

4.3.4.2 Field emission scanning electron microscopy

Distinctive differences in the morphology of pure RTG and lyophilized RTG-Nanosuspension were observed in **Figure 4.5**. **Figure 4.5A** shows that pure RTG predominantly appeared as orthorhombic-shaped crystals [18]. Poloxamer 407 were spherical with smooth surface **Figure 4.5B** [51]. The FESEM image of lyophilized RTG-Nanosuspension **Figure 4.5C** showed no evidence of characteristic morphology of pure drug. The optimized method could form desired RTG-Nanosuspension, and the selected stabilizer effectively influenced the morphology of lyophilized RTG-Nanosuspension.

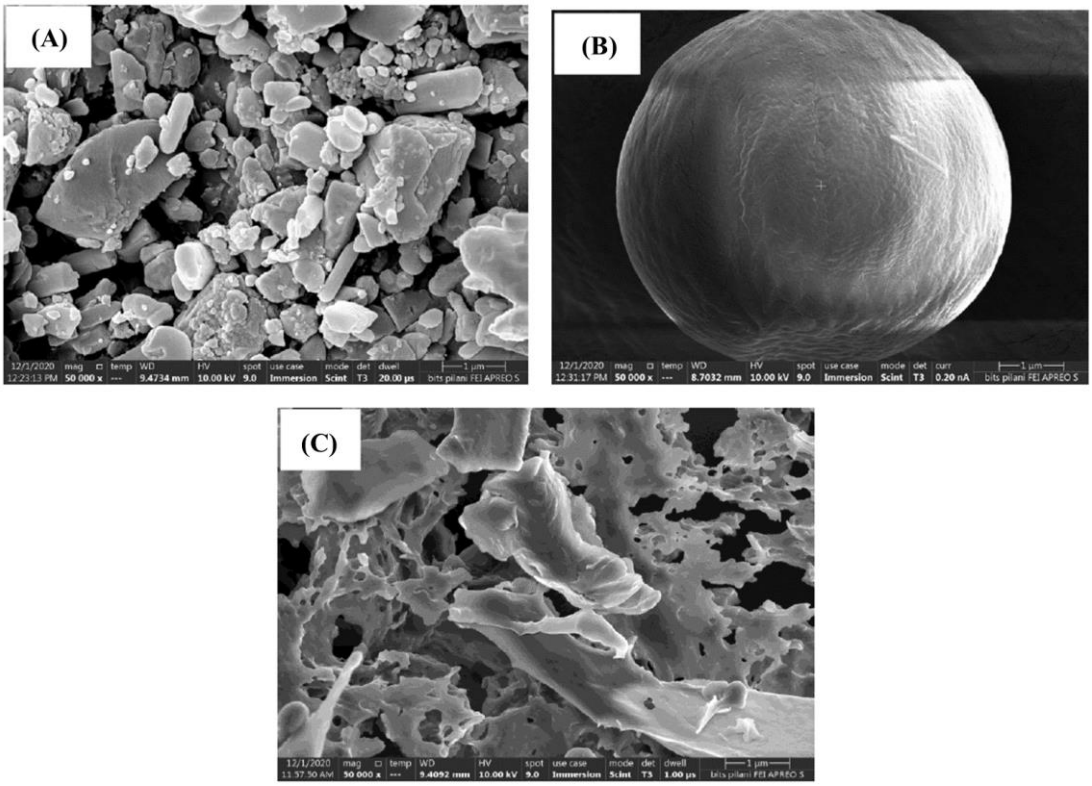

Figure 4.5 FESEM images (A) Crystalline (orthorhombic) structure of pure-RTG, (B) Smooth spherical structure of pure Poloxamer 407, (C) Porous amorphous structure of lyophilized RTG-Nanosuspension

4.3.4.3 Transmission electron microscopy

The shape and size of pure RTG and RTG-Nanosuspension were further characterized by TEM analysis. TEM image of pure RTG showed that the particle size of drug is significantly higher with sharp edges (**Figure 4.6A**). The morphological analysis of RTG-Nanosuspension

is shown in **Figure 4.6B**. The particles are nearly spherical in shape and size was in the similar range of the hydrodynamic size of the RTG-Nanosuspension.

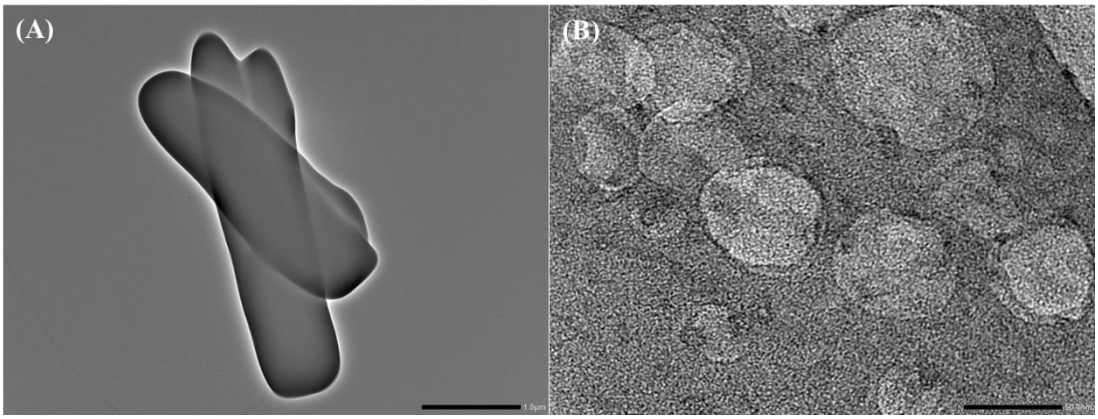

Figure 4.6 TEM images (A) pure RTG, (B) Optimized RTG-Nanosuspension

4.3.4.4 Differential scanning calorimetry

DSC defines the thermotropic phase transition behavior quantitatively [52]. The DSC thermograms of pure RTG, Poloxamer 407, and the lyophilized nanosuspension formulation are presented in **Figure 4.7A**. The pure drug showed a sharp endothermic melting peak at 97.93 ^{o}C as reported for polymorphic Form II of RTG [53]. Poloxamer 407 exhibited a strong endothermic peak at 51.29 ^{o}C [54]. But endothermic peak of the drug was found to be completely abolished in the lyophilized RTG-Nanosuspension formulation. Absence of endothermic peak of RTG in DSC thermogram indicates that the drug has been completely converted into amorphous from in the prepared lyophilized nanosuspension formulation [55].

4.3.4.5 Powder X-ray diffraction

The PXRD patterns of pure RTG, Poloxamer 407, physical mixture and the lyophilized RTG-Nanosuspension are presented in **Figure 4.7B**. The PXRD pattern of RTG presented intense peaks, at diffraction angles ($^{o}2\theta$): 12.140^{o}, 13.775^{o}, 17.855^{o}, 20.525^{o}, 22.085^{o}, and 22.955^{o} affirming its crystalline nature [21,56]. The X-ray diffractogram for Poloxamer 407 showed two distinct characteristic peaks at 20.450^{o} and 24.535^{o} suggesting the crystalline nature of the surfactant [57,58]. The characteristic peaks of RTG and Poloxamer 407 were present in

the physical mixture, indicating that the crystallinity of pure drug was unchanged in the physical mixture. The absence of characteristic PXRD peaks of RTG in the lyophilized RTG-Nanosuspension suggested its amorphous form, which is also supported by the DSC results.

4.3.4.6 Fourier-transform infrared spectroscopy

FT-IR spectrum of pure RTG, Poloxamer 407, and lyophilized RTG-Nanosuspension is shown in **Figure 4.7C**. FT-IR spectrum of pure RTG showed characteristic stretching vibrations at 3550 cm^{-1}, 1524 cm^{-1}, and 1269 cm^{-1} [21]. In pure RTG, intermolecular hydrogen bonding between -N group of one drug molecule and (OH group) is formed. The formation of hydrogen bonding caused the characteristic crystal structure of the drug [53]. Several IR absorption bands of RTG were observable in the FT-IR spectrum of lyophilized RTG-Nanosuspension, but with less intensity, which indicates an interaction between RTG and Poloxamer 407.

4.3.4.7 Raman-spectroscopy

Surface-enhanced Raman spectroscopy further investigated the conversion of crystalline RTG into amorphous form in the lyophilized RTG-Nanosuspension. In pure RTG, intermolecular hydrogen bonding between –OH group of one drug molecule and with -N group of another drug molecule is formed [53]. The Raman spectra of pure drug **Figure 4.7D** exhibited characteristic spectra at wavenumbers 683.09 cm^{-1}, 1054.9 cm^{-1}, and 1437.7 cm^{-1} corresponding to aliphatic C–S vibrations (630 – 790 cm^{-1}), amines (1000 – 1350 cm^{-1}) and asymmetrical CH_2–CH_2 chains (1400 – 1470 cm^{-1}), respectively [59]. The Raman spectrum of lyophilized RTG-Nanosuspension **Figure 4.7D** showed broader and less intense spectra at 683.7 cm^{-1}, 1053.9 cm^{-1}, and 1437.9 cm^{-1} compared to pure crystalline RTG. The typically crystalline form produces a Raman spectrum with very sharp, intense Raman bands, whereas an amorphous form shows comparatively broader and less intense bands [59–61]. These

results again confirmed that the crystalline RTG converted into an amorphous form in lyophilized RTG-Nanosuspension. The Raman spectroscopy results endorse FT-IR results, and both studies complement each other.

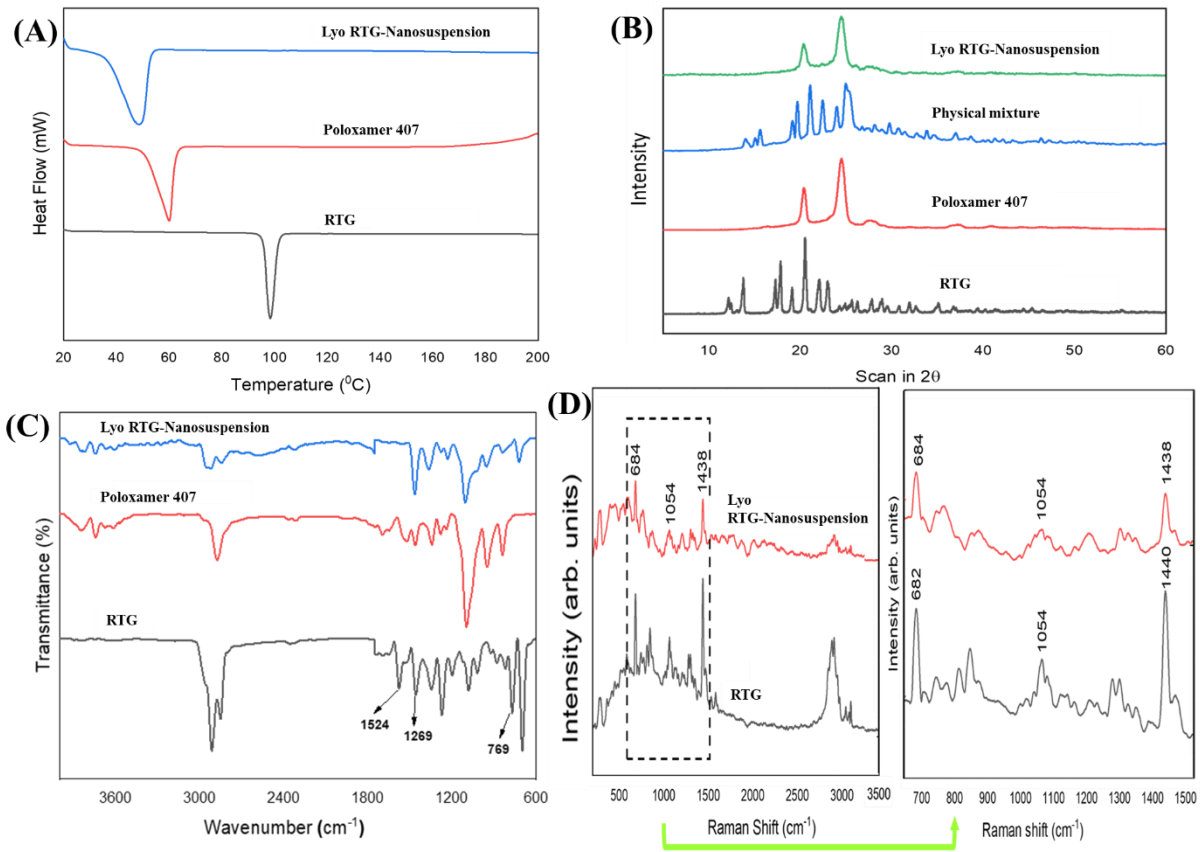

Figure 4.7 (A) DSC thermograms, (B) PXRD spectra, (C) FT-IR spectra, (D) Raman spectra for pure RTG and optimized RTG-Nanosuspension with magnified view of Raman spectra of pure RTG and RTG-Nanosuspension: Broadening of aliphatic C–S vibrations peak (682 cm^{-1}); amines peak (1054 cm^{-1}); and asymmetrical CH_2–CH_2 chains peak (1440 cm^{-1})

4.3.5 *In vitro* dissolution

The dissolution profile of the optimized RTG-Nanosuspension was compared with pure RTG and presented in **Figure 4.8A**. A significant improvement in nanosuspension's rate and extent of dissolution compared to the pure drug was seen. In the first 15 min, % cumulative drug dissolved from RTG-Nanosuspension was found to be greater than 95%, whereas, in the case of pure drug, it was observed to be less than 2% within the same period. Furthermore, pure RTG demonstrated very poor dissolution, as only 6.32% of the drug was dissolved in 1 h. The DE at 60 min, MDT, MDR, and f_2 were calculated and used to effectively compare the

dissolution behaviour of nanosuspension and pure drug (**Table 4.5**). The f_2 was significantly lower than 50, demonstrating that the two dissolution profiles are not similar. Lower MDT and higher MDR of RTG-Nanosuspension further show the significant dissolution enhancement of RTG. This enhancement in the RTG dissolution from the RTG-Nanosuspension can be attributed to the various properties of the formulation. Firstly, the conversion of crystalline form into amorphous in RTG-Nanosuspension is one of the reasons [31]. Secondly, nanosize particles can cause improvement in the apparent solubility [36]. Nernst–Brunner postulated that particle size reduction below 50 μm results in decreased effective boundary layer thickness and increased particle surface area [62,63]. This causes significant improvement in the dissolution rate of a substance. The Prandtl boundary layer equation states that particle size reduction beyond 2 μm creates a thin hydrodynamic layer around it. Thin hydrodynamic layer formation around particles is ascribed to their enhanced curvature, resulting in an improved dissolution rate [64,65].

Table 4.5 Model-independent dissolution parameters of pure RTG and RTG-Nanosuspension

Parameters	Pure RTG	RTG-Nanosuspension
Q_5	0.56	76.5
Q_{15}	1.57	95.11
Q_{60}	6.32	100
DE_5	0.002	0.383
DE_{15}	0.007	0.709
DE_{60}	0.311	0.918
MDT	0.508	0.082
MDR	3.84	15.66

4.3.6 *Ex vivo* nasal permeation

Ex vivo nasal permeation study was performed to evaluate the permeation behaviour of pure RTG and the RTG-Nanosuspension. **Figure 4.8B** shows the drug dispersion's permeation profile and the formulated nanosuspension across the goat nasal mucosa. The study revealed

that the amount of drug permeated per unit area from RTG-Nanosuspension was enhanced by 20-fold compared to pure drug suspension ($p < 0.0001$, Two-way ANOVA-Tukey test) over 360 min. The % cumulative drug permeated after 360 min from RTG-Nanosuspension and pure-drug suspension was 82.23 ± 3.85% and 10.85 ± 3.52%, respectively. The result demonstrates that formulation of nanosuspension has caused substantial improvement in drug permeability across the nasal mucosa. The improved nasal absorption could be predominantly due to the reduction in particle size and higher drug dissolution rate in nanosuspension formulation [66]. Higher permeability might also be attributed to the surface area of nanosuspension attained due to low particle size [32]. Further, the presence of Poloxamer 407 in the formulation might also help increase the nasal permeation of optimized nanosuspension. Poloxamer 407 is reported to increase drug transport via nasal mucosa by reducing the viscosity and elasticity of mucus [67,68]. Furthermore, characteristic property of surfactant to alter the tight junction of nasal mucosa could also improve the permeability of RTG-Nanosuspension [69]. The nasal permeation study result indicates that the optimized RTG-Nanosuspension is an interesting nanocarrier for i.n. delivery of RTG that might enhance the brain availability of the drug.

4.3.7 Nasal ciliotoxicity study

Nasal ciliotoxicity study was performed to determine the effect of pure RTG and RTG-Nanosuspension on nasal mucosa. Effect of negative control (PBS pH 6.4), positive control (isopropyl alcohol), pure drug suspension and RTG-Nanosuspension on nasal mucosa is shown in **Figure 4.9** (**A** – **D**), respectively. Negative control (PBS pH 6.4) treated nasal mucosa **Figure 4.9A** showed intact epithelial lining and no damage of mucosa. In **Figure 4.9B**, positive control (isopropyl alcohol) sample showed substantial damage to the epithelial cell lining of nasal mucosa. Isopropyl alcohol (mucociliary toxic agent) treated tissue appeared necrotized and also shown atrophy of glands (shown using arrow).

Histopathological structure of both nasal mucosae treated with pure drug suspension **Figure 4.9C** and optimized RTG-Nanosuspension **Figure 4.9D** appeared similar to the tissue structure of negative control and showed no sign of toxicity. The ciliotoxicity evaluation indicates that RTG-Nanosuspension is safe due to its non-toxic nature and can be used to deliver RTG into brain via i.n. route.

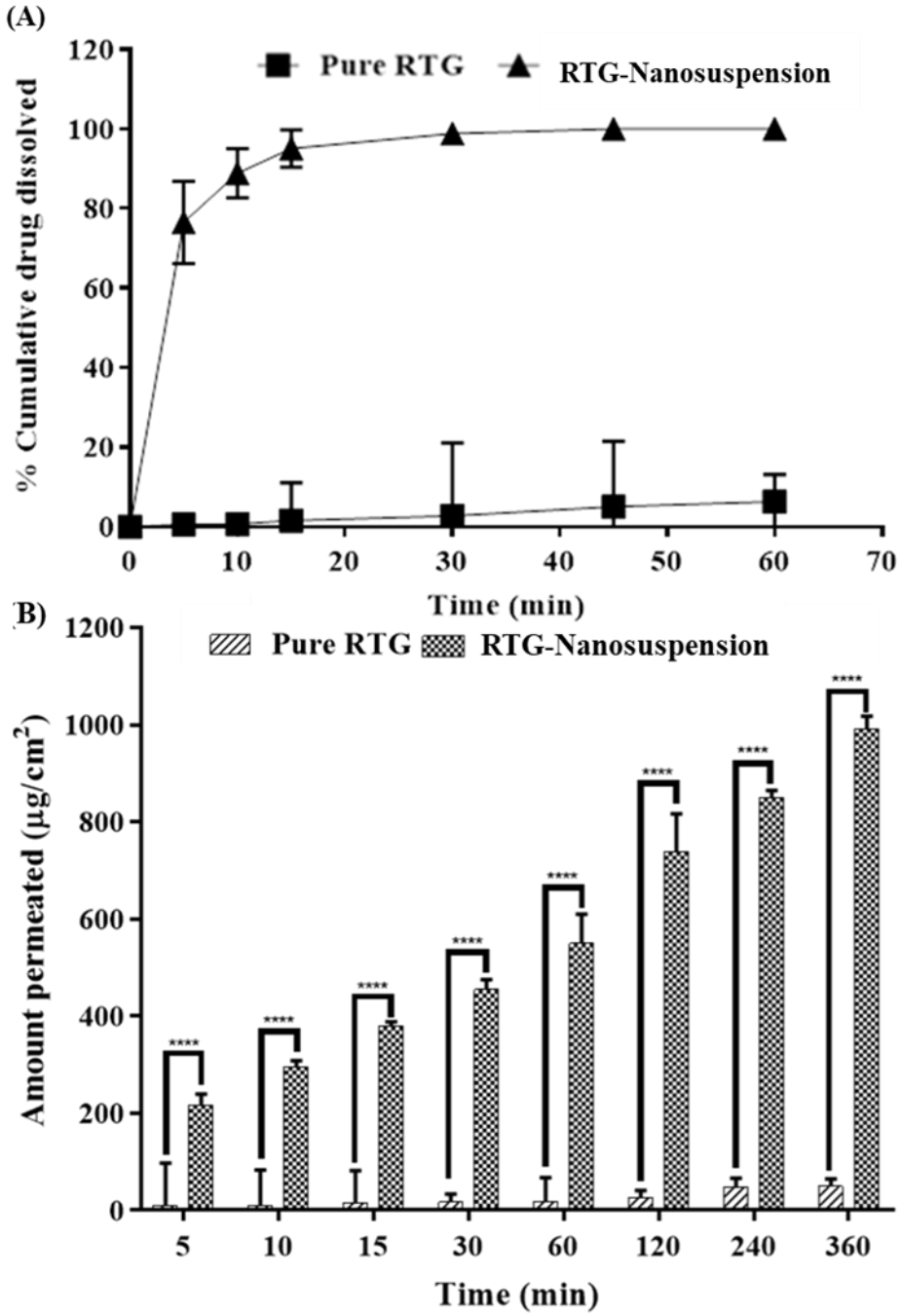

Figure 4.8 (A) Dissolution profiles of pure RTG and RTG-Nanosuspension (data are the means and standard deviations of three determinations; n = 3), (B) *Ex vivo* amount of drug

permeated/unit area from optimized RTG-Nanosuspension and drug suspension via goat nasal mucosa (n = 3, Mean ± SD)

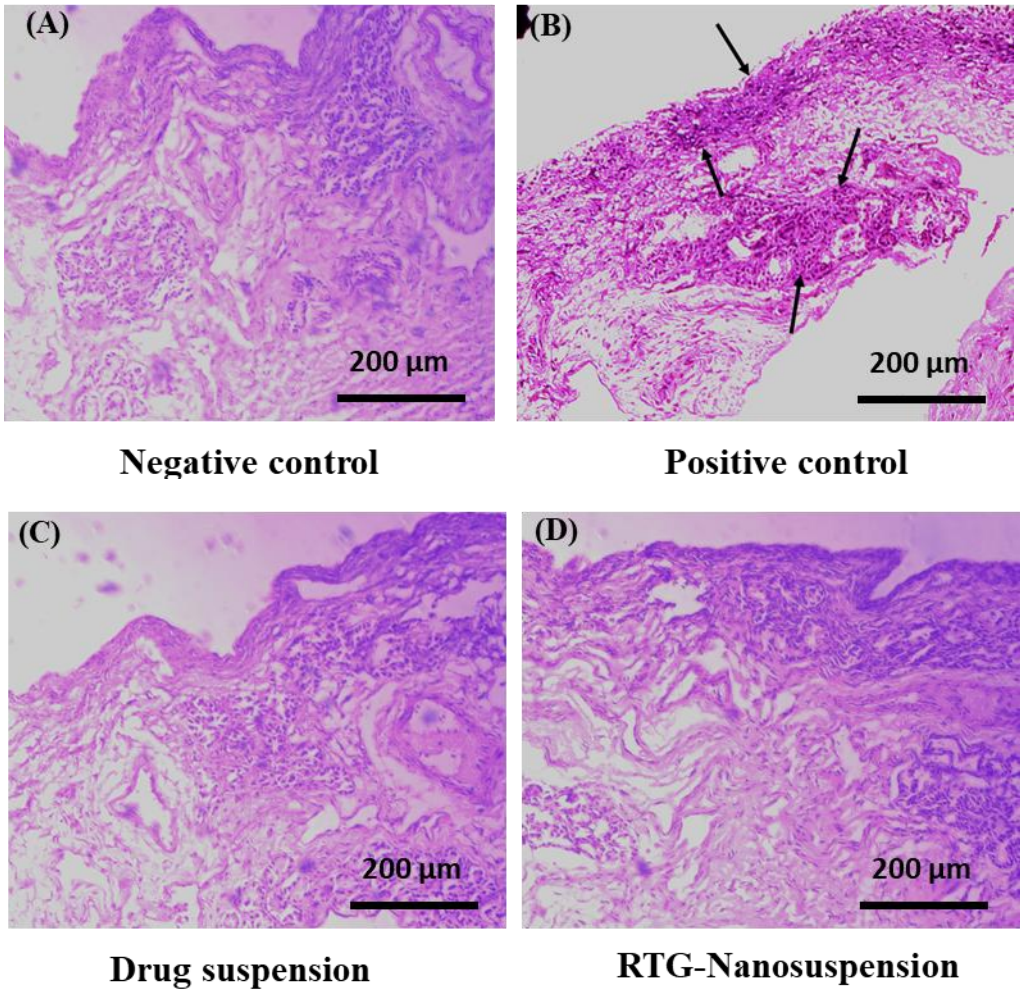

Figure 4.9 Histopathological micrograph (at 100X magnification) structure of goat nasal mucosa treated with (A) Phosphate buffer saline pH 6.4, (B) Isopropyl alcohol, (C) Drug suspension; (D) Optimized RTG-Nanosuspension

4.3.8 Stability study

Lyophilized RTG-Nanosuspension was evaluated for its stability over a period of three months in terms of particle size (nm), PDI and drug content. Results obtained from the stability study are shown in **Table 4.6**. No significant changes in terms of the mean particle size (nm), PDI and drug content of the lyophilized RTG-Nanosuspension were observed during 3 months of storage at refrigerated condition. This result indicates that the lyophilized RTG-Nanosuspension was stable.

Table 4.6 Stability studies data of RTG-Nanosuspension (n = 3)

Time (Months)	Particle size (nm)	PDI	Drug content (% w/w)
0	73.55 ± 4.04	0.286 ± 0.028	101.61 ± 3.69
1	76.25 ± 2.11	0.223 ± 0.017	100.50 ± 1.57
2	80.44 ± 1.33	0.257 ± 0.053	99.47 ± 1.60
3	82.88 ± 6.41	0.339 ± 0.049	97.89 ± 2.90

4.3.9 *In vivo* studies

4.3.9.1 Mucociliary transport time

Mucociliary transport time values for pure RTG suspension and RTG-Nanosuspension were found to be 7.5 ± 3.53 min and 20.0 ± 5.00 min, respectively. RTG-Nanosuspension demonstrated significantly higher ($P < 0.05$, one-tailed unpaired t-test) mucociliary clearance transport time than that of RTG suspension (**Figure 4.10**). Increased residence time of RTG-Nanosuspension compared to pure drug suspension can be attributed to the presence of Poloxamer 407 in the nanosuspension formulation which is well known for its mucoadhesive property [70]. The high mucociliary clearance transport time value of RTG-Nanosuspension compared to pure drug suspension indicated that the nanosuspension was capable of resist the process of mucocilliary clearance and increased the retention time of nanosuspension in the nasal cavity.

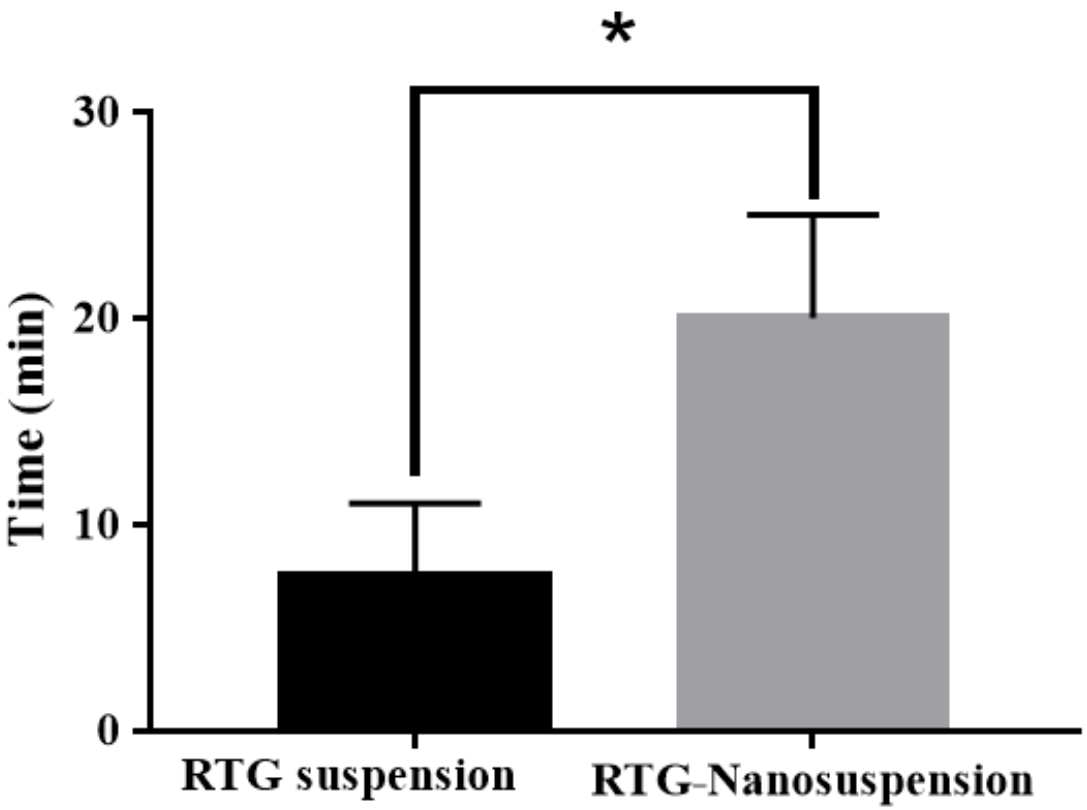

Figure 4.10 Mucociliary transport time of aqueous RTG suspension and RTG-Nanosuspension. Independent student t-test with one-tail was applied. '*' shows p-value < 0.05

4.3.9.2 Brain and plasma PK analysis

The brain and plasma PK profile of RTG-Nanosuspension and pure drug suspension are shown in **Figure 4.11**. The important brain and plasma PK parameters are presented in **Table 4.7**. For optimized nanosuspension, RTG brain concentration at all time points was much higher than RTG suspension (**Figure 4.11A**). The brain C_{max} for RTG-Nanosuspension was significantly ($P < 0.0005$, one-tailed, unpaired t-test) higher than pure drug suspension (**Table 4.7**). RTG-nanosuspension showed 1.86-fold increase in brain C_{max} and 2.56-fold increment in brain $AUC_{0\rightarrow tlast}$. This increase in brain C_{max} and $AUC_{0\rightarrow tlast}$ is supported by the longer residence time of optimized nanosuspension in the nasal cavity. The higher residence time would allow higher absorption of RTG to brain via olfactory and trigeminal transport pathways from nose.

Though RTG-Nanosuspension also showed a significant improvement in plasma PK parameters than RTG suspension; however, brain PK parameters were better than plasma showing the selective delivery to the brain (**Figure 4.11B**). For RTG-Nanosuspension, C_{max} and $AUC_{0\rightarrow tlast}$ for brain was higher than plasma. The higher brain concentration of RTG than plasma would ensure better therapeutic effect, while lower systemic exposure and associated side-effects. The higher plasma concentration for RTG-Nanosuspension than suspension could be due to increased transport through other pathways via the respiratory route. The increased absorption to other transport pathways from nose to plasma can be attributed to faster dissolution of RTG-Nanosuspension than suspension [71].

DTE (%) for RTG-Nanosuspension was 885.13 whereas, for suspension was 438.18. For RTG-Nanosuspension, DTP (%) was 88.7 while for drug suspension it was 77.18. DTE (%) compares the brain exposure of the drug when administered via the i.n. route vs a systemic route. In this study i.v. administration of RTG was considered as the systemic route. DTE (%) of optimized RTG-Nanosuspension more than 100 signifies the brain exposure of RTG after i.n. administration was superior to that of systemic route. This is regard as a measure of direct nose-to-brain uptake efficacy. The positive DTP (%) obtained from RTG-Nanosuspension representing efficient direct nose to brain uptake. The observed results for both DTE (%) and DTP (%) may be ascribed to the better residence times of RTG-nanosuspension in nasal cavity as compared to RTG suspension.

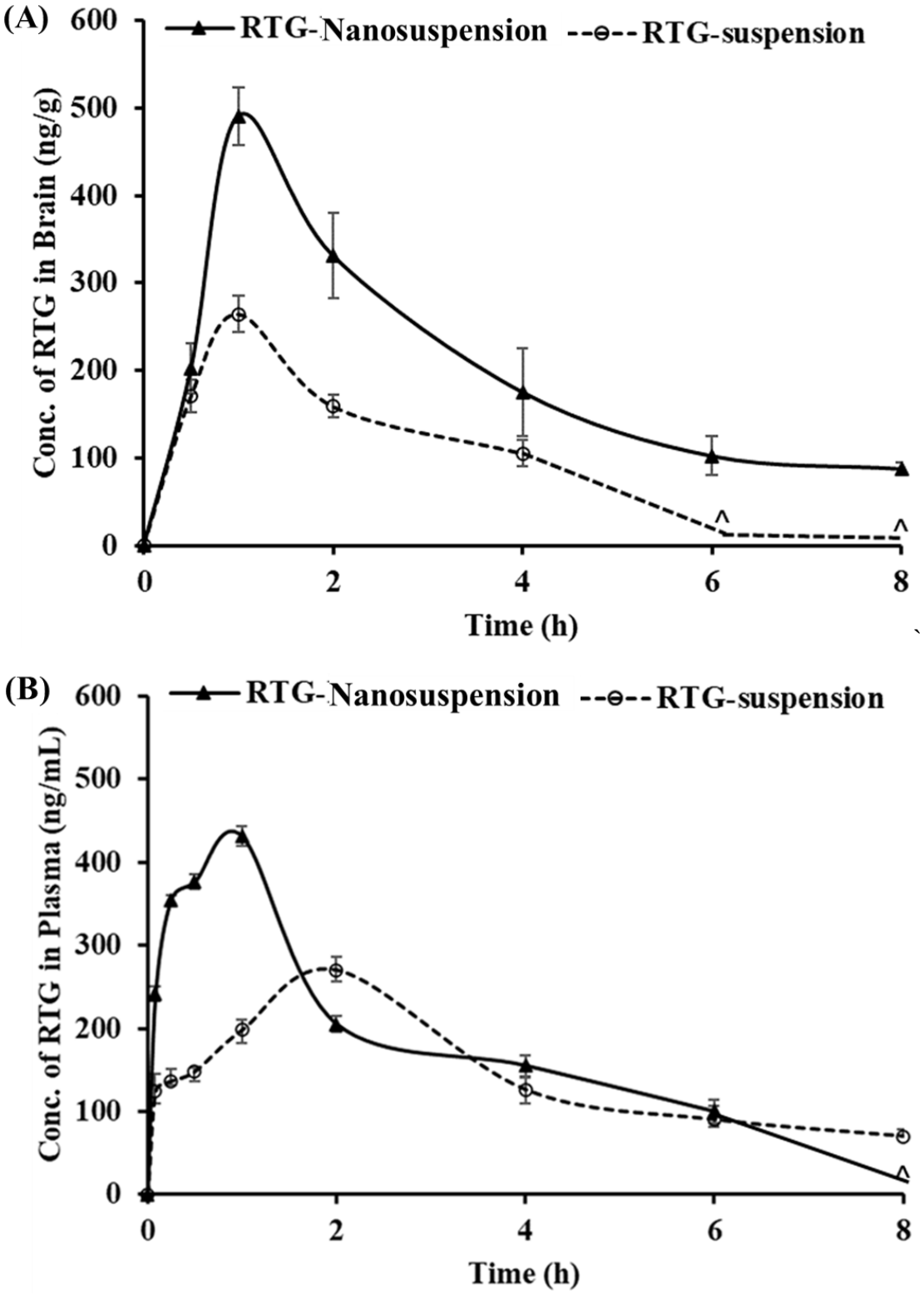

Figure 4.11 PK profiles of RTG attained after i.n. administration of RTG-Nanosuspension and RTG suspension in (A) Brain and (B) Plasma; '^' in both the profiles denote that the concentration of RTG was not detected at those time points in brain matrices and plasma

Table 4.7 Brain and plasma PK parameters for RTG-Nanosuspension and RTG suspension after i.n. administration

PK parameters	Brain		Plasma	
	RTG-Nanosuspension	RTG suspension	RTG-Nanosuspension	RTG suspension
$AUC_{0\rightarrow tlast}$ (ng*h/g)[b], (ng*h/mL)[p]	1609.49 ± 34.92	628.11 ± 12.21	1286.29 ± 14.07	779.01 ± 14.11
C_{max} (ng/g)[b], (ng/mL)[p]	490.79 ± 48.93	264.71 ± 21.12	430.87 ± 9.20	270.12 ± 18.50
T_{max} (h)	1	1	1	2
MRT (h)	2.95	1.82	2.23	3.15
Clearance (g/h)[b], (mL/h)[p]	255.30	-	276.71	312.65

[b] unit for brain PK parameters, [p] unit for plasma PK parameters. RTG dose for all i.n. formulations = 2 mg/Kg; for plasma PK n = 4 animals were used, and n = 4 animals' brains were used for brain PK at every time point; The brain and plasma data are represented as mean ± SD.

4.3.10 Histopathology of brain

The morphology of hippocampal region on brain slides at 0 h and after administration of i.n. nanosuspension at 8th h was studied for any sign of toxicity (**Figure 4.12**) [72]. The results showed similar morphology for treated animal's hippocampal region (**Figure 4.12C** and **D**) as compared to the control (**Figure 4.12A** and **B)**. Any symptoms of neuronal damage *viz.*, shrinkage of cell body or cell undergoing necrosis were not observed in the treated brain (**Figure 4.12D**). This result suggests that the i.n. RTG-Nanosuspension was safe and did not cause any brain damage.

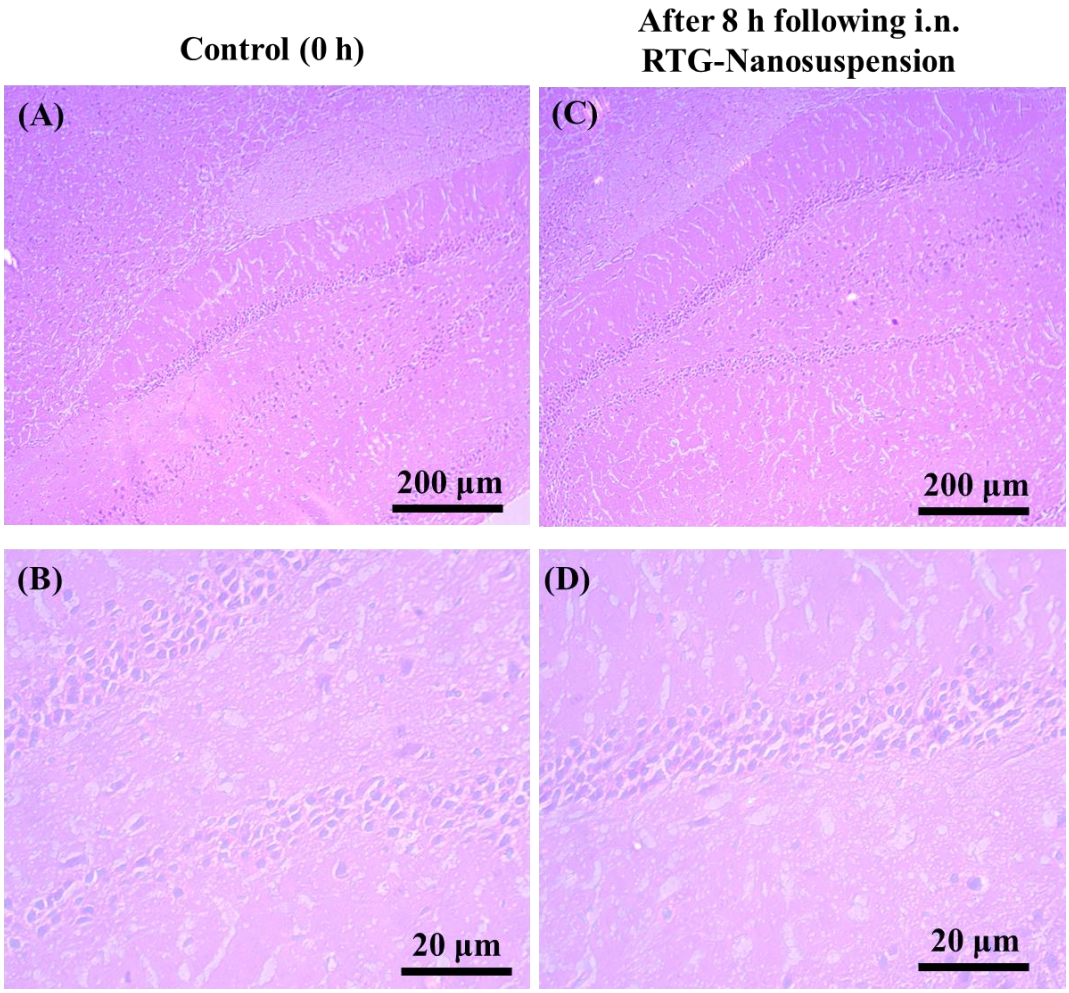

Figure 4.12 Histopathological evaluations of brain (hippocampal region) in different conditions (A) Control animal at 100X magnification, (B) Control animal at 400X magnification, (C) RTG-Nanosuspension treated animal at 100X magnification, (D) RTG-Nanosuspension treated animal at 400X magnification

4.4 Conclusion

This chapter describes the design, optimization, *in vitro*, *ex vivo* and *in vivo* characterization of RTG-Nanosuspension. RTG-Nanosuspension were prepared by antisolvent precipitation-ultrasonication procedure. RTG-Nanosuspensions were characterized for their particle size, PDI, and drug content. The crystalline state of RTG was altered in the optimized nanosuspension formulation and was confirmed by several analytical tools *viz.*, DSC, PXRD, Raman spectroscopic methods. The stability study confirmed that the optimized lyophilized nanosuspension is stable up to 3 months. Furthermore, the amorphous conversion of RTG from crystalline state in the optimized nanosuspension formulation significantly enhanced the

in vitro dissolution behaviour, *ex vivo* nasal permeation of the drug. Moreover, nasal ciliotoxicity study established the safety and non-toxic nature of the optimized RTG-Nanosuspension. *In vivo* brain and plasma PK studies were performed by administering the nanosuspension via i.n. route and compared with the i.n. pure RTG suspension. Results demonstrated that i.n. RTG-Nanosuspension showed significantly increased brain uptake in term of both DTE (%) and DTE (%) as compared to i.n. drug suspension. The results from present work indicate that intranasally administered nanosuspension formulation of RTG would be advantageous for enhancing the brain delivery of the drug.

References

1. Nordling-David, M.M.; Yaffe, R.; Guez, D.; Meirow, H.; Last, D.; Grad, E.; Salomon, S.; Sharabi, S.; Levi-Kalisman, Y.; Golomb, G.; et al. Liposomal Temozolomide Drug Delivery Using Convection Enhanced Delivery. *Journal of Controlled Release* **2017**, *261*, 138–146, doi:10.1016/j.jconrel.2017.06.028.

2. Asadi, S.; Roohbakhsh, A.; Shamsizadeh, A.; Fereidoni, M.; Kordijaz, E.; Moghimi, A. The Effect of Intracerebroventricular Administration of Orexin Receptor Type 2 Antagonist on Pentylenetetrazol-Induced Kindled Seizures and Anxiety in Rats. *BMC Neuroscience* **2018**, *19*, 49, doi:10.1186/S12868-018-0445-9.

3. Dalvi, A. V.; Ravi, P.R.; Uppuluri, C.T.; Mahajan, R.R.; Katke, S. V.; Deshpande, V.S. Thermosensitive Nasal in Situ Gelling Systems of Rufinamide Formulated Using Modified Tamarind Seed Xyloglucan for Direct Nose-to-Brain Delivery: Design, Physical Characterization, and in Vivo Evaluation. *Journal of Pharmaceutical Investigation* **2021**, *51*, 199–211, doi:10.1007/s40005-020-00505-9.

4. Dhaliwal, H.K.; Fan, Y.; Kim, J.; Amiji, M.M. Intranasal Delivery and Transfection of MRNA Therapeutics in the Brain Using Cationic Liposomes. *Molecular pharmaceutics* **2020**, *17*, 1996–2005, doi:10.1021/acs.molpharmaceut.0c00170.

5. Bourganis, V.; Kammona, O.; Alexopoulos, A.; Kiparissides, C. Recent Advances in Carrier Mediated Nose-to-Brain Delivery of Pharmaceutics. *European Journal of Pharmaceutics and Biopharmaceutics* **2018**, *128*, 337–362, doi:10.1016/j.ejpb.2018.05.009.

6. Prajapati, J.B.; Patel, G.C. Nose to Brain Delivery of Rotigotine Loaded Solid Lipid Nanoparticles: Quality by Design Based Optimization and Characterization. *Journal of Drug Delivery Science and Technology* **2021**, *63*, 102377,

doi:10.1016/j.jddst.2021.102377.

7. Bi, C.C.; Wang, A.P.; Chu, Y.C.; Liu, S.; Mu, H.J.; Liu, W.H.; Wu, Z.M.; Sun, K.X.; Li, Y.X. Intranasal Delivery of Rotigotine to the Brain with Lactoferrin-Modified PEG-PLGA Nanoparticles for Parkinson's Disease Treatment. *International Journal of Nanomedicine* **2016**, *11*, 6547–6559, doi:10.2147/IJN.S120939.

8. Wang, F.; Yang, Z.; Liu, M.; Tao, Y.; Li, Z.; Wu, Z.; Gui, S. Facile Nose-to-Brain Delivery of Rotigotine-Loaded Polymer Micelles Thermosensitive Hydrogels: In Vitro Characterization and in Vivo Behavior Study. *International Journal of Pharmaceutics* **2020**, *577*, 119046, doi:10.1016/j.ijpharm.2020.119046.

9. Bhattamisra, S.K.; Shak, A.T.; Xi, L.W.; Safian, N.H.; Choudhury, H.; Lim, W.M.; Shahzad, N.; Alhakamy, N.A.; Anwer, M.K.; Radhakrishnan, A.K.; et al. Nose to Brain Delivery of Rotigotine Loaded Chitosan Nanoparticles in Human SH-SY5Y Neuroblastoma Cells and Animal Model of Parkinson's Disease. *International Journal of Pharmaceutics* **2020**, *579*, 119148, doi:10.1016/j.ijpharm.2020.119148.

10. Choudhury, H.; Zakaria, N.F.B.; Tilang, P.A.B.; Tzeyung, A.S.; Pandey, M.; Chatterjee, B.; Alhakamy, N.; Bhattamishra, S.K.; Kesharwani, P.; Gorain, B.; et al. Formulation Development and Evaluation of Rotigotine Mucoadhesive Nanoemulsion for Intranasal Delivery. *Journal of Drug Delivery Science and Technology* **2019**, *54*, 101301, doi:https://doi.org/10.1016/j.jddst.2019.101301.

11. Saindane, N.S.; Pagar, K.P.; Vavia, P.R. Nanosuspension Based in Situ Gelling Nasal Spray of Carvedilol: Development, in Vitro and in Vivo Characterization. *AAPS PharmSciTech* 2013, *14*, 189–199.

12. Lu, Y.; Li, Y.; Wu, W. Injected Nanocrystals for Targeted Drug Delivery. *Acta*

Pharmaceutica Sinica B **2016**, *6*, 106–113, doi:10.1016/J.APSB.2015.11.005.

13. Fuhrmann, K.; Połomska, A.; Aeberli, C.; Castagner, B.; Gauthier, M.A.; Leroux, J.C. Modular Design of Redox-Responsive Stabilizers for Nanocrystals. *ACS Nano* **2013**, *7*, 8243–8250, doi:10.1021/nn4037317.

14. Bonaccorso, A.; Gigliobianco, M.R.; Pellitteri, R.; Santonocito, D.; Carbone, C.; Di Martino, P.; Puglisi, G.; Musumeci, T. Optimization of Curcumin Nanocrystals as Promising Strategy for Nose-to-Brain Delivery Application. *Pharmaceutics* **2020**, *12*, 476, doi:10.3390/pharmaceutics12050476.

15. Moakes, R.J.A.; Davies, S.P.; Stamataki, Z.; Grover, L.M.; Moakes, R.J.A.; Grover, L.M.; Davies, S.P.; Stamataki, Z. Formulation of a Composite Nasal Spray Enabling Enhanced Surface Coverage and Prophylaxis of SARS-COV-2. **2021**, doi:10.1002/adma.202008304.

16. Djupesland, P.G. Nasal Drug Delivery Devices: Characteristics and Performance in a Clinical Perspective-a Review. *Drug delivery and translational research* **2013**, *3*, 42–62, doi:10.1007/S13346-012-0108-9.

17. Sinha, B.; Müller, R.H.; Möschwitzer, J.P. Bottom-up Approaches for Preparing Drug Nanocrystals: Formulations and Factors Affecting Particle Size. *International journal of pharmaceutics* **2013**, *453*, 126–141, doi:10.1016/J.IJPHARM.2013.01.019.

18. Saha, P.; Pandey, M.M. Spectrochimica Acta Part A : Molecular and Biomolecular Spectroscopy A New Fluorescence-Based Method for Rapid and Specific Quantification of Rotigotine in Chitosan Nanoparticles. *Spectrochimica Acta Part A: Molecular and Biomolecular Spectroscopy* **2022**, *267*, 120555, doi:10.1016/j.saa.2021.120555.

19. Tuomela, A.; Hirvonen, J.; Peltonen, L. Stabilizing Agents for Drug Nanocrystals : Effect on Bioavailability. *Pharmaceutics* **2016**, *8*, doi:10.3390/PHARMACEUTICS8020016.

20. Saha, P.; Pandey, M.M. DoE-Based Validation of a HPLC–UV Method for Quantification of Rotigotine Nanocrystals: Application to in Vitro Dissolution and Ex Vivo Nasal Permeation Studies. *Electrophoresis* **2022**, *43*, 590–600, doi:10.1002/ELPS.202100157.

21. Tzeyung, A.S.; Md, S.; Bhattamisra, S.K.; Madheswaran, T.; Alhakamy, N.A.; Aldawsari, H.M.; Radhakrishnan, A.K. Fabrication, Optimization, and Evaluation of Rotigotine-Loaded Chitosan Nanoparticles for Nose-to-Brain Delivery. *Pharmaceutics* **2019**, *11*, 1–17, doi:10.3390/pharmaceutics11010026.

22. Pandey, M.M.; Jaipal, A.; Charde, S.Y.; Goel, P.; Kumar, L. Dissolution Enhancement of Felodipine by Amorphous Nanodispersions Using an Amphiphilic Polymer: Insight into the Role of Drug–Polymer Interactions on Drug Dissolution. *http://dx.doi.org/10.3109/10837450.2015.1022785* **2015**, *21*, 463–474, doi:10.3109/10837450.2015.1022785.

23. Jug, M.; Hafner, A.; Lovrić, J.; Kregar, M.L.; Pepić, I.; Vanić, Ž.; Cetina-Čižmek, B.; Filipović-Grčić, J. An Overview of in Vitro Dissolution/Release Methods for Novel Mucosal Drug Delivery Systems. *Journal of Pharmaceutical and Biomedical Analysis* **2018**, *147*, 350–366, doi:10.1016/j.jpba.2017.06.072.

24. Yu, S.; Sun, X.Z.; Liu, Y.X. Numerical Analysis of the Relationship between Nasal Structure and Its Function. *The Scientific World Journal* **2014**, *2014*, doi:10.1155/2014/581975.

25. Abdou, E.M.; Kandil, S.M.; Miniawy, H.M.F.E. Brain Targeting Efficiency of Antimigrain Drug Loaded Mucoadhesive Intranasal Nanoemulsion. *International Journal of Pharmaceutics* **2017**, *529*, 667–677, doi:10.1016/j.ijpharm.2017.07.030.

26. Patel, H.P.; Chaudhari, P.S.; Gandhi, P.A.; Desai, B. V.; Desai, D.T.; Dedhiya, P.P.; Vyas, B.A.; Maulvi, F.A. Nose to Brain Delivery of Tailored Clozapine Nanosuspension Stabilized Using (+)-Alpha-Tocopherol Polyethylene Glycol 1000 Succinate: Optimization and in Vivo Pharmacokinetic Studies. *International Journal of Pharmaceutics* **2021**, *600*, 120474, doi:10.1016/j.ijpharm.2021.120474.

27. Ravi, P.R.; Aditya, N.; Patil, S.; Cherian, L. Nasal In-Situ Gels for Delivery of Rasagiline Mesylate: Improvement in Bioavailability and Brain Localization. *Drug Delivery* **2015**, *22*, 903–910, doi:10.3109/10717544.2013.860501.

28. Sita, V.G.; Jadhav, D.; Vavia, P. Niosomes for Nose-to-Brain Delivery of Bromocriptine: Formulation Development, Efficacy Evaluation and Toxicity Profiling. *Journal of Drug Delivery Science and Technology* **2020**, *58*, 101791, doi:10.1016/j.jddst.2020.101791.

29. Lee, D.; Minko, T. Nanotherapeutics for Nose-to-Brain Drug Delivery: An Approach to Bypass the Blood Brain Barrier. *Pharmaceutics* **2021**, *13*, doi:10.3390/pharmaceutics13122049.

30. ICH International Council for Harmonisation of Technical Requirements for Pharmaceuticals for Human Use ICH Harmonised Guideline Impurities: Guideline For Residual Solvents Q3C(R6) Final Version. **2016**.

31. Hao, J.; Gao, Y.; Zhao, J.; Zhang, J.; Li, Q.; Zhao, Z.; Liu, J. Preparation and Optimization of Resveratrol Nanosuspensions by Antisolvent Precipitation Using Box-Behnken Design. *AAPS PharmSciTech* **2014**, *16*, 118–128, doi:10.1208/s12249-014-

0211-y.

32. Alshweiat, A.; Csóka, Ii.I.; Tömösi, F.; Janáky, T.; Kovács, A.; Gáspár, R.; Sztojkov-Ivanov, A.; Ducza, E.; Márki, Á.; Szabó-Révész, P.; et al. Nasal Delivery of Nanosuspension-Based Mucoadhesive Formulation with Improved Bioavailability of Loratadine: Preparation, Characterization, and in Vivo Evaluation. *International Journal of Pharmaceutics* **2020**, *579*, 119166, doi:10.1016/j.ijpharm.2020.119166.

33. Chen, C.; Wang, L.; Cao, F.; Miao, X.; Chen, T.; Chang, Q.; Zheng, Y. Formulation of 20(S)-Protopanaxadiol Nanocrystals to Improve Oral Bioavailability and Brain Delivery. *International Journal of Pharmaceutics* **2016**, *497*, 239–247, doi:10.1016/j.ijpharm.2015.12.014.

34. Rachmawati, H.; Shaal, L. Al; Müller, R.; Keck, C. Development of Curcumin Nanocrystal: Physical Aspects. *Journal of pharmaceutical sciences* **2013**, *102*, 204–214, doi:10.1002/JPS.23335.

35. Chin, W.W.L.; Parmentier, J.; Widzinski, M.; Tan, E.H.; Gokhale, R. A Brief Literature and Patent Review of Nanosuspensions to a Final Drug Product. *Journal of Pharmaceutical Sciences* **2014**, *103*, 2980–2999, doi:10.1002/JPS.24098.

36. Patravale, V.B.; Date, A.A.; Kulkarni, R.M. Nanosuspensions: A Promising Drug Delivery Strategy. *The Journal of pharmacy and pharmacology* **2004**, *56*, 827–840, doi:10.1211/0022357023691.

37. Wen, H.; Morris, K.R.; Park, K. Synergic Effects of Polymeric Additives on Dissolution and Crystallization of Acetaminophen. *Pharmaceutical Research* **2008**, *25*, 349–358, doi:10.1007/s11095-007-9468-0.

38. Dalvi, S. V.; Dave, R.N. Controlling Particle Size of a Poorly Water-Soluble Drug

Using Ultrasound and Stabilizers in Antisolvent Precipitation. *Industrial and Engineering Chemistry Research* **2009**, *48*, 7581–7593, doi:10.1021/ie900248f.

39. Shegokar, R.; H.Müller, R. Nanocrystals: Industrially Feasible Multifunctional Formulation Technology for Poorly Soluble Actives. *Elsevier* **2010**, *399*, 129–139.

40. Mishra, V.; Bansal, K.; Verma, A.; Yadav, N.; Pharmaceutics, S.T.-; 2018, U. Solid Lipid Nanoparticles: Emerging Colloidal Nano Drug Delivery Systems. *Pharmaceutics* **2018**, *10*, 191, doi:10.3390/pharmaceutics10040191.

41. Na, Y.G.; Pham, T.M.A.; Byeon, J.J.; Kim, M.K.; Han, M.G.; Baek, J.S.; Lee, H.K.; Cho, C.W. Development and Evaluation of TPGS/PVA-Based Nanosuspension for Enhancing Dissolution and Oral Bioavailability of Ticagrelor. *International Journal of Pharmaceutics* **2020**, *581*, 119287, doi:10.1016/J.IJPHARM.2020.119287.

42. Gajera, B.Y.; Shah, D.A.; Dave, R.H. Development of an Amorphous Nanosuspension by Sonoprecipitation-Formulation and Process Optimization Using Design of Experiment Methodology. *International Journal of Pharmaceutics* **2019**, *559*, 348–359, doi:10.1016/J.IJPHARM.2019.01.054.

43. Park, M.-W.; Yeo, S.-D. Antisolvent Crystallization of Roxithromycin and the Effect of Ultrasound. *Separation Science and Technology* **2010**, *45*, 1402–1410, doi:10.1080/01496391003689538.

44. Deshpande, R.D.; Sravan Kumar Varma, N. V; Vaghela, R. Effect of Nanonization on Poorly Water Soluble Glibenclamide Using Liquid Anti-Solvent Precipitation Technique: Aqueous Solubility, In Vitro and In Vivo Study. *RSC Advances* **2015**, *5*, 81728–81738, doi:10.1039/c5ra12678a.

45. Lonare, A.A.; Patel, S.R. Antisolvent Crystallization of Poorly Water Soluble Drugs.

International Journal of Chemical Engineering and Applications **2013**, *4*, 337–341, doi:10.7763/IJCEA.2013.V4.321.

46. Verma, S.; Kumar, S.; Gokhale, R.; Burgess, D.J. Physical Stability of Nanosuspensions: Investigation of the Role of Stabilizers on Ostwald Ripening. *International Journal of Pharmaceutics* **2011**, *406*, 145–152, doi:10.1016/J.IJPHARM.2010.12.027.

47. Wang, H.; Mustaffar, A.; Phan, A.N.; Zivkovic, V.; Reay, D.; Law, R.; Boodhoo, K. A Review of Process Intensification Applied to Solids Handling. *Chemical Engineering and Processing: Process Intensification* **2017**, *118*, 78–107, doi:10.1016/J.CEP.2017.04.007.

48. Danaei, M.; Dehghankhold, M.; Ataei, S.; Hasanzadeh Davarani, F.; Javanmard, R.; Dokhani, A.; Khorasani, S.; Mozafari, M.R. Impact of Particle Size and Polydispersity Index on the Clinical Applications of Lipidic Nanocarrier Systems. *Pharmaceutics* **2018**, *10*, 1–17, doi:10.3390/pharmaceutics10020057.

49. Jacobs, C.; Müller, R.H. Production and Characterization of a Budesonide Nanosuspension for Pulmonary Administration. *Pharmaceutical Research* **2002**, *19*, 189–194, doi:10.1023/A:1014276917363.

50. Kuk, D.H.; Ha, E.S.; Ha, D.H.; Sim, W.Y.; Lee, S.K.; Jeong, J.S.; Kim, J.S.; Baek, I.H.; Park, H.; Choi, D.H.; et al. Development of a Resveratrol Nanosuspension Using the Antisolvent Precipitation Method without Solvent Removal, Based on a Quality by Design (QbD) Approach. *Pharmaceutics* **2019**, *11*, 688, doi:10.3390/pharmaceutics11120688.

51. Ei-Badry, M.; Hassan, M.A.; Ibrahim, M.A.; Elsaghir, H. Performance of Poloxamer

407 as Hydrophilic Carrier on the Binary Mixtures with Nimesulide. *Farmacia* **2013**, *61*, 1137–1150.

52. Lopez, C.; Cristelle, M.; David-briand, E.; Bizien, T.; Artzner, F.; Riaublanc, A.; Anton, M. Loading of Lutein in Egg-Sphingomyelin Vesicles as Lipid Carriers : Thermotropic Phase Behaviour , Structure of Sphingosome Membranes and Lutein Crystals. **2020**, *138*, doi:10.1016/j.foodres.2020.109770.

53. Wolff, H.-M.; Quere, L.; Riedner, J. Polymorphic Form of Rotigotine 2008.

54. Jin, G.; Ngo, H. V.; Cui, J.H.; Wang, J.; Park, C.; Lee, B.J. Role of Surfactant Micellization for Enhanced Dissolution of Poorly Water-soluble Cilostazol Using Poloxamer 407-based Solid Dispersion via the Anti-solvent Method. *Pharmaceutics* **2021**, *13*, 1–14, doi:10.3390/pharmaceutics13050662.

55. Aukunuru, J.; Nanam, P.; Rambabu, B.; Sailu, C.; Thadkala, K. Preparation and Characterization of Amorphous Ezetimibe Nanosuspensions Intended for Enhancement of Oral Bioavailability. *International Journal of Pharmaceutical Investigation* **2014**, *4*, 131, doi:10.4103/2230-973x.138344.

56. Hans-Michael Wolff; Quere, L.; Riedner, J. Polymorphic Form of Rotigotine and Process for Production.

57. Eloy, J.O.; Marchetti, J.M. Solid Dispersions Containing Ursolic Acid in Poloxamer 407 and PEG 6000: A Comparative Study of Fusion and Solvent Methods. *Powder Technology* **2014**, *253*, 98–106, doi:10.1016/J.POWTEC.2013.11.017.

58. Shariare, M.H.; Altamimi, M.A.; Marzan, A.L.; Tabassum, R.; Jahan, B.; Reza, H.M.; Rahman, M.; Ahsan, G.U.; Kazi, M. In Vitro Dissolution and Bioavailability Study of Furosemide Nanosuspension Prepared Using Design of Experiment (DoE). *Saudi*

Pharmaceutical Journal **2019**, *27*, 96–105, doi:10.1016/J.JSPS.2018.09.002.

59. Oh, D.; Chon, J.; Na, M.; Kang, J.; Park, E.; Rhee, Y.; Kim, J.; Hwan, D.; Kim, D.; Park, C. Preparation and Physicochemical Characterization of Rotigotine Drug-in-Adhesive Patch Containing Crystal Growth Inhibitor. *Journal of Drug Delivery Science and Technology* **2019**, *53*, 101193, doi:10.1016/j.jddst.2019.101193.

60. Tang, X.C.; Pikal, M.J.; Taylor, L.S. A Spectroscopic Investigation of Hydrogen Bond Patterns in Crystalline and Amorphous Phases in Dihydropyridine Calcium Channel Blockers. *Pharmaceutical Research* **2002**, *19*, 484–490, doi:10.1023/a:1015147729564.

61. Kuroiwa, Y.; Higashi, K.; Ueda, K.; Yamamoto, K.; Moribe, K. Nano-Scale and Molecular-Level Understanding of Wet-Milled Indomethacin/Poloxamer 407 Nanosuspension with TEM, Suspended-State NMR, and Raman Measurements. *International Journal of Pharmaceutics* **2018**, *537*, 30–39, doi:10.1016/J.IJPHARM.2017.12.028.

62. Nernst, W. Theorie Der Reaktionsgeschwindigkeit in Heterogenen Systemen. *Zeitschrift für Physikalische Chemie* **1904**, *47*, 52–55, doi:10.1515/ZPCH-1904-4704.

63. Brunner, E. Reaktionsgeschwindigkeit in Heterogenen Systemen. *Zeitschrift für Physikalische Chemie* **1904**, *47U*, 56–102, doi:10.1515/ZPCH-1904-4705.

64. Mosharraf, M.; Nyström, C. The Effect of Particle Size and Shape on the Surface Specific Dissolution Rate of Microsized Practically Insoluble Drugs. *International Journal of Pharmaceutics* **1995**, *122*, 35–47, doi:10.1016/0378-5173(95)00033-F.

65. Wang, A.; Wang, L.; Sun, K.; Liu, W.; Sha, C.; Li, Y. Preparation of Rotigotine-Loaded Microspheres and Their Combination Use with L-DOPA to Modify

Dyskinesias in 6-OHDA-Lesioned Rats. *Pharmaceutical Research* **2012**, *29*, 2367–2376, doi:10.1007/s11095-012-0762-0.

66. Attari, Z.; Bhandari, A.; Jagadish, P.C.; Lewis, S. Enhanced Ex Vivo Intestinal Absorption of Olmesartan Medoxomil Nanosuspension: Preparation by Combinative Technology. *Saudi Pharmaceutical Journal* **2016**, *24*, 57–63, doi:10.1016/J.JSPS.2015.03.008.

67. Marttin, E.; Verhoef, J.C.; Romeijn, S.G.; Merkus, F.W.H.M. Effects of Absorption Enhancers on Rat Nasal Epithelium in Vivo: Release of Marker Compounds in the Nasal Cavity. *Pharmaceutical research* **1995**, *12*, 1151–1157, doi:10.1023/A:1016207809199.

68. Pailla, S.R.; Talluri, S.; Rangaraj, N.; Ramavath, R.; Challa, V.S.; Doijad, N.; Sampathi, S. Intranasal Zotepine Nanosuspension: Intended for Improved Brain Distribution in Rats. *DARU, Journal of Pharmaceutical Sciences* **2019**, *27*, 541–556, doi:10.1007/s40199-019-00281-4.

69. Wavikar, P.; Pai, R.; Vavia, P. Nose to Brain Delivery of Rivastigmine by In Situ Gelling Cationic Nanostructured Lipid Carriers: Enhanced Brain Distribution and Pharmacodynamics. *Journal of Pharmaceutical Sciences* **2017**, *106*, 3613–3622, doi:10.1016/J.XPHS.2017.08.024.

70. Giuliano, E.; Paolino, D.; Fresta, M.; Cosco, D. Mucosal Applications of Poloxamer 407-Based Hydrogels: An Overview. *Pharmaceutics* **2018**, *10*, 159, doi:10.3390/PHARMACEUTICS10030159.

71. Dalvi, A.; Ravi, P.R.; Uppuluri, C.T. Design and Evaluation of Ru Fi Namide Nanocrystals Loaded Thermoresponsive Nasal in Situ Gelling System for Improved Drug Distribution to Brain. *Frontiers in Pharmacology* **2022**, *13*, 943772,

doi:10.3389/fphar.2022.943772.

72. Sita, V.G.; Jadhav, D.; Vavia, P. Niosomes for Nose-to-Brain Delivery of Bromocriptine: Formulation Development, Efficacy Evaluation and Toxicity Profiling. *Journal of Drug Delivery Science and Technology* **2020**, *58*, doi:10.1016/j.jddst.2020.101791.

Chapter 5: Development, *In vitro*, *Ex vivo* and *In vivo* Evaluation of Rotigotine Proposomes for Improved N2B Delivery

5.1 Introduction

Treatment of central nervous system (CNS) diseases has been a potential challenge due to the presence of blood-brain barrier (BBB). Nanocarrier-based drug delivery systems have made sufficient advancements in the management of CNS diseases by either transporting the drugs to brain through BBB or by evading it. Nose-to-brain (N2B) delivery of nanocarriers has shown remarkable improvement in treating CNS diseases by avoiding BBB. Nanocarriers due to their properties *viz.*, size, shape, and surface charge are able to increase nasal permeation of drugs.

Literature suggests that intranasal (i.n.) liposomes are effective for the treatment of CNS diseases such as Alzheimer's disease, schizophrenia, stroke, and epilepsy [1–3]. These nanoformulations are known to improve brain availability of CNS drugs with minimal or no toxicity to the nasal mucosa [1,3,4]. Different modified versions of liposomes such as ethanol based ethosomes [5], glycerol based glycerosomes, and propylene glycol (PG) based proposomes [6] have been developed to further improve the advantages of liposomes for i.n. and other route of delivery. PG is widely used in combination with other excipients for i.n. nanoemulsions intended for brain delivery of CNS drugs. PG helped to increase stability of the vesicles, improve *in vivo* absorption of drugs, and exhibit rapid onset of action following i.n. administration [7–9].

Proposomes are reported to improve liposomal stability, and the combination of phospholipids and PG synergistically could increase drug permeation by blending the lipid bilayer with the cellular lipids. Thus, in this study, we have prepared Rotigotine (RTG) loaded proposomes (RTG-Proposomes) for i.n. delivery to enhance the brain availability of drug. The RTG-

Proposomes were characterized for size distribution, zeta potential, microscopic morphology, and *in vitro* drug release. An *ex vivo* nasal permeation study was performed to evaluate the nasal permeability of drug from RTG-Proposomes. The *in vivo* study was performed to assess the direct N2B delivery and brain targeting efficiency of the formulation by calculating drug targeting efficiency percentage (DTE (%)) and direct transport percentage (DTP (%)).

5.2 Materials and methods

5.2.1 Materials

RTG was a kind gift from Mylan Laboratories Ltd. (Hyderabad, India). Glipizide, used as internal standard (IS) was purchased from TCI Chemicals Pvt Ltd. (Chennai, India). Soya phosphatidylcholine (SPC), Lipoid S 100, was kindly gifted by Lipoid (GmBH, Germany). PG was purchased from SRL Chemicals Pvt. Ltd. (Mumbai, India). Milli-Q water obtained from an in-house Milli-Q® Reference water purification system (GmbH, Germany) was used in all experimental processes and analysis.

5.2.2 Preparation of RTG-Proposomes

The proposomes were prepared by cold mixing followed by ultrasonication as previously reported [6], with slight modification (**Figure 5.1**). Briefly, SPC was dissolved in PG at 60 ^{o}C and cooled down to room temperature. 24 mg of RTG was added into the solution of SPC and PG, and dissolved under magnetic stirring. The aqueous phase (pure Milli-Q water) was dispensed via ‘pump A’ of Mitos Duo XS-Pump, part no 3200401 (Dolomite, Royston, UK). The aqueous phase (10 mL) was dropwise added at a flow rate of 500 µL/min to the drug solution under magnetic stirring at 750 rpm. The dispersion was kept at room temperature under continuous stirring for further 30 min. The dispersion was subjected to ultrasonication (Vibra cell model, Sonics & Materials, Inc., Connecticut, USA) for 1.5 min at 25% amplitude in a pulse mode for obtaining proposomes. Ultrasonication time, SPC concentration (%w/v), and

PG concentration (%v/v) were varied at different levels during optimization of particle size, PDI, and % entrapment efficiency (%EE) of RTG-Proposomes.

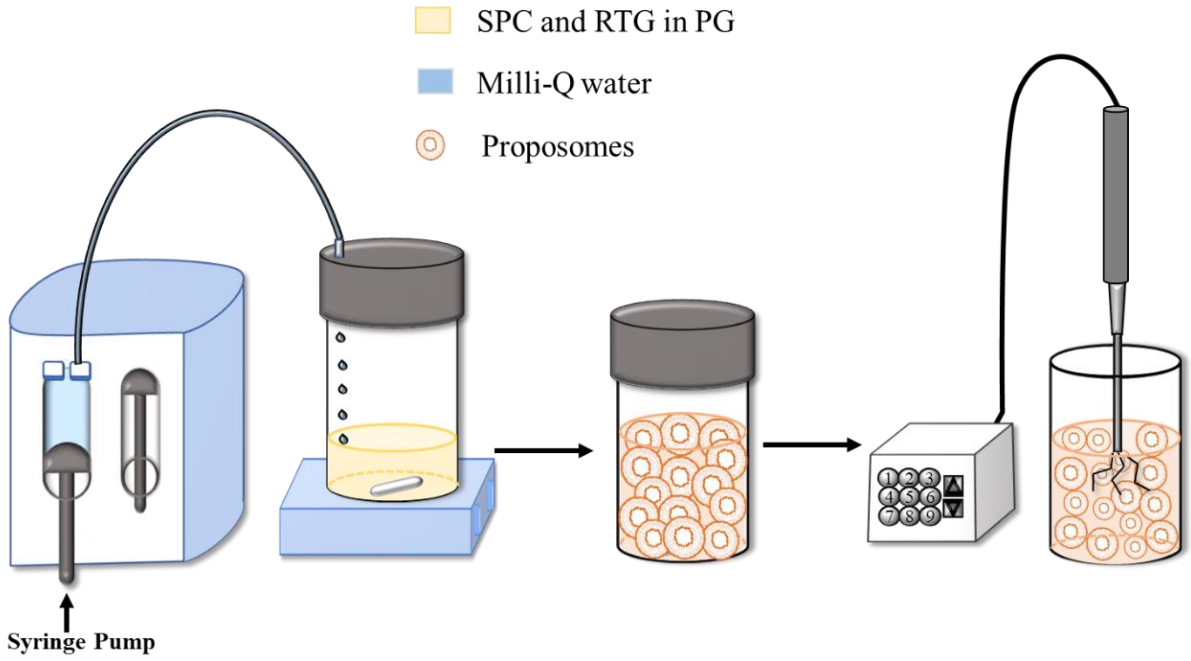

Figure 5.1 Schematic representation of the preparation process of RTG-Proposomes

5.2.3 Characterization of RTG-Proposomes

5.2.3.1 Particle size, PDI, and zeta potential

Dynamic light scattering technique (Zetasizer nano ZS, Malvern Instruments, UK) was used for determining the particle size, PDI, and zeta potential of formulated RTG-Proposomes. The samples were diluted 10 times with Milli-Q water and equilibrated at 25 ^{o}C for 2 min before every measurement. Three independent measurements were performed for each proposomes formulation, and the mean values were reported for particle size, PDI, and zeta potential.

5.2.3.2 Entrapment efficiency

Entrapment efficiency (%EE) was determined using dialysis bag (molecular weight cut-off 3,500 Da, Himedia, India). %EE was calculated from the amount of free RTG ($W_{Free\ drug}$) present in the formulation. 0.4 mL of formulation was added into dialysis bag and dialyzed against Milli-Q water (80 mL) for 45 min with constant stirring at 100 rpm using magnetic

bead. 45 min dialysis time was identified based on free drug release from the dialysis bag. The time, at which 90% free drug (of 0.4 mL in dialysis bag) was dialyzed, was taken as the endpoint for free drug dialysis. Drug content present in the filtrate was determined using a validated RP-HPLC analytical method discussed in **Chapter 3**. Equation 5.1 was used for the calculation %EE:

$$\%EE = \frac{W_{Total\ drug} - W_{Free\ drug}}{W_{Total\ drug}} \times 100 \quad (5.1)$$

where, $W_{Total\ drug}$ is the amount of RTG used in the preparation of RTG-Proposomes, and $W_{Free\ drug}$ is the amount of unentrapped RTG.

5.2.4 Transmission electron microscopy (TEM)

The morphology of RTG-Proposomes and pure-RTG was evaluated using transmission electron microscopy (TEM) (JEOL, Tokyo, Japan). An accelerating voltage of 120 kV was used during the analysis. A simple drop caste method was used to prepare the samples for the analysis. Briefly, a small drop of diluted sample was dropped on the carbon coated copper grid, allowed to caste for few minutes on the grid, then excess liquid was soaked using blotting paper before measurement.

5.2.5 *In vitro* release

In vitro release study of RTG-Proposomes was performed by dialysis bag method (Molecular weight cut-off of 12 kDa, Himedia, India). The membrane was soaked for 2 h prior to the experiment for its activation. The study was carried out in 50 mL phosphate buffer saline (PBS), pH 7.4 as release media, and stirred at 100 rpm, temperature maintained at 37 ± 2 ^{o}C [11]. RTG-Proposomes containing 1 mg equivalent RTG was taken in the activated dialysis membrane, sealed, and immersed into the release media. At predetermined time points (0.5, 1, 2, 4, 6, 8, 12, 18, and 24 h) samples of 1 mL were withdrawn and replenished with fresh medium. Percentage cumulative drug released was analyzed by suitably diluting the samples

using validated RP-HPLC analytical method described in **Chapter 3**, **Method II** [12]. To understand the kinetics and mechanism of drug release from the optimized proposomes, release profile results were fitted into several mathematical models *viz.*, first order, Higuchi model, and Korsmeyer-Peppas. Best fitted mathematical model was selected based on high correlation coefficient (R^2) value for the release data. For the Korsmeyer-Peppas model, obtained *n* value was used to evaluate the drug release mechanism. Similarity factor (f_2) was used to evaluate the release profiles of RTG-Proposomes and RTG suspension.

5.2.6 *Ex vivo* nasal permeation

Goat nasal mucosa was obtained immediately after the sacrifice of goat from a local slaughterhouse. Permeation study was performed using Franz diffusion cell (Orchid Scientific, Nashik, India) with a diffusion area of 0.785 cm^2. The mucosa was hydrated in PBS (pH 6.4) for 15 min prior use. Receptor compartment of the diffusion cell was filled with 5 mL of PBS (pH 6.4) as permeation media. Nasal mucosa was kept in contact with receptor compartment keeping the mucosal side facing toward the donor compartment. The whole diffusion assembly was kept under magnetic stirring at 50 rpm and the temperature was maintained at 33 ± 1 ^oC. *Ex vivo* nasal permeation study was performed using 2.4 mg drug equivalent RTG-Proposomes. 1 mL of final RTG-proposomes and pure RTG suspension were placed separately in the donor compartment. At predetermined time intervals (5, 10, 15, 30, 60, 120, 240, and 360 min), 500 µL of samples were withdrawn and replaced with the same amount of pre-heated fresh media. All the samples were centrifuged (Eppendorf®, Hamburg, Germany) at 15,000 rpm for 15 min at 4 ^oC, and supernatants were collected. The supernatants were suitably processed and analysed using validated RP-HPLC analytical method described in **Chapter 3**, **Method II** [12].

5.2.7 Stability of RTG-Proposomes

Stability of optimized proposomes (n = 3) was evaluated by determining average particle size, PDI, zeta potential and %EE at various time points (7^{th} day, 1^{st} month, and 2^{nd} month) over 2

months. Optimized RTG-Proposomes were stored in 15 mL glass container and kept at refrigerated conditions (4 °C).

5.2.8 *In vivo* studies in Wistar rats

All *in vivo* experiments were prior approved by the Institute's Animal Ethics Committee (IAEC), Protocol number- IAEC/RES/26/07/REV-1/30/19. Male Wistar rats of 9 – 10 weeks old and weighed between 250 – 260 g were used in all *in vivo* studies conducted for RTG-Proposomes and suspension. RTG suspension was prepared as described in the previous **Chapter 4**, **Section 4.2.11**. Formulations were administered at 2 mg/Kg of rat weight. Animals were fasted overnight having only access to water before dosing.

5.2.8.1 Intranasal (i.n.) administration

Formulations were intranasally administered using a soft cannula (Instech Laboratories, PA, USA). To ensure delivery to the olfactory region of nasal cavity, 1.3 cm long cannula was attached in front of a 100 µL microtip. Isoflurane was used in the anaesthetic chamber to anesthetize the rats before dosing and during blood sample collection. After dosing of each formulation, rats were kept in supine position till recovery. Formulations were administered at 2 mg/Kg (75 µL) of rat weight. Rats were fasted overnight with only access to water prior dosing.

5.2.8.2 Evaluation of mucociliary transport time

Mucociliary clearance transport time for RTG-Proposome was evaluated using a method previously described in **Chapter 4, Section 4.2.11.2**. RTG-Proposomes were administered (75 µL) to each nostril as mentioned in **Chapter 4, Section 4.2.11.1**. After administration of formulation, oropharyngeal cavity of rat was swabbed using cotton buds at every 5 min interval upto 90 min. Rats were not allowed access to food for 1 h after initiation of the study. Samples collected at each time point were diluted using mobile phase (ACN:KH_2PO_4,pH 5::54:46). RTG was estimated in each swab with the validated RP-HPL analytical method discussed in

Chapter 3, **Method II** [12]. The time point at which presence of RTG was detected in oropharyngeal cavity was reported as mucociliary transport time for the RTG-Proposomes. Mucociliary transport time for pure drug suspension data was taken from **Chapter 4, Section 4.3.9.1** [13].

5.2.8.3 Brain and plasma PK analysis

PK studies for brain and plasma were performed for RTG-Proposomes following i.n. administration to rats. Dosing of each formulation was completed using the setup and technique discussed in **Chapter 4, Section 4.2.11.1**. For plasma PK study, blood samples were collected from rats (n = 4) via retro-orbital puncture technique. At each time point, 200 µL of blood was collected in 1.5 mL centrifuge tubes already containing anticoagulant (4.5% w/v disodium EDTA in water). Blood was collected at predetermined time intervals of 0 min i.e., before dose and 0.08, 0.25, 0.5, 1, 2, 4, 6, and 8 h after dosing. After dosing, brains were collected at 0.5, 1, 2, 4, 6, and 8 h. At each time (n = 4) rats were sacrificed, and brains were collected as described in **Chapter 3**, **Section 3.5.2.1**. Samples were processed using protein-precipitation method as described in **Chapter 3**, **Sections 3.5.2.1** and **3.5.2.2**, respectively. The samples were analysed using the validated RP-HPLC bioanalytical method discussed in **Chapter 3**, **Method III**. For aqueous drug suspension, the plasma and brain PK data were taken from **Chapter 4**, **Section 4.3.9.2**. PK parameters *viz.*, C_{max}, T_{max}, $AUC_{0\rightarrow tlast,}$ clearance, and MRT were determined by non-compartmental analysis (NCA) using Phoenix WinNonlin (Version 8.0, Pharsight Corporation, NC, USA) for RTG-Proposomes. To compare the brain uptake efficiency of pure drug and optimized RTG-Proposomes, DTP (%) and DTE (%) [14,15] were calculated using Equation 4.1 and Equation 4.2, respectively as described in **Chapter 4, Section 4.2.11.3**.

High and positive values of DTP (%) and DTE (%) suggest effective brain delivery of the drug [15]. DTP (%) indicates percentage of drugs reaching directly to the brain via N2B pathways. DTE (%) indicates total amount of drug transported to the brain which includes direct nose-to-brain and indirect nose-to-systemic circulation-to-brain [14].

5.2.9 Histopathology of brain

Rat brains were collected at 0 time (as control) and at 8 h following i.n. administration of RTG-Proposomes. The isolated brains were washed with PBS (pH 7.4) to get rid of any remaining blood or connective tissues. The cleaned brains were weighed and stored at 10% v/v formalin solution. A series of ethanol concentration (*v/v*) i.e., 70%, 80%, 95%, and finally using 100%, dehydration of brain tissue was performed. The brain tissue was embedded in paraffin wax and sectioned using microtome. The deparaffinization process was performed using xylene. Slides were first treated with xylene, then ethanol concentrations (*v/v)*of 100%, 80%, and 70%, and finally using phosphate buffer saline (pH 7.4) rehydration was achieved. Finally the slides were stained with hematoxylin and eosin. The histopathological slides were evaluated using an inverted light microscope (Carl Zeiss, Jena, Germany) for toxicity. Three rats from each group were used for the study [15].

5.3 Results and Discussion

5.3.1 Preparation of RTG-Proposomes

5.3.1.1 Effect of ultrasonication on particle size and PDI

Proposomes was prepared by cold mixing process followed by the ultrasonication method. It was found that ultrasonication time has an effect on the vesicle size of proposomes (**Table 5.1**). Proposomes prepared without the assistance of ultrasonication showed significantly high particle size. Ultrasonication might cause several cavitation events that increase the diffusion of lipid used for the preparation of proposomes [16]. It was observed that after 0.5, 1 and 1.5

min of ultrasonication, the particle size and PDI of proposomes were significantly decreased. However, further increase in the ultrasonication time up to 2.5 min did not result in significant decrease in the particle size and PDI. Thus, further optimization studies of RTG-Proposomes were carried out at a fixed ultrasonication time of 1.5 min. Change in concentration of PG also showed an effect on the particle size. Thus, to understand the exact effect of PG on particle size, a detailed study was performed in the following section.

Table 5.1 Effect of ultrasonication time on particle size and PDI

Formulation code [a]	Ultrasonication time (min)	Particle size (nm)	PDI
P 1 (1, 5)	0	198.00 ± 7.54	0.183 ± 0.038
P 1A (1, 5)	0.5	173.80 ± 9.52	0.354 ± 0.076
P 1B (1, 5)	1.0	116.26 ± 8.02	0.419 ± 0.024
P 1C (1, 5)	1.5	94.95 ± 3.17	0.255 ± 0.003
P 1D (1, 5)	2.0	95.43 ± 5.25	0.247 ± 0.009
P 1E (1, 5)	2.5	99.51 ± 2.58	0.278 ± 0.028
P 2 (1, 10)	0	168.73 ± 8.11	0.103 ± 0.086
P 2A (1, 10)	0.5	85.88 ± 6.42	0.339 ± 0.049
P 2B (1, 10)	1.0	59.54 ± 1.62	0.394 ± 0.003
P 2C (1, 10)	1.5	57.94 ± 2.95	0.354 ± 0.020
P 2D (1, 10)	2.0	63.89 ± 7.88	0.371 ± 0.016
P 2E (1, 10)	2.5	71.12 ± 0.90	0.385± 0.018

[a] The values in bracket with labels show the concentration of SPC (1% w/v) and concentration of PG (5% and 10% v/v)

5.3.1.2 Effect of PG (%v/v) on particle size PDI and %EE

In case of nasal delivery, PG content in a formulation should be limited [17]. Hence, amount of PG was considered as an essential parameter for RTG-Proposomes. All three concentrations (5%, 7.5%, and 10% v/v) of PG resulted desired particle size below 150 nm. Increased concentration of PG resulted in decreased particle size**.** This result might be ascribed to the fact that PG shows stabilizing effect that avoids aggregation of vesicles. PG might also help in modification of surface tension of proposomes resulting in spatial stability that leads to lower particle size [18]. High concentration PG might also cause increased disorders on bilayer structure of lipid, which further reduces particle size [6].

All three concentrations of PG yielded good %EE between 76.40 ± 1.68 to 87.01 ± 1.86. Increase in PG concentration caused an increase in the %EE of proposomes (**Table 5.2**). This might be because due to PG, the solubility and distribution of RTG gets increased inside the vesicle of proposomes [19,20]. Though the highest concentration of PG showed better particle size and %EE but, it resulted in higher PDI (**Table 5.2**). Hence, medium concentration (7.5%) of PG was fixed for further studies.

Table 5.2 Effect of PG on particle size, PDI, and %EE of different proposomes

Formulation Code [a]	Particle size (nm)	PDI	% EE
P 3 (1, 5)	146.77 ± 11.29	0.275 ± 0.009	76.40 ± 1.68
P 4 (1, 7.5)	105.37 ± 2.04	0.266 ± 0.004	81.44 ± 2.21
P 5 (1, 10)	93.65 ± 3.83	0.349 ± 0.34	87.01 ± 1.86

[a] The values in bracket with labels show the concentration of SPC (1% w/v) and concentration of propylene glycol (5%, 7.5%, and 10% v/v). P3 to P5 contains 24 mg of RTG

5.3.1.3 Effect of SPC (%w/v) on particle size, PDI, and %EE

Phospholipid, SPC, is the primary component of RTG-Proposomes layer and has an immediate effect on particle size and the PDI. As shown in **Table 5.3**, increased concentration of SPC resulted in proposomes of significantly large particle size and high PDI. An increased amount of SPC leads to increased aggregation, resulting in higher particle size and wide range of distribution [21,22].

Increase in SPC concentration also resulted in increase in %EE (**Table 5.3**). An increase in the SPC concentration forms more vesicles and leads to high %EE. Although 2.5% w/v concentration of SPC showed highest %EE but, also resulted to high particle size and PDI.

Table 5.3 Effect of SPC on particle size, PDI, and %EE of different proposome formulations

Formulation Code [a]	Particle size (nm)	PDI	% EE
P 6 (7.5, 1)	115.63 ± 5.22	0.267 ± 0.028	82.97 ± 0.18
P 7 (7.5, 1.5)	149.53 ± 2.64	0.396 ± 0.023	85.20 ± 0.03
P 8 (7.5, 2)	190.80 ± 0.98	0.447 ± 0.024	86.55 ± 0.19
P 9 (7.5, 2.5)	231.23 ± 7.22	0.274 ± 0.019	90.80 ± 0.10

[a] The values in bracket with labels show the concentration of propylene glycol (7.5% v/v) and concentration of SPC (1%, 1.5%, 2%, and 2.5% w/v). P6 to P9 contains 24 mg of RTG

Hence, formulation P 6 (**Table 5.3**) that resulted in a good %EE (82.97 ± 0.18), particle size of 115.63 ± 5.22 nm with PDI of 0.267 ± 0.028 was selected as final optimized RTG-Proposomes formulation. The hydrodynamic particle size of RTG-Proposomes is presented in **Figure 5.2A**. The zeta potential of formulation P6 was measured (−14.8 ± 1.2 mV) and data presented in **Figure 5.2B**.

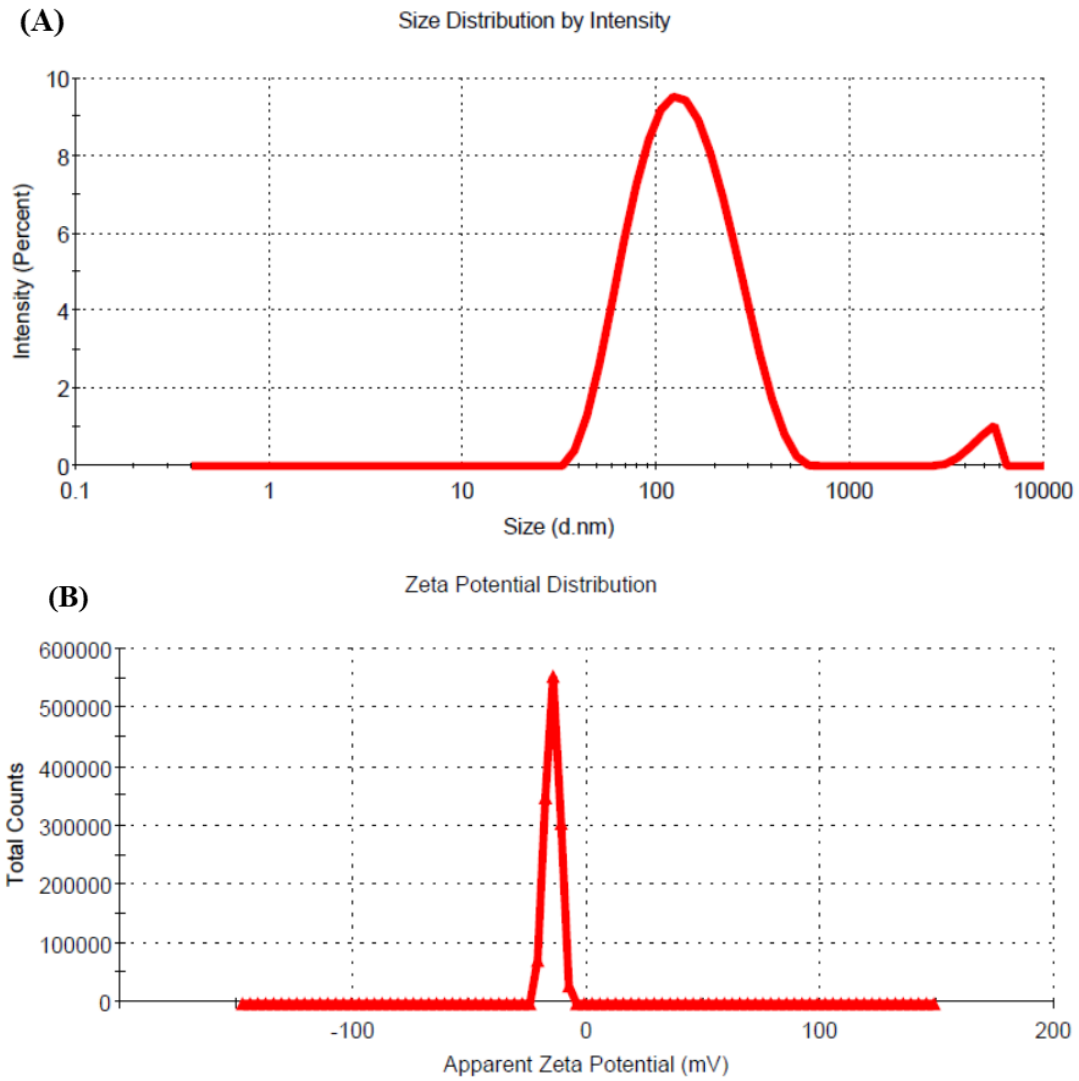

Figure 5.2 (A) Hydrodynamic diameter of optimized RTG-Proposomes based on the % intensity, (B) Zeta potential of optimized RTG-Proposomes

5.3.2 Transmission electron microscopy

The morphology of pure-RTG and optimized RTG-Proposomes analyzed using TEM showed in **Figure 5.3**. TEM images showed that the size and shape of pure drug are significantly different from the optimized proposomes (**Figure 5.3A**). TEM analysis revealed that the prepared proposomes were primarily spherical with a consistent size distribution. The proposomes surface was found to be smooth and regular. No evidence of vesicle agglomeration was observed on the surface which revealed stability of the optimized proposomes. The diameters of prepared proposomes were found to be in the range of 100 nm approximately (**Figure 5.3B**).

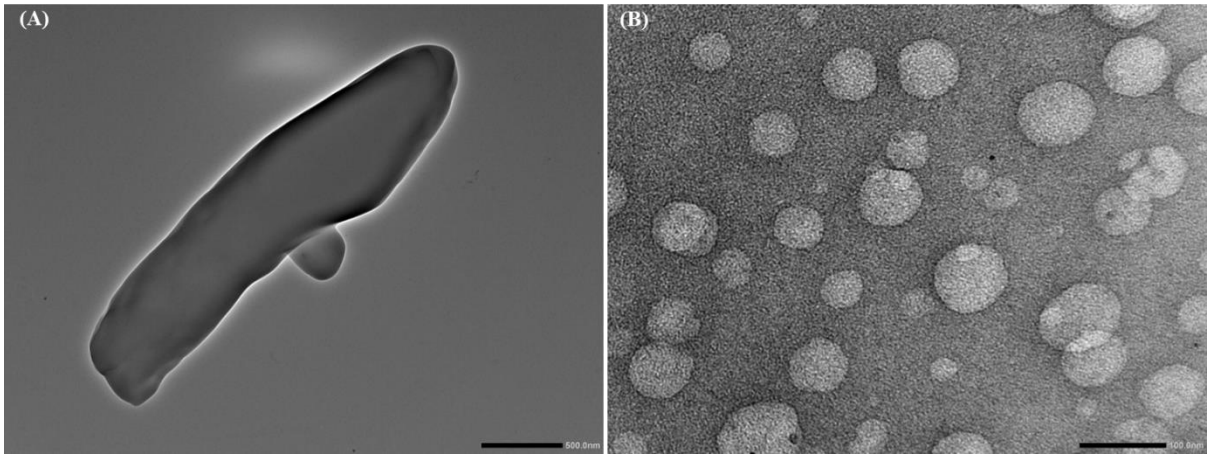

Figure 5.3 TEM images of (A) Pure RTG, (B) Optimized RTG-Proposomes

5.3.3 *In vitro* release

The *in vitro* drug release study of optimized RTG-Proposomes and pure RTG suspension was performed, and result is presented in **Figure 5.4**. From the pure drug suspension, almost 100% drug released within 24 h. Form RTG-Proposomes, cumulative drug released was found up to 45% after 24 h. The release data confirmed that RTG-Proposomes prolonged the release of drug **Figure 5.4**. The release kinetics showed that optimized proposomes followed Korsmeyer-Peppas model (R^2 = 0.9645) (**Table 5.4**) and showed a non-Fickian diffusion release mechanism with a '*n'* value of 0.347 [23]. This result indicated that the vesicle successfully controlled release of RTG from the optimized proposomes [4,11]. The release profiles of RTG-Proposomes and RTG suspension were evaluated for similarity factor (f_2), which showed that the two release profiles are significantly not similar to each other.

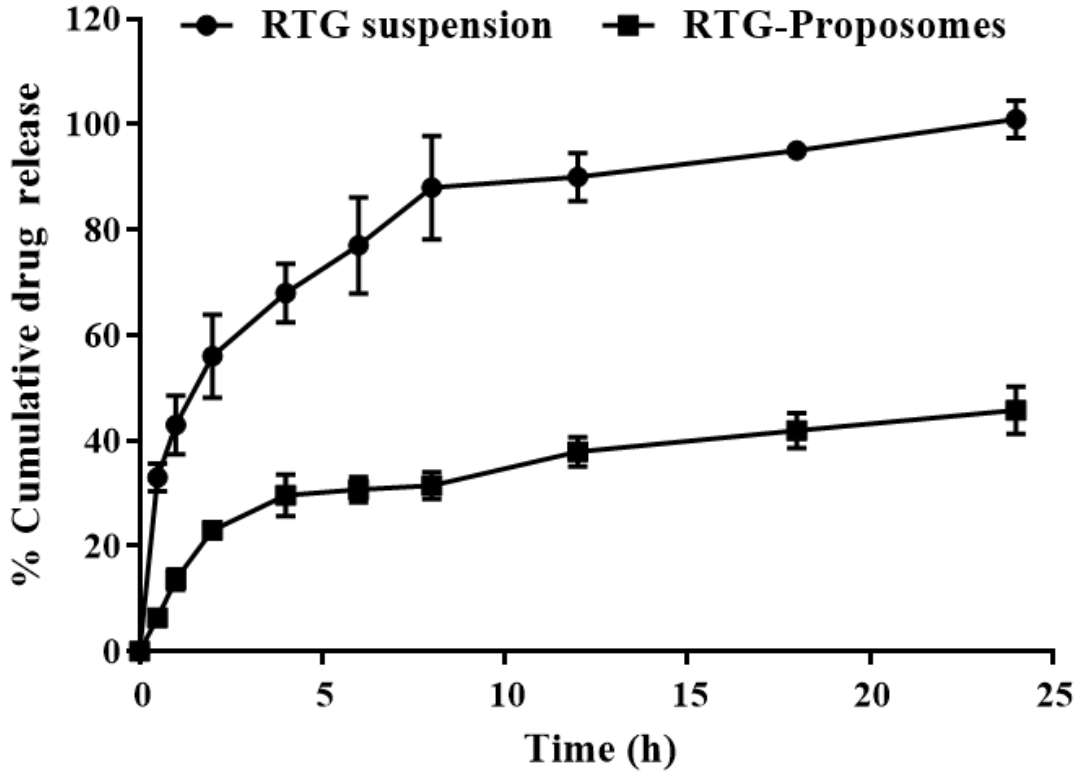

Figure 5.4 *In vitro* release profiles of RTG suspension and optimized RTG-Proposomes in PBS (pH 7.4)

Table 5.4 Kinetic model application to *in vitro* release data of RTG-Proposomes

Model	R^2 value
First-order	0.5186
Higuchi Model	0.8942
Korsmeyer-Peppas	**0.9645**

5.3.4 *Ex vivo* nasal permeation

Ex vivo nasal permeation study was performed to compare pure RTG suspension and RTG-Proposomes. The mean cumulative *ex vivo* RTG permeated/unit area *vs* time through the goat nasal mucosa is presented in **Figure 5.5**. The permeation behaviour showed that RTG amount permeated (386.26 ± 18.62 μg/cm^2) from proposomes was significantly higher than that of pure drug suspension ($p < 0.05$). Optimized RTG-Proposome showed 8.04-fold increase in amount permeated as compared to the pure drug suspension. The result indicated that proposome formulation provides better permeability than pure drug [24]. Better permeation of RTG from

proposome can be attributed to the combined effect of PG and SPC present in the formulation. . SPC increases affinity towards biological membrane which might also enhance the permeation behaviour of proposome [25]. The bilayer proposomes vesicles, due to its fluidity, might also have helped in opening tight junction pores of the nasal mucosa [26].

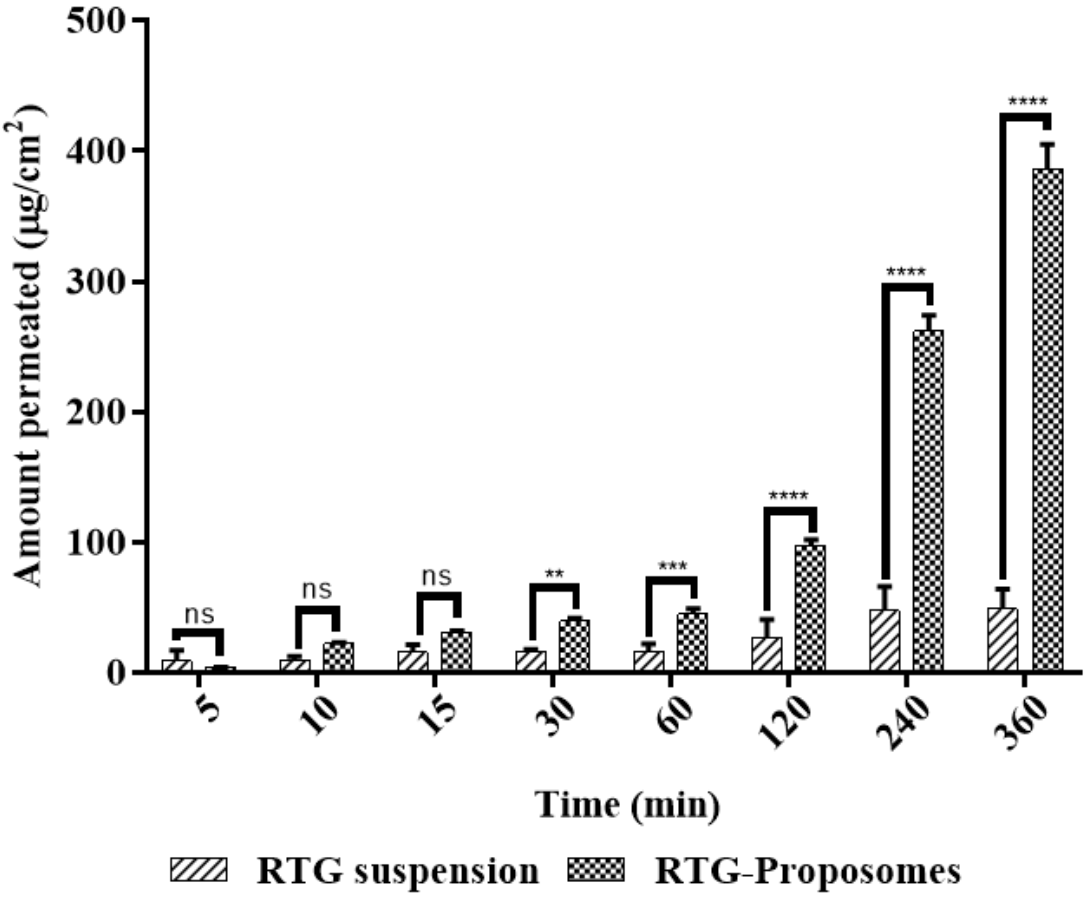

Figure 5.5 *Ex vivo* amount of drug permeated/unit area from optimized RTG-Proposomes and drug suspension via goat nasal mucosa (n = 3, Mean ± SD)

5.3.5 Stability under refrigerated condition

Stability study results of RTG-Proposomes are given in **Table 5.5**. No significant difference was noted in any of the parameters such as particle size (nm), PDI, zeta potential, and %EE between freshly prepared proposomes and RTG-Proposomes stored at the refrigerated conditions over 60 days ($P > 0.05$).

Table 5.5 Stability data of RTG-Proposomes

Parameters	0th Day	7th Day	30th Day	60th Day
Particle size (nm)	115.63 ± 5.22	118.23 ± 1.01	112.52 ± 1.12	120.11 ± 3.91
PDI	0.267 ± 0.028	0.301 ± 0.002	0.291 ± 0.001	0.302 ± 0.005
Zeta potential (mV)	–14.8 ± 1.2	–16.8 ± 1.1	–15.1 ± 0.5	–16.7 ± 2.1
%EE	82.97 ± 0.18	81.77 ± 0.11	85.10 ± 1.11	80.68± 2.90

5.3.6 *In vivo* studies

5.3.6.1 Mucociliary transport time

Mucociliary clearance transport time for pure RTG suspension and RTG-Proposomes were found to be 7.5 ± 3.53 min and 32.5 ± 3.53 min, respectively. RTG-Proposomes demonstrated higher ($P < 0.05$) mucociliary clearance transport time than that of RTG suspension (**Figure 5.6**). Increased mucociliary transport time of RTG-Proposomes indicates its higher residence time in the nasal cavity. This might be attributed to presence of SPC in the proposomes. High mucociliary clearance transport time of RTG-Proposomes indicated that proposomes could resist the process of mucociliary clearance resulting in its increased retention in nasal cavity.

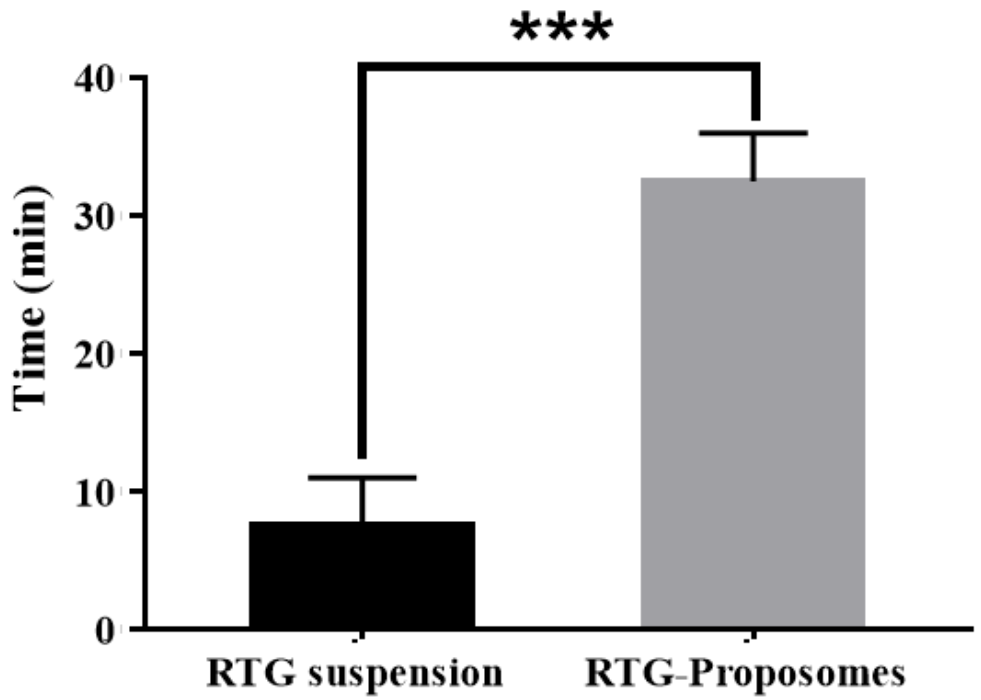

Figure 5.6 Mucociliary transport time of aqueous RTG suspension and RTG-Proposomes. Independent student t-test with one-tail was applied. '***' shows p-value < 0.05.

5.3.6.2 Brain and plasma PK analysis

In vivo PK studies after i.n. administration of RTG-Proposomes and RTG suspension were conducted at a dose of 2 mg/Kg and dose volume of 75 µL in each nostril. Brain and plasma concentration *vs* time profiles were constructed and presented in **Figure 5.7**. A comparison of the PK performances (in brain and plasma) of RTG-Proposomes and pure drug suspension is given in **Table 5.6**. PK data for RTG suspension was taken from **Chapter 3**, **Section 3.5.6** [13].

Table 5.6 Brain and plasma PK parameters for RTG-Proposomes and RTG suspension after i.n. administration

PK parameters	**Brain**		**Plasma**	
	RTG-Proposomes	**RTG suspension**	**RTG-Proposomes**	**RTG suspension**
$AUC_{0\rightarrow tlast}$ $(ng*h/g)^b$, $(ng*h/mL)^p$	3271.10 ± 13.12	628.11 ± 12.21	1491.89 ± 16.34	779.01 ± 14.11
C_{max} $(ng/g)^b$, $(ng/mL)^p$	708.61 ± 29.95	264.71 ± 21.12	321.87 ± 11.90	270.12 ± 18.50
T_{max} (h)	2	1	0.5	2
MRT (h)	3.34	1.82	2.74	3.15

[b] unit for brain PK parameters, [p] unit for plasma PK parameters. RTG dose for both i.n. formulations: 2 mg/Kg; for plasma PK n = 4 animals were used, and n = 4 animals' brains were used for brain PK at every time point; The brain and plasma data are represented as mean ± SD.

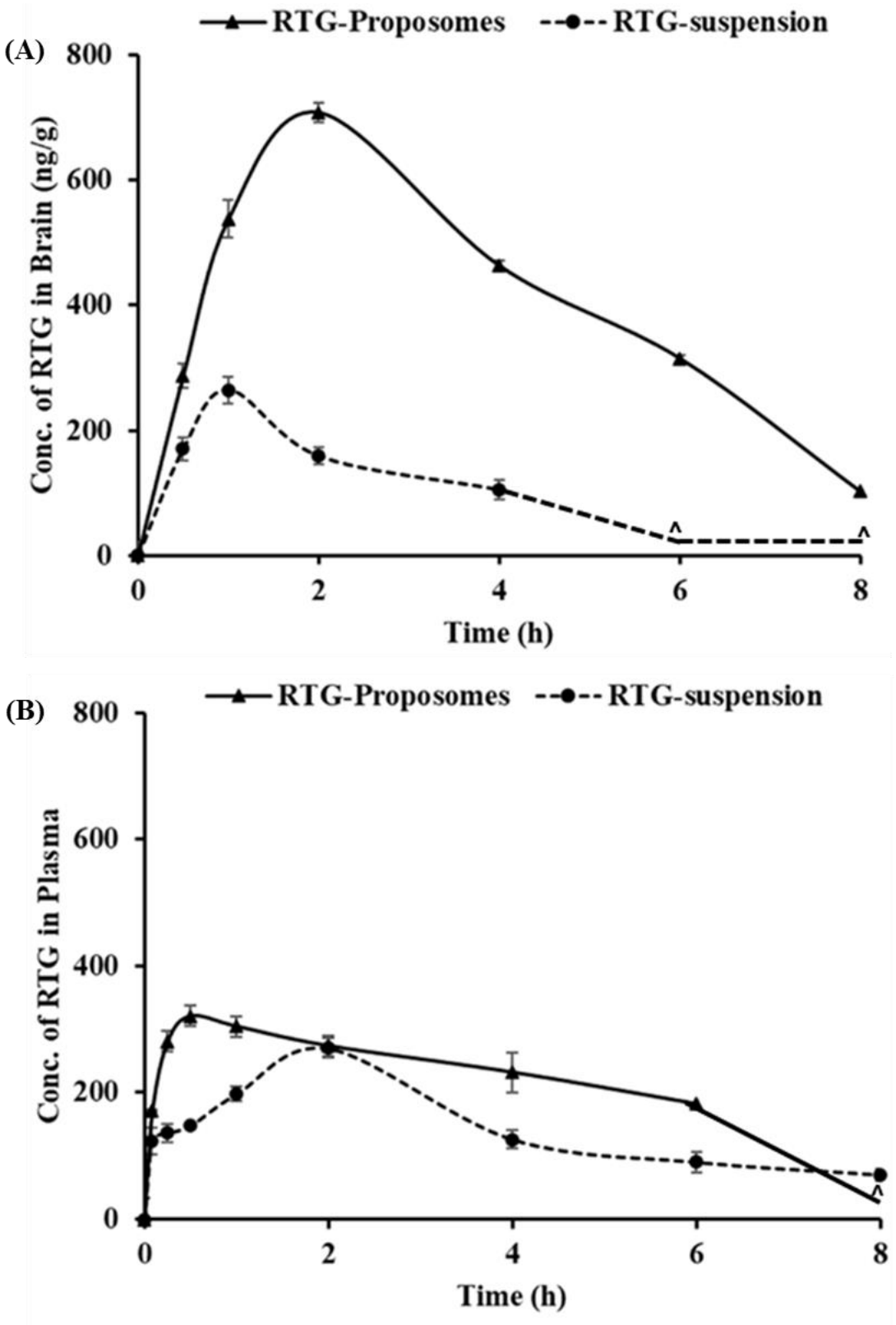

Figure 5.7 PK profiles of RTG attained after i.n. administration of RTG-Proposomes and RTG suspension in (A) Brain and (B) Plasma. '^' in both the profiles denote that the concentration of RTG was not detected at those time points in brain matrices and plasma.

The brain $AUC_{0\rightarrow tlast}$ value for RTG-Proposomes was around 5.21-fold higher than that of the brain $AUC_{0\rightarrow tlast}$ of pure drug suspension. The brain C_{max} of RTG-Proposomes showed a 2.68-fold increment as compared to pure RTG suspension after i.n. administration. An unpair t-test comparison for brain $AUC_{0\rightarrow tlast}$ values for both formulations showed a statistically significant ($p < 0.0001$) difference between the two formulations. The brain concentrations of RTG were compared at different time points for both treatments using t-tests. At all-time points, brain drug concentrations from proposomes were significantly higher than that of RTG suspension at a 5% confidence interval level. To further evaluate the performance of formulations, DTP (%) and DTE (%) values were calculated as per Equation 4.1 and Equation 4.2, describe in **Chapter 4**, **Section 4.2.11.3**. The DTE (%) evaluates the brain exposure of drug when administered via the i.n. route *vs* a systemic route. DTE (%) value for RTG-Proposomes was found 1556.4 which is significantly higher than 100. This result implies that the brain exposure of proposomes after i.n. administration was superior to that was attained via systemic route following intravenous administration of pure RTG solution. This result finally showed that the prepared proposomes improve the direct N2B uptake efficacy of RTG. The DTP (%) was found to be 93.6 for RTG-Proposomes representing effective direct N2B uptake. The observed results for both DTE (%) and DTP (%) of RTG-Proposomes may be ascribed to the increased residence of the formulation in nasal cavity. This might have helped in better uptake of the proposomes to brain after i.n. administration. Furthermore, the smaller particle size of RTG-Proposomes might also have helped to enter through the olfactory neurons of brain via different endocytic transport in nasal mucosa and resulted in higher DTP (%) and DTE (%) as compared to RTG suspension [27,28].

5.3.7 Histopathology of brain

Morphology of the hippocampus region on brain slides was examined at 0 h and at 8 h following RTG-Proposomes administration (**Figure 5.8**) to show any signs of toxicity [29]. **Figure 5.8C** and **5.8D** depicts the morphology of hippocampus area of treated rats compared to control rats (**Figure 5.8A** and **B**). There were no signs of neuronal injury, such as cell body shrinkage or necrosis, in the rats' brain (**Figure 5.8D**). This indicated that RTG-Proposomes were safe and did not induce brain injury.

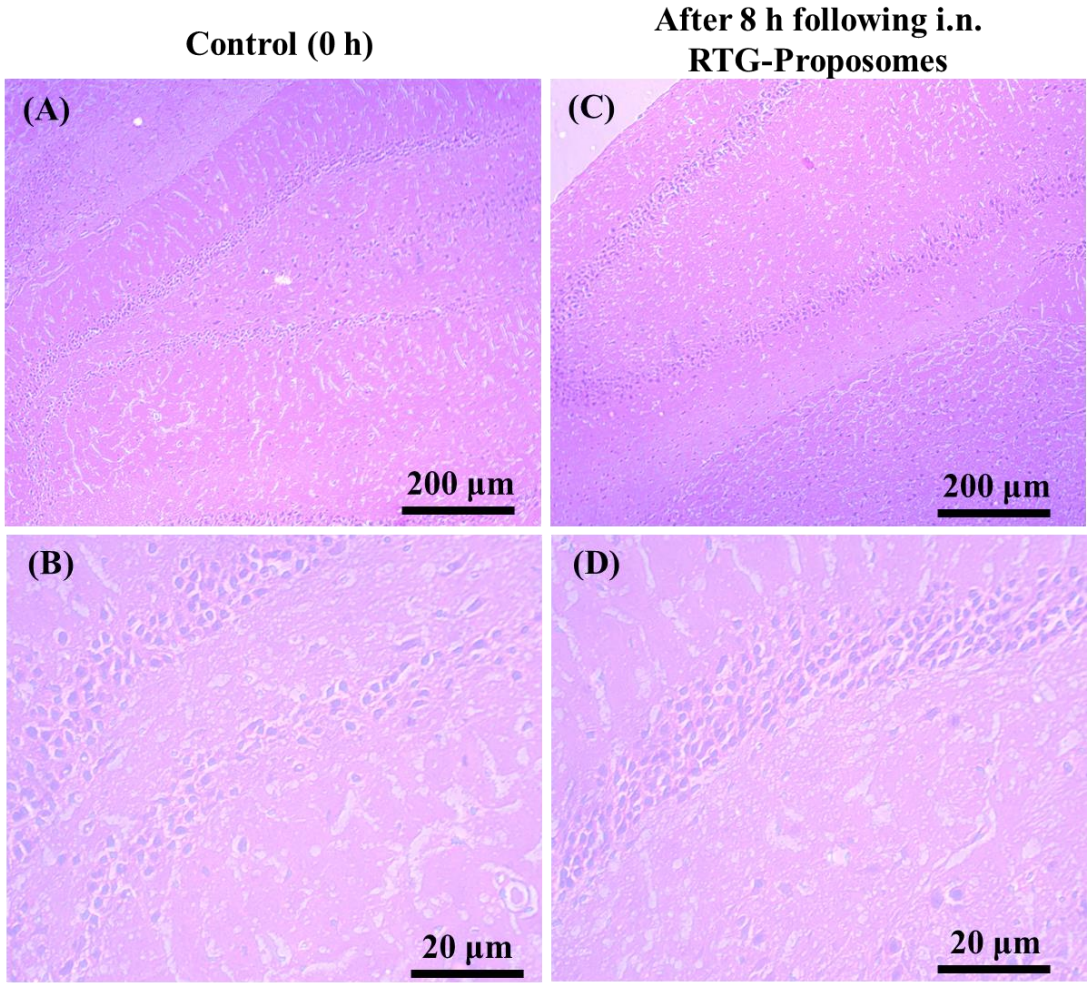

Figure 5.8 Histopathological evaluations of brain (hippocampal region) in different conditions (A) Control animal at 100X magnification, (B) Control animal at 400X magnification, (C) RTG-Proposomes treated animal at 100X magnification, (D) RTG-Proposomes treated animal at 400X magnification

5.4 Conclusion

This chapter describes the design, optimization, *in vitro*, *ex vivo*, and *in vivo* characterization of RTG-Proposomes. RTG-Proposomes were prepared using cold mixing process followed by ultrasonication. RTG-Proposomes were developed and optimized for improved N2B delivery of the drug. Presence of PG improved *ex vivo* permeability of the drug in proposomes formulation. RTG-Proposomes showed controlled release of RTG as compared to pure RTG. *In vivo* PK studies in Wistar rats demonstrated that the developed RTG-Proposomes showed significant high DTE (%) and DTP (%) of 1556.4 and 93.6, respectively. High DTE (%) and DTP (%) value of proposomes indicate better direct N2B delivery of drug compared to pure RTG suspension via olfactory or trigeminal pathway upon i.n. administration. Brain histopathology study further confirmed that the prepared proposomes are non-toxic and safe for N2B delivery of RTG. The overall results demonstrate superiority of the optimized RTG-Proposomes for the better management of PD via i.n. route in comparison to pure drug suspension given via same route.

References

1. Yang, Z.Z.; Zhang, Y.Q.; Wang, Z.Z.; Wu, K.; Lou, J.N.; Qi, X.R. Enhanced Brain Distribution and Pharmacodynamics of Rivastigmine by Liposomes Following Intranasal Administration. *International Journal of Pharmaceutics* **2013**, *452*, 344–354, doi:10.1016/j.ijpharm.2013.05.009.

2. Al Asmari, A.K.; Ullah, Z.; Tariq, M.; Fatani, A. Preparation, Characterization, and in Vivo Evaluation of Intranasally Administered Liposomal Formulation of Donepezil. *Drug design, development and therapy* **2016**, *10*, 205–215, doi:10.2147/DDDT.S93937.

3. Praveen, A.; Aqil, M.; Imam, S.S.; Ahad, A.; Moolakkadath, T.; Ahmad, F.J. Lamotrigine Encapsulated Intra-Nasal Nanoliposome Formulation for Epilepsy Treatment: Formulation Design, Characterization and Nasal Toxicity Study. *Colloids and Surfaces B: Biointerfaces* **2019**, *174*, 553–562, doi:10.1016/j.colsurfb.2018.11.025.

4. Narayan, R.; Singh, M.; Ranjan, O.P.; Nayak, Y.; Garg, S.; Shavi, G. V.; Nayak, U.Y. Development of Risperidone Liposomes for Brain Targeting through Intranasal Route. *Life Sciences* **2016**, *163*, 38–45, doi:10.1016/J.LFS.2016.08.033.

5. Bahadur, S.; Pardhi, D.M.; Rautio, J.; Rosenholm, J.M.; Pathak, K. Intranasal Nanoemulsions for Direct Nose-to-Brain Delivery of Actives for CNS Disorders. *Pharmaceutics* **2020**, *12*, 1230, doi:10.3390/pharmaceutics12121230.

6. Kathuria, H.; Nguyen, D.T.P.; Handral, H.K.; Cai, J.; Cao, T.; Kang, L. Proposome for Transdermal Delivery of Tofacitinib. *International Journal of Pharmaceutics* **2020**, *585*, 119558, doi:10.1016/J.IJPHARM.2020.119558.

7. Yogendra Raj Pandey, S.K.; Gupta, B.K.; Ali, J.; Baboota, S. Intranasal Delivery of Paroxetine Nanoemulsion via the Olfactory Region for the Management of Depression:

Formulation, Behavioural and Biochemical Estimation. *Nanotechnology* **2016**, *27*, 025102, doi:10.1088/0957-4484/27/2/025102.

8. Li, L.; Nandi, I.; Kim, K.H. Development of an Ethyl Laurate-Based Microemulsion for Rapid-Onset Intranasal Delivery of Diazepam. *International Journal of Pharmaceutics* **2002**, *237*, 77–85, doi:10.1016/S0378-5173(02)00029-7.

9. Shelke, S.; Shahi, S.; Jadhav, K.; Dhamecha, D.; Tiwari, R.; Patil, H. Thermoreversible Nanoethosomal Gel for the Intranasal Delivery of Eletriptan Hydrobromide. *Journal of Materials Science: Materials in Medicine* **2016**, *27*, 103, doi:10.1007/s10856-016-5713-6.

10. Zhang, Y.; Pu, C.; Tang, W.; Wang, S.; Sun, Q. Gallic Acid Liposomes Decorated with Lactoferrin: Characterization, in Vitro Digestion and Antibacterial Activity. *Food Chemistry* **2019**, *293*, 315–322, doi:10.1016/j.foodchem.2019.04.116.

11. Saka, R.; Chella, N.; Khan, W. Development of Imatinib Mesylate-Loaded Liposomes for Nose to Brain Delivery: In Vitro and in Vivo Evaluation. *AAPS PharmSciTech* **2021**, *22*, 192, doi:10.1208/s12249-021-02072-0.

12. Saha, P.; Pandey, M.M. DoE-Based Validation of a HPLC–UV Method for Quantification of Rotigotine Nanocrystals: Application to in Vitro Dissolution and Ex Vivo Nasal Permeation Studies. *Electrophoresis* **2022**, *43*, 590–600, doi:10.1002/ELPS.202100157.

13. Saha, P.; Kathuria, H.; Pandey, M.M. Nose-to-Brain Delivery of Rotigotine Redispersible Nanosuspension: In Vitro and in Vivo Characterization. *Journal of Drug Delivery Science and Technology* **2023**, *79*, 104049, doi:10.1016/j.jddst.2022.104049.

14. Lee, D.; Minko, T. Nanotherapeutics for Nose-to-Brain Drug Delivery: An Approach to

Bypass the Blood Brain Barrier. *Pharmaceutics* **2021**, *13*, doi:10.3390/pharmaceutics13122049.

15. Sita, V.G.; Jadhav, D.; Vavia, P. Niosomes for Nose-to-Brain Delivery of Bromocriptine: Formulation Development, Efficacy Evaluation and Toxicity Profiling. *Journal of Drug Delivery Science and Technology* **2020**, *58*, 101791, doi:10.1016/j.jddst.2020.101791.

16. Huang, X.; Caddell, R.; Yu, B.O.; Xu, S.; Theobald, B.; Lee, L.J.; Lee, R.J. Ultrasound-Enhanced Microfluidic Synthesis of Liposomes. *Anticancer Research* **2010**, *30*, 463–466.

17. Inactive Ingredient Search for Approved Drug Products Available online: https://www.accessdata.fda.gov/scripts/cder/iig/index.cfm?event=BasicSearch.page (accessed on 5 May 2022).

18. Zhang, L.; Lu, C.T.; Li, W.F.; Cheng, J.G.; Tian, X.Q.; Zhao, Y.Z.; Li, X.; Lv, H.F.; Li, X.K. Physical Characterization and Cellular Uptake of Propylene Glycol Liposomes in Vitro. *Drug Development and Industrial Pharmacy* **2012**, *38*, 365–371, doi:10.3109/03639045.2011.604331.

19. Li, W.Z.; Hao, X.L.; Zhao, N.; Han, W.X.; Zhai, X.F.; Zhao, Q.; Wang, Y.E.; Zhou, Y.Q.; Cheng, Y.C.; Yue, Y.H.; et al. Propylene Glycol-Embodying Deformable Liposomes as a Novel Drug Delivery Carrier for Vaginal Fibrauretine Delivery Applications. *Journal of Controlled Release* **2016**, *226*, 107–114, doi:10.1016/J.JCONREL.2016.02.024.

20. Salem, H.F.; Gamal, A.; Saeed, H.; Tulbah, A.S. The Impact of Improving Dermal Permeation on the Efficacy and Targeting of Liposome Nanoparticles as a Potential

Treatment for Breast Cancer. *Pharmaceutics 2021, Vol. 13, Page 1633* **2021**, *13*, 1633, doi:10.3390/PHARMACEUTICS13101633.

21. Salem, H.F.; Kharshoum, R.M.; Mahmoud, M.; Azim, S.A.; Ebeid, E.-Z.M. Development and Characterization of a Novel Nano-Liposomal Formu- Lation of Alendronate Sodium Loaded with Biodegradable Polymer. *Ars Pharmaceutica* **2018**, *59*, 9–20, doi:10.4321/S2340-98942018000100001.

22. Nahar, K.; Absar, S.; Patel, B.; Ahsan, F. Starch-Coated Magnetic Liposomes as an Inhalable Carrier for Accumulation of Fasudil in the Pulmonary Vasculature. *International journal of pharmaceutics* **2014**, *464*, 185–195, doi:10.1016/J.IJPHARM.2014.01.007.

23. Lisik, A.; Witold Musial Conductomeric Evaluation of the Release Kinetics of Active Substances from Pharmaceutical Preparations Containing Iron Ions. *Materials* **2019**, *12*, 730, doi:10.3390/ma12050730.

24. Touitou, E.; Duchi, S.; Natsheh, H. A New Nanovesicular System for Nasal Drug Administration. *International Journal of Pharmaceutics* **2020**, *580*, 119243, doi:10.1016/J.IJPHARM.2020.119243.

25. Aboud, H.M.; Ali, A.A.; El-Menshawe, S.F.; Elbary, A.A. Nanotransfersomes of Carvedilol for Intranasal Delivery: Formulation, Characterization and in Vivo Evaluation. *Drug Delivery* **2015**, *23*, 2471–2481, doi:10.3109/10717544.2015.1013587.

26. Mara Mainardes, R.; Cristina Cocenza Urban, M.; Oliveira Cinto, P.; Vinicius Chaud, M.; Cesar Evangelista, R.; Palmira Daflon Gremiao, M. Liposomes and Micro/Nanoparticles as Colloidal Carriers for Nasal Drug Delivery. *Current Drug Delivery* **2006**, *3*, 275–285, doi:10.2174/156720106777731019.

27. Seju, U.; Kumar, A.; Sawant, K.K. Development and Evaluation of Olanzapine-Loaded PLGA Nanoparticles for Nose-to-Brain Delivery: In Vitro and in Vivo Studies. *Acta biomaterialia* **2011**, *7*, 4169–4176, doi:10.1016/J.ACTBIO.2011.07.025.

28. Wang, F.; Yang, Z.; Liu, M.; Tao, Y.; Li, Z.; Wu, Z.; Gui, S. Facile Nose-to-Brain Delivery Evaluation of Intranasal Delivery Route of Drug Administration for Brain Targeting of Rotigotine-Loaded Polymer Micelles Thermosensitive Hydrogels: In Vitro Characterization and in Vivo Behavior Study. *International Journal of Pharmaceutics* **2020**, *577*, 119046, doi:10.1016/j.ijpharm.2020.119046.

29. Sita, V.G.; Jadhav, D.; Vavia, P. Niosomes for Nose-to-Brain Delivery of Bromocriptine: Formulation Development, Efficacy Evaluation and Toxicity Profiling. *Journal of Drug Delivery Science and Technology* **2020**, *58*, doi:10.1016/j.jddst.2020.101791.

Chapter 6: Development, *In vitro*, *Ex vivo* and *In vivo* Evaluation of Rotigotine Loaded Lecithin Chitosan Nanoparticles for Improved N2B Delivery

6.1 Introduction

Chitosan (CS) is a positively charged biodegradable polysaccharide available in broad range of molecular weights from 50 – 400 kDa. CS is a promising polymer for pharmaceutical formulations due to its biocompatible and mucoadhesive nature. Intranasal (i.n.) formulations based on CS have shown improved nasal residence time and better mucoadhesion. CS is well reported for opening tight junctions reversibly which helps in the enhancement of paracellular/extracellular transport of nanocarriers via the olfactory neuronal pathway [1,2].

Soy lecithin is a negatively charged phospholipids combination consisting mainly of phosphatidylcholines. It is a biocompatible, safe, and non-immunogenic excipient. The interaction between lecithin and the CS can produce nanoparticles (NP) by self-assembling utilizing ionic interactions [3,4]. CS-lecithin NP of both hydrophilic and lipophilic drugs have been developed and reported for oral, transdermal, and i.n. delivery [5–9]. These NP have enhanced the drugs' oral, systemic, and brain bioavailability. In this present study, we have prepared and evaluated Rotigotine (RTG)-loaded CS-lecithin hybrid NP (RTG-LCNP) for i.n. administration to improve the brain availability of drug in comparison to pure RTG suspension. An *ex vivo* nasal permeation study was performed to evaluate the permeability properties of RTG-LCNP compared to pure RTG suspension. Finally, the nasal clearance time and *in vivo* study of the optimized LCNP were performed to assess the direct nose-to-brain (N2B) delivery and brain targeting efficiency.

6.2 Materials and methods

6.2.1 Materials

RTG was a gift sample from Mylan Laboratories (Hyderabad, India). Medium molecular weight CS (75 – 85% deacetylated), acetic acid glacial (GAA) was purchased from SISCO Research Laboratories (SRL) Pvt. Ltd (Delhi, India). Lecithin (Lipoid S 100, soybean lecithin with phosphatidylcholine) and Poloxamer 407 were obtained as gift samples from Lipoid (GmBH, Germany) and BASF (Mumbai, India), respectively. Sodium chloride, potassium chloride, mannitol, and different buffer salts (KH_2PO_4, K_2HPO_4) were obtained from SD Fine Chemicals Pvt. Ltd. (Mumbai, India). HPLC grade acetonitrile (ACN) was purchased from Merck (Mumbai, India).

Milli-Q water taken from an in-house Milli-Q® Reference water purification system (GmbH, Germany) was used in all experimental processes and analysis.

6.2.2 Preliminary studies for RTG-LCNP

Solubility of RTG, in the presence of different stabilizer was evaluated to identify the suitable stabilizer for the preparation of RTG-LCNP. A solubility study of RTG in presence of different stabilizers was performed as discussed in the previous **Chapter 4**, **Section 4.2.3**. The equilibrium solubility of RTG was assessed in different surfactants such as span 20, PVP K-30, Soluplus®, tween 20, sodium lauryl sulphate, Poloxamer 188, and Poloxamer 407. Briefly, an excess amount of RTG was added into the vials (n = 3) containing 5 mL of different surfactant solutions (0.1 %*w/v*) and kept on shaking in water bath shaker (Remi, Mumbai, India) for 24 h at 37 ± 1 ^oC temperature.

6.2.3 Preparation of RTG-LCNP

The LCNP was prepared by solvent injection method [8,10]. An ethanolic solution of the drug and lecithin was prepared by dissolving 20 mg of RTG and lecithin in 1 mL of ethanol. CS and Poloxamer 407 were dissolved in GAA, and pH of the solution was adjusted with sodium acetate buffer. The ethanolic solution was injected into the aqueous phase using 22G needle attached to a polypropylene syringe. The injection was done for 5 min under high-speed homogenization (Polytron PT 1300D, Kinematica, Lucerne, Switzerland) at 12,000 rpm. The organic solvent was evaporated from nano-dispersion using rotavapor (Buchi, Mumbai, India) for 10 min and was lyophilized (Labconco^{TM}, South Kansas City, USA). The obtained nano-dispersion of RTG-LCNP was ultracentrifuged (Thermo, Massachusetts, USA) at 45,000 rpm for 1 h at 4 °C to attain a pellet of RTG-LCNP. The supernatant was decanted, and the LCNP was collected. Further, LCNP pellets were washed thrice with Milli-Q water to remove any trace of free drug from the surface of LCNP. For lyophilization, the final collected pellet of RTG-LCNP was re-dispersed using Milli-Q water containing mannitol as a cryoprotectant (**Figure 6.1**). The lyophilized RTG-LCNP was stored under refrigerated conditions (4 °C) till further use. A control RTG suspension was prepared by dispersing RTG in 0.2 %*w/v* methyl cellulose (400 cps).

The effect of several formulation parameters *viz.*, ratio of drug:lecithin, ratio of lecithin:CS, amount of Poloxamer 407, pH of CS solution on particle size, PDI, % entrapment efficiency (%EE), % drug loading (%DL) were optimized to select the final LCNP batch.

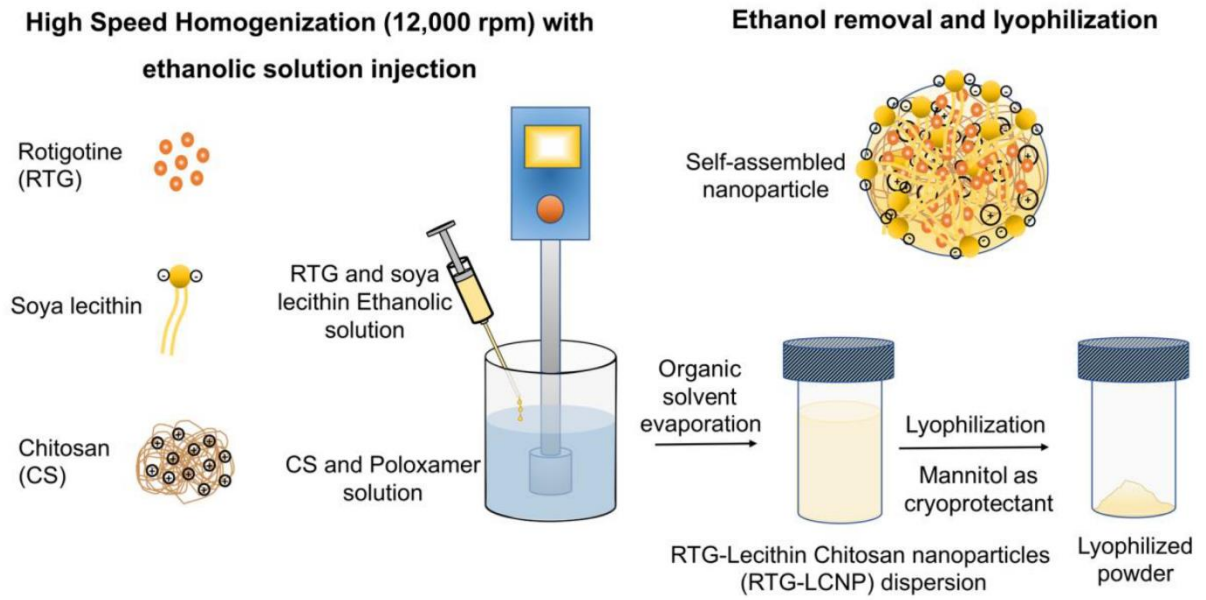

Figure 6.1 Schematic representation of preparation of LCNP

6.2.4 Characterization of RTG-LCNP

6.2.4.1 Particle size, PDI, and zeta potential

The average particle size (d.nm) and PDI of RTG-LCNP were determined using the dynamic light scattering technique (Zetasizer nano ZS, Malvern Instruments, UK). The zeta potential was measured using electrophoretic dynamic light scattering. The LCNP nano-dispersion were diluted ten times with sodium acetate buffer (pH 5.5) and allowed to equilibrate for 2 min at 25 ^{o}C before each measurement. Three measurements were performed for every LCNP nano-dispersion, and the mean values were reported for final particle size, PDI, and zeta potential.

6.2.4.2 Entrapment efficiency (%EE) and drug loading (%DL)

The %EE of LCNP were estimated from the amount of RTG unentrapped ($W_{Free\ drug}$). The free RTG was separated from LCNP nano-dispersion by ultracentrifugation at 45,000 rpm for 1 h. The amount of RTG present in the supernatant was analysed for determination of unentrapped drug ($W_{Free\ drug}$) using the RP-HPLC analytical method described in **Chapter 3**, **Method II** [11]. %EE for LCNP was calculated using the formula presented in Equation 6.1:

$$\%EE = \left(\frac{W_{Total\ drug} - W_{Free\ drug}}{W_{Total\ drug}}\right) \times 100 \quad (6.1)$$

where, $W_{Total\ drug}$ is the amount of RTG used in the preparation of RTG-LCNP.

For LCNP, %DL was estimated following the direct method. For this, after ultracentrifugation (45,000 rpm for 1h at 4 °C) pellets of RTG-LCNP was collected, washed, and dried under vacuum. The pellets were first weighed and dissolved in ACN to extract RTG, then diluted appropriately using mobile phase (ACN:KH_2PO_4, pH 5::54:46). The amount of RTG was quantified using the RP-HPLC analytical method described in **Chapter 3**, **Method II** previously. Finally, %DL was calculated using the formula given in Equation 6.2:

$$\%DL = \left(\frac{W_{RTG}}{W_{RTG-LCNP}}\right) \times 100 \quad (6.2)$$

where, W_{RTG} is the weighed of RTG loaded in the LCNP and $W_{RTG\text{-}LCNP}$ is the total weight of prepared NP.

6.2.4.3 Differential scanning calorimetry (DSC)

Thermal analysis was carried out using DSC to analyse the physical state of RTG encapsulated in the optimized RTG-LCNP. Lyophilised RTG-LCNP was accurately weighed inside an aluminium pan and crimped. The samples were analysed using DSC-60 Plus (Shimadzu, Kyoto, Japan) at a temperature range of 30 – 250 °C and heated at a rate of 5 °C/min in nitrogen environment (50 mL/min). DSC analysis was also performed for pure RTG, CS, lecithin, and mannitol (cryoprotectant).

6.2.4.4 Field emission scanning electron microscopy (FESEM)

Field emission scanning electron microscope (FEI, Washington, USA) was used for examination of surface morphology of optimised LCNP. Briefly, 5 µL of optimized RTG-LCNP nano-dispersion was dropped onto a glass coverslip and left overnight to dry under desiccator [12]. The sample containing glass coverslip was sticked to the aluminium stab using

double-sided carbon tape. Finally, the samples were sputter-coated for 50 s by Q150TES sputter coater (Quorum Technologies, East Sussex, England). Gold-coated samples were analysed using FESEM using 15 kV high-voltage vacuum pump.

6.2.4.5 Transmission electron microscopy (TEM)

The particle size and shape of RTG-LCNP and pure-RTG were further evaluated using transmission electron microscopy (JEOL, Tokyo, Japan) at an accelerating voltage of 120 kV. The samples were prepared by drop caste on carbon coated copper grids. The formulations droplet was dropped on the carbon grid and cast on the grid for a few min. Then the excess liquid was soaked using blotting paper before analysis. The cast grid was placed in TEM to take microscopic images for morphological analysis.

6.2.5 *In vitro* release

RTG-LCNP drug release was carried out using the dialysis bag method (Molecular weight cut-off of 12 kDa, Himedia, India). The dialysis bag was soaked in Milli-Q water for 2 h and then opened. 1 mg drug equivalent RTG-LCNP and RTG suspension were separately taken in a dialysis bag, sealed, and immersed in the 50 mL phosphate buffer saline (PBS), pH 7.4, as release media. The system was maintained at 37 ± 2 ^{o}C with constant stirring at 100 rpm [13]. At predetermined time (0.5, 1, 2, 4, 6, 8, 12, 18, and 24 h), 1 mL samples were withdrawn and replenished with pre-heated fresh medium. The samples were diluted with mobile phase and analysed using the validated RP-HPLC method described in previously in **Chapter 3**, **Method II**. The release profiles of RTG-LCNP were analysed using mathematical models, i.e., first-order, Higuchi model, and Korsmeyer-Peppas, to understand the kinetics and release mechanism. The high correlation coefficient (R^2) was taken as a best fit. The *n* value obtained in Korsmeyer-Peppas model was used to assess the drug release mechanism. The similarity

factor (f_2) was determined and used to compare RTG-LCNP and RTG suspension release profiles.

6.2.6 *Ex vivo* nasal permeation

Goat nasal mucosa samples were acquired immediately after the sacrifice of goat from slaughterhouse. Permeation study was performed using Franz diffusion cell (Orchid Scientific, Nasik, India) with a diffusion area of 0.785 cm^2. The mucosa was hydrated in PBS (pH 6.4) for 15 min prior use. The receptor compartment of diffusion cell was filled with 5 mL of PBS (pH 6.4) as release media. The nasal mucosa was kept in contact with receptor compartment keeping the mucosal side facing towards the donor compartment. The whole diffusion assembly was kept under magnetic stirring at 50 rpm and temperature was maintained at 33 ± 1 ^oC. Nasal permeation study was performed for optimized RTG-LCNP containing Separately, 1 mL of each formulations *viz.*, optimized RTG-LCNP dispersion and pure RTG suspension were placed onto the donor compartment. At predetermined time intervals (5, 10, 15, 30, 60, 120, 240, and 360 min), 500 µL of samples were withdrawn and replaced with the same amount of pre-heated fresh media. All the samples were centrifuged (Eppendorf®, Hamburg, Germany) at 15,000 rpm for 15 min at 4 ^oC and supernatants were collected and suitably diluted with mobile phase (ACN:KH_2PO_4, pH 5::54:46). To permeated amount of RTG was analysed using previously described RP-HPLC method discussed in **Chapter 3**, **Method II** [11].

6.2.7 Stability study of RTG-LCNP

The storage stability of the lyophilized RTG-LCNP was analysed over 60 days in refrigerated conditions. RTG-LCNP were taken in airtight glass containers (15 mL) and stored at 4 ^oC. Samples (n = 3) were collected on 7th day, 30th day, and 60th day and evaluated for particle size (nm), PDI, zeta potential (mV), and %DL.

6.2.8 *In vivo* studies in Wistar rats

Male Wistar rats of 9 – 10 weeks (250 – 260 g) were used for all the *in vivo* studies. All the animals were housed at the central animal facility. A previous approval from the Institute's Animal Ethics Committee (IAEC), Protocol number- IAEC/RES/26/07/REV-1/30/19 was attained for all the experimental procedures carried out on animals.

6.2.8.1 Intranasal (i.n.) administration

Formulations were administered intranasally using a 1.3 cm long soft cannula (Instech Laboratories, PA, USA) attached in front of a 100 µL microtip. Rats were anaesthetized using isoflurane for both dosing and plasma collection. 75 µL of formulation (dose of 2 mg/Kg) was carefully pipetted out and administered in each of the nostrils [14]. After the i.n. administration of RTG-LCNP and RTG suspension, the rats were kept in supine position till it recovered from the anaesthesia. The PK parameters of brain and plasma of LCNP formulation were compared with that of pure RTG suspension. Aqueous suspension of RTG was prepared similarly as described in **Chapter 4**, **Section 4.2.11.1**.

6.2.8.2 Evaluation of mucociliary transport time

Mucociliary transport time for RTG-LCNP was assessed as described in **Chapter 4**, **Section 4.2.11.2**. Both formulations were administered (75 µL) to each nostril as mentioned in **Chapter 4**, **Section 4.2.11.1**. After administration, oropharyngeal cavity of rat administered with nasal dose was swabbed using cotton buds at an interval of 5 min till 90 min. Rats were not allowed to access of food for 1 h after initiation of the study. The samples collected at each time points were diluted using mobile phase (ACN:KH_2PO_4, pH 5::54:46). RTG was estimated in each swab with the validated RP-HPL method as discussed in **Chapter 3**, **Method II**. The time point at which presence of RTG quantified in oropharyngeal cavity was reported as mucociliary

transport time for RTG-LCNP. Mucociliary transport time for pure drug suspension data was taken from the previously reported **Chapter 4**, **Section 4.3.9.1**.

6.2.8.3 Plasma and brain PK analysis

PK studies for brain and plasma were performed for two groups *viz.*, RTG-LCNP and RTG suspension following i.n. administration to the rats. For aqueous drug suspension, the plasma and brain PK data were taken from the previously discussed **Chapter 4**, **Section 4.3.9.2**. Dosing of RTG-LCNP was completed using the set up and technique discussed in **Chapter 4**, **Section 4.2.11.1**. For plasma PK study, blood sampling was done from rats (n = 4) via retro-orbital puncture technique. At each time point, 200 µL of blood was collected in 1.5 mL centrifuge tubes already containing anticoagulant (4.5 %*w/v* disodium EDTA in water) at time intervals of 0 min i.e., before dose and 0.08, 0.25, 0.5, 1, 2, 4, 6, and 8 h after dosing. After dosing, brains were collected at each time intervals as mentioned before. At each time point rats (n = 4) were sacrificed, and brains of animals were collected as described in previous **Chapter 3**, **Section 3.5.2.1**. Brain tissue samples were collected at 0.5, 1, 2, 4, 6, and 8 h post dosing. Plasma and brain matrices were separated, and samples were processed using protein-precipitation method as described in previous chapter, **Sections 3.5.2.1** and **3.5.2.2**, respectively. Further analysis of the bio samples was performed using the validated RP-HPLC bioanalytical method discussed in **Chapter 3**, **Method III**. PK parameters *viz.*, C_{max}, T_{max}, $AUC_{0\rightarrow tlast,}$ and MRT were determined by non-compartmental analysis (NCA) using Phoenix WinNonlin (Version 8.0, Pharsight Corporation, NC, USA). To evaluate and compare the brain uptake of pure drug to optimized RTG-LCNP after i.n. administration, brain direct transport percentage (DTP (%)) and drug targeting efficiency percentage (DTE (%)) [15,16] were calculated using Equation 4.1 and Equation 4.2, respectively as described in **Chapter 4**, **Section 4.2.11.3**.

Using the PK parameters, DTP (%) and DTE (%) were computed to assess the direct N2B delivery effectiveness of the RTG-LCNP. Values greater than 0 and 100 for DTP (%) and DTE (%), respectively, signify substantial direct N2B distribution of the drug.

6.2.9 Histopathology of brain

The brains were isolated from rats before i.n. administration (as control, 0 h) and at 8 h after i.n. administration of RTG-LCNP. The isolated brains were washed in PBS (pH 7.4) to remove traces of blood and connective tissues. The cleaned brains were weighed and then fixed in 10 %*v/v* formalin solution. A series of ethanol concentration (*v/v*) i.e., 70%, 80%, 95%, and finally using 100%, dehydration of brain tissue was performed. The brain tissue was embedded in paraffin wax and sectioned using microtome. The deparaffinization process was performed using xylene. Slides were first treated with xylene, then ethanol concentrations (*v/v)*of 100%, 80%, and 70%, and finally using phosphate buffer saline (pH 7.4) rehydration was achieved. Finally the slides were stained with hematoxylin and eosin. Then the rehydrated slides were stained with hematoxylin and eosin. The histopathological slides were examined using an inverted light microscope (Carl Zeiss, Jena, Germany). Three rats from each group were used for the study.

6.3 Results and discussion

6.3.1 Preparation and characterization of RTG-LCNP

6.3.1.1 Effect of drug:lecithin ratio particle size and PDI

The amount of lecithin played an essential role in the preparation of NP. Lecithin concentration directly affects %EE and %DL of RTG-loaded LCNP. Thus, first drug:lecithin ratio was optimized during the preparation of formulation. The drug:lecithin ratio also affects particle size and PDI of the drug-lecithin dispersion (**Table 6.1**). The NP suspension was also prepared

without CS. Drug:lecithin ratio between 1:1 to 1:6 (*w/w*) was used during the formulation optimization. An increase in drug:lecithin ratio from 1:1 to 1.3 (*w/w*) resulted in decreased particle size of dispersion. The further high drug:lecithin ratio caused increased particle size and PDI. The ratio of 1:3 (*w/w*) had the lowest particle size and PDI. Both lower and higher lecithin concentrations resulted in increased particle size and PDI. The result might be attributed to the fact that an increase in lecithin amount results in aggregation of particles whereas, a decrease in lecithin amount fails to suitably stabilise the dispersion. The drug:lecithin (1:3) ratio was the selected as the optimum.

Table 6.1 Effect of drug:lecithin ratio on particle size and PDI of RTG-LCNP

Formulation code[a]	Drug:lecithin ratio (*w/w*)	Particle size (nm)	PDI
LCNP 1	1:1	220 ± 1.33	0.451 ± 0.011
LCNP 2	1:2	182 ± 2.34	0.412 ± .014
LCNP 3	1:3	123 ± 2.12	0.292 ± .002
LCNP 4	1:4	263 ± 1.22	0.409 ± 0.009
LCNP 5	1:5	294 ± 1.56	0.495 ± 0.003
LCNP 6	1:6	322 ± 2.86	0.309 ± 0.001

[a] LCNP 1 to LCNP 6 contains 20 mg of RTG

6.3.1.2 Effect of lecithin:CS ratio on particle size and PDI

Lecithin:CS ratio also affects particle size and PDI of the LCNP. A proper complexation between lecithin and CS is a prerequisite for preparing self-assembled LCNP and resulting in desired particle size. Lecithin:CS ratio was varied between 10 to 30, where the lecithin amount was kept constant at 60 mg. The increased lecithin:CS ratio resulted in lower particle size (**Table 6.2**). Whereas, lower lecithin:CS ratio resulted higher particle size. These results might be attributed to the fact that at low lecithin:CS ratio, a greater number of CS chains available for complexation with lecithin [10]. Hence, the lecithin:CS ratio (30) was selected for further optimization of LCNP.

Table 6.2 Effect of lecithin-CS ratio on particle size and PDI of RTG-LCNP

Formulation Code[a]	Lecithin:CS ratio	Particle size (nm)	PDI
LCNP 7	10	203.6 ± 1.22	0.430 ± 0.001
LCNP 8	20	171.0 ± 2.31	0.394 ± 0.002
LCNP 9	30	102.0 ± 1.22	0.312 ± 0.006

[a] LCNP 7 to LCNP 9 contains 20 mg of RTG

6.3.1.3 Effect of amount of Poloxamer 407 on particle size, PDI and %EE

Poloxamer 407 can directly affect RTG-LCNP particle size, PDI, and %EE. The drug exhibited lower solubility in Poloxamer 407 than other stabilizers (data showed in **Chapter 4**) [17]. Thus, Poloxamer 407 was selected as the stabilizer. The amount of Poloxamer 407 was varied from 2.5 to 10 mg by keeping the previous two parameters constant (drug:lecithin ratio: 1:3 (*w/w*), and lecithin:CS ratio 30) (**Table 6.3**). Decrease in the amount of Poloxamer 407 significantly increased the particle size of LCNP. This can be attributed to the absence of sufficient Poloxamer 407 to stabilize the formulation. The high Poloxamer 407 also resulted in a larger particle size and PDI. Increase in Poloxamer 407 amount was observed to negatively affect the %EE (**Table 6.3**). The high Poloxamer 407 increased the drug solubility, negatively impacting the %EE of RTG-LCNP. Hence, 5 mg of Poloxamer 407 was selected for the further optimization of %DL of the NP.

Table 6.3 Effect of amount of Poloxamer 407 on particle size, PDI, and %EE of RTG-LCNP

Formulation Code[a]	Amount of Poloxamer 407 (mg)	Particle size (nm)	PDI	%EE
LCNP 10	2.5	259.8 ± 5.17	0.309 ± 0.009	93.1 ± 3.61
LCNP 11	5	110.3 ± 1.09	0.348 ± 0.012	87.6 ± 2.93
LCNP 12	10	193.7 ± 4.05	0.421 ± 0.018	83.2 ± 1.90

[a] LCNP 10 to LCNP 12 contains 20 mg of RTG

6.3.1.4 Effect of pH of CS Solution on particle size and %DL

pH of CS solution is already reported to have a significant effect in the preparation of LCNP by ionic gelation method. CS gets solubilized in water due to the ionization of $NH3^+$ group

present in polymer due to the amine group in the CS. The positive charge causes the ionic interaction with the negatively charged lecithin [18]. As per the literature, CS solubility is decreased at pH > 6, because of poor ionization of the amine group [19]. Furthermore, in case of i.n. delivery, the pH of formulation is an important factor. Formulation pH different from physiological pH (range) of nasal cavity results in nasal irritation. Additionally, pH of CS might affect the solubility of RTG in aqueous phase and finally effect the %DL. Hence, pH of CS solution for optimization %DL was varied between pH 5 – 6. The effect of pH of CS solution on %DL of prepared RTG-LCNP is presented in **Table 6.4**.

Table 6.4 Effect of pH of CS Solution on particle size and %DL of RTG-LCNP

Formulation code[a]	Effect of pH	Particle size (nm)	%DL
LCNP 13	5.0	102.0 ± 0.02	6.33 ± 3.35
LCNP 14	5.5	107.5 ± 1.60	10.72 ± 4.03
LCNP 15	6.0	108.2 ± 1.09	14.43 ± 2.77

[a] LCNP 13 to LCNP 15 contains 20 mg of RTG, lecithin:CS ratio of 30 and Poloxamer 407 of 5 mg

The result showed that with decrease in pH of CS solution the %DL was decreased when all the other formulation and process parameters were kept constant. This result might be attributed to the fact that the drug showed a pH dependent solubility. At lower pH of CS solution, the drug solubility increases resulting in a lower %DL. RTG is reported to be soluble between pH 1 – 5, and with increasing pH the solubility of drug decreases. The result showed that change in pH of CS Solution has no significant effect on particle size of the prepared LCNP. Hence, LCNP 15 which showed a better %DL (14.43 ± 2.77) and a particle size of 108.2 ± 1.09 nm (**Figure 6.2A**) was selected as the optimal formulation. The %EE for LCNP 15 was 85.22 ± 1.83. The zeta potential of the optimized formulation was 14.9 ± 0.5 mV (**Figure 6.2B**).

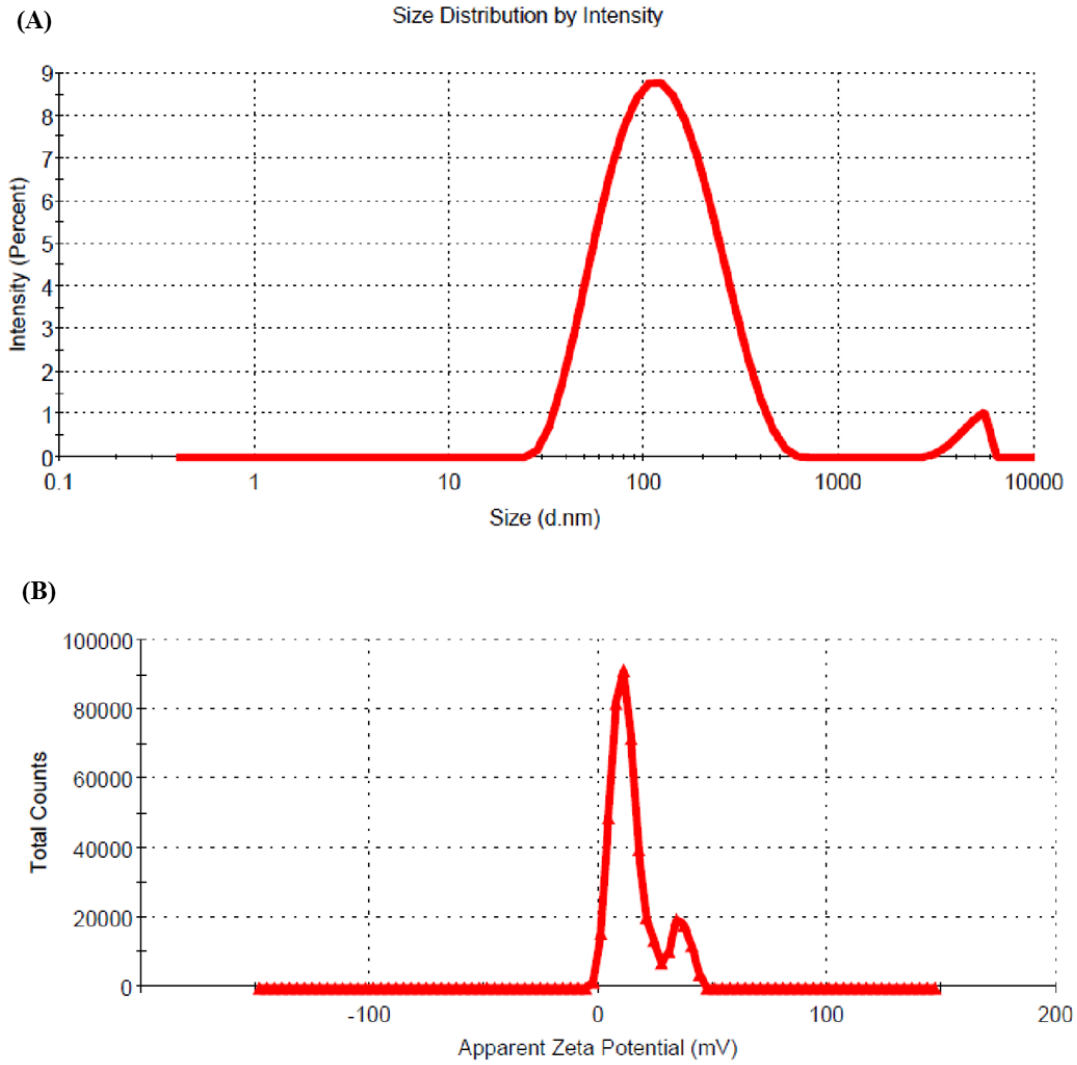

Figure 6.2 (A) Hydrodynamic diameter of optimized RTG-LCNP based on the % intensity, (B) Zeta potential of optimized RTG-LCNP

6.3.2 Characterization of RTG-LCNP

6.3.2.1 Differential scanning calorimetry

DSC thermograms of pure RTG, lecithin, CS, mannitol (cryoprotectant), and final lyophilized RTG-LCNP are presented in **Figure 6.3A**. The pure RTG showed a sharp endothermic melting peak at 97.87 ^{o}C [20], indicating that RTG is crystalline. Thermogram of CS shows no endothermic peak whereas, lecithin exhibits its characteristic sharp endothermic peak at 43.84 ^{o}C. Finally, the DSC thermogram of lyophilized RTG-LCNP exhibited a sharp endothermic peak at 166 °C which corresponds to the melting point of the cryoprotectant (mannitol) used

for lyophilization of LCNP [21]. The disappearance of RTG melting peak might be attributed to the entrapment of RTG in RTG-LCNP. The absence of peak might also be due to the conversion of RTG to its amorphous state within the LCNP.

6.3.2.2 Field emission scanning electron microscopy

The surface morphology of RTG-LCNP was characterized by FESEM. **Figure 6.3B** revealed almost spherical morphology of final RTG-LCNP. FESEM image revealed that the final RTG-LCNP were predominantly uniform in shape with smooth surfaces. The FESEM image also shows spherical particles of RTG-LCNP are of similar size as obtained by dynamic light scattering analysis. **Figure 6.3C** shows the FESEM images of crystalline RTG. The **Figure 6.3C** revealed that the RTG crystal are orthorhombic in shape [22].

6.3.2.3 Transmission electron microscopy

TEM image of pure RTG revealed that the drug shows high particle size with sharp edge (**Figure 6.4A**). In contrast, LCNP appeared to be nearly spherical in shape (**Figure 6.4B**). The image also revealed that core of the LCNP was surrounded by a compact outer layer which indicates formation of a core-shell structure [5,6].

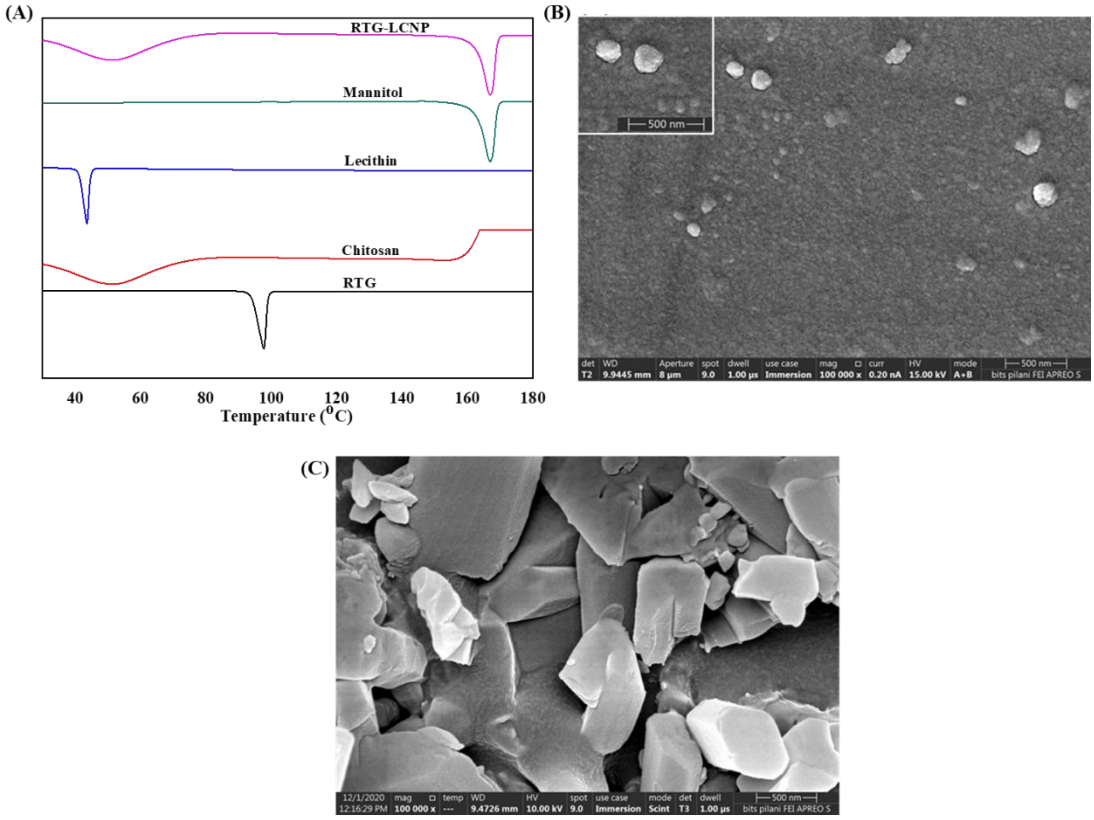

Figure 6.3 (A) DSC thermograms of RTG, Chitosan, Lecithin, and lyophilized RTG-LCNP, (B) Surface morphology of the optimized RTG-LCNP by FESEM, (C) Surface morphology of pure crystalline RTG by FESEM

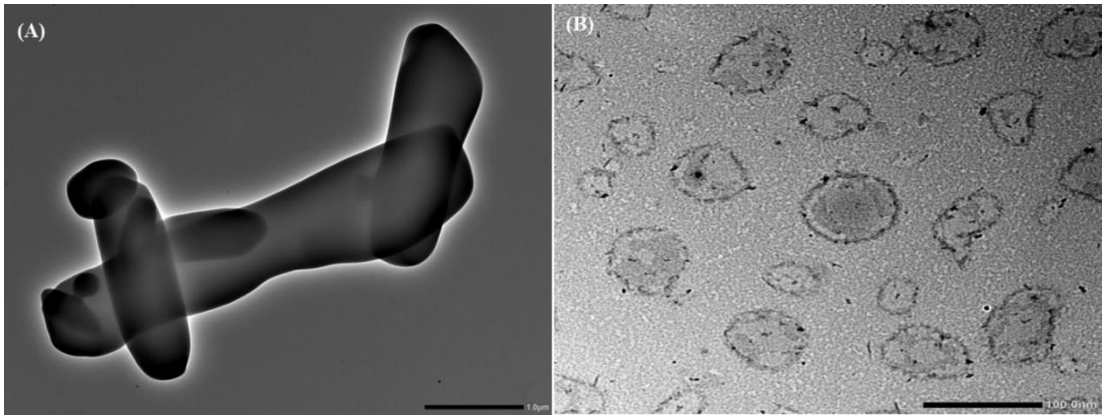

Figure 6.4 TEM images (A) Pure RTG, (B) Optimized RTG-LCNP by TEM

6.3.3 *In vitro* release

The *in vitro* drug release study of pure RTG suspension and optimized RTG-LCNP were performed, and the results are presented in **Figure 6.5**. From the pure drug suspension, almost 100% drug released was observed within 24 h. While from optimised LCNP, RTG released in a controlled pattern up to 24 h. Form RTG-LCNP, cumulative drug released (%CDR) was

found up to 32.44 ± 2.71 % after 24 h. The drug release from RTG-LCNP showed best fit with Korsmeyer–Peppas model with a R^2 value of 0.9296(**Table 6.5**). The R^2 with first-order was 0.3526, and R^2 with Higuchi model was 0.8289. The drug release mechanism from LCNP was best explained as non-Fickian diffusion type (n = 0.331) [23]. Another few lipophilic drugs i.e., 5-fluorouracil, kaempferol, and raloxifene also exhibited a similar Korsmeyer–Peppas model dependent release profile from lecithin-CS delivery systems [10,24,25]. Both the release profiles of RTG-LCNP and RTG suspension were evaluated for similarity factor (f_2), which showed that the two release profiles are not similar to each other, with a f_2 value of 20.

Table 6.5 Kinetic model application to *in vitro* release data of RTG-LCNP

Model	**R^2 value**
First-order	0.3562
Korsmeyer-Peppas	**0.9296**
Higuchi Model	0.8389

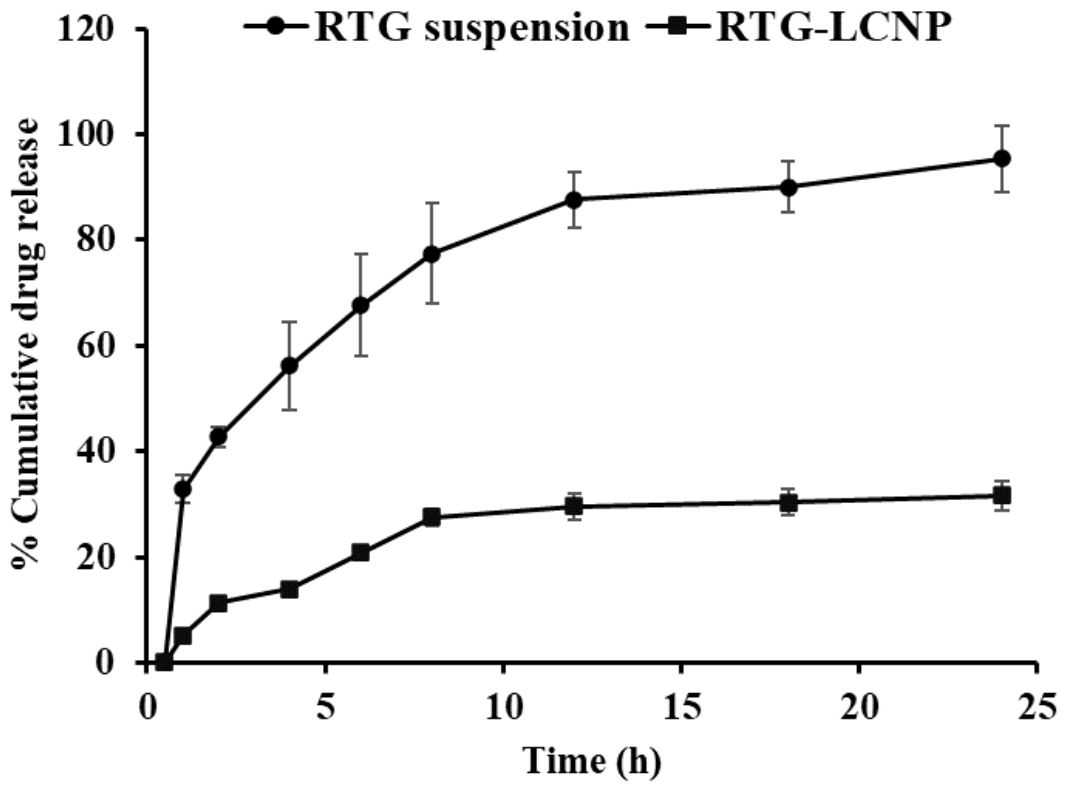

Figure 6.5 *In vitro* release profiles of RTG suspension and optimized RTG-LCNP in PBS (pH 7.4)

6.3.4 *Ex vivo* nasal permeation

An *ex vivo* nasal permeation study was performed to compare pure RTG suspension and RTG-LCNP. The mean cumulative *ex vivo* RTG permeated/unit area *vs* time through the goat nasal mucosa is presented in **Figure 6.6**. The permeation behaviour showed that RTG amount permeated (464.89 ± 58.22 μg/cm^2) from LCNP was significantly higher than that of pure RTG dispersion ($p < 0.05$). Optimized RTG-LCNP showed a 9.66-fold increase in amount permeated as compared to pure drug suspension. The result indicated that the LCNP formulation provides better permeability than pure drug. Better permeation of RTG from LCNP could be attributed to the presence of CS in the formulation. CS in the formulation might improve the *ex vivo* nasal permeation via paracellular transport by opening the tight junctions of biological membrane [6,26,27].

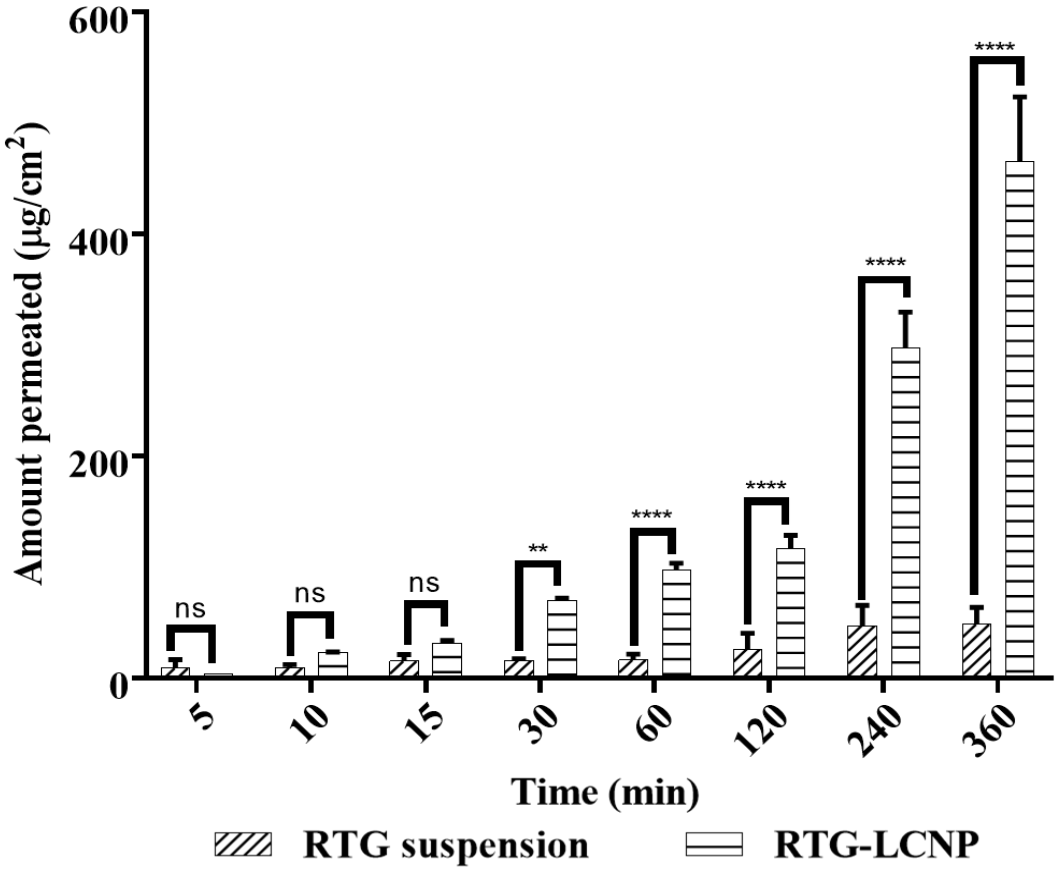

Figure 6.6 *Ex vivo* amount of drug permeated/unit area from optimized RTG-LCNP and drug suspension via goat nasal mucosa (n = 3, Mean ± SD)

6.3.5 Stability study of RTG-LCNP

Results obtained from stability study of RTG-LCNP in refrigerated conditions are shown in **Table 6.6**. No significant variation was observed in any of the parameters like particle size (nm), PDI, zeta potential and %DL between freshly prepared LCNP and LCNP stored at the refrigerated conditions over 60 days ($P > 0.05$).

Table 6.6 Stability data of lyophilized RTG-LCNP

Parameters	0 Day	7th Day	30th Day	60th Day
Particle size (nm)	108.2 ± 4.40	105.1 ± 4.38	103.3 ± 1.56	119.8 ± 11.10
PDI	0.312 ± 0.001	0.310 ± 0.002	0.297 ± 0.022	0.371 ± 0.325
Zeta potential (mV)	14.9 ± 0.5	14.1 ± 0.3	13.8 ± 0.3	16.2 ± 0.3
%DL	14.43 ± 2.77	14.75 ± 0.12	15.01 ± 2.39	12.85 ± 4.03

6.3.6 *In vivo* studies

6.3.6.1 Mucociliary transport time

Mucociliary transport time for pure RTG suspension and RTG-LCNP were 7.5 ± 3.53 min and 47.5 ± 3.53 min, respectively. RTG-LCNP demonstrated higher ($P < 0.05$) mucociliary transport time than that of RTG suspension (**Figure 6.7**). Increased mucociliary transport time value of RTG-LCNP compared to pure drug suspension indicates higher residence time in nasal cavity. The result might be attributed to the presence of mucoadhesive CS in formulation. The high mucociliary transport time of RTG-LCNP indicated that the nanocarrier could resist the mucocilliary clearance process and increased retention time of drug in the nasal cavity.

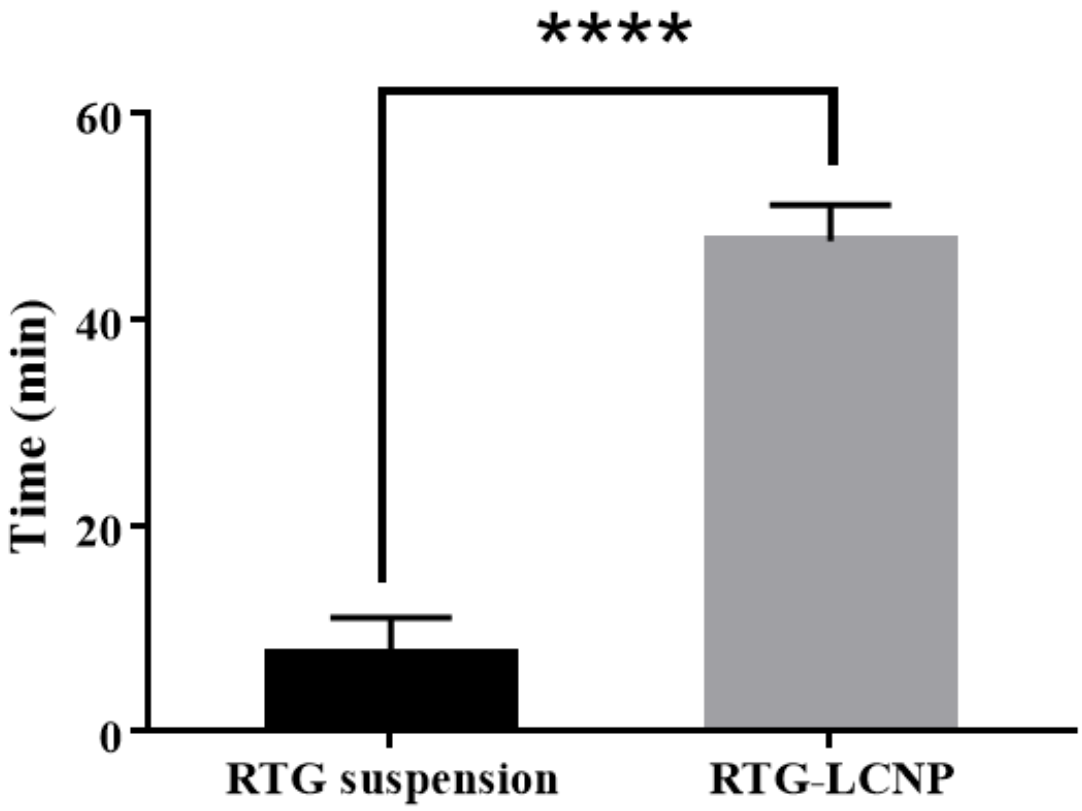

Figure 6.7 Mucociliary transport time of aqueous RTG suspension and RTG-LCNP. Independent student t-test with one-tail was applied. '****' shows p-value < 0.05.

6.3.6.2 Brain and plasma PK analysis

Brain and plasma concentration vs time profiles of RTG-LCNP and drug suspension following i.n. administration were constructed and presented in **Figure 6.8**. The brain and plasma PK parameters of RTG-LCNP and pure drug suspension were given in **Table 6.7**. PK data for RTG suspension was taken from **Chapter 3**, **Section 3.5.6**. The brain C_{max} of RTG-LCNP showed 3.84-fold increment compared to pure RTG suspension after i.n. administration. RTG-LCNP resulted increase in brain $AUC_{0\rightarrow tlast}$ by 8.76-fold than pure drug suspension. An unpair t-test comparison for brain $AUC_{0\rightarrow tlast}$ values for both formulations showed a statistically significant ($p < 0.0001$) difference between the two formulations. The brain concentrations of RTG were compared at all the time points, both RTG-LCNP and pure RTG suspension using t-tests. The drug concentrations from RTG-LCNP in the brain were significantly higher than RTG suspension at all respective time points at a 5% confidence interval (**Figure 6.8A**). To further

evaluate the *in vivo* performance of LCNP formulation, DTP (%) and DTE (%) were calculated as per Equation 4.1 and Equation 4.2, described in previous **Chapter 4**, **Section 4.2.11.3**. Here as a systemic route, the i.v. administration was used. DTE (%) value for RTG-LCNP was found 3673.7 which is significantly higher than 100. This result implies that the brain exposure of LCNP after i.n. administration is superior to that attained via the systemic route. This finally indicates the direct N2B uptake efficacy of the prepared LCNP. The DTP (%) was found to be 97.3 for RTG-LCNP showing effective direct N2B uptake of RTG to the brain. The high and positive DTE (%) and DTP (%) of RTG-LCNP may be ascribed to the better retention of formulation at the site of administration than drug suspension. CS in LCNP formulation improved mucoadhesion in the nasal cavity [28]. The presence of CS might further help in reversibly opening tight junctions, facilitating drug uptake to the brain via the olfactory nerve pathway.

Plasma $AUC_{0\rightarrow tlast}$ from RTG-LCNP was also significantly higher than drug suspension (**Table 6.7**). This result might be attributed to the fact that from LCNP via an indirect pathway RTG also reached the brain in higher amounts. CS present in the formulation might facilitate LCNP reach to the brain from systemic circulation by passing through BBB [29,30]. The presence of CS in LCNP might also result in opening a tight junction of the nasal epithelium, which finally leads to better systemic exposure of drug from LCNP from the respiratory region compared to pure suspension. The high plasma drug concentration from LCNP might be another reason for high DTE (%).

Table 6.7 Brain and plasma PK parameters for RTG-LCNP and RTG suspension after i.n. administration

PK parameters	Brain		Plasma	
	RTG-LCNP	**RTG suspension**	**RTG-LCNP**	**RTG suspension**
$AUC_{0\rightarrow tlast}$ (ng*h/g)[b], (ng*h/mL)[p]	5507.57 ± 23.91	628.11 ± 12.21	1060.44 ± 29.95	779.01 ± 14.11
C_{max} (ng/g)[b], (ng/mL)[p]	1013.47 ± 11.28	264.71 ± 21.12	230.87 ± 8.19	270.12 ± 18.50
T_{max} (h)	2	1	1	2
MRT (h)	3.81	1.82	1.58	3.15
Clearance (g/h)[b], (mL/h)[p]	78.57	-	-	312.65

[b] unit for brain PK parameters, [p] unit for plasma PK parameters. RTG dose for both i.n. formulations: 2 mg/Kg; for plasma PK n = 4 animals were used, and n = 4 animals' brains were used for brain PK at every time point; The brain and plasma data are represented as mean ± SD.

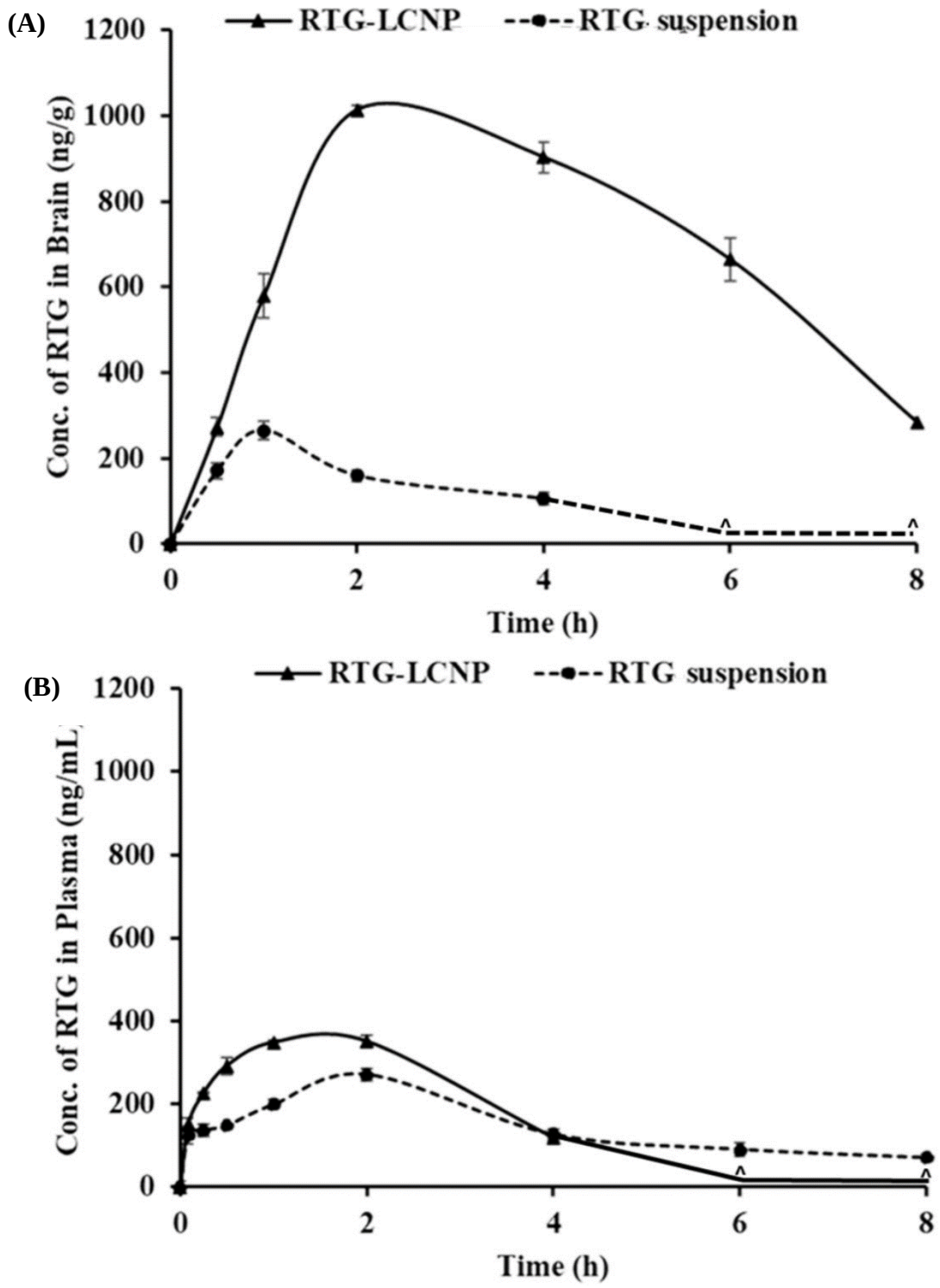

Figure 6.8 PK profiles of RTG attained after i.n. administration of RTG-LCNP and RTG suspension in (A) Brain and (B) Plasma. '^' in both the profiles denote that the concentration of RTG was not detected at those time points in brain matrices and plasma.

6.3.7 Histopathology of brain

At 0 h (control) and 8 h after receiving RTG-LCNP (treated), the morphology of the hippocampus region on brain slides was investigated for any toxicity (**Figure 6.9**) [31]. The morphology of the hippocampal area of LCNP treated rat (**Figure 6.9C** and **D**) was found to be similar to the control (**Figure 6.9A** and **B**). **Figure 6.8D** demonstrated that in the hippocampal region, there were no indications of neuronal damage, such as cell body necrosis or shrinking. This suggested that RTG-LCNP did not cause any damage to the brain and were safe for clinical use.

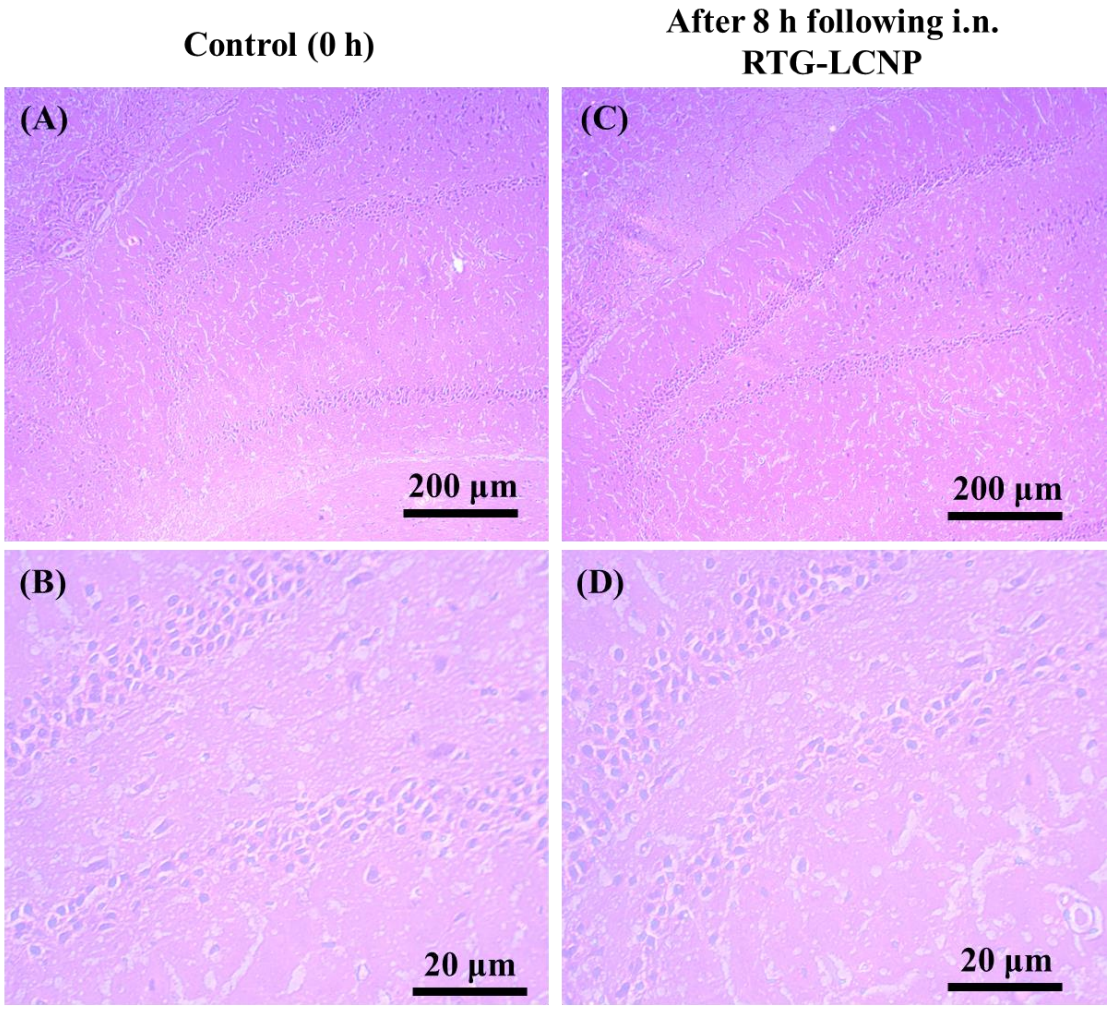

Figure 6.9 Histopathological evaluations of brain (hippocampal region) in different conditions (A) Control animal at 100X magnification, (B) Control animal at 400X magnification, (C) LCNP treated animal at 100X magnification, (D) LCNP treated animal at 400X magnification

6.4 Conclusion

RTG loaded LCNP were developed and optimized for better N2B delivery of RTG. In order to facilitate longer residence times at the olfactory region of RTG, RTG-LCNP was prepared in with CS in combination with lipid. Critical formulation variables of the RTG-LCNP were optimized for anticipated particle size, PDI, %EE, and %DL. The optimized RTG-LCNP was stable in refrigerated condition for atleast 2 months. *In vivo* PK studies in male Wistar rats showed that the developed RTG-LCNP demonstrated significant direct N2B delivery with 3.84-fold and 8.76-fold increased brain C_{max} and $AUC_{0\rightarrow tlast}$ as compared to pure RTG suspension. The results demonstrate the superiority of the optimized RTG-LCNP for the better management of PD when compared to the pure drug given in i.n. route. Furthermore, the brain histopathological study proves that the prepared LCNP was safe and non-toxic for i.n. administration. Overall, it can be concluded that RTG-LCNP would be advantageous for improving brain distribution of RTG following i.n. administration and has the potential for clinical application.

Reference

1. Trotta, V.; Pavan, B.; Ferraro, L.; Beggiato, S.; Traini, D.; Gomes, L.; Reis, D.; Scalia, S.; Dalpiaz, A. Brain Targeting of Resveratrol by Nasal Administration of Chitosan-Coated Lipid Microparticles. *European Journal of Pharmaceutics and Biopharmaceutics* **2018**, *127*, 250–259, doi:10.1016/j.ejpb.2018.02.010.

2. Rukmangathen, R.; Yallamalli, I.M.; Yalavarthi, P.R. Biopharmaceutical Potential of Selegiline Loaded Chitosan Nanoparticles in the Management of Parkinson's Disease. *Current Drug Discovery Technologies* **2018**, *16*, 417–425, doi:10.2174/1570163815666180418144019.

3. Khan, M.M.; Madni, A.; Torchilin, V.; Filipczak, N.; Pan, J.; Tahir, N.; Shah, H. Lipid-Chitosan Hybrid Nanoparticles for Controlled Delivery of Cisplatin. *Drug delivery* **2019**, *26*, 765–772, doi:10.1080/10717544.2019.1642420.

4. Sonvico, F.; Cagnani, A.; Rossi, A.; Motta, S.; Di Bari, M.T.; Cavatorta, F.; Alonso, M.J.; Deriu, A.; Colombo, P. Formation of Self-Organized Nanoparticles by Lecithin/Chitosan Ionic Interaction. *International journal of pharmaceutics* **2006**, *324*, 67–73, doi:10.1016/J.IJPHARM.2006.06.036.

5. Liu, L.; Zhou, C.; Xia, X.; Liu, Y. Self-Assembled Lecithin/Chitosan Nanoparticles for Oral Insulin Delivery: Preparation and Functional Evaluation. *International Journal of Nanomedicine* **2016**, *11*, 761–769, doi:10.2147/IJN.S96146.

6. Dong, W.; Ye, J.; Wang, W.; Yang, Y.; Wang, H.; Sun, T.; Gao, L.; Liu, Y. Self-Assembled Lecithin/Chitosan Nanoparticles Based on Phospholipid Complex: A Feasible Strategy to Improve Entrapment Efficiency and Transdermal Delivery of Poorly Lipophilic Drug. *International Journal of Nanomedicine* **2020**, *15*, 5629,

doi:10.2147/IJN.S261162.

7. Hafner, A.; Lovrić, J.; Pepić, I.; Filipović-Grčić, J. Lecithin/Chitosan Nanoparticles for Transdermal Delivery of Melatonin. *Journal of Microencapsulation* **2011**, *28*, 807–815, doi:10.3109/02652048.2011.622053.

8. Uppuluri, C.T.; Ravi, P.R.; Dalvi, A. V. Design and Evaluation of Thermo-Responsive Nasal in Situ Gelling System Dispersed with Piribedil Loaded Lecithin-Chitosan Hybrid Nanoparticles for Improved Brain Availability. *Neuropharmacology* **2021**, *201*, 108832, doi:10.1016/J.NEUROPHARM.2021.108832.

9. Murthy, A.; Ravi, P.R.; Kathuria, H.; Vats, R. Self-Assembled Lecithin-Chitosan Nanoparticles Improve the Oral Bioavailability and Alter the Pharmacokinetics of Raloxifene. *International Journal of Pharmaceutics* **2020**, *588*, 119731, doi:10.1016/j.ijpharm.2020.119731.

10. Murthy, A.; Ravi, P.R.; Kathuria, H.; Vats, R. Self-Assembled Lecithin-Chitosan Nanoparticles Improve the Oral Bioavailability and Alter the Pharmacokinetics of Raloxifene. *International Journal of Pharmaceutics* **2020**, *588*, 119731, doi:10.1016/J.IJPHARM.2020.119731.

11. Saha, P.; Pandey, M.M. DoE-Based Validation of a HPLC–UV Method for Quantification of Rotigotine Nanocrystals: Application to in Vitro Dissolution and Ex Vivo Nasal Permeation Studies. *Electrophoresis* **2022**, *43*, 590–600, doi:10.1002/ELPS.202100157.

12. Lujan, H.; Griffin, W.C.; Taube, J.H.; Sayes, C.M. Synthesis and Characterization of Nanometer-Sized Liposomes for Encapsulation and Microrna Transfer to Breast Cancer Cells. *International Journal of Nanomedicine* **2019**, *14*, 5159–5173,

doi:10.2147/IJN.S203330.

13. Saka, R.; Chella, N.; Khan, W. Development of Imatinib Mesylate-Loaded Liposomes for Nose to Brain Delivery: In Vitro and in Vivo Evaluation. *AAPS PharmSciTech* **2021**, *22*, 192, doi:10.1208/s12249-021-02072-0.

14. Wang, F.; Yang, Z.; Liu, M.; Tao, Y.; Li, Z.; Wu, Z.; Gui, S. Facile Nose-to-Brain Delivery of Rotigotine-Loaded Polymer Micelles Thermosensitive Hydrogels: In Vitro Characterization and in Vivo Behavior Study. *International Journal of Pharmaceutics* **2020**, *577*, 119046, doi:10.1016/j.ijpharm.2020.119046.

15. Lee, D.; Minko, T. Nanotherapeutics for Nose-to-Brain Drug Delivery: An Approach to Bypass the Blood Brain Barrier. *Pharmaceutics* **2021**, *13*, doi:10.3390/pharmaceutics13122049.

16. Sita, V.G.; Jadhav, D.; Vavia, P. Niosomes for Nose-to-Brain Delivery of Bromocriptine: Formulation Development, Efficacy Evaluation and Toxicity Profiling. *Journal of Drug Delivery Science and Technology* **2020**, *58*, 101791, doi:10.1016/j.jddst.2020.101791.

17. Saha, P.; Kathuria, H.; Pandey, M.M. Nose-to-Brain Delivery of Rotigotine Redispersible Nanosuspension: In Vitro and in Vivo Characterization. *Journal of Drug Delivery Science and Technology* **2023**, *79*, 104049, doi:10.1016/j.jddst.2022.104049.

18. Hafner, A.; Lovrić, J.; Pepić, I.; Filipović-Grčić, J. Lecithin/Chitosan Nanoparticles for Transdermal Delivery of Melatonin. *Journal of Microencapsulation* **2011**, *28*, 807–815, doi:10.3109/02652048.2011.622053.

19. Roy, J.C.; Salaün, F.; Giraud, S.; Ferri, A.; Roy, J.C.; Salaün, F.; Giraud, S.; Ferri, A.

Solubility of Chitin: Solvents, Solution Behaviors and Their Related Mechanisms. In *Solubility of Polysaccharides*, 2017, 20–60, doi: 10.5772/intechopen.71385.

20. Wolff, H.-M.; Quere, L.; Riedner, J. Polymorphic Form of Rotigotine 2008.

21. Paul, A.; Shi, L.; Bielawski, C.W. A Eutectic Mixture of Galactitol and Mannitol as a Phase Change Material for Latent Heat Storage. *Energy Conversion and Management* **2015**, *103*, 139–146, doi:10.1016/J.ENCONMAN.2015.06.013.

22. Saha, P.; Pandey, M.M. Spectrochimica Acta Part A : Molecular and Biomolecular Spectroscopy A New Fluorescence-Based Method for Rapid and Specific Quantification of Rotigotine in Chitosan Nanoparticles. *Spectrochimica Acta Part A: Molecular and Biomolecular Spectroscopy* **2022**, *267*, 120555, doi:10.1016/j.saa.2021.120555.

23. Lisik, A.; Witold Musial Conductomeric Evaluation of the Release Kinetics of Active Substances from Pharmaceutical Preparations Containing Iron Ions. *Materials* **2019**, *12*, 730, doi:10.3390/ma12050730.

24. Alomrani, A.; Badran, M.; Harisa, G.; … M.Al.-S.P.; 2019, U. The Use of Chitosan-Coated Flexible Liposomes as a Remarkable Carrier to Enhance the Antitumor Efficacy of 5-Fluorouracil against Colorectal Cancer. *Saudi Pharmaceutical Journal* **2019**, *27*, 603–611,doi: 10.1016/j.jsps.2019.02.008.

25. Ilk, S.; Saglam, N.; Özgen, M. Kaempferol Loaded Lecithin/Chitosan Nanoparticles: Preparation, Characterization, and Their Potential Applications as a Sustainable Antifungal Agent. *Artificial Cells, Nanomedicine and Biotechnology* **2016**, *45*, 907–916, doi:10.1080/21691401.2016.1192040.

26. Şenyiğit, T.; Sonvico, F.; Rossi, A.; Tekmen, I.; Santi, P.; Colombo, P.; Nicoli, S.; Özer, Ö. In Vivo Assessment of Clobetasol Propionate-Loaded Lecithin-Chitosan

Nanoparticles for Skin Delivery. *International Journal of Molecular Sciences* **2016**, *18*, 32, doi:10.3390/IJMS18010032.

27. Şenyiğit, T.; Sonvico, F.; Barbieri, S.; Özer, Ö.; Santi, P.; Colombo, P. Lecithin/Chitosan Nanoparticles of Clobetasol-17-Propionate Capable of Accumulation in Pig Skin. *Journal of Controlled Release* **2010**, *142*, 368–373, doi:10.1016/J.JCONREL.2009.11.013.

28. Jafarieh, O.; Md, S.; Ali, M.; Baboota, S.; Sahni, J.K.; Kumari, B.; Bhatnagar, A.; Ali, J. Design, Characterization, and Evaluation of Intranasal Delivery of Ropinirole-Loaded Mucoadhesive Nanoparticles for Brain Targeting. *Drug Development and Industrial Pharmacy* **2015**, *41*, 1674–1681, doi:10.3109/03639045.2014.991400.

29. Caprifico, A.E.; Foot, P.J.S.; Polycarpou, E.; Calabrese, G. Overcoming the Blood-Brain Barrier: Functionalised Chitosan Nanocarriers. *Pharmaceutics* **2020**, *12*, 1–20, doi:10.3390/pharmaceutics12111013.

30. Pourtalebi Jahromi, L.; Moghaddam Panah, F.; Azadi, A.; Ashrafi, H. A Mechanistic Investigation on Methotrexate-Loaded Chitosan-Based Hydrogel Nanoparticles Intended for CNS Drug Delivery: Trojan Horse Effect or Not? *International Journal of Biological Macromolecules* **2019**, *125*, 785–790, doi:10.1016/j.ijbiomac.2018.12.093.

31. Sita, V.G.; Jadhav, D.; Vavia, P. Niosomes for Nose-to-Brain Delivery of Bromocriptine: Formulation Development, Efficacy Evaluation and Toxicity Profiling. *Journal of Drug Delivery Science and Technology* **2020**, *58*, 101791, doi:10.1016/j.jddst.2020.101791.

Chapter 7: Comparison of the Various Optimized Nanocarriers of Rotigotine for N2B Delivery

7.1 Introduction

In this research work, we have designed and optimized three intranasal (i.n.) nanocarriers to enhance distribution of Rotigotine (RTG) to the brain via direct nose-to-brain (N2B) pathways. We have further evaluated the pharmacokinetic (PK) profiles of all three RTG-loaded nanocarriers in both brain and plasma following i.n. administration along with pure drug suspension.

We have evaluated the following formulations for N2B delivery of RTG:

1. Suspension of pure RTG (RTG suspension)
2. Nanosuspension for RTG (RTG-Nanosuspension)
3. Proposomes for RTG (RTG-Proposomes)
4. Lecithin-chitosan nanoparticles for RTG (RTG-LCNP).

Brain and plasma PK studies of intravenously administered pure RTG solution were also performed to demonstrate brain targeting efficiency of the developed RTG-loaded i.n. nanocarriers.

In this chapter, all three nanocarriers *viz.*, RTG-Nanosuspension, RTG-Proposomes, and RTG-LCNP were compared in terms of particle size, polydispersity index (PDI), zeta potential, entrapment efficiency (%EE) etc. The *ex vivo* nasal permeation and mucociliary transport time of RTG suspension, RTG-Nanosuspension, RTG-Proposomes, and RTG-LCNP were compared. Finally, the *in vivo* performance of all three nanocarrier systems was compared with RTG suspension after i.n. administration for N2B uptake of the drug.

7.2 Comparison of formulation processes of nanocarriers for RTG

RTG-Nanosuspension was prepared using antisolvent precipitation-ultrasonication method. In this process, the type of solvent and stabilizers preliminarily played a critical role in optimizing desired particle size. Furthermore, concentration of stabilizer, concentration of drug, and solvent:antisolvent ratio were identified as the most important critical variables for nanosuspension's particle size and PDI.

For the preparation of proposomes, effect of magnetic stirring, addition of droplets were initially optimized to obtain a desired particle size. Finally, ultrasonication time, propylene glycol (PG) concentration, and soya phosphatidylcholine (SPC) were found as the critically affecting method variables for the optimization of particle size, PDI, and %EE of the proposomes.

RTG-LCNP was prepared by solvent injection technique. Positively charged chitosan (CS) interacted with negatively charged lecithin to produce the LCNP. Lecithin:CS ratio, pH of CS solution, etc. act as critical factors for the preparation of optimized LCNP.

7.3 Comparison of particle size, zeta potential, %EE, drug content and *in vitro* drug release of RTG nanocarriers

The particle size, PDI, zeta potential, drug content, %EE for all three nanocarriers are presented in **Table 7.1**. RTG-Nanosuspension showed the lowest particle size amongst all three nanocarriers. RTG-LCNP showed a slightly higher %EE than the RTG-Proposomes.

In vitro drug dissolution study was performed for RTG-Nanosuspension whereas, *in vitro* release study was performed for RTG-Proposomes and RTG-LCNP. *In vitro* dissolution revealed that the drug dissolved was significantly faster from nanosuspension formulation.

Table 7.1 Comparison of physical characteristics of the nanocarriers for RTG

Physical characteristics	RTG-Nanosuspension	RTG-Proposomes	RTG-LCNP
Particle Size (nm)	73.55 ± 4.04	115.63 ± 5.22	108.2 ± 1.09
PDI	0.286 ± 0.028	0.267 ± 0.028	0.312 ± 0.006
Zeta potential (mV)	−24.7 ± 0.7	–14.8 ± 1.2	14.9 ± 0.5
%EE	NA	82.97 ± 0.18	85.22 ± 1.83
Drug content (%w/w)	101.61 ± 3.69	NA	NA

In vitro release study demonstrated that release was extended from the RTG-LCNP as compared to RTG-Proposomes formulation. The dissolution profile from RTG-Nanosuspension was not similar to the profile of pure drug (f_2 = 3.8). The release profile of RTG-Proposomes was similar to RTG-LCNP (f_2 = 62). But RTG-Proposomes and RTG-LCNP release profiles were not similar to pure RTG suspension (f_2 = 20) and (f_2 = 18), respectively.

7.4 Comparison of *ex vivo* permeation behaviour of RTG formulations

Ex vivo nasal permeation of pure RTG suspension, RTG-Nanosuspension, RTG-Proposomes, and RTG-LCNP were evaluated using goat nasal mucosa. Amount of RTG permeated/unit area after 360 min of all the formulations were presented in **Table 7.2**. Amongst all the formulations, nanosuspension showed the highest amount permeated/unit area at the end of 360 min.

Statistical comparison (**Figure 7.1**) revealed that the *ex vivo* permeation for pure drug suspension was substantially lower than the other three nanocarriers. The amount permeated/unit area from RTG-Nanosuspension was significantly higher than RTG-Proposomes and RTG-LCNP. The study results revealed that the smaller particle size and high dissolution rate of RTG-Nanosuspension might substantially improve the ex vivo performance of nanosuspension compared to the other two nanocarriers.

Table 7.2 Comparison of *ex vivo* amount permeated/unit area of RTG formulations

Formulations	Amount permeated/unit area (µg/cm^2)
RTG suspension	48.70 ± 15.43
RTG-Nanosuspension	992.45 ± 25.80
RTG-Proposomes	386.26 ± 18.62
RTG-LCNP	464.89 ± 58.22

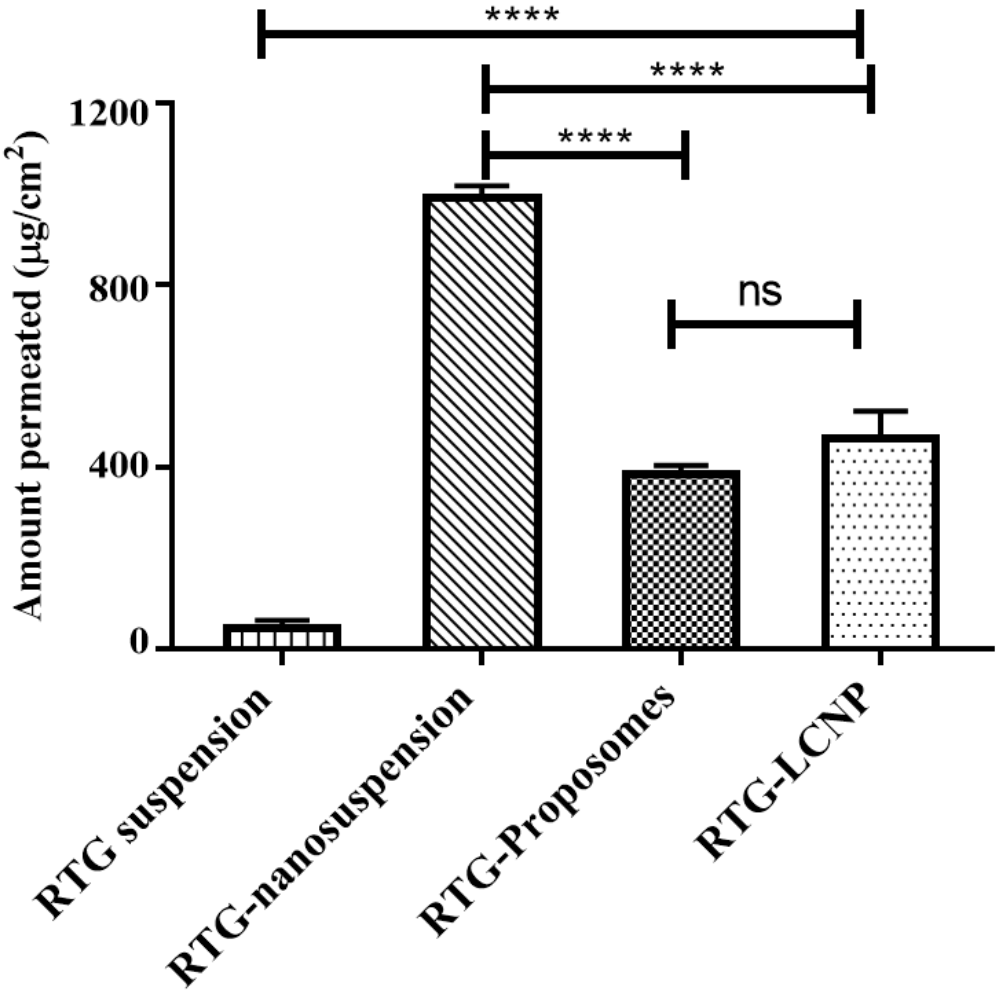

Figure 7.1 Comparison of *ex vivo* amount permeated/unit area of RTG formulations

7.5 Comparison of mucociliary transport time of RTG formulations

Mucociliary transport time following i.n. administration of RTG suspension, RTG-Nanosuspension, RTG-Proposomes, and RTG-LCNP was measured. The mucociliary transport time for all the formulations is presented in **Table 7.3**.

Table 7.3 Comparison of mucociliary transport time of RTG formulations

Formulations	Mucociliary transport time (min)
RTG suspension	7.5 ± 3.53
RTG-Nanosuspension	20.0 ± 5.00
RTG-Proposomes	32.5 ± 3.53
RTG-LCNP	47.5 ± 3.53

Statistical comparison (**Figure 7.2**) revealed that the mucociliary transport time for pure drug suspension was significantly lower than the other three nanocarriers. A significant ($P < 0.009$) difference was noted between the mucociliary transport time of RTG-Proposomes and RTG-LCNP. But, both the nanocarriers were statistically superior to that of RTG-Nanosuspension at P value of 0.0347 and < 0.0002, respectively. The results reveal that polymer or lipidic excipients (CS or SPC) were more helpful in retaining the formulation in nasal cavity than Poloxamer 407. The significantly high mucociliary transport time for RTG-LCNP compared to all other formulations indicate that CS helped delay mucociliary clearance.

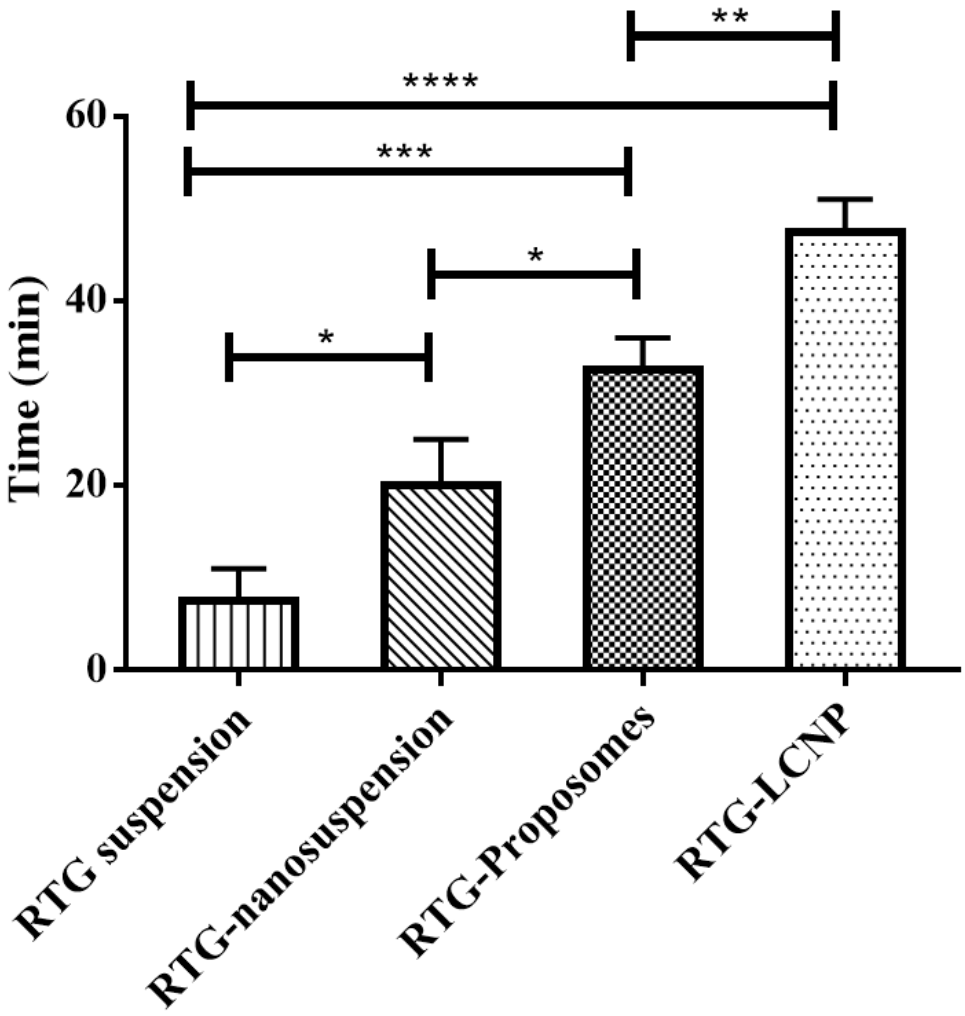

Figure 7.2 Mucociliary transport time for RTG following i.n. administration of various formulations. One-way ANOVA with Tukey's test applied. '****' shows p-value < 0.0001, '***' shows p-value 0.0005, '**' shows p-value 0.009 and '*' shows p-value 0.02.

7.6 Comparison of brain and plasma pharmacokinetic (PK) studies of RTG formulations

Data obtained from the brain and plasma PK studies of RTG nanocarriers are presented in **Table 7.4**. The RTG-LCNP showed the best results amongst all the formulations in terms of brain C_{max}, $AUC_{0\rightarrow tlast}$, DTE (%), and DTP(%). The result could be attributed to the fact that presence of CS and lecithin might have caused significant permeation enhancement leading to better brain availability. Furthermore, CS also had mucoadhesive property, resulting in longer residence time in the administration site (nose). All these advantages of RTG-LCNP

formulation finally exhibited in a better direct N2B delivery of RTG to brain via i.n. administration. Comparison of brain concentration *vs* time profiles for all the formulations following i.n. administration was constructed and presented in (**Figure 7.3**). RTG concentration in the brain was significantly higher from all three nanocarriers (p-value 0.0001) than RTG suspension at the first 4 time points (**Figure 7.3**). In contrast, from drug suspension, RTG was detected in brain at 4th h, which indicated that pure suspension was not sufficient enough to facilitate the availability of drug in the organ. Whereas all three nanocarriers enhanced and sustained the brain availability of RTG till 8th h (**Figure 7.3**).

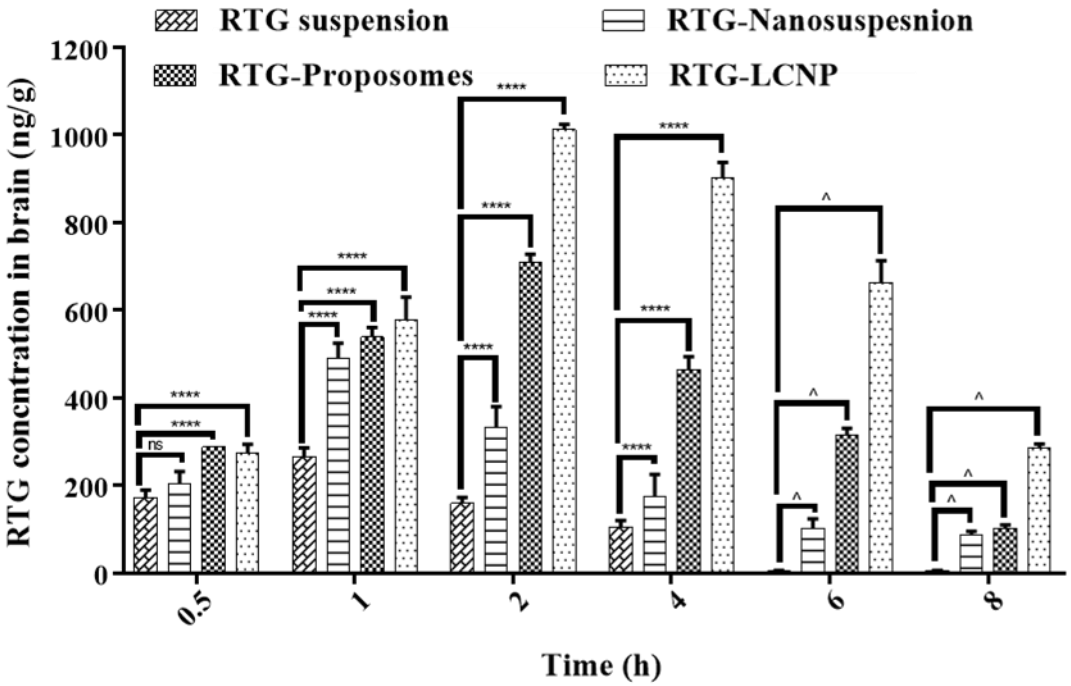

Figure 7.3 Concentration of RTG in brain at different time point after i.n. administration of RTG formulations. '^' in both the profiles denote that the concentration of RTG was not detected at those time points in brain matrices. Two-way ANOVA with Tukey's test applied. '****' shows p-value < 0.0001

Table 7.4 Comparison of brain and plasma PK parameters for different formulations of RTG

Matrix	PK parameters	RTG suspension	RTG-Nanosuspension	RTG-Proposomes	RTG-LCNP
Brain	$AUC_{0\rightarrow tlast}$ (ng/g*h)[b]	628.11 ± 12.21	1609.49 ± 34.92	3271.10 ± 13.12	5507.57 ± 23.91
	C_{max} (ng/g)[b]	264.71 ± 21.12	490.79 ± 48.93	708.61 ± 29.95	1013.47 ± 11.28
	T_{max} (h)	1	1	2	2
	MRT (h)	1.82	2.95	3.34	3.81
Plasma	$AUC_{0\rightarrow tlast}$ (ng/mL*h)[p]	779.01 ± 14.11	1286.29 ± 14.07	1491.89 ± 16.34	1060.44 ± 29.95
	C_{max} (ng/mL)[p]	270.12 ± 18.50	430.87 ± 9.20	321.87 ± 11.90	230.87 ± 8.19
	T_{max} (h)	2	1	0.5	1
	MRT (h)	3.15	2.23	2.74	1.58
DTE (%)			885.1	1556.4	3673.7
DTP (%)			88.7	93.6	97.3

[b] unit for brain PK parameters, [p] unit for plasma PK parameters. RTG dose for all i.n. formulations = 2 mg/kg; n = 4 rats were used for plasma PK, and for brain PK n = 4 animals' brains were used at every time point; The brain and plasma data are represented as mean ± SD.

7.7 Conclusion

Ex vivo nasal permeation, brain, and plasma PK data of all three nanocarriers demonstrated that the RTG-LCNP formulation was superior to the other two nanocarriers in terms of permeability behavior and direct transport of RTG to the brain. However, in comparison i.n. RTG suspension and intravenously administered RTG solution, all three optimized nanocarriers demonstrated improved performance in terms of *in vivo* brain distribution of RTG following N2B delivery.

Chapter 8: Future Scope of Work

In this research work, we have developed, optimized, and evaluated different nanocarriers to enhance the brain availability of Rotigotine (RTG) via intranasal (i.n.) administration. The developed nanocarriers demonstrated significant enhancement in the direct nose-to-brain (N2B) uptake of RTG. The *in vivo* pharmacokinetics (PK) studies performed in male Wistar rats revealed that a substantial amount of RTG has been taken up via the direct N2B pathways when administered as nanocarriers. Although, transit time in the nasal cavity was increased due to the nanocarriers but, we believe that loading of nanocarriers in any *in situ* gelling system will further improve the brain PK performance of the developed nanocarriers. Nanocarriers loaded *in situ* gel can also result in lower drug transport to the systemic circulation from the nasal cavity.

In this present study, we only evaluated the PK parameters of the optimized nanocarriers. The pharmacodynamic studies required to perform in disease model to further confirm the efficacy of the optimized nanocarriers for actual management of Parkinson's disease in pre-clinical setup.

Furthermore, the actual mechanisms of nanocarriers uptake via i.n. route is still not clear. Thus, it is necessary to perform mechanistic studies to determine different mechanisms involved in the uptake of drugs and/or nanocarriers via N2B route. This can facilitate advanced optimization of various nanocarriers for the effective uptake via i.n. route.

Recently, various devices are marketed to deliver liquid formulations as a spray dosage form to the olfactory region in humans via i.n. route. Appropriate installation of drug and/or formulations in the nasal cavity plays a critical role for direct N2B delivery of drug. A suitable

delivery device can further improve the PK performance of the optimized nanocarriers and ease the i.n. administration of nanocarriers.

Finally, several clinical trials are also ongoing investigating the direct N2B uptake of drugs in humans. These suggest that N2B delivery is one of futuristic approaches in the domain of drug delivery. Considering the results attained in the present research work at pre-clinical level, it is important to perform advanced studies in human to check the future prospective of nanocarriers based formulation intended for direct N2B delivery of RTG.

APPENDIX

List of Publications and Presentations

List of Publications (From Thesis Work)

1. **Paramita Saha**, Himanshu Kathuria, Murali Monohar Pandey. Intranasal nanotherapeutics for brain targeting and clinical studies in Parkinson's disease. Journal of Controlled Release. 2023 June; 358, 293-318. doi: 10.1016/j.jconrel.2023.04.021 (**IF: 11.467**)
2. **Paramita Saha**, Prabhjeet Singh, Himanshu Kathuria, Deepak Chitkara, Murali Monohar Pandey. Self-assembled lecithin-chitosan nanoparticles improved Rotigotine nose-to-brain delivery and brain targeting efficiency. Pharmaceutics. 2023 March; 15(3), 851, doi: 10.3390/pharmaceutics15030851 (**IF: 6.525)**
3. **Paramita Saha**, Deepak Chitkara, Murali Monohar Pandey. (Re)Formulating rotigotine: A potential molecule with unmet needs. Therapeutic Delivery. 2023 January; 13(9), 445-448. doi: 10.4155/tde-2022-0046 (**IF: 3.11**)
4. **Paramita Saha**, Himanshu Kathuria, Murali Monohar Pandey. Nose-to-brain delivery of rotigotine redispersible nanosuspension: In vitro and in vivo characterization. Journal of Drug Delivery Science and Technology. 2022 November; 79, 104049, doi: 10.1016/j.jddst.2022.104049 (**IF: 5.062**)
5. **Paramita Saha**, Murali Monohar Pandey. A new fluorescence-based method for rapid and specific quantification of rotigotine in chitosan nanoparticles. Spectrochimica Acta Part A: Molecular and Biomolecular Spectroscopy. 2022 February; 267 (Part 2), 120555. doi: 10.1016/j.saa.2021.120555. (**IF: 4.831**)
6. **Paramita Saha**, Murali Monohar Pandey. DoE-based validation of a HPLC-UV method for quantification of rotigotine nanocrystals: Application to in vitro dissolution and ex vivo

nasal permeation studies. Electrophoresis. 2022 February; 43(4), 590-600. doi: 10.1002/elps.202100157. (**IF: 3.595**)

Other Publication

1. **Paramita Saha,** Murali Monohar Pandey. Design of Experiment (DoE)-Approach Based RP-HPLC Analytical Method Development and Validation for Estimation of Efavirenz in Bulk and Formulations. Journal Chromatographic Science. 2022 January; 60(1), 35-44. doi: 10.1093/chromsci/bmab029. (**IF: 1.555**)

List of Conference Presentation (From Thesis Work)

1. **Paramita Saha,** Murali Monohar Pandey, "Development and Validation of Spectrophotometric Method for the Estimation of Rotigotine" at 'Biological Science and Bio-Engineering Conference' in Students' Research Convention 2021, Indian Institute of Technology (IIT), Kanpur on 27^{th} – 28^{th} Mar 2021. (**Awarded with 'Best Research Award' and cash prize**).

List of other Conference Presentations

1. **Paramita Saha**, Murali Monohar Pandey, "Solid Dispersion Technique for Dissolution Rate Enhancement of Cefpodoxime Proxetil" at 'National Conference on Advances in Microscopy and Foldscope' at Motilal Nehru National Institute of Technology (MNNIT), Allahabad on 15^{th} – 16^{th} Mar 2019.
2. **Paramita Saha**, Chandani Lulla, Ankita Sehgal, Murali Monohar Pandey, "Dissolution Enhancement of Curcumin by Preparing Nanocrystals" at 'International Conference on Life Science Research & its Interface with Engineering and Allied Sciences' at Birla Institute of Technology and Science – Pilani, Pilani Campus on 1^{st} – 3^{rd} Nov 2018.

Workshops

1. 'Pharmacokinetic & Pharmacodynamic Modeling and Simulation using Pumas' at Birla Institute of Technology and Science – Pilani, Pilani Campus, Pilani on 24th – 25th Feb 2020.
2. 'Workshop on Analytical Instrument for Chemical and Environmental Engineers' at Birla Institute of Technology and Science – Pilani, Pilani Campus on 25th – 26th Mar 2019.
3. 'National Workshop on Foldscope' at Motilal Nehru National Institute of Technology (MNNIT), Allahabad on 31st Aug – 1st Sep 2018.

Brief Biography of the Candidate

Ms. Paramita Saha completed her B.Pharm. from West Bengal University and Technology (WBUT, newly named as MAKAUT), West Bengal in 2013 and M.Pharm. (Pharmaceutics) from BITS Pilani, Hyderabad Campus, in 2016. After completing her M.Pharm., she worked as Research Associate at Lupin Research Park, Pune (Aug 2016 – Feb 2018). In 2018, she joined BITS Pilani, Pilani Campus, to pursue her doctoral studies under the supervision of Dr. Murali Monohar Pandey. During her masters and doctoral studies, she has authored several research and review papers in renowned international peer-reviewed journals and delivered presentations at international and national conferences.

Brief Biography of the Supervisor

Dr. Murali Monohar Pandey is currently working as an Assistant Professor in Department of Pharmacy, BITS Pilani, Pilani Campus. He has completed B.Pharm., M.Tech. (Biotechnology) from Jadavpur University, Kolkata, and Ph.D. (Pharmaceutics) from BITS Pilani, Pilani Campus. He is associated with BITS Pilani since 2007. He is having 17 years of teaching experience. He has guided more than 40 (B. Pharm.) and 35 (M.Pharm.) students in various laboratory and study-oriented projects. He has also guided 4 (B.Pharm.) and 3 (M.Pharm.) students for their dissertation/thesis works. He is a member of Academic Counseling Cell, BITS Pilani. He has many publications in reputed international and national peer-reviewed journals and has presented papers in scientific conferences in India and abroad. He has successfully completed several government-sponsored and industry-sponsored research projects.